

**DYNAMIC ANALYSIS OF
DELAMINATED COMPOSITE
PRETWISTED STIFFENED CYLINDRICAL
SHELLS -
A FINITE ELEMENT APPROACH**

*A Thesis
Submitted
By*

MRUTYUNJAY ROUT

Doctor of Philosophy (Engineering)

**DEPARTMENT OF MECHANICAL ENGINEERING
FACULTY COUNCIL OF ENGINEERING & TECHNOLOGY
JADAVPUR UNIVERSITY
KOLKATA, INDIA-700 032
2018**

**JADAVPUR UNIVERSITY
KOLKATA - 700 032, INDIA**

INDEX NO.: 230/16/E

1. Title of the thesis:

Dynamic Analysis of Delaminated Composite Pretwisted Stiffened Cylindrical Shells - A Finite Element Approach

2. Name, Designation & Institution of the Supervisor:

Dr. Amit Karmakar,
Associate Professor,
Mechanical Engineering Department,
Jadavpur University, Kolkata - 700 032.

3. List of Publication:

- a. Mrutyunjay Rout, Sasank Shekhara Hota and Amit Karmakar. "Free vibration characteristics of delaminated composite pretwisted stiffened cylindrical shell." *Proceedings of the Institution of Mechanical Engineers, Part C: Journal of Mechanical Engineering Science* 232, no. 4 (2018): 595-611.
- b. Mrutyunjay Rout, Tanmoy Bandyopadhyay, and Amit Karmakar. "Free vibration analysis of pretwisted delaminated composite stiffened shallow shells: A finite element approach." *Journal of Reinforced Plastics and Composites* 36, no. 8 (2017): 619-636.
- c. Mrutyunjay Rout, Sasank Shekhar Hota and Amit Karmakar. "Transient response of pretwisted delaminated stiffened shell under low velocity impact." *International Journal for Computational Methods in Engineering Science and Mechanics*, (2018): DOI: 10.1080/15502287.2018.1430080.
- d. Mrutyunjay Rout and Amit Karmakar. "Free vibration of rotating pretwisted CNTs-reinforced shallow shells in thermal environment" *Mechanics of Advanced Materials and Structures*, (2018): DOI: 10.1080/15376494.2018.1452317.
- e. Mrutyunjay Rout, Sasank Shekhar Hota, and Amit Karmakar. "Prediction of impact response of delaminated pretwisted stiffened shell" *Australian Journal of Mechanical Engineering*. (2019):

DOI: <https://doi.org/10.1080/14484846.2019.1600212>.

- f.* Mrutyunjay Rout and Amit Karmakar. "Low Velocity Impact Performance of Delaminated Composite Stiffened Shell." *Procedia Engineering* 173 (2017): 306-313.

4. List of Patents: Nil

5. List of Presentations in National/International/Conferences/Workshops:

- a.* Low Velocity Impact Performance of Delaminated Composite Stiffened Shell, 11th International Symposium on Plasticity and Impact Mechanics, *Implast 2016*, December 12-14, 2016, IIT Delhi, India.
- b.* Multiple Low Velocity Impact on Twisted Composite Stiffened Blade-A Finite Element Approach, 5th ASME Gas Turbine India Conference, *GTIndia 2017*, December 7-8, 2017, Bengaluru, Karnataka, India.
- c.* Effect of delamination on stiffened and un-stiffened shell-A comparative study, International Conference on Theoretical, Applied, Computational and Experimental Mechanics, *ICTACEM 2017*, December 28-30, 2017, IIT Kharagpur, India.
- d.* Low velocity impact performance of CNTs-reinforced composite plate, 2nd National Conference on Multi-Dimensional Advancement in Mechanical Engineering, *NCMAME 2017*, December 27-28, 2017, Govt. College of Engg., Kalahandi, Odisha, India.
- e.* Free Vibration of Rotating Twisted Composite Stiffened Plate, 1st International Conference on Mechanical Engineering, *INCOM 2018*, January 4-6, 2018, Jadavpur University, Kolkata, India.

**JADAVPUR UNIVERSITY
KOLKATA-700 032, INDIA**

CERTIFICATE FROM THE SUPERVISOR

This is to certify that the thesis entitled “**Dynamic Analysis of Delaminated Composite Pretwisted Stiffened Cylindrical Shells - A Finite Element Approach**” submitted by Shri Mrutyunjay Rout, who got his name registered on 04/04/2016 for the award of **Ph.D.(Engineering) degree of Jadavpur University** is absolutely based upon his own work under the supervision of **Dr. Amit Karmakar, Associate Professor, Dept. of Mechanical Engineering** and that neither his thesis nor any part of the same has been submitted for any degree / diploma or any other academic award anywhere before.

Dr. Amit Karmakar,
Associate Professor,
Dept. of Mechanical Engineering,
Jadavpur University, Kolkata - 700 032.

ACKNOWLEDGEMENT

First and above all, I praise God, the almighty for providing me this opportunity and granting me the capability to proceed successfully. This thesis appears in its current form due to the assistance and guidance of several people. Therefore, I would like to offer my sincere thanks to all of them.

I express my deep sense of gratitude to my supervisor Dr. Amit Karmakar, Associate Professor, Department of Mechanical Engineering, Jadavpur University, Kolkata for his active guidance and prudent suggestions throughout the course of my Ph. D work. I would also like to thank all the faculty members of the Mechanical Engg. Department, Jadavpur University, for their constant support and encouragement.

I also owe my sincere thanks to Dr. Sasank Shekhar Hota, Professor, Department of Civil Engineering, CVR College of Engineering, Hyderabad, Telangana for introducing me to the field of finite element analysis (FEM) during the initial stages of my Ph.D work. I admire his great qualities and feel happy to be associated with him.

I am thankful to Dr. Dulu Patnaik, Principal of my parent institute, Government College of Engineering, Kalahandi, Bhawanipatna for granting me deputation-cum-study leave for this program. I owe my gratitude to Dr. Chitaranjan Dash, Head, Department of Basic Science, Govt. College of Engg., Kalahandi, Bhawanipatna for his constant encouragement and moral support to complete this research work.

The excellent cooperation and support provided by many of my friends and co-research scholars, namely Mr. Laxminarayan Rout, Dr. Tanmoy Bandopadhyaya, Mr. Apurba Das, Mr. Jayanarayan Mahakud and Mr. Pabitra Maji are thankfully acknowledged.

I extend sincerest gratitude to my parents for their blessings and my brothers and sister for standing by me with lots of encouragement.

It was a difficult proposition for me to undertake this mission away from home with the responsibilities of my wife and little son. However, I am indebted to my in-laws for taking care of my family in my absence. My wife, Sthiti deserves a special word of praise for extending her support in preparing all the drawing in AutoCAD. Last but not the least; I thank my little son, Shriyans for enduring with the diversion of my time and missing a lot of his enjoyable moments because of my absence during the research work. This thesis, a fruit of the combined efforts of my family members, is dedicated to them as a token of love and gratitude.

Mrutyunjay Rout

LIST OF PUBLICATIONS

The following research publications are based on the present research work:

1. Mrutyunjay Rout, Sasank Shekhara Hota, and Amit Karmakar. "Free vibration characteristics of delaminated composite pretwisted stiffened cylindrical shell." *Proceedings of the Institution of Mechanical Engineers, Part C: Journal of Mechanical Engineering Science* 232, no. 4 (2018): 595-611.
2. Mrutyunjay Rout, Tanmoy Bandyopadhyay, and Amit Karmakar. "Free vibration analysis of pretwisted delaminated composite stiffened shallow shells: A finite element approach." *Journal of Reinforced Plastics and Composites* 36, no. 8 (2017): 619-636.
3. Mrutyunjay Rout, Sasank Shekhar Hota, and Amit Karmakar. "Transient response of pretwisted delaminated stiffened shell under low velocity impact." *International Journal for Computational Methods in Engineering Science and Mechanics*, (2018) :DOI: 10.1080/15502287.2018.1430080.
4. Mrutyunjay Rout and Amit Karmakar. "Free vibration of rotating pretwisted CNTs-reinforced shallow shells in thermal environment" *Mechanics of Advanced Materials and Structures*, (2018): DOI: 10.1080/15376494.2018.1452317.
5. Mrutyunjay Rout, Sasank Shekhar Hota, and Amit Karmakar. "Prediction of impact response of delaminated pretwisted stiffened shell" *Australian Journal of Mechanical Engineering*. (2019):DOI: <https://doi.org/10.1080/14484846.2019.1600212>.
6. Mrutyunjay Rout and Amit Karmakar. "Low Velocity Impact Performance of Delaminated Composite Stiffened Shell." *Procedia Engineering* 173 (2017): 306-313.

ABSTRACT

Advances in composite technology have led the extensive application of composite materials in energy, aviation and marine engineering. A cantilevered twisted composite cylindrical shell idealized as turbo machinery blade offers higher strength to weight ratio, durability and design flexibility with tailoring of fiber angles in different layers. Delamination is the most common cause of failure of laminated composite structures, particularly under compressive loads. The presence of delamination in the composite turbomachinery blades reduces its overall strength and attenuates the desired vibration characteristics. Moreover, the delamination tends to increase rapidly under impact loads, causing further reduction in structural strength. In order to improve the safety and durability, stiffeners are integrated at suitable orientations of such composite shell structures. Stiffeners also help to improve the vibration and impact response of such structures. Therefore, the composite turbomachinery blade is idealized as twisted laminated cylindrical shell with laminated composite stiffener. Dynamic analyses in respect of free vibration characteristics and impact response of pretwisted delaminated stiffened cylindrical shells are studied in this present work using finite element method.

The element stiffness and mass matrices for the laminated stiffened shell elements have been computed by appropriate combinations of the eight noded isoparametric shell element with three noded isoparametric curved beam element. In the present method, the effect of mass and stiffness of the stiffener are being lumped at the nodal points of the shell element considering their eccentricity and curvature. Multi-point constraint algorithm is utilized to model delamination within the shell. A generalized in-house computer code is developed to compute numerical results. The present method is validated with benchmark problems of free vibration and low velocity impact problem available in the open literature. Furthermore, additional problems have been taken up with different parametric variations for both free vibration and low velocity impact analyses to arrive at some meaningful conclusions.

For free vibration analysis a generalized cylindrical stiffened shell as well as long, intermediate and short cylindrical stiffened shells based on Aas-Jakobsen's parameters is considered. Parametric studies have been performed to predict the effects of stiffener orientation, twist angle, fibre orientation, delamination along span and across thickness, stiffener thickness to shell thickness ratio, eccentricity of stiffener and rotational speed on the fundamental frequency of the stiffened shell. Some basic guidelines are suggested to select the useful design parameters of the panel such as x-directional eccentric top stiffeners with fiber orientation within the range of 60^0 to 70^0 are beneficial.

Low velocity impact response of pretwisted laminated composite stiffened shells under the impact of single and multiple masses have been investigated. The modified Hertzian contact law is utilized to compute the contact force between shell and impactor while Newmark's time integration algorithm is used to solve time dependent equations of cylindrical stiffened shell and the impactor. A detailed parametric study in terms of stiffener orientation, delamination across the thickness, eccentricity of stiffener, stiffener depth to shell thickness ratio, initial twist, diameter of impactor, velocity of impactor and rotation of stiffened shell are performed for low velocity single impact, multi-impact and time delayed multi-impact cases to arrive at some significant conclusions. The work reported in this study provides an efficient modeling approach.

NOMENCLATURE

A_0, \dots, A_8	Constants of displacement polynomial
$[D]$	Elasticity matrix of shell element
$[D^{sx}]$	Elasticity matrix of x- stiffener
$[D^{sy}]$	Elasticity matrix of y- stiffener
E_1, E_2	Young's moduli of laminated shell and stiffener, respectively
E_i	Modulus of elasticity of the spherical impactor
F_C	Contact force during impact
F_m	Maximum contact force just before unloading
G_{12}, G_{13}, G_{23}	Shear moduli of laminated shell and stiffener
L	Length of shell in plan
M_x, M_y, M_{xy}	Moment resultants of shell per unit length
M_x^{sx}, M_y^{sy}	Moment resultants per unit length of x-and y-directional stiffeners, respectively
N_x, N_y, N_{xy}	In-plane force resultants of shell per unit length
N_x^{sx}, N_y^{sy}	In-plane force resultants per unit length of x-and y-directional stiffeners, respectively
Q_{xz}^{sx}, Q_{yz}^{sy}	Transverse shear resultants per unit length of x-and y-directional stiffeners, respectively
Q_{ij}	Elastic constants of stiffness matrix
$[\bar{Q}_{ij}]$	Off axis elastic constants
Q_{xz}, Q_{yz}	Transverse shear resultants of shell per unit length
T_x^{sx}, T_y^{sy}	Torsion resultants per unit length of x-and y-directional stiffeners, respectively
X, Y, Z	Global coordinate axes
a	Length of delamination
b	width of shell in plan
b_{st}	width of the stiffener
d	Distance of centre of delamination from fixed end.
d_{st}	thickness of the stiffener.
$\{d_n\}$	Vector containing element nodal displacements and rotations.
e_{sx}, e_{sy}	Eccentricities of x and y direction stiffeners with respect to shell mid-surface, respectively.
h	Thickness of shell
h'	Distance of delamination across the thickness from top ply

k	Contact stiffness of the shell
m_i	Mass of the impactor
nl, nl_x, nl_y	Number of layers in laminated shell, x-directional stiffener and y-directional stiffener, respectively
n_x, n_y	number of stiffeners in x and y directions, respectively
p	intensity of uniformly distributed load per unit area
r_i	Radius of the spherical impactor
u, u^{sx}	Tangential displacements along x axis of shell and x-directional stiffener elements, respectively
v, v^{sy}	Tangential displacements along y axis of shell and y-directional elements, respectively
w, w^{sx}, w^{sy}	Transverse displacements along z axis of shell, x-directional stiffener and y-directional elements, respectively
w_i	Displacement of the spherical impactor
ν	Poisson's ratio of the spherical impactor
ξ, η	Local natural coordinates of an element
$\alpha, \alpha^{sx}, \alpha^{sy}$	Rotations along x axis of shell, x-directional stiffener and y-directional elements, respectively
$\beta, \beta^{sx}, \beta^{sy}$	Rotations along y axis of shell, x-directional stiffener and y-directional elements, respectively
$\bar{\alpha}$	Depth of indentation
$\bar{\alpha}_m$	Maximum indentation
$\bar{\alpha}_{cr}$	Critical indentation beyond which permanent indentation
$\nu_{12}, \nu_{13}, \nu_{23}$	Poisson's ratios of laminated shell and stiffener
θ	Orientation of fiber in the lamina with respect to x-axis.
ϵ_x, ϵ_y	Normal strains
$\gamma_{xy}, \gamma_{xz}, \gamma_{yz}$	Shear strains
κ_x, κ_y	Parameters of curvature variation of shell
κ_{xy}	Parameter of torsion
σ_x, σ_y	Normal stresses in the shell along X- and Y- directions respectively.
$\tau_{xy}, \tau_{xz}, \tau_{yz}$	Shear stresses in YZ, XY and XZ planes of shell, respectively.
$\sigma_x^{sx}, \sigma_y^{sy}$	Normal stresses in the x- and y- directional stiffeners, respectively
$\tau_{xy}^{sx}, \tau_{xz}^{sx}$	Shear stresses in YZ plane of x-directional stiffener, along Y and Z axes, respectively
$\tau_{yx}^{sy}, \tau_{yz}^{sy}$	Shear stresses in XZ plane of y-directional stiffener, along X and Z axes, respectively

k_s, k_s^{sx}, k_s^{sy}	Shear correction factor for shell, x-and y- directional stiffeners, respectively
ρ	mass density of shell and stiffeners
ρ_k	Mass density of the k^{th} layer of the laminated shell and stiffener
Ω'	Actual angular speed of rotation of the stiffened shell about Z-axis
Φ	Twist angle of the stiffened shell
Ω	Non-dimensional rotational speed [$\Omega = \Omega' / \omega_n$]
ω_n	Fundamental natural frequency of stationary stiffened shell
ϖ	Non-dimensional fundamental frequency [$\varpi = \omega_n L^2 \sqrt{\rho / E_1 h^2}$]
Δt	time step

Numbering of Figures, Tables and Equations

Figures, tables and equations have been numbered in accordance with the chapters in which they appear. Each table, figure or equation has two distinct numbers. The first number indicates the number of the chapter and the second number refers to the actual number of the figure, table or equation in that chapter.

Representation of References

The list of references has been furnished at the end of the thesis. These references have been represented by the respective name of the author(s) along with the year of publication.

CONTENTS

		Page No.
		i
		ii
		iii
		iv
		vi
		xii
		xiv
Chapter 1	INTRODUCTION	
1	General	1
1.1	Method of analysis	3
1.2	Present study-its relevance in research	5
1.3	Remarks	6
1.4	Literature Review	6
1.5	1.5.1 Plate and shell theories	7
	1.5.2 Turbomachinery blades	10
	1.5.3 Pretwisted plates & shells	10
	1.5.4 Composite stiffened structure	12
	1.5.5 Bending behavior of stiffened plate/shell	14
	1.5.6 Free vibration behavior of stiffened plate/shell	17
	1.5.7 Transient response under low velocity impact	21
	1.5.7.1 Composite plates and shells:	21
	1.5.7.2 Composite stiffened plate/shell	28
	1.5.8 Delaminated composite plate/shell structures	30
	1.5.9 Delaminated composite stiffened plate/shell	35
	1.5.10 Other Aspects	39
	1.5.11 Critical observaions	40
1.6	Research Gaps Identified	41
1.7	Scope of the Present Investigation	42
1.8	Organization of the Thesis	44
Chapter 2	THERORETICAL FORMULATION	
2	General	46
2.1	Shell Element	47
2.2	2.2.1 Shape Functions	48
	2.2.2 Generalized Displacement Fields and Nodal Degrees of Freedom	48
	2.2.3 Strain-Displacement Equations	49
	2.2.4 Force-Strain Relationships	51
	2.2.5 Generalized Inertia Matrix	54
2.3	Stiffener Element	55
	2.3.1 Shape Functions	55
	2.3.2 Generalized Displacement Fields and Nodal Degrees of Freedom	56
	2.3.3 Strain-Displacement Equations	58
	2.3.4 Force-Strain Relationships	59
	2.3.5 Generalized Inertia Matrix	64
2.4	Compatibility Between Shell and Stiffener	65

2.5	Multipoint Constraints Algorithm For Delamination	68
2.6	Formulating The General Dynamic Problem	69
2.6.1	Strain Energy of rotating stiffened shell	69
2.6.2	Kinetic Energy of rotating stiffened shell	72
2.6.3	Work done due to external load	76
2.6.4	Governing equation	77
2.7	Imposition Of Boundary Conditions And Solution Procedure	79
2.7.1	Formulating Static Problem	79
2.7.2	Formulating Free Vibration Problem	80
2.7.3	Formulating low velocity Impact Problem	81
Chapter 3	FREE VIBRATION ANALYSIS OF DELAMINATED COMPOSITE PRETWISTED ROTATING CYLINDRICAL STIFFENED SHELLS	
3	3.1 General	84
	3.2 Convergence And Validation	85
	3.3 Free Vibration of a Generalized Delaminated Stiffened Cylindrical Shell	89
	3.3.1 Effect of delamination on un-stiffened shell, stiffened shell and twisted stiffened shell	90
	3.3.2 Effect of delamination along the span of the laminated shell	92
	3.3.3 Effect of delamination along the thickness of the laminated stiffened shell	93
	3.3.4 Effect of stiffener depth to shell thickness	94
	3.3.5 Effect of stacking sequence, angle of twist, and rotation	95
	3.3.6 Mode shapes	98
	3.4 Free Vibration of Long, Intermediate and Short Cylindrical Stiffened Shells	101
	3.4.1 Effects of delamination	102
	3.4.2 Effect of eccentricity of stiffeners	103
	3.4.3 Effect of twist angle and rotation	105
	3.4.4 Effect of number of layers in the laminate	107
	3.4.5 Mode shapes	108
Chapter 4	TRANSIENT RESPONSE OF DELAMINATED COMPOSITE PRETWISTED CYLINDRICAL STIFFENED SHELL SUBJECTED TO LOW VELOCITY IMPACT	
4	4.1 General	113
	4.2 Convergence and validation	114
	4.3 Response of pretwisted delaminated stiffened shell	118
	4.3.1 Effect of stiffener orientation	118
	4.3.2 Effect of delamination across the thickness	120
	4.3.3 Effect of Eccentricity of stiffeners	122
	4.3.4 Effect of stiffener depth to shell thickness ratio	124
	4.3.5 Effect of initial twist	124
	4.3.6 Effect of diameter of impactor	127
	4.4 Response of delaminated stiffened shell under multiple impact	129
	4.4.1 Effect of stiffener	129
	4.4.2 Effect of twist angle	130

	4.4.3	Effect of delamination	131
	4.4.4	Effect of stiffener depth to shell thickness ratio	133
	4.4.5	Effect of delayed impact	134
Chapter 5		CONCLUSIONS	
5	5.1	General	137
	5.2	Conclusions	137
	5.2.1	Free vibration analysis	137
	5.2.2	Transient response due to low velocity impact	139
	5.2.2.1	Impact by single mass	139
	5.2.2.2	Impact by multiple masses	140
	5.3	Contributions of the present work	141
	5.4	Scope of future work	141
		REFERENCES	143
		APPENDIX	165

LIST OF TABLES

Table Number	Caption	Page Number
3.1	Convergence study for non-dimensional fundamental frequencies ($\varpi = \omega_n L^2 \sqrt{\rho / E_{11} h^2}$) of eight layered symmetric cross ply and angle ply stiffened cylindrical shell. ($L / b = 1, b / h = 100, b / R_y = 0.5, b_{st} = 2h$ and $d_{st} = 4h, E_1 = 138.0$ GPa, $E_2 = 8.96$ GPa, $G_{12} = G_{13} = 7.1$ GPa, $G_{23} = 2.84$ GPa, $\nu_{12} = 0.3, n_x = n_y = 1$)	85
3.2	Non-dimensional fundamental frequencies ($\varpi = \omega_n L^2 \sqrt{\rho h / D}$) of an isotropic rotating cantilever plate. ($L / b = 1, h / L = 0.12, D = E h^3 / 12(1 - \nu^2), \nu = 0.3, E$ is the Young's Modulus of Elasticity)	86
3.3	Non-dimensional fundamental frequencies ($\varpi = \omega_n L^2 \sqrt{\rho / E_{11} h^2}$) of three layer $[\theta, -\theta, \theta]$ graphite-epoxy twisted plates. ($L / b = 1, b / h = 20, \text{Twist angle}(\phi) = 30^\circ, E_{11} = 138.70$ GPa, $E_{22} = 8.96$ GPa, $G_{12} = 7.1$ GPa, $\nu_{12} = 0.3$)	86
3.4	Natural frequencies (Hz) of simply supported antisymmetric cross-ply ($0^\circ/90^\circ$) crossed stiffened plate with "eccentric at bottom" stiffeners ($0^\circ/90^\circ$) ($L = b = 254$ mm, $h = 12.7$ mm, $b_{st} = 6.35$ mm, $d_{st} = 25.4$ mm, $E_{11} = 144.8$ GPa, $E_{22} = 9.67$ GPa, $G_{12} = G_{13} = 4.14$ GPa, $G_{23} = 3.45$ GPa, $\nu = 0.3, \rho = 1389.23$ kg/m ³ and $n_x = n_y = 1$, stiffeners are centrally placed)	87
3.5	Natural frequency (Hz) of cantilever cylindrical shell with eccentric orthogonal stiffeners. ($L = b = 0.3048$ m, $R = 2L, h = 3.175$ mm, $\rho = 7800$ kg/m ³ , $E = 209 \times 10^9$ N/m ² , $\nu = 0.30, n_x = 3, n_y = 2$, stiffeners divide the planform of the shell equally)	87
3.6	Fundamental frequencies (Hz) of composite ($[0^\circ/90^\circ]_2$) cylindrical shells for different extents of centrally located mid-surface delamination for simply supported boundary conditions. $E_{11} = 172.5$ GPa, $E_{22} = 6.9$ GPa, $G_{12} = G_{13} = 3.45$ GPa, $G_{23} = 1.38$ GPa, $\rho = 1600$ kg/m ³ , $\nu_{12} = 0.25, L = b = 0.5$ m, $c = d, L / h = 100$, lamination: $(0^\circ/90^\circ)_2$.	88
3.7	Variation of non-dimensional fundamental frequency of delaminated angle ply symmetrical composite ($[\theta / -\theta / \theta / -\theta]_s$) cylindrical stiffened shells for various fibre orientations and twist angles at different rotational speeds. $L / b = 1, b / h = 100, b / R_y = 0.5, a / L = 0.333, d / L = 0.5, h' / h = 0.5, n_x = n_y = 1, b_{st} = 2h, d_{st} = 4h$, eccentric stiffener at bottom.	96
3.8	Effect of stiffener on First four mode shapes of eight layered symmetric angle ply $[45 / -45 / 45 / -45]_s$ cylindrical shell, $n_x = n_y = 1, b_{st} = 2h,$	99

	$d_{st} = 4h$	
3.9	Effect of twist angle and rotation on first four mode shapes of eight-layered symmetric mid-plane delaminated angle ply composite ($[45/-45/45/-45]_s$) stiffened cylindrical shell, $a/L=0.333$, $d/L=0.5$, $n_x = n_y = 1$, $b_{st} = 2h$, $d_{st} = 4h$.	100
3.10	Fundamental frequencies (ω_n) of graphite-epoxy composite (angle-ply $[45/-45/-45/45]$ and cross-ply $[0/90/90/0]$) delaminated cylindrical shells with three different types of stiffeners. $b_{st} = 2h$, $d_{st} = 4h$, $a/L = 0.50$, $d/L = 0.5$, $n_x = n_y = 3$, $\rho = 22,080 \text{ kg/m}^3$.	104
3.11	Non-dimensional fundamental frequency (NDFP) of delaminated four layered angle ply $[45/-45/-45/45]$ stiffened long, intermediate and short shells at rotating state for different twist angles. $b_{st} = 2h$, $d_{st} = 4h$, $a/L = 0.50$, $d/L = 0.5$, $n_x = n_y = 3$.	106
3.12	Effect of rotation and twist angle on first four mode shapes of symmetric delaminated cross-ply $[0/90/90/0]$ un-stiffened and stiffened cylindrical long shell $a/L = 0.333$, $d/L = 0.5$, $n_x = n_y = 1$, $b_{st} = 2h$, $d_{st} = 4h$.	111

LIST OF FIGURES

Figure Number	Caption	Page Number
2.1	Typical cantilevered laminated composite cylindrical stiffened shells in the global Cartesian coordinate system. (a) Untwisted stiffened shell (b) Twisted stiffened shell.	47
2.2	Curved isoparametric shell element with nodes	48
2.3	Fiber orientation of a shell lamina	52
2.4	Three-noded isoparametric stiffener element	55
2.5	Vertical displacement of x-directional stiffener on account of shell rotation.	56
2.6	Stresses in x-directional stiffener cross-section.	60
2.7	Effect of curvature and eccentricity on axial displacement of stiffener.	66
2.8	Shell elements at a delamination crack tip	68
2.9	Rotational and translational offsets of rotating cylindrical shell about local and inertial frames of reference	73
3.1	The influence of relative position of delamination on the first natural frequency of composite $[0^0/0^0/0^0/0^0/0^0/0^0]$ cantilever beam. ($E_1=57.864\text{GPa}$, $E_2=4.2742\text{ GPa}$, $\nu_{12}=0.32$, $G_{12} = G_{13} = G_{23}=1.583\text{ GPa}$, $\rho = 1380\text{ kg/m}^3$, $L=600\text{ mm}$, $b=50\text{ mm}$, $h=25\text{ mm}$, $a=37.5\text{ mm}$, $h'/h=0.5$, Relative position of delamination= d/L)	88
3.2	Effect of fiber orientation on non-dimensional fundamental frequency for crossed stiffened shell without delamination (WD), delaminated stiffened shell(D), undelaminated unstiffened shell (WA) and delaminated unstiffened shell(A). $L/b = 1, b/h = 100, b/R_y = 0.5$, $b_{st} = 2h$ and $d_{st} = 4h$, $\Phi = 0^0$	90
3.3	Effect of percentage of delamination at the mid plane on NDFF of $[45/-45/45/-45]_s$ laminated stiffened shell along the length. $L/b = 1$, $b/h = 100, b/R_y = 0.5$, $b_{st} = 2h$ and $d_{st} = 4h$	91
3.4	Variation of non-dimensional fundamental frequency of symmetric cross ply composite ($[0/90/0/90]_s$) stiffened shell with relative position of delamination along the span(d/L). $L/b = 1, b/h = 100, b/R_y = 0.5$, $b_{st} = 2h$ and $d_{st} = 4h$	92
3.5	Variation of non-dimensional fundamental frequency by varying relative position of delamination across the thickness. $L/b = 1$, $b/h = 100, b/R_y = 0.5$, $b_{st} = 2h$, $d_{st} = 4h$, $a/L = 0.333$, $d/L = 0.5$	93
3.6	Variation of Non-dimensional fundamental frequency with stiffener depth to shell thickness ratio of delaminated stiffened composite($[0/90/0/90]_s$) cylindrical shell, $L/b = 1$, $b/h = 100$, $b/R_y = 0.5$, $b_{st} = 2h$, $a/L = 0.666$, $d/L = 0.5$ $h'/h = 0.5$	95
3.7	Variation of relative frequency with fiber angle orientation. Relative Frequency=Delaminated frequency/undelaminated frequency.	97

3.8	Variation of NDFF with fibre angle orientation at stationary ($\Omega=0.0$) and rotating ($\Omega=0.5$ and 1.0) conditions with one and two stiffener in each directions. $L/b=1$, $b/h=100$, $b/R_y=0.5$, $b_{st}=2h$, $d_{st}=4h$, $a/L=0.333$, $d/L=0.5$, $h'/h=0.5$	98
3.9	Variation of fundamental frequency with relative position of delamination across the thickness of un-stiffened and stiffened composite([0/90/0/90] _s) cylindrical shells at $\Phi=0^0$ and 15^0 , $b_{st}=2h$, $d_{st}=4h$, $a/L=0.50$, $d/L=0.5$, $n_x=n_y=1$, $\rho=22080$ kg/m ³ , LS: Long Shell, IS: Intermediate Shell, SS: Short Shell	103
3.10	Percentage increase in rotating frequencies with respect to twist angles of composite ([45/-45/-45/45]) stiffened shells at $\Omega=0.5$ and $\Omega=1.0$. $b_{st}=2h$, $d_{st}=4h$, $a/L=0.50$, $d/L=0.5$, $n_x=n_y=3$. Note: LS: Long shell, IS: Intermediate shell, SS: Short shell, ET: Eccentric at top, EB: Eccentric at Bottom, CO: Concentric	106
3.11a	Variation of non-dimensional fundamental frequencies with number of layers in undelaminated and delaminated untwisted/twisted stiffened shells Note: CP: Cross-ply without delamination, AP: Angle-ply without delamination, DEL CP: Cross-ply with delamination, DEL AP: Angle-ply with delamination, $n_x=n_y=1$, $b_{st}=2h$, $d_{st}=4h$, $a/L=0.50$, $d/L=0.5$.	109
3.11b	Variation of non-dimensional fundamental frequencies with number of layers in undelaminated and delaminated untwisted/twisted stiffened shells Note: CP: Cross-ply without delamination, AP: Angle-ply without delamination, DEL CP: Cross-ply with delamination, DEL AP: Angle-ply with delamination, $n_x=n_y=1$, $b_{st}=2h$, $d_{st}=4h$, $a/L=0.50$, $d/L=0.5$.	110
3.12	Percentage reduction in fundamental frequency of Long, intermediate and short crossed stiffened (eccentric at top) shell with number of layer due to 50% delamination at different twist angles. Note: CP: Cross ply, AP: Angle ply, $n_x=n_y=1$, $b_{st}=2h$, $d_{st}=4h$, $a/L=0.50$, $d/L=0.5$.	110
4.1	Convergence of transient response with respect to different time steps for cantilevered delaminated composite ([0/90/0/90/0] _s) cylindrical crossed stiffened shell under low velocity impact. $L=0.5$ m, $b=0.3$ m, $h=0.005$ m, $b_{st}=2h$, $d_{st}=4h$, $n_x=n_y=1$, $a/L=0.5$, $d/L=0.5$, $\Phi=30^0$, $v_i=3$ m/s, $E_i=210$ GPa, $r_i=6.35$ mm, $\rho_i=7960$ kg/m ³ , $\nu_i=0.3$.	115
4.2	Contact force and in-plane stress history of a clamped square composite plate, impacted at the center of the plate. $E_1=142.73$ GPa, $E_2=13.79$ GPa, $G_{12}=4.64$ GPa, $\nu_{12}=0.30$, $\rho=1.61 \times 10^3$ kg/m ³ , $L=b=0.14$ m, $h=3.81 \times 10^{-3}$ m, mass of striker = 0.014175 kg, velocity of striker = 22.6 m/s, contact stiffness ($k_C=1 \times 10^8$ N/m ^{1.5})	116
4.3	Impact responses of a cross ply ([0/90/0/90/0] _s) composite plate	117

- impacted centrally by spherical steel ball under simply supported boundary conditions. $L = 20$ cm, $b = 20$ cm, $h = 0.269$ cm, $E_1 = 120$ GPa, $E_2 = 7.9$ GPa, $G_{12} = G_{23} = G_{13} = 5.5$ GPa, $\nu_{12} = 0.30$, $\rho = 1.58 \times 10^{-5}$ N-sec²/cm⁴, $V_i = 300$ cm/sec, $\rho_i = 7.96 \times 10^{-5}$ N-sec²/cm⁴. (a) Contact force history (b) Central deflections.
- 4.4 Contact force and beam displacement histories of a cantilever composite ([0⁰/90⁰/90⁰/0⁰]) beam at locations *A* and *B*. $L = 0.3$ m, $b = 0.01$ m, $h = 0.01$ m, $r_{iA} = r_{iB} = 0.01$ m, $v_{iA} = v_{iB} = 2.0$ m/s, $E_1 = 144.80$ GPa, $E_2 = 9.65$ GPa, $G_{12} = G_{13} = 4.14$ GPa, $G_{23} = 3.45$ GPa, $\nu_{12} = 0.30$, $\rho = 1389.23$ kg/m³. *A* ($L/6, b/2$), *B* ($5L/6, b/2$) 117
- 4.5 Effect of adding stiffener along x- and y-direction on the transient impact responses of the delaminated composite cylindrical shell, $a/L = 0.50$, $d/L = 0.5$, $b_{st} = h$, $d_{st} = 2h$, $d_i = 1.27$ cm, $v_i = 5$ m/s. (a) Time history of contact force; (b) Time history of shell displacement/thickness; (c) Time history of impactor velocity; (d) Time history of impactor displacement; (e) Time history of σ_x ; (f) Time history of σ_y . 119
- 4.6 Dynamic impact response of delaminated composite ([0/90/0/90/0]_s) stiffened cylindrical shell for various position of delamination across the thickness, $n_x = 1$, $a/L = 0.75$, $d/L = 0.5$, $b_{st} = h$, $d_{st} = 2h$, $v_i = 5$ m/s, $d_i = 1.27$ cm. (a) Time history of contact force; (b) Time history of shell displacement/thickness; (c) Time history of impactor velocity; (d) Time history of impactor displacement; (e) Time history of σ_x ; (f) Time history of σ_y . 121
- 4.7 Effects of eccentricity of stiffeners on the transient response of the composite ([0/90/0/90/0]_s) stiffened cylindrical shell, $n_x = n_y = 3$, $d/L = 0.5$, $a/L = 0.5$, $b_{st} = 2h$, $d_{st} = 4h$, $d_i = 1.27$ cm, $v_i = 3$ m/s. (a) Time history of contact force; (b) Time history of shell displacement/thickness; (c) Time history of shell velocity; (d) Time history of impactor displacement; (e) Time history of σ_x ; (f) Time history of σ_y . Note: B: Eccentric bottom, C: Concentric, T: Eccentric top. 123
- 4.8 Effect of stiffener depth to shell thickness ratio on the transient response of the composite ([0/90/0/90/0]_s) stiffened cylindrical shell, $n_x = 1$, $d/L = 0.5$, $a/L = 0.5$, $b_{st} = 2h$, $d_i = 1.27$ cm, $v_i = 3$ m/s. (a) Time history of contact force; (b) Time history of shell displacement/thickness; (c) Time history of impactor velocity; (d) Time history of impactor displacement; (e) Time history of σ_x ; (f) Time history of σ_y . 125
- 4.9 Effect of twist angle on the dynamic impact response of the delaminated composite ([0/90/0]_s) stiffened cylindrical shell, $n_x = 1$, $a/L = 0.75$, $d/L = 0.5$, $b_{st} = h$, $d_{st} = 2h$, $d_i = 1.27$ cm, $v_i = 7$ m/s. (a) Time history of contact force; (b) Time history of shell displacement/thickness; (c) Time history of impactor velocity; (d) Time history of impactor displacement; (e) Time history of σ_x ; (f) Time history of σ_y . 126
- 4.10 Transient impact response of the delaminated twisted composite ([0/90/0]_s) stiffened cylindrical shell for various impactor diameters, $n_x = 1$, $d/L = 0.75$, $a/L = 0.5$, $b_{st} = h$, $d_{st} = 2h$, $\Phi = 30^\circ$, $v_i = 7$ 128

	m/s.(a) Time history of contact force; (b) Time history of shell displacement/thickness; (c) Time history of impactor velocity; (d) Time history of impactor displacement; (e) Time history of σ_x ; (f) Time history of σ_y .	
4.11	Effect of orientation of stiffener on the transient response of the undelaminated untwisted composite stiffened cylindrical shell $v_c=v_f=3$ m/s, $b_{st}=d_{st}=h$.	130
4.12	Effect of twist angle on the transient response of the delaminated composite stiffened cylindrical shell $v_c=v_f=3$ m/s, $n_x=1$, $a/L=0.50$, $d/L=0.5$, $h'/h=0.5$, $b_{st}=d_{st}=h$.	131
4.13	Effect of percentage of delamination on the transient response of the composite stiffened cylindrical shell. $n_x=1$, $v_c=v_f=3$ m/s, $\Phi=30^0$, $d/L=0.5$, $b_{st}=d_{st}=h$.	132
4.14	Effect of stiffener depth to shell thickness ratio on the transient response of the delaminated composite stiffened cylindrical shell $v_c=v_f=5$ m/s, $n_x=1$, $a/L=0.50$, $d/L=0.5$, $h'/h=0.5$, $\Phi=15^0$.	133
4.15	Effect of delay impact on the transient response of the delaminated composite stiffened cylindrical shell. $v_c=v_f=4$ m/s, $n_x=1$, $a/L=0.50$, $d/L=0.5$, $h'/h=0.5$, $\Phi=15^0$, $b_{st}=d_{st}=h$.	134
4.16	The magnified deformation configuration of the mid-plane of the delaminated composite shells with and without stiffener at the times corresponding to their peak value of contact forces. Stiffeners are placed eccentrically at bottom. $a/L=0.50$, $d/L=0.5$, $b_{st}=h$, $d_{st}=2h$, $v_i=5$ m/s	136

Dedicated
to
My Family

CHAPTER 1

INTRODUCTION

1.1 GENERAL

Fibre reinforced polymer (FRP) composites have been introduced into a wide range of industrial applications as found their superior performance over alternative materials. FRP composites are favored in many practical applications because of their high strength to weight ratios, excellent fatigue and corrosion resistance, longer durability, high tailorability and also have greater resistance to environmental degradation. Plates and shells consisting of composite layers with different fibre orientation, possess high specific strength and specific stiffness and are used as structural elements for aircrafts, ships, automobiles, turbomachinery blades, impellers etc. Application of shell structures in mechanical engineering which found in automobile, marine and other industries covers turbine blades, helicopter blades, and impeller of pumps etc.

The engineers have attempted to make the composite shell as thin as practicable so as to reduce the dead weight is reduced and structure function as a membrane, free from large initial bending stresses but not at the cost of its strength. This idea of achieving increased strength-to-weight ratio was led to a step forward by integrating the skin with a row of ribs called as stiffeners. These are so named because the presence of the ribs makes any thin-walled structure such as composite plates /shells stiffer due to the addition of the stiffness of the stiffener itself. Such structures are not purely human innovation. Examples also exist in nature in the form of fish, mushroom, leaf etc. The wide use of stiffened structural elements in engineering has started in the nineteenth century, mainly with the application of steel plates for hull of ships, steel bridges and aircraft structures. The composite stiffened structures are widely used in the engineering applications and have found applications in several fields of modern industry. The stiffeners used in these structures may consist of open or closed sections. The open sections are I, T, Z, L inverted T or rectangular sections and closed sections are box and hat stiffeners. The open sections are less rigid in torsion than the closed ones. Depending on the arrangement of stiffeners with respect to the shell mid surface, it can be classified as concentric or eccentric. The stiffener is concentric, if the centroid of the stiffener cross section coincides with the shell mid-surface and is eccentric, if the stiffener centroid remains above or below the shell midsurface.

Owing to its laminated construction of the stiffened shell, delamination happens to be one of the most feared damage modes in composite structures. Because of its insidious nature, the detection and prediction of delamination presence and growth becomes very difficult for the designers. Delamination tendencies of structures are higher near holes, cracks, free edges, and bonded joints wherein the stress concentration effect are generally higher. Presence of delamination reduces the strength and stiffness of the composite laminates which resulting in reduced service life of the components. Moreover, high rotational speeds in turbomachinery blades results in centrifugal forces of considerable magnitude manifest itself through geometric stiffening, which known as centrifugal stiffening. This could be regarded as problem of initial stresses of the shell element. Existence of initial stresses usually aggravates the delamination damage and hence the study of delaminated shell is of prime concerned. In early 1950's the development of high-speed turbomachineries such as turbines, compressors, fans and blowers search for advanced materials that could resist the high temperature and the associated dynamic stress generated on the turbomachinery components. Failure of the turbine or turbo-compressor blades due to fatigue became a critical issue for researchers especially the turbine blades vibrating near their resonant frequencies. The accurate prediction of the natural frequencies of the turbomachinery blades became a topic of considerable research interest during the design phase itself. Pretwisted open cylindrical shells are special shells where the curvature of the mid-surface along one of the orthogonal direction is absent ($R_x=\infty$) and the pretwist provides for the initial stress-stiffening of the composite structure. Turbomachinery, impeller or fan blades can be idealized as composite cylindrical stiffened shells of low aspect ratio. Owing to the fact that there are numerous fixed and rotating blades in a turbo-machine the accurate point of failure of such a system is extremely complex and hence requires the help of numerical techniques such as finite element method.

The impact load in general results large deflection bending of the blades, generating high local stresses and deformations ensuing complex damage modes in the blades because of heterogeneous and anisotropic behavior of composites. Among these loads, low velocity impact loading due to its high strain rate causes more damage in composite structures than their metallic counterparts. Damage mechanisms typically caused by low velocity impacts in laminates are matrix cracking, fiber fracture and delamination at resin-rich interfaces within the composite structure. Impact damages cause a substantial reduction in the material's compressive strength

and stiffness. Hence, for effective design of the stiffened shell it is very significant to understand the low velocity impact response of the structure. Consequently, the present investigation is concerned with the free vibration and low velocity impact analysis of rotating delaminated pretwisted stiffened cylindrical shell.

1.2 METHODS OF ANALYSIS

The exact analysis of rotating delaminated pretwisted stiffened shells is based on the theory of elasticity. This is rarely performed due to its tedious and difficult computational procedures for evaluation of deflection and stresses of this complex structure. Considering the early modeling of stiffener, three types of models were created to idealize the structure to simpler one for which solution methods were known. In the first category, the elastic properties of stiffeners are distributed uniformly along the orthogonal directions and the stiffened shell is replaced by an equivalent orthotropic shell of constant thickness. The orthotropic shell theory demands equal and close spacing of stiffeners. Also the stiffeners are to be of identical profiles. Moreover, as the shell and the stiffeners are converted into an equivalent shell, the evaluation of stresses in the shell and the stiffeners separately becomes difficult. Further, the evaluation of properties of the equivalent shell becomes a difficult proposition. This restricts the usefulness of the technique.

In the second type of model, the stiffened shell is idealized as grillage, which is a plane structure of intersecting beams and carry lateral load through the action of beam bending. There are basically two drawbacks in this approach. First, the centroidal planes of beams in different directions are assumed to be same, which affect the accuracy of stresses calculated. Secondly, that the beam properties are derived based on effective breadth of plate/shell is an issue, which still remains inconclusive. Further, a part of same plating (effective breadth) is considered to be effective for both the intersecting beams. Therefore, this model has restrictive usage.

The third category of model is more realistic and accurate. Here, the stiffened plate/shell structures are replaced by discrete plate/shell and beam idealization, where the plate/shell and the stiffener are modeled separately maintaining the compatibility at the interface of the two. The plate/shell-beam idealization makes the analysis sufficiently involved and complex, but it gives a better picture of structural behavior. However, the advent of digital computers and parallel development of techniques of structural analysis, have made the analysis of structures simpler

and more accurate. There are a number of numerical methods in which the plate/shell and the stiffeners are treated as separate entities. These are

Finite difference method,

Energy method, such as Rayleigh's method, Rayleigh-Ritz method, Galerkin method, etc,

Dynamic stiffness method,

Finite element method.

Out of these, finite element method is considered to be the most versatile due to its ability to cater to any arbitrary geometry, incorporate complicating effect, ease of formulation and include wide range of elements. Finite element method for stiffened structure has various approaches such as finite strip method, discrete stiffener approach, lumped model approach and arbitrary orientated stiffener approach. Out of these approaches, the arbitrary oriented stiffener approach is considered to be the most flexible model as the stiffener can be placed anywhere within the plate element and need not necessarily be connected at the nodes.

Delamination is the most feared major damage mode as delaminated composite under sustained loading may prompt the delamination layer to buckle under compression, or may prompt delamination crack to grow further. In the present analysis, pre-existing delamination is also included in the composite shell to investigate its effect on free vibration and transient response due to low velocity impact. Virtual crack closure technique is generally used in classical fracture mechanics to model debonding of laminated composites which requires the computation of strain energy release rate at the delamination crack front. But in the present formulation, it is not possible to obtain the strain energy release rate directly, so an adequate algorithm called Multipoint Constraints Algorithm based on shear deformable lamination theory is used along with finite element method to formulate delamination in the shell. The compatibility of deformation and equilibrium of resultant forces and moments are ensured at the delamination crack front. In the model of delaminations in the laminated stiffened shells, the undelaminated region is modeled by a single layer of shell elements, while the delaminated region is modeled by two layers of shell elements whose interface contains the delamination. Based on the multipoint constraint conditions, the formulation of stiffness matrices of the elements at the delamination crack tip is modified accordingly.

In addition to this, rotational speed of the stiffened shell can result in centrifugal forces of considerable magnitude. Because of this rotation, when we apply Lagrange's equation an

additional stiffness term emerges which is generally called the ‘additional stiffness’ or ‘supplementary stiffness’. Effect of the initial stresses is due to the second-order strain components, and, when the displacements are small, manifests itself through ‘geometric stiffness’ or ‘stress-stiffness’ matrix. It is to be noted that the analysis is performed for moderate rotational speeds and the Coriolis component resulting from rotation is neglected as in an earlier study. Sreenivasamurthy and Ramamurthi (1985) reveals that, it has no effect at moderate rotational speed while it becomes prominent at higher rotational speed.

Regarding low velocity impact, local deformation in the contact region is accounted for the investigation in order to accurately predict the contact force history. Impactor mass and stiffened structure can be considered as two solids in contact and the impact problem can be considered as a dynamic problem. However, this approach cannot describe the effect of permanent deformation and local damage in the unloading process. Unloading part of the indentation process can be modeled only using experimentally determined contact laws. A simple relation between the contact force and the indentation has been used by Sun and Chen (1985) to study the impact of laminated plate by spherical impactor employed in this formulation. This contact law includes both loading and unloading phases. During the first loading phase, the contact laws closely follows Hertz’s law of contact while in unloading phase, the contact law is changed and depends upon the maximum contact force and maximum indentation. Both the loading and unloading curves are of two distinct curves. Several types of mathematical models are used to study the impact of structures by foreign objects, which include equivalent spring mass system, energy balance method etc. The equilibrium equations derived from Lagrange’s equation of the stiffened shell panel and the impactor are solved by using Newmark’s time integration technique.

1.3 PRESENT STUDY - ITS RELAVANCE IN RESEARCH

Laminated composite twisted shells find many advanced engineering applications as compressor or turbine blades, flow guide vanes, helicopter blades, aircraft / marine propellers, etc. Delamination or separation of two adjacent plies in laminated composite, which is one of the most common modes of damages, may occur due to manufacturing defects, dynamic loading, impact of foreign objects, etc. Presence of delaminations and their growth during the service life may seriously affect the structural integrity by reducing the strength and stiffness of composite

twisted shells. Hence, the delaminated shell is often stiffened to achieve greater strength with relatively less amount of material and thus satisfy the objective of minimum weight design with economy of the material. Moreover, delamination and stiffener in the structure may result in a change in dynamic characteristics. Therefore, it is very much important to know the natural frequencies of the stiffened panel accurately with delamination.

It is evident that recent research has focused on the dynamic analysis of damaged structures. In the present study, an attempt has been made to investigate the response of the damaged cylindrical shell with stiffener. Though the response of stiffened shell structures has received some attention from the researches, but damaged structures with stiffener is unexpressed.

1.4 REMARKS

The present literature in the field of shell research indicates that study of rotating composite pretwisted stiffened shell with or without delamination is of recent problem. It is worth mentioning that laminated composite stiffened shells, delamination in shells and rotating pretwisted shells need a comprehensive investigation to realize the full potentialities of the structures.

A thorough review of earlier literature in this field explores the scope of further research. The review of the existing literature along with the gap is presented in the next section.

1.5 LITERATURE REVIEW

Research, design and construction of shell structures with or without stiffeners have a long history and the literature that has accumulated in this area is vast. Shell structures have been used in different places of which, the use of these forms as turbomachinery blades is of the present interest. In this chapter, a historical review of shell structures is presented. Section 1.5.1 gives a picture of the course of development of studies on composite shell structures, starting with plate and shell theories to its application in tubromachinery blades. Section 1.5.2 to 1.5.11 present the detail review of the studies on the dynamic response of delaminated twisted composite stiffened shell, so as to find out the actual scope and objective of the present study in these areas. Finally, based on the earlier contributions of the researchers, the possible research gaps in this field are identified and objectives of the work are defined.

1.5.1 Plate and shell theories

An elastic shell is a body made of elastic substance whose one dimension (especially in the thickness direction) is extremely small compared to the other dimensions. The behavior of an elastic shell under the influence of an external load is governed by the three dimensional theory of elasticity. A boundary and/or initial value problem is solved in this theory to understand how the shell behaves under the given loading conditions. However the boundary or initial value problems are extremely difficult to be solved directly even in the simplest cases and hence various approximation techniques like the finite element method, finite difference method, perturbation method or the calculus of variations have been adopted for obtaining approximate solutions of such problems in most practical scenarios.

Classical laminated plate theory (CLPT) has been widely used as the basis of the analysis and design in structural laminates though it possesses some serious deficiencies like assumption of plane stress state in the constitutive relations and elimination of shear deformation as per the Kirchoff's hypothesis (normal sections remains normal). Classical laminated plate theory, which is primarily an extension of the Kirchoff's thin plate bending theory which neglects the transverse shear deformation and transverse normal strain effect was analyzed in by Ashton and Whitney (1970). This theory was later elaborated for very thin laminates by Jones (1975) and Tsai (1988). Longitudinal modulus of advanced carbon/graphite fiber reinforced composites is much higher in comparison to their transverse shear modulus. This significant material anisotropy may cause an appreciable amount of transverse shear deformation and warping in the case of moderately thick to thick laminated composite plates. It must therefore be first ensured that the transverse shear deformation must be accounted effectively in order to ensure accurate determination of interlaminar shear stresses. Yang, Norris and Stavsky (YNS) theory (1966) which is an extension of the Mindlin's two-dimensional theory (1951) was the first one to account for the transverse shear deformation in symmetrically laminated aeolotropic, orthotropic and isotropic plates. They showed that the effect of transverse shear deformations is always significant in the dynamic theory of heterogeneous plates.

The credibility and limitations of the classical plate theory were later analyzed by Pagano (1969, 1970a) who formulated the three-dimensional linear elasticity solutions for the static bending of bidirectional composite laminates. It was found that the conventional plate theory leads to a very poor description of laminate response at low span-to-depth ratios, but converges

to the exact solution as this ratio increases. These exact solutions along with the extended works of Pagano (1970b) on the effect of shear coupling established the range of validity of the classical laminated plate theory. It was concluded that the stresses generally converge more rapidly to the exact solution than plate deflection using classical plate theory while incorporating shear deformation can substantially reproduce the deflections predicted by elasticity theory in most cases. Whitney and Pagano (1970) analyzed the YNS theory in details by employing transverse shear stress coefficient and showed better agreement with exact solutions. Pagano and Hatfield (1972) further considered the response of multi-ply laminates and showed that a conservative estimate of the magnitude of the error obtained in CLPT compared to exact solutions could be achieved for laminates consisting of only several layers. Whitney (1972) addressed the concern that the bending moments and stresses may either converge towards a wrong solution or may not converge at all due to the existence of cross-elasticity bending stiffness terms in homogeneous or symmetrically laminated anisotropic plates, by using a classical Fourier analysis that satisfied both the geometric and natural boundary conditions.

Reddy (1984) developed a higher-order shear deformation theory for laminated composite plates having the same dependent unknowns as in the first-order shear deformation theory of Whitney and Pagano (1970) and also accounted for the parabolic distribution of the transverse shear strains through the thickness of the plate. The theory reveals the deflections and stresses more accurately compared to the first-order theory. Later, Phan and Reddy (1985) developed a higher-order shear deformation theory that accounted for parabolic distribution of the transverse shear stresses, but required no shear correction coefficients. A displacement finite element model of the theory is developed and used to analyze laminated anisotropic composite plates for deflections, stresses, natural frequencies and buckling loads. Murthy (1981) presented an improved transverse shear deformation theory for laminated anisotropic plates under bending and eliminates the need for an arbitrarily chosen shear correction factor. Lu and Liu (1992) developed a theory that accounted for the interlaminar shear stress continuity and transverse shear deformation. Lee and Chen (1996) developed a generalized laminate theory which incorporated both single-layer and multiple-layer approaches for computation of interlaminar shear stresses. This layer reduction technique is computationally efficient and retains the accuracy of the predicted stress within $\pm 8\%$.

Whitney (1969) obtained closed form solutions for off-axis symmetric laminates and showed that transverse shear deformation could significantly affect the plate response in case of highly anisotropic laminates. Sun and Whitney (1973) investigated the effect of heterogeneous shear deformation over the thickness of the plate on the dynamic behavior of laminates. It was found that local shear deformation depended highly on the transverse shear rigidities of the constituent layers. Sciuva (1986) formulated a displacement field incorporating transverse shear deformation, in-plane and rotary inertia effect in predicting deflection, natural frequencies and buckling loads for thick-multi layered orthotropic plates. The new displacement model satisfies the contact conditions at the interfaces. A review on the first-order shear deformation theories for multi-layered composite plates based on linear displacement assumptions in the thickness direction was made by Noor and Burton (1989).

Bert and Malik (1996) reviewed the application of differential quadrature method (A numerical solution technique for initial and or boundary problems in computational mechanics) in comparison to conventional numerical solution techniques such as the finite difference and finite element methods. Malik and Bert (1995,1996, 1996) presented a quantitative assessment of the relative effect of shear deformation and rotary inertia on the free vibration of symmetric cross-ply laminated plates. Eigenvalue equations for the problem were derived from the governing differential equations using the differential quadrature method (DQM). Differences in the frequencies based on shear deformation only and those based on shear deformation with rotatory inertia were found to be less than 1 per cent. Craig and Dawe (1986) predicted that the scale of the influence of transverse shear, and of rotary inertia increases with increase in the ratio of plate thickness and an increase in the transverse shear flexibility of the plate. Classical plate theory was found to often give unacceptable errors except for lowest modes of vibration of very thin plates.

Sun and Whitney (1976) studied the dynamic behavior of symmetrically laminated composite plates under initial stress including the effect of transverse shear deformation. Numerical results depicted that the influence of initial in-plane tensile stress resultant was considerable in comparison to the static solution. Yang and Shieh (1987) studied the vibration behavior of antisymmetric cross ply laminates using virtual work theorem and included the effect of transverse shear deformation and rotary inertia. In 1990, Professor J.N. Reddy revised a variety of the current third-order plate theories (Reddy, 1990). Differences and similarities

between such theories were pointed to identify the actual contributions. After compiling all of these third-order theories, Reddy proposed a general, consistent-strain plate theory from which any of the reviewed theories can be derived. He also accounted for nonlinear strains by using von Kármán's assumptions.

Finally, the question of which plate or shell theory presents the best results, especially in intricate cases such as those of laminated stiffened structures, remains open. As more and more references are seen, it is possible to say that a linear plate theory can give better results than a sophisticated non-linear one, if it is better solved, numerically and/or physically. This means that numerical errors will be minimized, or the solution will not neglect the relevance of physical behaviors and dimensions of the problem. Therefore, the first-order shear deformation theory of plate/shell is used to solve the current problem using mainly the FEM.

1.5.2 Turbomachinery blades

Dynamic behavior of rotating turbomachinery blades with a pretwist has been a field where extensive research works have been conducted. Rao (1973, 1977, 1980, 1983) carried out an exhaustive survey of turbomachinery blades including important aspects of blade vibrations like estimation of the natural frequencies, blade excitation forces, effect of blade aspect ratios, blade geometry, resonant vibrations in addition to the analytical and experimental determination of these aspects.

1.5.3 Pretwisted plates & shells

Vibration analysis of turbomachinery blades has traditionally been carried out by means of beam theory. One can find literally hundreds of references in the literature incorporating considerations such as coupling between bending and torsion, taper, shear deformation, rotary inertia, pretwist and rotational effect into one-dimensional beam vibration analyses. However, beam analysis becomes inadequate for low aspect ratio blades. Most obviously, vibration modes which involve predominantly chordwise bending are completely missed. These modes become more important as blade thicknesses and aspect ratios decrease. Furthermore, another important question arises. Even for those modes obtainable from beam analysis (i.e., spanwise bending and torsion), accuracy of beam theory is a major concern. In 1980s two-dimensional methods of blade vibration analysis have been developed. As seen from Leissa (1980), most of these utilize finite elements and tend to require considerable computation time. However, the chordwise bending effect are accounted for and, with properly conformable finite elements, accurate results

are obtainable if sufficient elements are employed. Carnegie (1959a, 1959b, 1964) studied the vibrations of pre-twisted cantilever blades pre-twisted linearly about the centroid of its cross-section up to an angle of $\pi/2$ radian and assumed to be mounted encastre at the root.

Achenbach et al. (1968) studied the vibrations of a laminated body employing the governing equations and boundary conditions to study the thickness-twist motion of a laminated layer. Whitney and Leissa (1969) obtained the closed form solutions to the linearized equations for heterogeneous anisotropic plates where the coupling between bending and stretching is unavoidable. The governing equations of the laminated anisotropic plate were formulated using the basic assumptions of thin-plate theory, including nonlinear terms in the von Karman sense. Dokainish and Rawtani (1969a, 1969b, 1971) carried out vibration analysis of a cantilever plate mounted on the periphery of a rotating disc using the finite element method wherein the distributed centrifugal force is resolved into two components: one acting in the plane of the plate and the other normal to the plate. Macbain (1975) studied the effect of varying tip twist and increasing centrifugal loading on the resonant characteristics of a cantilevered plate using numerical and experimental methods. Later on, Kirkhope and Wilson (1976) studied the coupled vibration modes of a rotating blade-disc system using finite element method. Rao and Banerjee (1977) calculated the natural frequencies of a cantilever blade with an asymmetric cross-section mounted on a rotating disc using a polynomial frequency equation method. Crawley (1979) determined the natural frequencies and mode shapes of a number of Graphite/Epoxy plates and shells while Crawley and Dugundji (1980) developed a method for estimating the natural frequencies of composite cantilever plates and for non-dimensionalizing the frequency data. Leissa (1980, 1981) studied the vibrational aspects of turbomachinery blades by shell analysis. Vibration characteristic of rotating pretwisted cantilever plates was studied by Sreenwasamurthy and Ramamurti (1980, 1981). Ravn-Jensen (1982) studied the free vibrations of turbine blades numerically using a general shell theory taking into account the centrifugal forces. Ramamurti and Kielb (1984) determined the natural frequencies of twisted rotating plates. Kielb et al. (1985) compared the results related to the vibration of twisted cantilever plates. Rao and Gupta (1987) studied the free vibration characteristics of a rotating pretwisted small aspect ratio blade, mounted on a disc at a stagger angle, using classical bending theory of thin shells. Qatu and Leissa (1991a, 1991b) presented the first known natural frequencies and mode shapes of laminated composite twisted cantilever plates using the Ritz's method.

Navi and Ganesan(1996) compared the free vibration results of pretwisted composite blades using beam and plate theories and reported that for the accurate prediction of natural frequencies of metal matrix composite twisted blades one could use plate elements. Lim et al. (1997) presented the free vibration results of pretwisted composite conical shell incorporating the effect of pretwist based on Ritz extremum energy method. Karmakar and Sinha (2001) examined the first ply failure load based on the tensor polynomial failure criterion of rotating pretwisted blade employing finite element method. Chandiramani et al. (2003) carried out the free and forced vibration of a rotating, pretwisted laminated composite blade using beam theory wherein the structural model includes transverse shear flexibility, restrained warping and centrifugal and Coriolis effect. Kee and Kim (2004) carried out the vibration analysis of initially twisted rotating thick cylindrical shell including the effect of centrifugal force and Coriolis acceleration. Their investigation was based on the concept of the degenerated shell element with the Reissner–Mindlin’s assumptions while the governing equations were solved by FEM. Sinha and Turner (2011) studied the natural frequencies of a typical turbo-machinery cantilevered airfoil blade by considering it as a plate of an equivalent rectangular cross-section subjected to a quasi-static load due to centrifugal force field. Asha and Sahoo (2011) carried out vibration, buckling and parametric instability characteristics of general laminated cross-ply pre-twisted cantilever flat and curved panels wherein the linear part of the strain was used to derive the elastic stiffness matrix and the non-linear part of the strain was used to derive the geometric stiffness matrix. Dey and Karmakar (2012) studied the free vibration response of delaminated pretwisted rotating conical shell neglecting Coriolis component for moderate rotational speed using FEM. Carrera et al. (2013) used a self unified formulation to study the free vibration of rotating composite blade. They used finite element method to solve the governing equations derived in a weak form by means of Hamilton’s principle. Cao et al.(2017) investigated a pretwisted rotating cantilever sandwich-plate model with thermal barrier coating (TBC) layers wherein the classic von Karman plate theory and the first-order shear deformation theory were applied to derive the energy equations of the rotating TBC blade.

1.5.4 Composite stiffened structure

While many researchers were simplified and improved the theory of shell structures with isotropic and laminated composite materials from time to time, a group of investigators started working on stiffened shells due to their superior performance under different load conditions and

cost effectiveness, and have wide applications in varieties of structures, such as aircraft, ships, automobile, turbomachinery applications, etc. There were two main types of analysis in the considerable literature on this subject depending upon whether the stiffening rings were treated by averaging their properties over the surface of the shell or by considering these as discrete element. The first method was particularly applicable to geometry having a large number of closely and equally spaced rings. On the other hand, second method could be more general as it could accommodate any distribution of the stiffeners and present a clear picture of the behavior of the structures. Earlier, the usual method of analyzing the structure was to treat as an orthotropic continuum with effective extensional and flexural stiffness by considering the stiffeners to be closely spaced and to average the stiffening effect over the surface of the shell as was done by Miller(1957) and Hoppmann II (1958). Weingarten (1965) predicted the natural frequencies of the ring stiffened simply supported conical shells by finding the equivalent orthotropic shell in which Galerkin method was adopted for the solution. The free flexural vibration of cylindrical shells stiffened by equidistant frame was investigated by Wah(1966) using finite difference method. Egle and Sewall (1968) studied the vibration of orthogonally stiffened cylindrical shells with stiffeners treated as discrete elements. McDonald (1970) reported the vibration of rib-stiffened freely supported cylindrical shells by solving the coupled equations of motion of the shell and stiffener directly, neglecting the shell in-plane and rotary inertia. Wang and Rinehart (1974) performed an exact analysis of longitudinal stiffened cylindrical shells with any edge supporting conditions. After arrival of digital computers and parallel development of the techniques of structural analysis like finite difference, finite element, boundary element, energy methods, etc. made the analysis of structures simpler and more accurate. Out of these, the finite element method was considered to be the most versatile due to its ability to cater to any arbitrary geometry, incorporate complicating effect, ease of formulation and include wide range of elements. As a result, the research on stiffened shells got a new dimension.

From the present discussion, it is evident that the primary attention of research on stiffened shell structures gradually shifted from one aspect to another in the course of time. Presently, the attention of some researchers is mostly on laminated stiffened shells based on finite element method. Therefore, the detailed study of earlier investigations on the composite stiffened shells are summarized and presented in the following with four headings viz. bending

analysis, free vibration analysis, transient analysis and other aspects to identify the inherent lacunae and gap of research.

1.5.5 Bending behavior of stiffened plate/shell

Venkatesh and Rao(1983) introduced a finite element analysis of laminated shallow shells reinforced with laminated stiffeners using a rectangular laminated anisotropic shallow thin finite element with 48 d.o.f conjunction with a laminated anisotropic curved beam and shell stiffening finite element having 16 d.o.f.. Compatibility between shell and stiffener was maintained all along their junction line. Further, a finite element analysis of laminated shells of revolution reinforced with laminated stiffeners was reported by the same author (Venkatesh and Rao, 1985) employing doubly curved quadrilateral laminated anisotropic shells of revolution finite element with 48 d.o.f. and two stiffener elements with 16 d.o.f. namely; (i) a laminated anisotropic parallel circle stiffener element (PCSE); (ii) a laminated anisotropic meridional stiffener element (MSE). However, the above two analyses made by Venkatesh and Rao(1983, 1985) were based on classical thin shell and beam theory and thus, transverse shear deformation was neglected.

Liao and Reddy (1990) presented a continuum based, two-dimensional degenerated shell element with a compatible degenerated beam element for stiffeners to study the geometric non-linear analysis of laminated, anisotropic stiffened shells. Chattopadhyay et al.(1993) studied the effect of the number of layers on the flexural response of the blade stiffened plates, where stiffeners can be placed anywhere and in any orientation within the plate element, and need not follow nodal lines and the formulation is based on finite element method. Goswami and Mukhopadhyay (1994) reported the static analysis of composite stiffened shells with the help of two different elements- the nine noded Lagrangian isoparametric element and Heterosis element. In the formulation, the stiffeners need not be placed along the nodal lines as it could take care of the placement of the stiffener anywhere within the shell element. Biswal and Ghosh (1994) investigated the flexural response of stiffened laminated plates wherein a standard four-noded rectangular element with seven degrees of freedom at each node was considered for the laminated plate and the stiffness of the stiffener was reflected at all four nodes of the plate element where the stiffeners were placed. The finite element formulation uses a higher order displacement function. Mukherjee et al.(1994) developed a higher order theory to study the

displacement and stress of the stiffened plate wherein a special smoothing technique was employed to evaluate the stresses at the nodal points of the stiffed plate.

Kolli and Chandrashekhara(1996) presented a model of composite stiffened plate to study the bending of angle ply and cross ply stiffened plate under different loading and boundary conditions based on first-order shear deformation theory. Stiffeners were modeled as laminated beams and placed along the nodal lines. Effect of the depth, number, and location of stiffeners were also examined. Sadek and Tawfik (2000) presented a model based on a higher order shear deformation theory wherein a realistic cross-sectional deformation pattern was assumed. Non-linear variations of longitudinal displacements through the thickness were included in the model. Thus the use shear correction coefficient was eliminated and the model was applicable for both moderately thick and thin stiffened composite plates. The model was developed using a nine-noded plate element with seven degrees of freedom at each node and a three-noded stiffener element with four degrees of freedom at each node. Static analyses on the isotropic and composite stiffened plates under different loading condition were reported. Effect of eccentricity of the stiffener and the stacking sequence of both plate and stiffener were also examined.

Prusty(2003) used the finite element method to investigate the static behavior of the stiffened shell using different types of stiffener such as open and closed section stiffeners. This formulation is based on concept of equal displacements at the shell–stiffener interface. Formulation of the shell was made by eight-noded isoparametric quadratic element, which has been derived on the basis of Mindlin-Reissner's theory and satisfying C^0 continuity for the interpolation functions, where stiffener was modeled as a three-noded curved beam element. Nath et al. (2007) presented an analytical solution of the elastic field of a deep stiffened cantilever beam of orthotropic composite material subjected to a parabolic shear loading at the free lateral end and the two opposing longitudinal edges were stiffened. Numerical Solutions obtained in the form of infinite series and the distribution of different stresses and displacement components were reported. Ojeda et al. (2007) reported a new approach for the large deflection analysis of isotropic and composite stiffened plates considering eight node isoparametric plate elements combined with three node beam elements wherein the concept of equal displacements at the plate–stiffener interface were adopted. Non-linear equilibrium equations were derived using the principle of virtual work applied to a continuum with a total Lagrangian description of motion. In addition to this Newton–Raphson incremental iterative solution technique was used to

obtain the non-linear response path. Nath and Ahmed (2009) investigated elastic behavior of stiffened struts of orthotropic composite material under an eccentric loading using displacement potential formulation. The authors presented the solutions of stresses and displacements of boron/epoxy composite struts wherein the effect of material orthotropy and different stiffeners on the elastic field were also investigated.

Bhar et al. (2010) presented the significance of using higher order theory over first-order shear deformation theory of laminated composite stiffened plate employing finite element method. The authors used Taylor series expansion to derive the spatial displacement fields of both the plate and the stiffener as functions of reference plane variables. Think and Quoc (2010) investigated the bending failure of laminated stiffened glass fiber/polyester composite plates with laminated open section (rectangular or T-shaped) and closed section (hat shaped) of stiffeners employing finite element method wherein a 9-noded isoparametric element with 9 degrees of freedom per node was combined with a 3-noded isoparametric beam element with 5 degrees of freedom per node to model the stiffened panel. Li et al.(2010) proposed , a finite element model based on the higher-order global–local theory to study the flexural behavior of stiffened laminated plates wherein the stiffeners were treated as a part of the laminated plate to ensure the compatibility of displacements and stresses between plate and stiffener and distributions of the displacements and stresses through the thickness of laminates were presented.

Bhaskar and Pydah (2014) investigated the static deflection of blade stiffened plate employing three dimensional models for plate and two dimensional plane stress model for stiffener with simply supported boundary conditions. Ahmed and Modak (2015) developed a finite-difference computational scheme wherein a new displacement potential was introduced to model the problem of laminated composites and obtained strain and stresses at different plies of the laminated cantilever. They investigated the elastic field of a laminated cantilever beam under the influence of symmetric and anti-symmetric arrangements of discrete stiffeners. Pydah and Bhaskar (2015) presented an analytical approach for simply supported blade-stiffened rectangular plates. Here, plane stress idealization was used to model the kinematics of transverse bending of the stiffener while simple one-dimensional classical models were employed for lateral bending and torsion. Nguyen-Thoi et al. (2017) reported a cell-based smoothed discrete shear gap method (CS-FEM-DSG3) using three-node triangular element for static analysis of stiffened

Mindlin plates wherein the compatibility of displacement field of stiffeners and shell was applied at the contact positions.

It is observed from the above discussion that most of the researchers developed their finite element models or other type of models and verified their efficiencies in the flexural bending analysis of composite stiffened shells. Further, several aspects of bending analysis of composite stiffened shells are yet to be taken up such as effect of delamination or debonding between skin and stiffener on the bending response of the twisted panel.

1.5.6 Free vibration behavior of stiffened plate/shell

Chao et al.(1980) studied the natural frequencies of rectangular laminated plates reinforced by stiffeners based on the solution of equation of motion of the plate segments, stiffeners and related displacement compatibilities. Stiffener-plate coupling was based on the equivalent orthotropic idealization. The shear lag effect was neglected and the extensional displacements in the laminate are assumed uniform. Bhimaraddi et al.(1989) considered a shear deformable shell of revolution element and a shear deformable curved beam element based on the higher-order theories to model the shell and the stiffener. Further, finite element method was used to find the frequency response of the orthogonally stiffened shell. The limitation of this element was that it could only handle the shells of revolution.

Chattopadhyay et al.(1992) reported the free vibration of eccentrically stiffened shell employing finite element method considering an isoparametric quadratic plate bending element wherein the properties of the stiffener element found at the Gaussian integration points in a direction tangential to the stiffener which results in a skew axes system and the strains were transformed from this system to the global axes system. Lee and Lee (1995) presented the vibration response of anisotropic plates with eccentric stiffeners based on finite element method wherein the stiffeners were modeled based on Timoshenko beam theory and used nine-noded quadrilateral elements for the skin plate and three-noded quadratic elements for the stiffener.

Ghosh and Biswal(1996) used a realistic cross-sectional deformation pattern, which eliminates the use of shear correction coefficients to study the free vibration response of stiffened laminated plates on the basis of higher order shear deformation theory. The finite element results were experimentally verified wherein a four-noded rectangular element with seven degrees of freedom at each node was used for the discretization of the stiffened plate. Stiffness of the stiffener element was counted at all four nodes of the plate element. Chandrashekhara et

al.(1997) presented the results of free vibration characteristics of laminated plates with discrete stiffeners considering the same model (Kolli and Chandrashekhara, 1996) by finite element method wherein the inertia effect due to in plane, flexural and rotary motions of the plate and stiffeners were included and effect of ply orientation and boundary conditions on vibration response of the stiffened plate were investigated. Kumar and Mukhopadhyay(2000) developed a new element, which was the combination of Allman's plane stress triangular element and the Discrete Kirchhoff-Mindlin triangular plate bending element to investigate the static and free vibration response of laminated plates stiffened with blade and parallel stiffeners based on first-order shear deformation theory. They used the same shape functions for both plate and stiffener to ensure the displacement compatibility. This element can adjust numerically to both thin and thick plate without any problem of shear lock.

Guo et al. (2002) presented the layered (zigzag) finite element method based on the first order shear deformation theory to investigate free vibration analysis of stiffened laminated composite plates wherein the laminated plate was modeled using nine-noded isoparametric degenerated flat shell element and the stiffeners as three-noded isoparametric beam elements based on Timoshenko beam theory where bilinear inplane displacement constraints is used to maintain the inter-layer continuity. Prusty and Ray (2004) used eight-noded isoparametric quadratic shell element and a three-noded curved beam element having the same displacement functions as that of the shell for modeling the shell and the stiffener, respectively. Free vibration characteristics of pannel was analyzed for both open and closed type stiffeners, which includes rectangular, L, T and I shaped stiffeners. A spline fine strip method for prediction of the natural frequencies, buckling stresses and modes of stiffened sandwich plates was reported by Yuan and Dawe (2004),wherein the formulation was established on the basis of a three-layer, third-order plate theory for the main sandwich plate, and an equivalent-single-layer plate theory for the compact stiffeners. The structure was modeled in the contexts of both first-order shear deformation plate theory and classical plate theory. Solution procedure was adopted based on the superstrip concept. Nayak and Bandyopadhyay (2005) made use of hyperbolic paraboloid, hyper, and conoidal shell forms to study the free vibration response of the laminated composite anticlastic doubly curved stiffened shells. In their investigation, a nine-noded isoparametric doubly curved thin shallow shell element and a three-noded isoparametric curved shallow beam elements were combined to model the stiffened structure. The effect of stiffness and mass of the

stiffener were lumped at the nodes of the shell using appropriate transformations for eccentricity, curvature and position of stiffener based on Sanders' first-approximation theory of thin shells. They presented the effect of stacking sequence, number of stiffeners, and orientations of stiffeners, stiffener depth to shell thickness ratio for different type of shell forms on the fundamental frequency.

Free vibration characteristics of stiffened laminated plate was studied by Qing et al. (2006) on the basis of the state-vector equation theory, where the plate and stiffeners were considered as two and three-dimensional elastic bodies. Effect of transverse shear deformation and the rotary inertia were included in the model, and the thickness of plate and the height of stiffeners had no restriction. Compatibility of displacements and stresses on the interface between the plate and the stiffeners were ensured through uniting the algebraic equation of the plate and the stiffeners. Sahoo and Chakravorty (2006) investigated the free vibration response of stiffened composite shell roofs using eight noded shell element and three noded beam element for the structure based on finite element method. They presented the distinctiveness of the response by varying the number and depth of stiffeners, laminations and boundary conditions. Effect of different stiffener arrangements on fundamental frequency were also presented by the authors. Prusty (2008) used the same formulation (Prusty and Ray, 2004) to investigate the free vibration and buckling behavior of the stiffened shell using different types of stiffener such as open and closed section stiffeners and reported the comparison between the two types of stiffeners. Torkamani et al. (2009) investigated the free vibration of orthogonally stiffened cylindrical shells employing the similitude theory wherein Donnell-type nonlinear strain-displacement relations along with the smearing theory were used to model the structure. Bhar et al. (2010) reported the significance of using higher order shear deformation theory (HSST) over the first order shear deformation theory (FSDT) based finite element method. The spatial displacement fields of both the plate and the stiffener were derived as functions of reference plane variables using Taylor series expansion. Both static and free vibration results of the stiffened plate using both HSST and FSDT were reported and compared. Thinh and Quoc (2010) used 9-noded isoparametric element with 9 degrees of freedom per node and a 3-noded isoparametric beam element with 5 degrees of freedom per node for finite element modeling of the plate and the stiffener, respectively to study bending failure and free vibration of the stiffened

plate. In addition to this, Dewebok device and DasyLab 7.0 software were used for obtaining the experimental results of the stiffened plates and compared with the computational results.

Li et al. (2013) proposed a layerwise/solid-element (LW/SE) method, which was established, based on the layerwise theory and the finite element method (FEM) to obtain the static and free vibration response. The layerwise theory was used to model the composite cylindrical shell and the eight-noded solid element was employed for discrete the stiffeners. Displacements coordination was used to ensure the compatibility of displacements at the interface between shells and stiffeners. Bhaskar and Pydah (2014) presented the analytical elasticity solution for static and free vibration of blade stiffened plates wherein the plate was modeled as 3D solid and the stiffener as plane stress problem, so that non-classical effect such as transverse shear deformation and rotary inertia were automatically accounted for any types of boundary conditions. Pydah and Bhaskar (2015) reported an analytical model based on the elasticity approach to investigate the statics and dynamics of simply supported plates stiffened by multiple blade stiffeners. Influence of the non-classical effect of transverse shear deformation, thickness stretch and rotary inertia in the analysis of stiffened plates were investigated. Sahoo (2015) presented the natural frequency and mode shapes of laminated composite stiffened elliptic parabolic shell employing finite element method wherein and eight noded shell element was combined with a three noded beam element. The author included the modeling of cutout in the stiffened panel and reported the effect of cutout size and position on the natural frequency of the stiffened panel.

Tuan et al. (2016) reported the frequency response of the laminated stiffened cylindrical shell based on finite element method wherein both the shell and the stiffener were modeled employing eight-noded isoparametric degenerated shell element. Zhao and Kapania (2016) developed an efficient finite element method to study vibration mode results of a curvilinear stiffened composite panel subjected to in-plane axial and shear loads. Displacement compatibility conditions were imposed at the panel-stiffener interfaces. They examined influence of the stiffener geometric curvature and placement, the stiffener depth ratio and that of the in-plane load factor on the panel vibrational responses. Castro and Donadon (2017) presented a semi-analytical approach to carry out the numerical investigation on the effect of skin-stiffener bonding flaw size on the vibration and linear buckling behavior of T stiffened composite panels wherein the penalty-based approach was used to assemble the domains and to model the

debonded region between the stiffener flange base and the plate. Compatibility of displacement and rotation between stiffener and panel was guaranteed. Damnjanovic' et al. (2017) reported the free vibration of stiffened plate based on FSDT and HSDT employing dynamic stiffness method. Dynamic stiffness matrices for transverse vibration of laminated composite plate based on the HSDT and FSDT previously derived by authors were coupled with the dynamic stiffness matrix of laminated composite plate undergoing in-plane vibration. Fang et al.(2017) reported an analytical and more cost-effective method to study the free vibration of a finite ring-stiffened elliptic cylindrical shell. Stiffeners were simulated by smearing technique wherein the effects of the stiffeners were averaged over the shell surface. Vibration equations of the elliptic cylindrical shell were derived based on Flugge shell theory. Nguyen-Thoi et al. (2017) presented a cell-based smoothed discrete shear gap method (CS-FEM-DSG3) using three-noded triangular element to carry out static, free vibration and buckling analyses of stiffened Mindlin plates by combining the original plate element CS-FEM-DSG3 with Allman's plane stress element and a linearly isotropic two-node stiffened beam element. Sheng and Wang (2018) developed a theoretical model to study the dynamic stability and nonlinear vibrations of the stiffened functionally graded (FG) cylindrical shell in thermal environment, wherein Von Kármán nonlinear theory, first-order shear deformation theory, smearing stiffener approach and Bolotin method were used to model stiffened FG cylindrical shells. Galerkin method and modal analysis technique were used to obtain the discrete nonlinear ordinary differential equations.

It is evident from the above that most of the researchers studied the free vibration aspects of composite stiffened shells without delamination, pretwist and rotation. Free vibration analysis of stiffened structure especially in the field of turbomachinery blades is yet to receive its due attention.

1.5.7 Transient response under low velocity impact

1.5.7.1 Composite plates and shells:

Advantages of these composites structures discussed before, however, are overshadowed by their relatively poor resistance to the impact loadings, which has prevented the application of these materials to many applications such as turbine fan blade and many more. Many other reports dealing with the responses of advanced composites to various type of impact have further increased the need for a better understanding of the problem so that the survivability of these composites can be improved. Low-velocity impact problems refers to the situations where, the

entire structure deforms as the elastic waves during the contact duration and propagates to the boundary and finally are reflected back several times. Failure modes of composite structures under low-velocity impact are quite different from those of the metallic structures where the damage starts from the surface and can be detected by routine visual inspection.

Goldsmith (1960) examined the vibrational aspects of impact, contact phenomenon involved in the impact of elastic solids and the results of impact experiments. Moon (1972, 1973) studied the stress waves due to impact on anisotropic plates and composite plates using a Mindlin's plate theory. It was shown that both extensional and bending waves were generated due to transverse impact. The Mindlin's plate theory was used to perform stress wave calculations in composite plates. This model was valid as long as the scale of the changes in stress levels (e.g., wavelength) was much longer than the sizes of the composite constituents (e.g., fiber diameter, ply-spacing's etc). Sun (1973) studied the shock fronts in laminated plates subjected to impact loading employing the ray theory. Kinematic conditions of compatibility and dynamic conditions on the wave front were also derived. Sun and Lai (1974) proposed that when a plate is subjected to an impulsive load, the reflections of waves from the top and bottom surfaces cannot be accounted for by the plate theories and investigated the transient waves set up in composite materials subjected to lateral impulsive loadings described by pressure distribution according to the Dirac delta function and Heaviside function. Sun and Chattopadhyay (1975) studied the impact of a mass on a simply supported laminated composite plate under initial stress by solving a nonlinear integral equation and found that higher initial tensile stress elevates the maximum contact force but reduces the contact time, deflections and stresses. Kubo and Nelson (1975) studied analytically the two-dimensional response of an elastic laminated composite plate subjected to an impact load on its surface. Behavior of the plate along the thickness direction was modeled by a sufficiently large number of generalized coordinates to capture the propagation and dispersion of stress waves due to the surface impact thereby calculating the stresses at the laminate interfaces. Sun and Yang (1980) performed static indentation tests to determine the law of contact between a steel ball and graphite/epoxy laminated composites and found that an index of 1.5 in the power law was adequate for the loading and unloading curves.

Thereafter, many researchers have attempted to match experimental results with the vibration theories by postulating the existence of a quasi-elastic layer beneath the contact point. Previous work of Hertz (1882) involved a theory based on the local indentation analogous to an

electrostatic problem. The Hertzian contact law between an elastic sphere and an elastic half-space provides an expression for the local indentation in respect of the contact force and a constant parameter which depends upon the radii of curvature at contact and elastic properties of the impactor and target. However, this relation was found to be valid for static loading only and neglects the effect of the elastic vibration in the local indentation and thus this theory was valid only for impact between very compact bodies.

Yang and Sun (1982) conducted static indentation tests on glass/epoxy and graphite/epoxy composite laminates by steel balls and loading, unloading, and reloading data were fitted into power laws. They established the critical indentation (α_{cr}) that was used to predict permanent indentations in composite materials during unloading. Lal (1983) analyzed the behavior of 8-ply, quasi-isotropic, graphite epoxy laminates subjected to low velocity transverse impact loading assuming that the indentation, flexural and shear stiffnesses could be represented by 3-equivalent springs in series. Ramkumar and Chen (1983) studied the low velocity impact of laminated plates and transversely isotropic beams and plates respectively.

Shivakumar et al. (1985a) developed an energy-balance model and a spring-mass model to predict the impact force and duration during low-velocity impact on circular composite plates and included the effect of contact deformation, bending, transverse shear and membrane deformations. Shivakumar et al. (1985b) also studied the low-velocity impact damage in clamped circular composite plates and predicted that failure would initiate as splitting in the bottom-most ply and then propagate to the other plies. Tan and Sun (1985) studied the impact response of graphite/epoxy laminates both theoretically and experimentally using a 9-node isoparametric finite element in conjunction with an empirical contact law. Sankar and Sun (1985) presented an efficient numerical algorithm for transverse impact problems wherein the iterations of the nonlinear problem were separated from the structural response computations. Joshi and Sun (1985) studied the impact induced fracture in graphite/epoxy laminates and established the importance of transverse shear stress in crack initiation. Schonberg et al. (1987) studied the dynamic structural contact problems of a rigid, smooth cylindrical striker impacting an elastically supported transversely isotropic beam and plate. Liu (1988) studied the damage characteristics of composite plates made of glass/epoxy, Kevlar/epoxy, and graphite/epoxy and proposed that the mismatching of bending stiffness between two adjacent laminae was an indicator of delamination initiation in the composite laminates subjected to subperforation

impact. Cairns and Legace (1989) presented an analytical method to study the transient response of graphite/epoxy and kevlar/epoxy laminates subjected to impact considering the effect of shearing deformation, bending-twisting coupling, and nonlinear contact behavior. It was predicted that mass of the impactor at a fixed-impact kinetic energy has a strong influence on impact event due to the relative inertia between the projectile and target.

Qian and Swanson (1990) compared the results of different solution techniques of the governing differential equations for impact response of composite plates. The analysis was based on two theories: one based on the Rayleigh-Ritz approach with numerical integration while the other involved an analytical approach using Laplace transformation. Christoforou and Swanson (1991) studied the impact on laminated plates based on the Fourier series expansion for simply-supported plates, combined with Laplace transform techniques for the solution of the impact problems. Abrate (1991) studied the impact dynamics on laminate composite materials in order to predict the location, type, induced damage size and the residual properties of the laminate. Yigit and Christoforou (1995) developed an impact model based on static contact laws incorporating the damage effect, to investigate the impact response of thin composite laminate supported by a rigid substrate. Maiti and Sinha(1996) reported the low velocity impact response of thin and thick plates based on FSDT and HSDT employing FEM. The variations of impact induced stresses were also presented. Christoforou and Yigit (1996) studied the impact on a simply-supported composite beam using an analytical method based on the impulse-momentum principle wherein the effect of local contact behavior is accounted for through the use of an appropriate coefficient of restitution obtained from an elastic-plastic contact law. Christoforou and Yigit (1998) studied the nature of impact response of composite plates through normalization of the governing equations and identified key parameters to governing the transition from locally dominated to globally dominated responses in order to characterize the impact response. On the other way, impact problems have also been investigated using several analytical methods like the integral method, energy balance method, lumped parameter method, spring-mass model, wave propagation method and the numerical analysis methods. Abrate (2001) reported three models: (1) energy-balance models assuming a quasi-static behavior of the structure; (2) spring-mass models accounting for the dynamics of the structure; (3) complete models in which the dynamic behavior of the structure is fully modeled.

Lee et al. (1984) presented a three dimensional finite element and dynamic analysis for fiber-reinforced composite laminates subjected to a given impact loading using the Central difference method. Sun and Chen (1985) studied the impact response of initially stressed composite laminates using the finite element method employing the Newmark time integration algorithm in solving the time dependent equations of the plate and the impactor. Effect of initial stress, impactor velocity, mass and size of impactor on the transient response were investigated. Chen and Sun (1985a) studied the nonlinear transient response of initially stressed composite plates. Chen and Sun (1985b) also studied the impact response of composite laminates with and without initial stresses using the finite element method employing an experimentally established contact law which accounted for the permanent indentation.

Aggour and Sun (1988) presented a two-dimensional finite element analysis for fiber-reinforced composite laminates subjected to circular distributed impact load resulting the impact of a blunt-end impactor. Wu and Springer (1988) calculated the impact induced stresses and strains in a rectangular fiber-reinforced plate after low velocity impact by a solid object using a three-dimensional, transient finite element method comprising of 8-node brick elements. The locations, lengths, and widths of delaminations were predicted by means of a proposed failure criterion based on the concept of dimensional analysis. Sun and Liou (1989) analyzed the deflection and stresses of the laminated composite plate subject to central small area impact loading using a three-dimensional hybrid stress finite element method in the space domain along with the Newmark direct integration method in the time domain. Wu and Fu-Kuo (1989) presented a transient dynamic finite element analysis for studying the response of laminated composite plates due to transverse foreign object impact using a 8-point brick element with incompatible modes wherein the direct Gauss quadrature integration scheme was used throughout the element thickness to account for the changes in the material properties from layer to layer within the element.

Vaziri et al. (1996) presented a numerical procedure in predicting low-velocity impact response of laminated composite plates and shells using super finite elements. The governing finite element formulation took into account the classical Kirchoff-Love laminate theory for thin elastic plates and shells (neglecting the effect of transverse shear deformation) while the impact force was calculated using a non-linear Hertzian-type contact law that accounted for the curvatures of the colliding bodies. Kim et al. (1997) investigated the dynamic behavior and

impact-induced damage of laminated curved composite structures using incompatible eight-noded brick elements with Taylor's modification and predicted that the maximum impact force increased with curvature for the same impact velocity. Chun and Lam (1998) studied the dynamic response of fully-clamped laminated composite plates subjected to low-velocity impact of a mass using a numerical method wherein the non-linear, second-order differential governing equations are derived by the Lagrange's principle and the Hertzian contact law with modified contact constant.

Mili and Necib (2001) studied the impact behavior of cross-ply laminated composite plates under low velocity impact where the Hertzian contact law was developed using spring-mass model approximation. Johnson et al. (2001) developed a continuum damage-mechanics (CDM) model for fabric-reinforced composites for modeling the in-ply and delamination failure wherein the structural response and failure modes from numerical simulations and impact tests were found to be in good agreement. Aslan et al. (2003) performed a numerical simulation for evaluating the stresses and contact forces of a composite plate during impact along with the associated failure analysis for predicting the impact damage and initiation of delaminations. Krishnamurthy et al. (2003) determined the impact response of a laminated composite cylindrical shell by the classical Fourier series and the finite element methods. The finite element method was included to predict the impact-induced damage using the semi-empirical damage model and the effect of controlling parameters like impactor mass, approach velocity and shell curvature were studied. Whittingham et al. (2004) experimentally quantified the effect of an initial pre-stress on the response of laminated plates subjected to low velocity impact and observed that the effect of the pre-stress on the permanent indentation depth, absorbed energy and peak impact loads becomes significant at higher impact loads ($>10\text{J}$). Swanson (2004, 2005) studied the contact loading of orthotropic materials using numerical contour integration to determine the size and aspect ratio of the elliptical contact area, contact pressure distribution and then obtained a detailed stress fields by general solution for transverse pressure loading of the laminated orthotropic materials.

Mikkor et al. (2006) developed an explicit finite element (FE) model (*software package: Pam-Crash*), incorporating a bi-phase material degradation model, to predict the behavior of loaded carbon/epoxy panels when impacted over a range of low energy levels. Chen et al. (2008) studied the effect of thickness, in-plane dimensions and boundary conditions on the contact

problem of a laminated plate indented by a rigid sphere and concluded that thickness has significant effect on the force-indentation response if the plate thickness is less than 2 mm. Heimbs et al. (2009) studied the effect of a compressive preload on the low velocity impact behavior of different carbon fibre-reinforced plastic (CFRP) materials using the commercial explicit finite element code LS-DYNA. An increase in deflection and energy absorption was observed for composite plates with a preload of 80% of the buckling load while the Non-destructive inspections showed large extents of delamination occurring between individual plies. Aktas et al. (2009) studied the impact response of unidirectional glass/epoxy laminates by considering energy profile diagrams and associated load–deflection curves and discussed on the damage modes and the damage process of laminates under varied impact energies. Olsson (2010, 2015) presented an analytical model to study delamination initiation and growth and the resulting response during small mass impact on orthotropic laminated composite plates fast stepwise numerical solution of a single integral equation. Yang and Cantwell (2010) performed a series of low velocity impact tests on $(0^0/90^0)$ glass fiber-reinforced epoxy resin and predicted that impact force required to initiate damage, P_{crit} , varies linearly with $t^{3/2}$, where t is the target thickness at test temperatures between 23^0C and 90^0C , indicating the temperature effect on damage. Caputo et al. (2014) developed a numerical procedure based on finite element models and simulation techniques to study the structural behavior of laminated composite plates under low velocity impact loading conditions. Sanga et al. (2016) developed a robust model using homogenized shells based on degenerated tri-dimensional brick elements to study the low velocity barely visible impact damage (BVID) in laminated carbon composite structures based on the Hashin and the Benzeggagh-Kenane damage criteria's. English et al. (2016) performed simulations of low velocity impact with a flat cylindrical indenter upon a carbon fiber fabric reinforced polymer laminate in order to ensure quantifiable confidence in material characterization and model physics when simulating low velocity impact in structures of interest. Choi (2016) numerically studied the transient response of a composite laminated plates and cylindrical shells subjected to low-velocity impacts using the shear deformation theory of a doubly curved shell and von Karman's large deflection theory. Park (2017) investigated the behavior of steel plates and graphite/epoxy composite laminated plates under low velocity impact based finite element method wherein it was observed that the composite laminated plate showed about two times more displacement difference than the steel plate.

Impact response of laminated composite structures having an preexisting delamination has been a research topic in the recent years. Sekine et al. (1997) and Hu et al. (1999) studied the impact response of partially delaminated and multiple delaminated composite laminates. McCallum (2015) studied the influence of preload and boundary condition on pre-damaged composite plates subjected to soft-body impact using LS-DYNA 971.

1.5.7.2 Composite stiffened plate/shell

Gong and Lam (1999) studied the transient response of a eccentric stiffened composite plate subjected to low velocity impact using finite element method wherein an impact force function based on Hertz contact law was linked into a commercial FE code. Effect of stiffener spacing and thickness, anisotropic material properties, impact mass, and contact stiffness on the impact response were investigated. Structures impacted by a solid striker were simulated by well-established commercial software LS-DYNA3D using the three-dimensional contact-impact algorithm, in which both striker and structure were modeled. Seydel and Chang (2001a) developed a real-time identification technique for the prediction of the location and force history of low-velocity impacts on composite panels with beam stiffeners. Numerical results verified with the experimental results wherein piezoceramic sensors were used to reconstruct the force history using the smoother-filter algorithm. Seydel and Chang (2001b) experimentally investigated the importance of modeling boundary conditions and sensor placement for the success of model-based impact identification technique of stiffened plate. Sekine and Atobe (2009) reported identification of locations and force histories of multiple point impacts on composite isogrid-stiffened panels using measured longitudinal strain response of isogrid to adjust the modal coordinates determined from the longitudinal strains measured on the free edge side of isogrid. Identification of location and force history of a single point impact at an oblique impact angle was also examined. Based on a continuum damage mechanics approach, an intralaminar damage stiffened composite panel was proposed by Faggiani and Falzon (2010) implemented in a finite element package. A detailed finite element model was used to simulate the response of a stiffened composite panel subjected to low-velocity impact wherein fiber tensile and compressive breakage, matrix tensile and compressive fracture, and shear failure were observed. In their investigation, the contact algorithms and friction between delaminated plies were also included for better simulation of the impact event. Li and Chakka (2010) fabricated a sandwich structure with a hybrid cellular core (periodic isogrid stiffened stochastic

syntactic foam) using the pin-guided dry-weaving technology wherein Instron Dynatup 8250HV impact testing machine was used to carry out impact (CAI) tests of the said panel. Ultrasonic inspection was performed for damage identification. Sharif-Khodaei et al. (2012) presented a methodology for impact identification on composite stiffened panels using piezoceramic sensors. A large number of impacts at various locations of a composite stiffened panel were simulated using the finite element (FE) method and the data generated from FE analyses were used in artificial neural networks to predict the impact location. Li et al. (2014) investigated the response and impact induced damage of stiffened laminated plates due to low velocity impact based on Layerwise/solid elements method (LW/SE) and progressive failure model. Nonlinear Hertz's contact law used to obtain the contact force at the interface of impactor and the impacted surface while the initiation of the impact-induced damages were predicted by employing 3D Hashin criteria. Further continuum damage mechanics used to observe the effect of accumulation of damages in the composite plate and stiffener. Sun and Tong (2014) reported nonlinear finite element method, combined with the user-defined materials subroutine (VUMAT) of the ABAQUS software to predict low-velocity impact damage on the stiffened composite structure, which represents a real aircraft structure.

Kim et al. (2015) experimentally investigated a complex stiffened composite structures subjected to low-velocity impact. Impact tests were conducted on the composite panel in which four multiplexed fiber Bragg grating (FBG) sensors were attached on the bottom surface. Verification of results indicated that 20 verification points were successfully localized with the maximum error of 43.98 mm and average error of 14.23 mm using four FBG sensors. Dai et al. (2016) investigated the thermo-mechanical behavior of a rectangular high-strength low alloy (HSLA)-stiffened plate under low-velocity impact based on von Kármán equation and classical thin plate theory. The authors used modified nonlinear Hertzian contact law for computation of contact force without considering the effect of friction. This investigation was based on the assumption that stiffener cross section does not deform in its plane for the derivation of the nonlinear governing equations using the Hamilton's variational principle. Li and Chen (2016) experimentally studied the effect of low velocity edge impact damage on the damage tolerance of wing relevant composite panels stiffened with both T-shaped and I-shaped stiffeners under uniaxial compression load. Ricco et al. (2016) used non-linear explicit FEM to predict the low velocity impact induced damages of omega shaped stiffened panel. Cohesive Zone Model

(CZM) was adopted by the authors to study the onset and the propagation of the inter-laminar damage while intra-laminar damage model was based on the Continuum Damage Mechanics. Gurben et al. (2017) investigated the failure behavior of steel stiffened panel experimentally and numerically. Finite element simulation of the model was based on the elastic-viscoplastic J2 flow theory and a one-parameter fracture criterion wherein a method for mesh refinement based on h-adaptively was proposed for handling fracture in large-element simulations. Kumar and Babu (2017) presented a pre-damaged I-stiffened panel to study the effect of delamination location and mode for delamination initiation and propagation under load. Effect of delamination location on crack growth and collapse behavior was based on the Virtual Crack Closure Technique. Morin et al. (2017) investigated the failure behavior of an aluminum alloy stiffened (T-shaped) shell under quasi-static and low-velocity impact loading conditions. Based on the obtained experimental data, a constitutive model and a failure criterion suitable for numerical simulation of large-scale offshore structures were identified and evaluated using finite element models with different mesh sizes. Sun et al. (2018) studied experimentally the effect of stiffener damage caused by low velocity impact (LVI) on compressive buckling and failure load of the three T-stiffened composite panels. They used a vertical drop-weight impact test system to introduce the impact damage in the panel. Failure loads drops to a maximum of 44% compared to the undamaged specimen.

The above discussion reveals that large attention is focused on low velocity impact of unstiffened shells/plates while limited attention is received on low velocity impact response of composite stiffened shells. However, such studies on rotating delaminated twisted cylindrical shell appear to be a major field for research.

1.5.8 Delaminated composite plate/shell structures

Delamination is the most feared damage mode of failure in composite, hence cannot be ignored. Presence of delamination may result in a progressive stiffness reduction, material degradation and structural disintegration, which may lead to final failure of the composite. Delamination is a matrix dominated mechanism mostly takes place in resin-rich interlaminar regions in the form of separation of plies. Delamination is commonly initiated at the geometric boundaries, manufacturing defects, and service-induced-damage. Wang (1980) investigated the initiation of delamination from a surface notch of an angle ply laminate in the form of broken plies and studied its failure mechanics and mechanism using hybrid-stress finite-element

formulation wherein Muskhelishvili's complex stress functions was used to examine the failure mechanics and mechanism of delamination. Chai and Babcock (1985) developed an analytical model to evaluate the compressive strength criticality of near-surface interlaminar defects in composite wherein the low velocity impact application was emphasized. The analysis was subdivided into two parts namely elastic stability problem and the fracture problem and was solved by Rayleigh-Ritz method and simple energy balance criteria, respectively. Simites et al. (1985) analyzed a simple 1-dimensional model of a laminated plate with simple supported and clamped ends to check the effect of location, size, and thickness of delamination on buckling and load carrying capacity. Pardoen (1989) investigated the effect of delamination position and size on the natural frequency of the beam wherein the contact between the delaminated layers was included without considering the bending/extension coupling.

Cheng and Dharan (1990) used the fracture mechanics approach to analyze delamination during drilling wherein the crack growth was considered collinear and the crack was in the plane of material symmetry. The whole system was modeled and analyzed based on classical plate theory and linear elastic fracture mechanics. Peck and Springer (1991) studied both the experimental and analytical results of elliptically delaminated composite plate subjected to in plane forces and thermal loads. The authors used Rayleigh-Ritz energy method to predict the bending and buckling characteristic in the sublaminates wherein the growth of delamination was also included. Ju et al. (1995) carried out the free vibration study of multiple delaminated composite plate based on finite element method wherein the sublaminates arising from delamination were meshed separately and displacement continuity at the connecting boundaries were established by transforming stiffness and mass matrices. The effect of contact in delaminated layers and delamination growth were not considered by the authors. Identification of delamination in the laminated composites and its behavior up to rupture was reported by Allix et al. (1998) wherein the identification process based on initiation and propagation delamination tests. The authors conducted standard edge-delamination tension tests to identify the other parameters of the interface damage model. Geubelle and Baylor (1998) simulated the delamination process in cohesive/volumetric finite element method which includes a volumetric constitutive model to represent the bulk behavior and a cohesive model to simulate the spontaneous creation of internal failure surfaces. They introduced cohesive elements along the boundaries of the inner layers and inside the transverse plies to simulate the spontaneous

initiation and propagation of transverse matrix cracks and delamination fronts. Allixa and Corigliano (1999) proposed an elastic-damage interface law to study the interactions between delamination and geometrical nonlinearities of composite beam in which interface models were used for the description of material degradation along the layer connections and of a large displacement formulation. A detailed study of delamination processes i.e. from initiation to structural failure was reported.

Alfano and Crisfield (2001) carried out an analysis of delamination in composite plate using interface elements and an interface damage law based on linear elastic fracture mechanics and discussed some issues related to numerical solution and factors influencing mechanical strength. Numerical results for analyses of a double cantilever beam specimen and for a problem involving multiple delaminations for which comparisons were made with experimental results were reported. Fleming (2001) reported the predictions of delamination growth using the virtual crack closure technique were implemented using the finite element crash code MSC/DYTRAN and compared with other methods of modeling delamination in finite element crash analyses. Parhi et al. (2001) carried out the free vibration and transient response of multiple delaminated composite plates under hygrothermal loading. Cho and Kim (2001) developed a higher-order zig-zag theory for laminated plate with multiple delaminations for buckling analysis wherein the opening as well as slipping behavior of the delaminated parts were considered. The displacement fields assumed for multiple delaminations were supplemented with unit step-functions which allow discontinuities in the displacement fields. The authors developed a multiple delaminated model based on finite element method. Hu et al. (2002) reported the free vibration results of delaminated composite beam and plates wherein the least-square technique was used to establish the continuity condition at the delamination front. This analysis is based on higher order shear deformation theory and penalty function method was also adopted to enforce the constraint conditions. Grassi and Zhang (2003) performed finite element analyses of mode-I interlaminar delamination in z-fibre reinforced composite laminates, which was based on a double cantilever beam configuration. The authors emphasized on the advantage of z-fibre technique to improve the crack growth resistance. Yam et al. (2004) reported a numerical method to determine the natural frequency of delaminated composite plate where delamination was modeled by inserting a virtual/artificial spring at the nodes of the upper and lower sublaminates within the delaminated

region. Further, the structure was coupled to a vibroacoustic system to bring desirable effect to the interface in the delaminated region.

Karmakar et al. (2005) used multipoint constraint algorithm to model delamination in pretwisted composite shells to study the free vibration response. The compatibility of deformation and equilibrium of resultant forces and moments at the delamination crack front were well established by the said algorithm. Oh et al. (2005) used the higher-order cubic zigzag theory of laminated composites with multiple delaminations proposed by Cho and Kim (2001) to investigate the natural frequency and transient response wherein the penetration at the delamination interfaces were prevented by using unilateral contact constraints by Lagrange multiplier method. Cappello and Tumino (2006) studied the buckling and post-buckling performance of unidirectional and cross-ply composite laminated plates with multiple delaminations using ANSYS and 2D meshes. This study reported on buckling results by the variation of delamination length and its position across the thickness. Davies et al. (2006) carried out the investigation dealt with the problem of modeling onset of delamination/debonding in composite structures and its consequent propagation wherein they developed a new interface element based on a monotonic force/displacement law. Johnson and Holzapfel (2006) used a continuum damage mechanics (CDM) model for fiber reinforced composite shell structures subjected to high velocity impacts to model both in-ply damage and delamination failure. Delamination failure model was based on delamination failure energy criterion. Jinhua and Yiming (2007) investigated the dynamic stability of delaminated cylindrical shell by incorporating the Heaviside step function into the displacement fields and finally Rayleigh–Ritz method was used to derive dynamic governing equations. Aymerich et al. (2008) reported the damage prediction in laminated structures subjected to low-velocity impact based on finite element technique with cohesive interface elements adopting a bilinear cohesive law. Alnefaie (2009) developed a three-dimensional (3D) finite element model of delaminated fiber-reinforced composite plates where a detachment of the nodes at the delaminated region was considered and their displacements on the upper and lower surfaces were not connected to each other. Nagashima and Suemasu (2010) presented buckling analyses of carbon fiber reinforced plastic laminate with delaminations wherein delamination was modeled independently of the finite element mesh through enrichment with the Heaviside and asymptotic basis functions.

Dey and Karmakar (2012a) carried out the free vibration analyses of multiple delaminated pretwisted angle ply conical shells based on Mindlin's theory and delamination was modeled by Multipoint constraint algorithm wherein the undelaminated region was modeled by a single layer of plate elements while the delaminated region was modeled using two layers of plate elements. The same authors (2012b) also investigated the effect of delamination on the natural frequencies of rotating conical shell. Mohanty et al.(2012) presented the free vibration of woven fiber glass/epoxy (G/E) composite plates with delamination experimentally and numerically wherein delamination mode was based on the multi point constraint algorithm. Nanda and Sahu (2012) adopted the same algorithm to model delamination to investigate the free vibration response of delaminated shells (cylindrical, spherical and hyperbolic paraboloid) based on different shell theories. Kumar et al. (2014) investigated the free vibration of delaminated composite plate considering mixed interpolation tensorial component, nine node quadrilateral (MITC9) element in finite element method. Delamination in laminate was modeled either using region based approach or layerwise approach. Region based delamination model was employed in ESL (Equivalent single layer theories) models and layerwise delamination model in LW (Layerwise theories) model. In layerwise theory, delamination was modeled by introducing a discontinuous function while in region based model delamination was introduced by splitting the delaminated structure in span wise direction into delaminated segment and integral segments. Muc and Stawiarski (2015) used finite element and damage index to identify delamination in cylindrical composite panels using guided waves and detect debonding using an inverse algorithm based guided wave signals activated and captured by surface-mounted PZT elements.

Hammami et al. (2016) presented the linear and nonlinear vibration response of delaminated composite beam experimentally wherein double superposed delaminations were artificially introduced using Teflon tape during the lay-up at the interfaces between plies having different stacking directions. Hirwani et al (2016) investigated both experimentally and numerically the effect of delamination on free vibration of the curved panels which includes cylindrical, spherical, elliptical, hyperboloid and flat. Two different higher-order shear deformable kinematic models are considered to model the delaminated curved panel. The response of the panel was computed experimentally using CDAQ-9178 (National Instruments) in conjunction with LABVIEW soft-ware. Sahoo et al. (2016) reported the effect of delamination on the static and dynamic response of the composite plate wherein the same method as reported

by Hirwani (2016) was employed to model delamination. Torabi et al. (2016) investigated theoretically and experimentally the transverse vibration of delaminated composite beam using two approaches. In the first approach it was assumed that delaminated layers deform freely without touching each other while in second approach the delaminated layers were allowed to slide over each other. In experimental work, delamination was artificially created by inserting a release film with proper thickness ($20\mu\text{m}$) at the desired location during manufacturing. Yazdani et al. (2016) presented an extended finite element method (XFEM) for modeling delamination in composites wherein the discontinuities were imposed within any arbitrary interface by enriching the displacement field. Thus two sub-domains defined the plane of the discontinuity. Arumugam and Rajamohan (2017) investigated theoretically and experimentally the free and forced vibration response of rotating delaminated tapered composite plate wherein the displacement fields of delaminated segments and intact segments with continuity condition was presented. In experimental work, a Teflon films was inserted at the interfaces of plies to create delamination. Shankar et al. (2017) reported the vibration analysis and control of delaminated smart composite plate under hygrothermal environment. Delamination was modeled by dividing the laminates into sublaminates then the upper and lower segments of the delaminated region were meshed separately. Hirwani et al. (2018) investigated the doubly curved shallow delaminated shells using higher order theory based finite element method. The delamination between the consecutive layers was included using two sub-laminate approaches including the intermittent displacement continuity conditions. Yazdani et al. (2018) used the extended finite element method (XFEM), the mixed-mode cohesive zone model, the contact formulation, and the damage criterion to study the interfacial delamination initiation and growth in composite shells with less computational effort.

1.5.9 Delaminated composite stiffened plate/shell

Studies conducted so far with delamination in the unstiffened shells or plates are available in literature but attention of a very few researchers have been focused on delaminated stiffened shells. Wang et al. (1995) used fracture mechanics approach to study the flange skin strip debond configuration and a skin-stiffener debond configuration of the stiffened panel wherein 4-node and 9-node shell elements were used to model the debond configurations where strain energy release rates for the debond configuration were computed by virtual crack closure technique (VCCT) and the gradient method. Naganarayana et al. (1996) presented a multidomain

modeling technique for modeling the delaminated stiffened composite shell structures for postbuckling solution under compressive load wherein stiffener was modeled as a two-noded curved element and shell as a three-noded element. This analysis also includes the delamination growth prediction using pointwise energy release rate obtained from the three-dimensional J integral.

Haoran et al. (2003) used virtual crack closure technique and a self-adaptive grid moving scheme to investigate the failure of the delaminated stiffened composite plate under compression and the delamination growth prediction was included in their investigation. Shape of the delamination was elliptical and circular and the continuity of displacement and rotation along the delamination front was satisfied by imposing the constraint equations. Armentani et al. (2004) used a hybrid (FEM/analytical) procedure based on virtual crack closure technique to compute the energy release rate for delamination at skin/stinger interface of a stiffened composite panel under longitudinal compression load. Rui-xiang and Hao-ran (2004) used total energy release rate as the criteria of estimating delamination growth with virtual crack closure technique (VCCT) wherein they reported the postbuckling and delamination propagation behavior in delaminated stiffened composite plates by finite element method. The authors developed a moving mesh technique to simulate the growth of the delamination front. Bisagni (2006) made use of an ultrasonic system obtaining C-scan and B-scan representations to predict the progressive debonding between the skin and the stringer under compression. The stiffened panel was analyzed numerically by using ABAQUS and experimental verifications were also reported. The growth of delamination was investigated by means of the Virtual Crack Closure Technique (VCCT) implemented within ABAQUS. Chen et al. (2006) studied the natural frequency of pre-damaged stiffened composite plate which includes delamination in the composite plate and debonding between skin and stiffener employing finite element method based on the principle of hump resonance. A virtual interface nonlinear contact element, called Hertz's discontinuous spring, was employed for simulating the separate/contact mode state along the interfaces of delamination and/or debonding regions. Suemasu et al. (2006) investigated the effect of localized damage on the compressive buckling as well as post buckling behaviors of blade stiffened composite plates wherein debonding between a skin panel and a flange and multiple delamination in the skin panel were considered. A contact problem between the skin and flange panels was approximated by a spring element with no restraint of the positive relative

displacement and a strong restraint of the negative displacement. Delamination in the skin panel closed during compression and the normal relative displacement was constrained to prevent the delaminated portions from overlapping.

A finite element formulation for a solid-like interface element based on the formulation of eight node continuum elements was proposed by Wagner and Balzani (2008) wherein a cohesive interface element was derived to predict both delamination and skin–stringer separation avoiding the interpenetration of the crack faces. An irreversible cohesive law was introduced a continuous cohesive free energy function of Smith–Ferrante type to detect the initiation and propagation of delamination. Riccio et al. (2013) investigated the skin delamination growth in stiffened composite panels using finite elements method, based on the Virtual Crack Closure Technique (VCCT) and on the fail release approach. This approach was used to simulate delamination growth while VCCT for computing the energy release rate along the delamination front. Riccio et al. (2014) reported skin–stringer debonding growth in composite panels under compressive load wherein the traction–separation law in Cohesive Zone Model (CZM) was presented. Virtual Crack Closure Technique (VCCT) based FEM analyses on Double Cantilever Beam (DCB) and End Notched Flexure (ENF) specimen were used to characterize the traction–separation law for fracture mode I and mode II, respectively. Riccio et al. (2014a) presented an experimental study on skin delamination buckling and growth phenomena in stiffened composite panels subjected to compression loading. In the lay out process of delamination a Teflon circular was inserted between the layers. To investigate the delamination phenomenon optical fibers were positioned very close to the delamination. Thermography test was conducted to monitor the artificial delamination status during the compression. Riccio et al. (2014b) investigated numerically the delamination buckling and growth of stiffened composite panels under compression wherein they made use of virtual crack closure technique with fail release approach for the simulation of the delamination propagation.

Borrelli et al. (2015) investigated kinematic coupling approaches for FE simulation of the mechanical behavior of stiffened composite panels. They made use of two coupling methods such as point-wise kinematic coupling and the weighted residual kinematic coupling. Area surrounding the delamination was modeled by two layers of solid elements, while all the other regions have been modeled by shell elements. Global–local elements were used to couple the two differently modeled regions. Contact elements were also placed on the initial delaminated

area in order to avoid overlapping between the two delaminated sub-laminates. Riccio et al. (2015) investigated the stinger-skin debonding growth in the composite stiffened panel under compression. Debonding growth was predicted by adopting standard Virtual Crack Closure Technique (VCCT) along with fail release approach. VCCT was used for calculating the energy release rate at delamination crack front. This approach was implemented in ANSYS by means of Ansys Parametric Design Language (APDL) to conduct the tests. A non-linear finite element model was proposed by Yetman et al. (2015) to study the effect of stinger-skin debonding of top hat stiffened panel on the failure modes, post-buckled ultimate strength and its damage tolerance. The model, which accounts for both geometric and material nonlinearities, was implemented in ABAQUS wherein the stiffeners, plate and cohesive interface were connected by multi-point constraints which restrict the degrees of freedom of the plate nodes to that of the connected flange nodes. Naini and Ramesh (2016) carried out the impact analysis of laminated composite stiffened panel embedded with delamination. The behavior of the panel was investigated with help of Abaqus and in respect to the location of the delamination and its propagation employing virtual crack closure technique (VCCT). Riccio et al. (2016) simulated inter laminar damage growth specially delamination in stiffened panels using a linear numerical methodology implemented in a commercial finite element platform.

Kumar (2017) numerical investigated the effect of delamination location on crack growth and collapse behavior of laminated composite stiffened panel with method of Virtual Crack Closure Technique. The authors adopted cohesive zone model with cohesive elements or interface elements to model delamination in Abaqus. Milazzo (2017) used Ritz approach to investigate the buckling and postbuckling of stiffened composite panels with through-the thickness cracks and/or delaminations. Decomposition strategy was implemented to model delamination while a node-to-node contact algorithm was used to prevent cases of interpenetration that may occur depending on the kind of damage, load, and constraints. Shah and Panda (2017) investigated the skin-stiffener debonding in stiffened composite panel with functionally graded (FG) bimodular material property under thermomechanical coupled field using work strain energy release rate (SERR) as a fracture parameter. The authors used the virtual crack closure technique (VCCT) equation along the delamination front at each pair of nodes to evaluate SERR for suitable growth criteria. An extended layerwise/solid-element (XLW/SE) method was developed by Lu et al. (2017) to investigate the flexural analysis of

composite stiffened plates with/without delaminations and/or transverse crack. In order to model the strain discontinuity resulted from the interfaces between the layers and displacement discontinuity of delaminations, the weak discontinuous function and the strong discontinuous function were used in the displacements field, respectively. Dávila and Bisagni (2017) investigated experimentally the quasi-static and fatigue damage progression in single-hat stringer compression specimens with delamination where a Teflon film was inserted between one flange of the stringer and the skin to create a delamination and pre-test finite element analyses were conducted using the virtual crack closure technique to select the range of defect sizes to be considered and the load levels to be applied during the fatigue tests.

From the above discussion, it is evident that delamination in the skin of the stiffened plates/shells receive less attention of the investigators. Considering delamination in the skin of a rotating stiffened cylindrical will be a good problem for the research work.

1.5.10 Other Aspects

The review of the literature further reveals that some of the investigators are concentrating on complicated aspects of the stiffened shell behavior. Study of static and dynamic instability characteristics of stiffened shell by Duffield and Willems (1972), Merritt and Willems (1973), Liao and Cheng (1994), Shrivastava et al.(2002, 2015) and Patel et al. (2006), respectively are some of notable works. First ply and progressive failure analysis of the composite stiffened shell/plate is another direction of work carried out by some of the investigators such as Kong et al. (1998), Ambur et al. (2004), Prusty (2005), Zhang et al. (2008), Anyfantis and Tsouvalis (2012) and Akterskaia et al. (2017), respectively. It may be found that extensive research work is also continuing in the fields of buckling analysis of stiffened structures with and without cutouts. Some of the outstanding works contributed by the investigators like Li and Wu (2015), Guo et al. (2016), Hao et al. (2017a, 2017b) and Tian et al. (2017) are still found in literature. These aspects are also to be studied with consideration of delamination and rotation in the twisted laminated stiffened shell.

It is, thus quite clear from the discussion that there lies a vast scope of research in the field of delaminated composite stiffened shell analysis. Furthermore, the study of composite stiffened shells is yet to reach the saturation. All the lacunae mentioned in the above discussion need due attention of the researchers. However, some of the areas pertaining to dynamic

behavior of laminated composite stiffened shell are to be taken up as the scope for future work, which have been outlined in the last chapter.

1.5.11 Critical Observations

The volume of literature that has accumulated on stiffened shell research when examined carefully shows that many important aspects have been explored and reported. It is also realized that there are some areas which need to be addressed and some other areas are to be studied yet more meticulously to fully understand the behaviour of stiffened shell forms. It is noted that many aspects of stiffened shell analysis and design need elaborate attention.

It is found that although many researchers have reported the vibration characteristics of stiffened shell panels, corresponding information regarding the behaviour of rotating twisted stiffened shells with and without delamination is missing in the literature.

The paper of Kolli and Chandrashekara (1996), Nayak and Bandyopadhyay (2005) reported the finite element formulation of different stiffened shell forms with simply supported boundary conditions. The work of Prusty and Satsangi (2001a) seems to be the only paper on bending analysis of stiffened shell panels although transverse deflections are only reported. Excellent review papers published from time to time by authors like Sinha and Mukhopadhyay (1995a), Yang et al.(2000), Qatu (2002a,2002b), echo the fact that static analysis of stiffened shell panels in general and particularly doubly curved panels have not figured in the existing body of literature. Stiffened conoidal shells which is very important in industrial applications have not been studied for static characteristics.

Among the vibration studies that have been carried out on stiffened shell configurations, cylindrical and spherical forms received maximum attention. Some vibration studies on truncated stiffened conoids were reported by Nayak and Bandyopadhyay (2002a, 2002b) for simply supported and clamped boundary conditions. Free vibration reports on stiffened conoidal shells for other practical boundary conditions are missing in the literature. Results on natural frequencies of full conoidal shells also need to be included in the research report. Cutouts are often provided on shell surfaces for creating passages for cables, conduits, pipes and chimneys. Sometimes cutouts are used to alter the resonating frequency. Hence, there is scope of working on stiffened conoids with cutouts as practically margins of cutouts are to be stiffened.

Forced vibration studies on stiffened shells appear at very few places like in the papers published by Sinha and Mukhopadhyay (1995b), Goswami and Mukhopadhyay (1955a) and

Mukhopadhyay and Goswami (1996). The above mentioned papers deals with cylindrical and spherical shells. Chakravorty et al. (1998) and Nayak and Bandyopadhyay (2006) reported limited studies on forced vibration of unstiffened and stiffened conoidals shells respectively. Although the work of Nayak and Bandyopadhyay (2006) was about stiffened shells but they reported transient deflections only.

Thus, it is felt that there are many areas of stiffened shells which need elaborate attention as indicated above. With this finding the actual scope of the present study is furnished in the next chapter.

1.6 RESEARCH GAPS IDENTIFIED

The present work is undertaken to fill in the following major research gaps broadly classified below as is evident from the literature review:

a) Idealization of turbomachinery blade with cylindrical stiffened shells of low aspect ratio

Almost all research works till date has idealized the turbomachinery blades as twisted thin plates or shells wherein the strength and natural frequencies of the blades are too low. Hence an effort has been made to increase the failure strength and natural frequencies of the turbomachinery, impeller or fan blades by idealizing as cantilevered composite pretwisted rotating cylindrical stiffened shells with low aspect ratio in the present analysis.

b) Effect of delamination

From the previous studies, it is observed that a few number of the works on debonding between skin and stinger based on facture mechanics are carried out on stiffened plate structures, Study related to delamination in stiffened shell with pretwist and rotation is found rare in literature. It is also predicted that there is a reduction in the natural frequencies of composite laminates due to the presence of delamination. Hence, the present study is intended to account for the effects of delamination on the free vibration and impact response of rotating pretwisted composite stiffened cylindrical shell structures.

c) Impact on composite cylindrical stiffened shell

Impact of low-velocity foreign masses with underwater vehicles, spacecrafts, leading edge of an aircraft wing, automobile bodies/protruded sections, blade of steam turbines and jet engines etc. is quite common in actual practice. The literature review reveals that a fair amount of research work has been devoted in the study of the impact response of composite stiffened

plates and shells. However, the rotation and pretwist effects on the transient response of delaminated composite cylindrical stiffened shells under arbitrary impact of foreign masses have not been attempted yet. Thus, a comprehensive study of the dynamic response of rotating delaminated composite cylindrical stiffened shells with pretwist subjected to impact stresses will be helpful in predicting the failure and reliability.

e) Multiple-impact on delaminated composite cylindrical stiffened shell

Most researchers till date have focused on single-site impact on composite plates and shell. However impact is never a localized phenomenon as in hailstorm or ballistic attacks. The superimposition of the contact stresses at different locations on the delaminated composite cylindrical stiffened shell makes the prediction of their transient response extremely complex. The present study aims to develop a numerical method capable of predicting the multiple-impact response of the pretwisted delaminated stiffened structure.

f) Delayed multiple Impacts

The delayed impact response of delaminated composite cylindrical stiffened shell based on the time-delay between the impactors has not been presented yet. The present work attempts to focus on the delayed impact response of delaminated composite stiffened cylindrical shell.

1.7 SCOPE OF THE PRESENT INVESTIGATION

A thorough review of the existing literature clearly suggests that though a plethora of research works on composite stiffened shells and pretwisted plates/shells have been presented but there is still a broad scope of further research especially in the field of dynamic analysis of rotating delaminated composite pretwisted stiffened cylindrical shells as well as their transient response under single or multiple impact of low-velocity masses. An analytical research effort is needed to be carried out to exploit the capability of the modern day high-speed computers in analyzing the response of composite stiffened cylindrical shells under impact loading. Accordingly, the present endeavor aims at investigating certain relevant problem areas so as to improve the understanding of free vibration and impact response of delaminated composite pretwisted stiffened shells employing finite element method. Present scope of the research aims to cover some of the lacuna as listed below keeping this objective in mind:

1. An eight-noded isoparametric shell element is developed to accurately model the complex geometry of pretwisted cylindrical shell while a three noded isoparametric

beam element is considered to model the stiffener. The Gauss quadrature integration scheme is used to compute the mass and stiffness matrices of the shell and stiffener elements. The formulation is based on the kinematic of first-order shear deformation (FSDT) theory. The general dynamic equilibrium equation is derived employing Lagrange's equation of motion. The finite element codes developed are capable of predicting the free vibration and transient response of delaminated composite pretwisted rotating stiffened cylindrical shells due to single and multiple low-velocity impacts. The computer codes developed are first validated against available published results to ensure their capability in performing further analysis accurately and reliably. The codes are then used for generating new numerical results and graphical data are interpreted from the numerical results

2. A pre-existing delamination of a definite size and at a particular location is assumed to be present and the free vibration characteristics of both stationary and rotating composite stiffened cylindrical shells will be investigated. Numerical studies on pretwisted composite stiffened cylindrical shells will be carried out for moderate rotational speeds for which the Coriolis effect will be neglected. Natural frequencies of delaminated composite pretwisted stiffened cylindrical shells will be obtained for different laminate configurations considering the combined effect of location/size of delamination, rotational speed, pretwist angle, and orientation of stiffener, thickness of stiffener and eccentricity of stiffener. Also, the free vibration behavior of long, intermediate and short stiffened cylindrical shells based on Aas-Jakobsen's parameters is studied.
3. Investigations will be carried out to study the single and multiple impact response of delaminated composite pretwisted stiffened cylindrical shells. The impact response will include the computation of contact force, shell/impactor displacements, impactor velocities, stress resultants and in-plane stresses at specified points of the cylindrical shells. The modified Hertzian contact laws that accounts for permanent indentation will be utilized to compute the contact force between the impactor and the delaminated stiffened shells. Graphical results will be presented to depict the influence of important parameters like twist angle, rotational speed, size and location of delamination, orientation of stiffener, thickness of stiffener, eccentricity of stiffener, time-delay

between subsequent impacts on the transient dynamic response of delaminated composite pretwisted stiffened cylindrical shell.

4. The results will be discussed in detail considering the effect of important parameters on the dynamic response of delaminated composite pretwisted stiffened cylindrical shells. A set of conclusions will be drawn summarizing the salient findings presented in this work. The scope of the future research work in this area will also be identified.

1.9 ORGANIZATION OF THE THESIS

This thesis consists of five chapters. The first chapter presents a general introduction of the delaminated composite pretwisted stiffened cylindrical shells along with its importance in relation to bending, free vibration, single and multiple impact response and associated finite element techniques used in predicting them. A detailed review of the existing literature is presented in this chapter and the scope of the present work is outlined based on the same. An extensive literature review is carried out with an emphasis on the following aspects:

- a) Laminated plate theory, shallow shell theory and pretwisted plate/shell.
- b) Bending analysis of stiffened plate/shell.
- c) Free vibration of composite stiffened plate/shell.
- d) Transient response of stiffened shell.
- e) Delamination modeling in plate/shell.
- f) Delamination modeling in stiffened plate/shell.
- g) Other aspects
- h) Critical observations

Chapter 2 presents the theoretical formulation which is used in the present analyses. Basic lamina stress-strain relations, constitutive equation of shell and stiffener are discussed followed by the derivation of geometric stiffness matrix for rotation. The finite element model is developed based on the Lagrange's equation of motion. An eight-noded isoparametric shell element is combined with a three noded beam element to develop the present finite element formulation. The modified Hertzian contact law that accounts for permanent deformation is utilized to compute the contact force between the stiffened shell and the impactor. The Gaussian quadrature is used in the integration for calculating the element stiffness, mass matrices and the element force vectors. The standard eigenvalue problem are solved by the QR iteration algorithm

is discussed. Newmark's time integration scheme used to solve the time dependent equations of the shell and the impactor/s is also reported.

Chapter 3 presents both numerical and graphical results of the free vibration analyses of delaminated composite pretwisted stiffened cylindrical shells. The computer codes are validated by comparing the results with those available in the existing literature. A concise study of the influence of the important parameters on the free vibration response of long, intermediate and short stiffened cylindrical based on Aas-Jakobsen's parameters are also presented in this chapter.

Chapter 4 deals with the single and multi-point impact response of delaminated composite pretwisted composite stiffened cylindrical shells. To establish the validity of the present finite element formulation in predicting the impact response of composite plates and shells, the results are first validated with those of previous investigators. Graphical results are presented to study the effect of important parameters on the transient response.

Significant conclusions drawn from the present investigations and the major contributions of the present research work are listed in **Chapter 5**. The major contributions of the present research work and the scope of the future research in the context of the present work and the related problem areas are also summarized.

A list of the references that are cited in the present work is given in the end. A flowchart of the computational procedure adopted to compute the low velocity impact response of the stiffened panel is given in **Appendix-I**.

CHAPTER 2

THEORETICAL FORMULATION

2.1 GENERAL

This chapter presents the theoretical formulation and solution procedures for free and transient vibration analyses of the rotating delaminated twisted composite stiffened shell. In the present analysis the surface of the composite stiffened shell is discretized into a number of finite elements. Each element of the composite stiffened shell is further considered as a combination of shell and beam elements. Formulation of the general curved shell element, having all the three radii of curvature using eight noded isoparametric quadratic elements, is derived on the basis of modified Sander's thin shell theory, satisfying C^0 continuity for the interpolation functions. The stiffeners are modeled as three noded curved beam elements having the same set of displacement functions as that of the shell excluding the one across the stiffener longitudinal axis. Suitable transformations account for the eccentricity and curvature of the stiffener as well as their positions anywhere parallel to the X- or Y-direction within the shell element. The stiffeners oriented along the X-direction are termed as x-stiffeners and those along the Y-direction are termed as y-stiffeners. Appropriate combinations of the element matrices of the shell and the beam elements; result in the overall element matrices of the stiffened shell element. A multi-point constraint algorithm is used to model delamination at desired location of the shell, wherein the undelaminated region is represented by a single layer and delaminated region as two layers. The compatibility of deformation and equilibrium of stress resultants are ensured at the delamination crack front. The governing dynamic equilibrium equation is derived using Lagrange's equation of motion. Standard Eigenvalue problems have been solved by using QR iteration algorithm. In low velocity impact problem, the contact force is computed using modified Hertzian contact law, which accounts for permanent indentation. The time dependent equations of the stiffened shell and the striker are solved by Newmark's time integration algorithm.

The mathematical formulation of the model is based on the following assumptions:

1. The middle plane the cylindrical shell is taken as the reference plane.

2. The laminated composite shell and the stiffener are made of number of layers bonded together, wherein each layer is treated as homogeneous and orthotropic.
3. The fibers are regularly spaced, perfectly aligned and perfectly bonded.
4. The matrix is homogeneous, linearly elastic and free from voids.
5. A two dimensional approach is employed to model the three dimensional shell and stiffener as one dimensional element.
6. The transverse normal is inextensible.
7. Normal to reference surface of the cylindrical shell before deformation remain straight but not necessarily normal after deformation.

2.2 SHELL ELEMENT

A doubly curved thin shallow shell of uniform thickness made of composite material is considered. The radii of principal curvature of the shell along the global Cartesian coordinates X and Y are R_x and R_y , respectively. The radius of the curvature of twist is R_{xy} . The projection of the shell on the XY plane is a rectangle of dimensions L and b which are parallel to X and Y axes respectively. The orientation of the stiffened shell in the global Cartesian coordinate system is shown in Fig. 2.1.

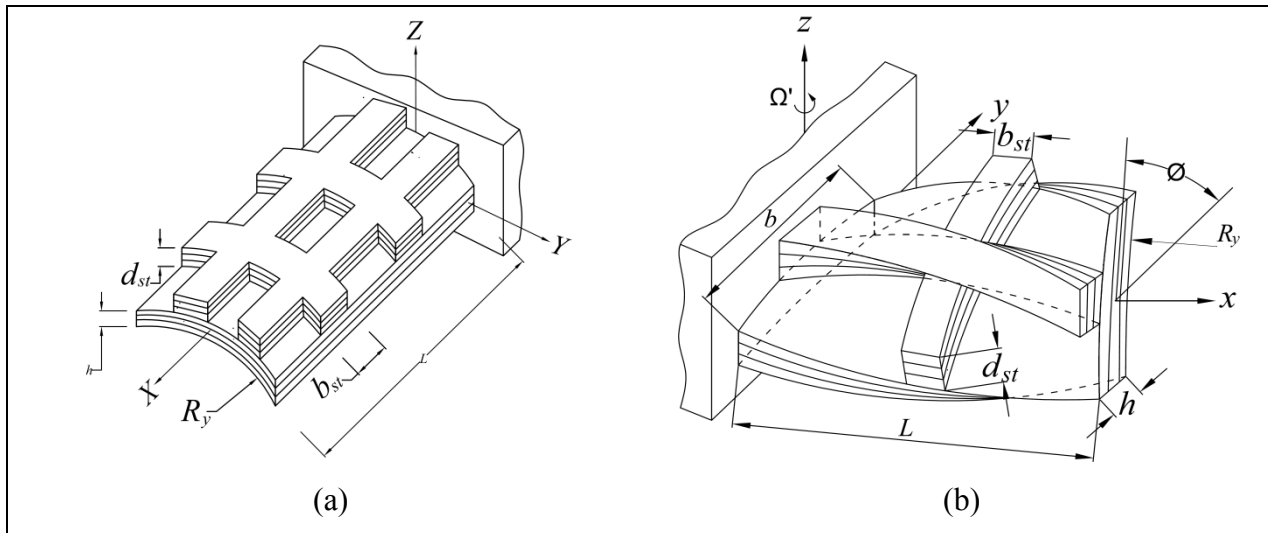


Figure 2.1 Typical cantilevered laminated composite cylindrical stiffened shells in the global Cartesian coordinate system. (a) Untwisted stiffened shell (b) Twisted stiffened shell.

The shell surface is discretized by curved quadratic elements, which are rectangles in plan. These rectangles are modeled as eight noded doubly curved isoparametric elements having four corner and four mid-side nodes as shown in Fig 2.2.

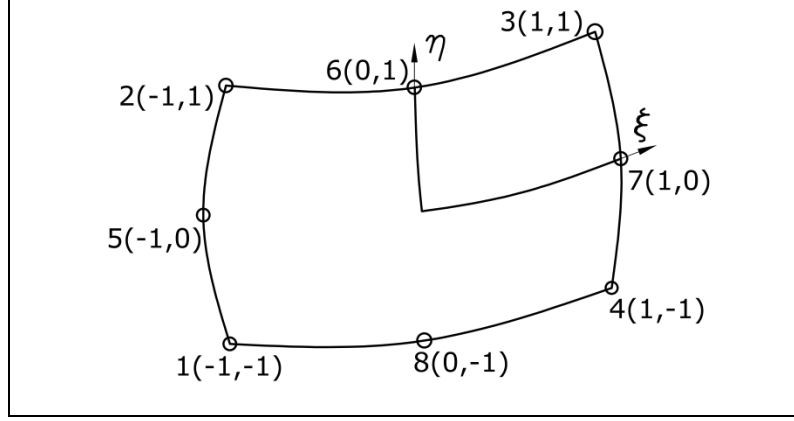


Figure 2.2 Curved isoparametric shell element with nodes

2.2.1 Shape Functions

For an isoparametric element the coordinates and displacements at any point within the element are represented by the coordinates and displacements of the nodes of the element and the shape functions. These are derived from an interpolation polynomial. In case of thin shell the final element is assumed to have mid-surface nodes only. Hence, the interpolation polynomial is a function of ξ and η and has the following form.

$$u(\xi, \eta) = A_0 + A_1\xi + A_2\eta + A_3\xi^2 + A_4\xi\eta + A_5\eta^2 + A_6\xi^2\eta + A_7\xi\eta^2 \quad (2.1)$$

The shape functions derived from the interpolation polynomial are as

$$\begin{aligned} N_i &= (1 + \xi\xi_i)(1 + \eta\eta_i)(\xi\xi_i + \eta\eta_i - 1)/4, & i = 1, 2, 3, 4 \\ N_i &= (1 + \xi\xi_i)(1 - \eta^2)/2, & i = 5, 7 \\ N_i &= (1 + \eta\eta_i)(1 - \xi^2)/2, & i = 6, 8 \end{aligned} \quad (2.2)$$

where N_i denotes the shape function at i th node having natural coordinates ξ_i and η_i .

The correctness of the shape functions is checked from the relations

$$\sum N_i = 1, \quad \sum \partial N_i / \partial \xi = 0 \quad \text{and} \quad \sum \partial N_i / \partial \eta = 0 \quad (2.3)$$

The coordinates of any point (x, y) within the element are obtained as

$$x = \sum N_i x_i \quad \text{and} \quad y = \sum N_i y_i, \quad i = 1, \dots, 8 \quad (2.4)$$

where x_i and y_i are the coordinates of the i th node.

2.2.2 Generalized Displacement Fields and Nodal Degrees of Freedom

Any shell surface can be modeled by three-dimensional solid elements. When the thickness dimension is considerably smaller than the other dimensions, the nodes along the thickness

direction supply additional degrees of freedom than needed and hence are not preferred. When a two-dimensional element is obtained by condensing the thickness direction nodes, the displacements of adjacent thickness direction nodes must be ensured to be equal to avoid numerical difficulties. Thus five degrees of freedom including three translations (u, v, w) and two rotations (α, β) are attached to each node. The final element has mid-surface nodes only and a line in the thickness direction remains straight but not necessarily normal to the mid-surface after deformations. The generalized displacements at any point within the element can be interpolated from the nodal values as

$$\{\delta\} = \begin{Bmatrix} u \\ v \\ w \\ \alpha \\ \beta \end{Bmatrix} = \sum_{i=1}^8 \begin{bmatrix} N_i & & & & \\ & N_i & & & \\ & & N_i & & \\ & & & N_i & \\ & & & & N_i \end{bmatrix} \begin{Bmatrix} u_i \\ v_i \\ w_i \\ \alpha_i \\ \beta_i \end{Bmatrix} \quad (2.5)$$

Equation (2.5) can be written in a compact form

$$\{\delta\} = [N] \{d_e\} \quad (2.6)$$

2.2.3 Strain-Displacement Equations

According to the modified Sanders' first approximation theory for thin shells (Sanders, 1959) the strain-displacement relationships are established as

$$\begin{bmatrix} \varepsilon_x & \varepsilon_y & \gamma_{xy} & \gamma_{xz} & \gamma_{yz} \end{bmatrix}^T = \begin{bmatrix} \varepsilon_x^0 & \varepsilon_y^0 & \gamma_{xy}^0 & \gamma_{xz}^0 & \gamma_{yz}^0 \end{bmatrix}^T + z \begin{bmatrix} \kappa_x & \kappa_y & \kappa_{xy} & \kappa_{xz} & \kappa_{yz} \end{bmatrix}^T \quad (2.7)$$

where the first vector on the right hand side represents the mid-surface strains and the second vector represents changes of the curvatures of the shell surface due to loading and are respectively related to the degrees of freedom as

$$\begin{Bmatrix} \varepsilon_x^0 \\ \varepsilon_y^0 \\ \gamma_{xy}^0 \\ \gamma_{xz}^0 \\ \gamma_{yz}^0 \end{Bmatrix} = \begin{Bmatrix} \partial u / \partial x + w / R_x \\ \partial v / \partial y + w / R_y \\ \partial u / \partial x + \partial v / \partial x + 2w / R_{xy} \\ \alpha + \partial w / \partial x \\ \beta + \partial w / \partial y \end{Bmatrix} \quad (2.8)$$

and

$$\begin{Bmatrix} \kappa_x \\ \kappa_y \\ \kappa_{xy} \\ \kappa_{xz} \\ \kappa_{yz} \end{Bmatrix} = \begin{Bmatrix} \partial\alpha/\partial x \\ \partial\beta/\partial y \\ \partial\alpha/\partial y + \partial\beta/\partial x \\ 0 \\ 0 \end{Bmatrix} \quad (2.9)$$

In the above relations R_x , R_y and R_{xy} are the three radii of curvature of the element. The surface equation of any shell form can be represented by the equation $z = f(x, y)$. For shallow shells where, according to Vlasov (1958), the ratio of the rise to the shorter plan dimension is less than 0.2, the surface curvatures can be approximately represented as,

$$\frac{1}{R_x} = \frac{\partial^2 z}{\partial x^2}, \quad \frac{1}{R_y} = \frac{\partial^2 z}{\partial y^2} \quad \text{and} \quad \frac{1}{R_{xy}} = \frac{\partial^2 z}{\partial x \partial y} \quad (2.10)$$

The strain components of equations (2.8) and (2.9) are to be considered together for generalized representation of the three-dimensional strain field and can be expressed in the form of

$$\{\varepsilon\} = [H]\{d_c\} \quad (2.11)$$

where $\{\varepsilon\} = [\varepsilon_x^0 \quad \varepsilon_y^0 \quad \gamma_{xy}^0 \quad \kappa_x \quad \kappa_y \quad \kappa_{xy} \quad \gamma_{xz}^0 \quad \gamma_{yz}^0]^T$ (2.12)

and $\{d_c\} = [\partial u/\partial x \quad \partial u/\partial y \quad \partial u/\partial z \quad \partial v/\partial x \quad \partial v/\partial y \quad \partial v/\partial z \quad \dots \\ \dots \quad \partial\beta/\partial x \quad \partial\beta/\partial y \quad \partial\beta/\partial z \quad u \quad v \quad w \quad \alpha \quad \beta]^T$ (2.13)

Since the displacements are interpolated from the nodal values by the shape functions, the derivatives of the displacements are obtained with respect to the natural coordinates and then proper transformation technique is applied. Thus the vector $\{d_c\}$ is expressed in terms of natural coordinates as:

$$\{d_c\} = [J]^{-1}\{d_n\} \quad (2.14)$$

where $\{d_n\} = [\partial u/\partial\xi \quad \partial u/\partial\eta \quad \partial u/\partial\zeta \quad \partial v/\partial\xi \quad \partial v/\partial\eta \quad \partial v/\partial\zeta \quad \dots \\ \dots \quad \partial\beta/\partial\xi \quad \partial\beta/\partial\eta \quad \partial\beta/\partial\zeta \quad u \quad v \quad w \quad \alpha \quad \beta]^T$ (2.15)

and $[J]$ is Jacobian matrix expressed as

$$[J] = \begin{bmatrix} \partial x/\partial\xi & \partial y/\partial\xi & \partial z/\partial\xi \\ \partial x/\partial\eta & \partial y/\partial\eta & \partial z/\partial\eta \\ \partial x/\partial\zeta & \partial y/\partial\zeta & \partial z/\partial\zeta \end{bmatrix} \quad (2.16)$$

For thin shells in which, according to Gioncu (1979), the ratio of thickness to minimum radius of curvature is less than 0.005, the terms with first power of ζ in the Jacobian matrix may be neglected.

From equation (2.15) it is evident that the vector $\{d_n\}$ can be obtained by multiplying the nodal displacement vector $\{d_e\}$ by a matrix $[\Lambda]$ containing the shape functions and their derivatives with respect to the natural coordinates. Thus

$$\{d_n\} = [\Lambda]\{d_e\} \quad (2.17)$$

where $[\Lambda]$ is 20×40 matrix and $\{d_e\}$ is given by

$$\{d_e\} = [u_1 \quad v_1 \quad w_1 \quad \alpha_1 \quad \beta_1 \cdots \cdots u_8 \quad v_8 \quad w_8 \quad \alpha_8 \quad \beta_8]^T \quad (2.18)$$

Combining equations (2.11), (2.14) and (2.17), one has

$$\{\varepsilon\} = [H]\{d_c\} = [H][J]^{-1}\{d_n\} = [H][J]^{-1}[\Lambda]\{d_e\} = [B]\{d_e\} \quad (2.19)$$

where $[B]$ is called the strain-displacement matrix and is expressed as

$$[B] = [H][J]^{-1}[\Lambda]$$

Twist angle of the shell is defined in terms of length (L) and curvature of twist (R_{xy}) as

$$\tan \Phi = -L / R_{xy} \quad (2.20)$$

2.2.4 Force-Strain Relationships

Force and moment resultants are obtained from the stresses as

$$\{F_e\} = \begin{Bmatrix} N_x \\ N_y \\ N_{xy} \\ M_x \\ M_y \\ M_{xy} \\ Q_{xz} \\ Q_{yz} \end{Bmatrix} = \int_{-h/2}^{h/2} \begin{Bmatrix} \sigma_x \\ \sigma_y \\ \tau_{xy} \\ \sigma_x z \\ \sigma_y z \\ \tau_{xy} z \\ \tau_{xz} \\ \tau_{yz} \end{Bmatrix} dz \quad (2.21)$$

where σ_x and σ_y are the normal stresses along X and Y directions, respectively and τ_{xy} , τ_{xz} and τ_{yz} are shear stresses in XY, XZ and YZ planes, respectively. Thickness of the shell is denoted by h .

A macro-mechanical analysis is required to establish the relationship between the forces and strains. The shell thickness is assumed to be made of a composite laminate which, in turn, may consist of a number of thin laminae. The principal material axes are indicated by 1 and 2 and the

moduli of elasticity of a lamina along these two directions are E_1 and E_2 , respectively and G_{12} , G_{23} and G_{13} be the shear moduli of the lamina along the subscripted directions.

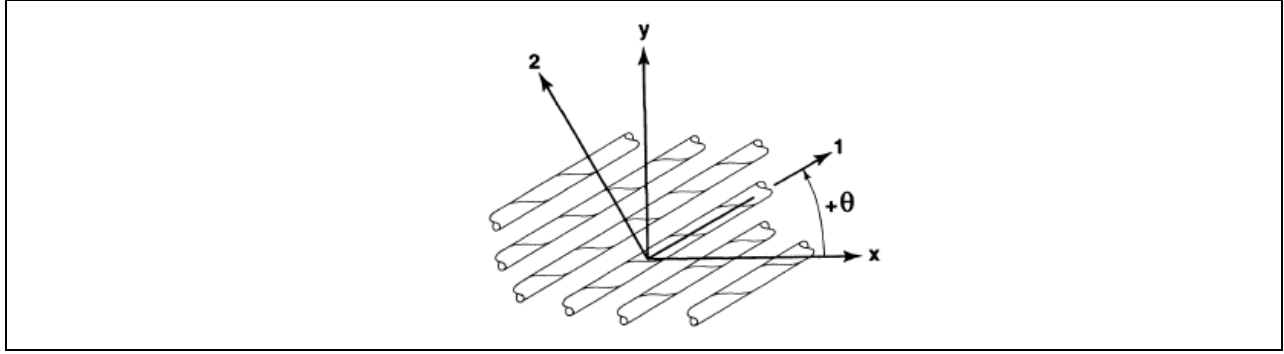


Figure 2.3 Fiber orientation of a shell lamina

Neglecting the normal stress perpendicular to the plane of the lamina, the stress-strain relations, in the principal material directions are given by

$$\begin{bmatrix} \sigma_1 \\ \sigma_2 \\ \tau_{12} \end{bmatrix} = \begin{bmatrix} Q_{11} & Q_{12} & 0 \\ Q_{12} & Q_{22} & 0 \\ 0 & 0 & Q_{66} \end{bmatrix} \begin{bmatrix} \varepsilon_1 \\ \varepsilon_2 \\ \varepsilon_3 \end{bmatrix} \quad (2.22)$$

$$\begin{bmatrix} \tau_{13} \\ \tau_{23} \end{bmatrix} = \begin{bmatrix} Q_{44} & 0 \\ 0 & Q_{55} \end{bmatrix} \begin{bmatrix} \gamma_{13} \\ \gamma_{23} \end{bmatrix} \quad (2.23)$$

where, $Q_{11} = \frac{E_1}{(1-\nu_{12}\nu_{21})}$, $Q_{22} = \frac{E_2}{(1-\nu_{12}\nu_{21})}$, $Q_{12} = \frac{\nu_{12}E_2}{(1-\nu_{12}\nu_{21})}$ and

$Q_{44} = G_{13}$, $Q_{55} = G_{23}$, $Q_{66} = G_{12}$ and $\nu_{21} = \frac{E_2}{E_1}\nu_{12}$.

Appropriate transformation is required in order to obtain the elastic constant matrices corresponding to arbitrary principle axes (X-Y) with which the material principle axes make an angle θ as shown in Fig. 2.3. Thus the off-axis elastic constant matrix is obtained from the on-axis elastic constant matrices.

$$\begin{aligned} [\bar{Q}_{ij}] &= \begin{bmatrix} \bar{Q}_{11} & \bar{Q}_{12} & \bar{Q}_{16} \\ \bar{Q}_{12} & \bar{Q}_{22} & \bar{Q}_{26} \\ \bar{Q}_{16} & \bar{Q}_{26} & \bar{Q}_{66} \end{bmatrix} \\ &= \begin{bmatrix} m^2 & n^2 & -2mn \\ n^2 & m^2 & 2mn \\ mn & -mn & m^2 - n^2 \end{bmatrix} \begin{bmatrix} Q_{11} & Q_{12} & 0 \\ Q_{12} & Q_{22} & 0 \\ 0 & 0 & Q_{66} \end{bmatrix} \begin{bmatrix} m^2 & n^2 & mn \\ n^2 & m^2 & -mn \\ -2mn & 2mn & m^2 - n^2 \end{bmatrix} \end{aligned} \quad (2.24)$$

where $m = \cos \theta$ and $n = \sin \theta$

Similarly, the following off-axis elastic constant for the transverse shear stresses can be obtained.

$$[\bar{Q}_{ij}] = \begin{bmatrix} \bar{Q}_{44} & \bar{Q}_{45} \\ \bar{Q}_{45} & \bar{Q}_{55} \end{bmatrix} \quad (2.25)$$

where

$$\left. \begin{aligned} \bar{Q}_{44} &= Q_{44}m^2 + Q_{55}n^2 \\ \bar{Q}_{45} &= (Q_{44} - Q_{55})mn \\ \bar{Q}_{55} &= Q_{44}n^2 + Q_{55}m^2 \end{aligned} \right\} \quad (2.26)$$

The stress-strain relations of the lamina, with respect to the x, y and z axes are expressed as

$$\begin{Bmatrix} \sigma_x \\ \sigma_y \\ \tau_{xy} \\ \tau_{xz} \\ \tau_{yz} \end{Bmatrix} = \begin{bmatrix} \bar{Q}_{11} & \bar{Q}_{12} & \bar{Q}_{16} & 0 & 0 \\ \bar{Q}_{21} & \bar{Q}_{22} & \bar{Q}_{26} & 0 & 0 \\ \bar{Q}_{16} & \bar{Q}_{26} & \bar{Q}_{66} & 0 & 0 \\ 0 & 0 & 0 & k_s \bar{Q}_{44} & k_s \bar{Q}_{45} \\ 0 & 0 & 0 & k_s \bar{Q}_{45} & k_s \bar{Q}_{55} \end{bmatrix} \begin{Bmatrix} \varepsilon_x \\ \varepsilon_y \\ \gamma_{xy} \\ \gamma_{xz} \\ \gamma_{yz} \end{Bmatrix} \quad (2.27)$$

where k_s is the shear correction factor to account for parabolic variation of the transverse shear strains and is approximately taken as 5/6.

Since the laminate consists of number of laminae, the total stress resultants for an nl -layered laminate are expressed as

$$\begin{Bmatrix} N_x \\ N_y \\ N_{xy} \end{Bmatrix} = \sum_{k=1}^{nl} \begin{bmatrix} \bar{Q}_{11} & \bar{Q}_{12} & \bar{Q}_{16} \\ \bar{Q}_{12} & \bar{Q}_{22} & \bar{Q}_{26} \\ \bar{Q}_{16} & \bar{Q}_{26} & \bar{Q}_{66} \end{bmatrix} \left\{ \int_{z_{k-1}}^{z_k} \begin{Bmatrix} \varepsilon_x^0 \\ \varepsilon_y^0 \\ \gamma_{xy}^0 \end{Bmatrix} dz + \int_{z_{k-1}}^{z_k} \begin{Bmatrix} \kappa_x \\ \kappa_y \\ \kappa_{xy} \end{Bmatrix} z dz \right\} \quad (2.28)$$

$$\begin{Bmatrix} M_x \\ M_y \\ M_{xy} \end{Bmatrix} = \sum_{k=1}^{nl} \begin{bmatrix} \bar{Q}_{11} & \bar{Q}_{12} & \bar{Q}_{16} \\ \bar{Q}_{12} & \bar{Q}_{22} & \bar{Q}_{26} \\ \bar{Q}_{16} & \bar{Q}_{26} & \bar{Q}_{66} \end{bmatrix} \left\{ \int_{z_{k-1}}^{z_k} \begin{Bmatrix} \varepsilon_x^0 \\ \varepsilon_y^0 \\ \gamma_{xy}^0 \end{Bmatrix} z dz + \int_{z_{k-1}}^{z_k} \begin{Bmatrix} \kappa_x \\ \kappa_y \\ \kappa_{xy} \end{Bmatrix} z^2 dz \right\} \quad (2.29)$$

$$\begin{Bmatrix} Q_{xz} \\ Q_{yz} \end{Bmatrix} = \sum_{k=1}^{nl} \begin{bmatrix} k_s \bar{Q}_{44} & k_s \bar{Q}_{45} \\ k_s \bar{Q}_{45} & k_s \bar{Q}_{55} \end{bmatrix} \left\{ \int_{z_{k-1}}^{z_k} \begin{Bmatrix} \gamma_{xz}^0 \\ \gamma_{yz}^0 \end{Bmatrix} dz \right\} \quad (2.30)$$

Combining the above relations (Eqs. 2.28, 2.29 and 2.30), the in-plane stress resultants $\{N\}$, the moments resultants $\{M\}$, and the transverse shear resultants $\{Q\}$, are related to the mid-plane strains and curvatures for a general laminated shell element is given by

$$\begin{Bmatrix} N_x \\ N_y \\ N_{xy} \\ M_x \\ M_y \\ M_{xy} \\ Q_{xz} \\ Q_{yz} \end{Bmatrix} = \begin{bmatrix} A_{11} & A_{12} & A_{16} & B_{11} & B_{12} & B_{16} & 0 & 0 \\ A_{12} & A_{22} & A_{26} & B_{12} & B_{22} & B_{26} & 0 & 0 \\ A_{16} & A_{26} & A_{66} & B_{16} & B_{26} & B_{66} & 0 & 0 \\ B_{11} & B_{12} & B_{16} & D_{11} & D_{12} & D_{16} & 0 & 0 \\ B_{12} & B_{22} & B_{26} & D_{12} & D_{22} & D_{26} & 0 & 0 \\ B_{16} & B_{26} & B_{66} & D_{16} & D_{26} & D_{66} & 0 & 0 \\ 0 & 0 & 0 & 0 & 0 & 0 & S_{44} & S_{45} \\ 0 & 0 & 0 & 0 & 0 & 0 & S_{45} & S_{55} \end{bmatrix} \begin{Bmatrix} \varepsilon_x^0 \\ \varepsilon_y^0 \\ \gamma_{xy}^0 \\ \kappa_x \\ \kappa_y \\ \kappa_{xy} \\ \gamma_{xz}^0 \\ \gamma_{yz}^0 \end{Bmatrix} \quad (2.31)$$

where, $(A_{ij}, B_{ij}, D_{ij}) = \sum_{k=1}^{nl} \int_{z_{k-1}}^{z_k} (\bar{Q}_{ij})_k (1, z, z^2) dz, \quad i, j = 1, 2, 6$

and $(S_{ij}) = k_s \sum_{k=1}^{nl} \int_{z_{k-1}}^{z_k} (\bar{Q}_{ij})_k dz, \quad i, j = 4, 5$

in which, z_k and z_{k-1} , are the distances measured from the mid-surface of a laminate to the bottom of the k th and $(k-1)$ th laminae $(\bar{Q}_{ij})_k$ is the element corresponding to i th row and j th column of the off-axis elastic constant matrix for the k th lamina.

Equation (2.31) is expressed in compact form as

$$\{F\} = [D]\{\varepsilon\} \quad (2.32)$$

2.2.5 Generalized Inertia Matrix

The generalized inertia matrix per unit area includes the translatory and rotary inertia terms. Mass and moment of inertia are the measures of translatory and rotary inertial resistances, respectively and are given by the following equations.

Mass per unit area is denoted by m and is given by

$$m = \sum_{k=1}^{nl} (z_k - z_{k-1}) \rho_k \quad (2.33)$$

where ρ is mass density of shell.

Moment of inertia per unit area is denoted by I and is given by

$$I = \frac{1}{3} \sum_{k=1}^{nl} (z_k^3 - z_{k-1}^3) \rho_k \quad (2.34)$$

Incorporating both the translatory and rotary inertia terms, the generalized inertia matrix $[m]$ takes the following form,

$$[m] = \begin{bmatrix} m & 0 & 0 & 0 & 0 \\ 0 & m & 0 & 0 & 0 \\ 0 & 0 & m & 0 & 0 \\ 0 & 0 & 0 & I & 0 \\ 0 & 0 & 0 & 0 & I \end{bmatrix} \quad (2.35)$$

2.3 STIFFENER ELEMENT

Curved beams of rectangular sections are considered for the stiffeners with constant width and depth made of laminated composite linearly elastic material. Stiffeners are oriented along X- and/or Y-directions. Stiffeners oriented along X- and Y-directions are called as the x- and y-directional stiffeners, respectively. The radius of curvature of the x-directional stiffener is R_x and that of the y-directional stiffener is R_y . The following steps are involved for the formulation of element matrices of the beam element.

An isoparametric curved three-noded beam element is chosen with two end nodes and one middle node to model the stiffeners. The isoparametric beam elements are oriented in natural coordinate system along ξ or η parallel to the global X or Y axes, respectively.

2.3.1 Shape Functions

The shape functions of three noded curved isoparametric beam elements for the x- and y-directional stiffeners as shown in Fig. 2.4 are taken as considered by Deb and Booton (1988) and are expressed as follows:

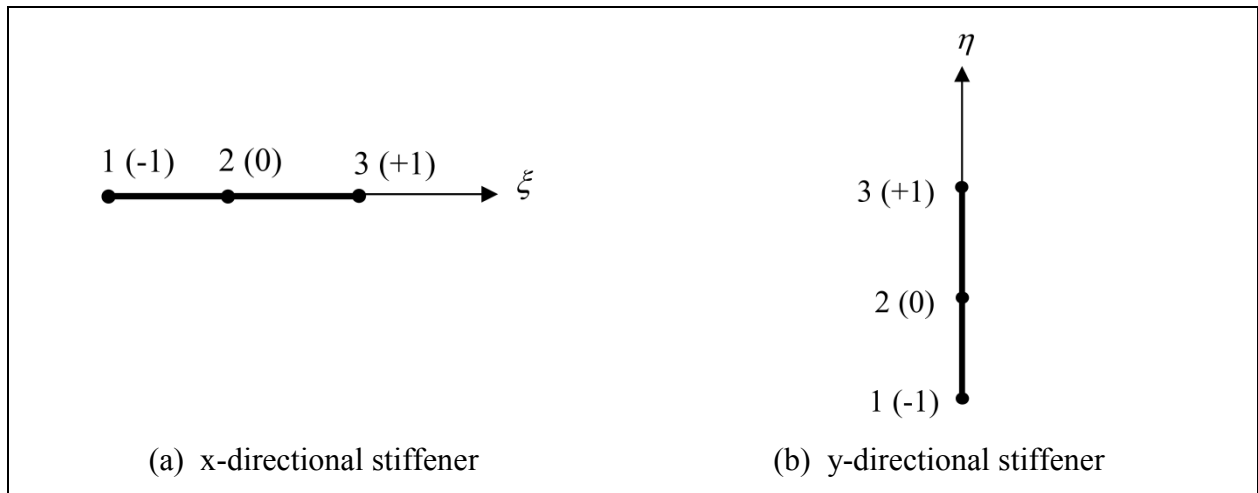


Figure 2.4 Three-noded isoparametric stiffener element

For x-directional stiffeners,

$$\left. \begin{aligned} N_i^{sx} &= 0.5\xi\xi_i(1 + \xi\xi_i) & \text{for } i = 1, 3 \\ N_i^{sx} &= (1 + \xi^2) & \text{for } i = 2 \end{aligned} \right\} \quad (2.36)$$

For y-directional stiffeners,

$$\left. \begin{aligned} N_i^{sy} &= 0.5\eta\eta_i(1 + \eta\eta_i) & \text{for } i = 1, 3 \\ N_i^{sy} &= (1 + \eta^2) & \text{for } i = 2 \end{aligned} \right\} \quad (2.37)$$

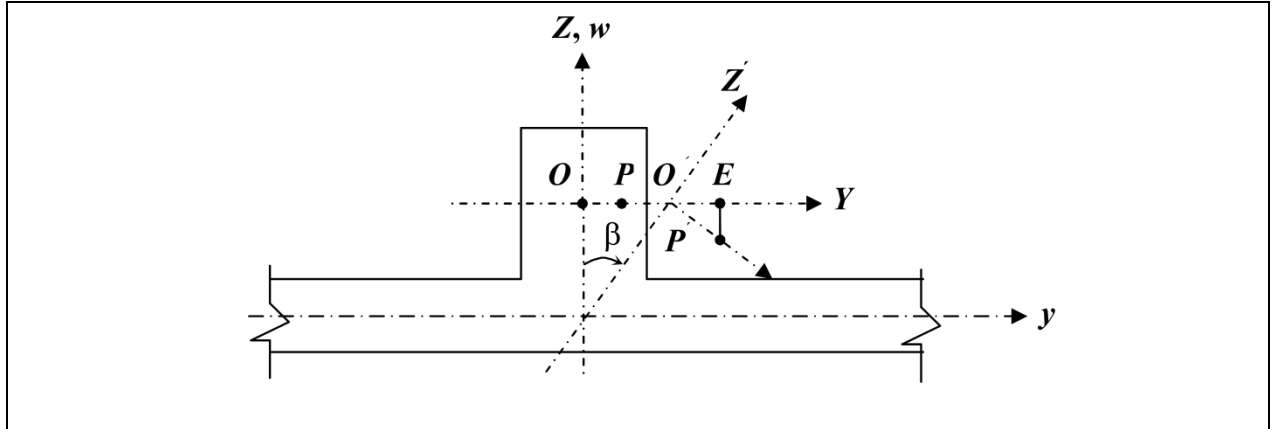
Since, the generalized displacements and coordinates are interpolated from their nodal values in an isoparametric formulation, the X-coordinate for the x-directional stiffener and Y-coordinate for the y-directional stiffener of any point within an element are obtained as

$$x = \sum N_i^{sx} x_i \quad i = 1, 2, 3 \quad (2.38)$$

$$y = \sum N_i^{sy} y_i \quad i = 1, 2, 3 \quad (2.39)$$

2.3.2 Generalized Displacement Fields and Nodal Degrees of Freedom

In the beam elements, each node has four degrees of freedom, u^{sx} , w^{sx} , α^{sx} and β^{sx} for x-directional stiffeners and v^{sy} , w^{sy} , α^{sy} and β^{sy} for y-directional stiffeners.



$$EP' = O'P'\beta = OP\beta_{sx} = y\beta_{sx}$$

Figure 2.5 Vertical displacement of x-directional stiffener on account of shell rotation.

The generalized displacement field of the x-directional stiffeners is of the following form:

$$\begin{Bmatrix} U^{sx} \\ V^{sx} \\ W^{sx} \end{Bmatrix} = \begin{Bmatrix} u^{sx} + z\alpha^{sx} \\ z\beta^{sx} \\ w^{sx} - y\beta^{sx} \end{Bmatrix} \quad (2.40)$$

where U^{sx} , V^{sx} and W^{sx} are the generalized displacements along X-, Y- and Z-directions at any point within the x-directional stiffener element, and u^{sx} and w^{sx} are those at the mid-plane of the x-directional stiffeners. α^{sx} and β^{sx} are the rotations of the normal to the undeformed mid-plane

of the x-directional stiffeners along X- and Y-directions, respectively. The vertical displacement of the x-directional stiffeners due to torsional rotation of the shell is shown in Fig. 2.5. The generalized displacement field is a function of x only. Hence derivatives of its components with respect to Y and Z axes do not exist.

Similarly, the generalized displacement field of the y-directional stiffeners is expressed as

$$\begin{Bmatrix} U^{sy} \\ V^{sy} \\ W^{sy} \end{Bmatrix} = \begin{Bmatrix} z\alpha^{sy} \\ v^{sy} + z\beta^{sy} \\ w^{sy} - x\alpha^{sy} \end{Bmatrix} \quad (2.41)$$

where U^{sy} , V^{sy} and W^{sy} are the generalized displacements along X-, Y- and Z-directions at any point within the y-directional stiffener element, and v^{sy} and w^{sy} are those at the mid-plane of the y-directional stiffener. α^{sy} and β^{sy} are the rotations of the normal to the undeformed mid-plane of the y-directional stiffeners along X- and Y-directions, respectively. The generalized displacement field is function of y only. Hence derivatives of its components with respect to X and Z axes do not exist.

The generalized displacement vector of the x-directional stiffener element is expressed in terms of the shape functions and nodal degrees freedom as

$$\{\delta^{sx}\} = \begin{Bmatrix} u^{sx} \\ w^{sx} \\ \alpha^{sx} \\ \beta^{sx} \end{Bmatrix} = \sum_{i=1}^3 \begin{bmatrix} N_i^{sx} & & & \\ & N_i^{sx} & & \\ & & N_i^{sx} & \\ & & & N_i^{sx} \end{bmatrix} \begin{Bmatrix} u_i^{sx} \\ w_i^{sx} \\ \alpha_i^{sx} \\ \beta_i^{sx} \end{Bmatrix} \quad (2.42)$$

which can be written in a compact form as

$$\{\delta^{sx}\} = [N^{sx}] \{d_e^{sx}\} \quad (2.43)$$

where $[N^{sx}]$ is the shape function matrix of the x-directional stiffener element.

Similarly, the generalized displacement vector of the y-directional stiffener element is expressed in a compact form as

$$\{\delta^{sy}\} = [N^{sy}] \{d_e^{sy}\} \quad (2.44)$$

where
$$\{\delta^{sy}\} = [v^{sy} \quad w^{sy} \quad \alpha^{sy} \quad \beta^{sy}]^T \quad (2.45)$$

$$\{d_e^{sy}\} = [v_1^{sy} \quad w_1^{sy} \quad \alpha_1^{sy} \quad \beta_1^{sy} \dots v_3^{sy} \quad w_3^{sy} \quad \alpha_3^{sy} \quad \beta_3^{sy}]^T \quad (2.46)$$

and $[N^{sy}]$ is the shape function matrix of the y-directional stiffener element.

2.3.3 Strain-Displacement Equations

The strain-displacement equations of the x- or y-directional stiffeners can be derived from the generalized displacement fields of the respective stiffeners. The strain components of the x-directional stiffeners considered are

$$\begin{Bmatrix} \varepsilon_x^{sx} \\ \gamma_{xy}^{sx} \\ \gamma_{xz}^{sx} \end{Bmatrix} = \begin{Bmatrix} \frac{\partial U^{sx}}{\partial x} \\ \frac{\partial U^{sx}}{\partial y} + \frac{\partial V^{sx}}{\partial x} \\ \frac{\partial U^{sx}}{\partial z} + \frac{\partial W^{sx}}{\partial x} \end{Bmatrix} = \begin{Bmatrix} \frac{\partial u^{sx}}{\partial x} + \frac{w^{sx}}{R_x} + z \frac{\partial \alpha^{sx}}{\partial x} \\ z \frac{\partial \beta^{sx}}{\partial x} \\ \alpha^{sx} + \frac{\partial w^{sx}}{\partial x} - y \frac{\partial \beta^{sx}}{\partial x} \end{Bmatrix} \quad (2.47)$$

The components of the above strain vector can be rearranged in terms of strain components of the stiffener mid-surface and changes of stiffener curvature due to loading to obtain the generalized strain vector so as to maintain compatibility with the force vector (given in the next section).

Thus the generalized strain components of the x-directional stiffeners are given by

$$\{\varepsilon^{sx}\} = \begin{Bmatrix} \varepsilon_x^{sx0} \\ k_x^{sx} \\ k_{xy}^{sx} \\ \gamma_{xz}^{sx} \end{Bmatrix} = \begin{Bmatrix} \frac{\partial u^{sx}}{\partial x} + \frac{w^{sx}}{R_x} \\ \frac{\partial \alpha^{sx}}{\partial x} \\ \frac{\partial \beta^{sx}}{\partial x} \\ \alpha^{sx} + \frac{\partial w^{sx}}{\partial x} \end{Bmatrix} = \sum_{i=1}^3 \begin{bmatrix} N_{i,x}^{sx} & \frac{N_i^{sx}}{R_x} & 0 & 0 \\ 0 & 0 & N_{i,x}^{sx} & 0 \\ 0 & 0 & 0 & N_{i,x}^{sx} \\ 0 & N_{i,x}^{sx} & N_i^{sx} & 0 \end{bmatrix} \begin{Bmatrix} u_i^{sx} \\ w_i^{sx} \\ \alpha_i^{sx} \\ \beta_i^{sx} \end{Bmatrix} \quad (2.48)$$

where subscript (,) denotes partial differentiation.

Derivatives with respect to x cannot be obtained directly. Hence these are obtained from the derivatives with respect to ξ as follows.

$$\frac{\partial N_i^{sx}}{\partial x} = \frac{\partial N_i^{sx}}{\partial \xi} \times \frac{\partial \xi}{\partial x} = \frac{1}{J^{sx}} \times \frac{\partial N_i^{sx}}{\partial \xi} \quad (2.49)$$

Where J^{sx} is the Jacobian of transformation for the x-stiffener and is given as

$$[J^{sx}] = \frac{\partial x}{\partial \xi} \quad (2.50)$$

The strain-displacement relationships of the x-directional stiffener given in Eq. (2.48) is written in a compact form as

$$\{\boldsymbol{\varepsilon}^{sx}\} = [B^{sx}] \{d_e^{sx}\} \quad (2.51)$$

The strain components of the y-directional stiffener considered are

$$\begin{Bmatrix} \varepsilon_y^{sy} \\ \gamma_{yx}^{sy} \\ \gamma_{yz}^{sy} \end{Bmatrix} = \begin{Bmatrix} \frac{\partial V^{sy}}{\partial y} \\ \frac{\partial V^{sy}}{\partial x} + \frac{\partial U^{sy}}{\partial y} \\ \frac{\partial V^{sy}}{\partial z} + \frac{\partial W^{sy}}{\partial y} \end{Bmatrix} = \begin{Bmatrix} \frac{\partial v^{sy}}{\partial y} + \frac{w^{sy}}{R_y} + z \frac{\partial \beta^{sy}}{\partial y} \\ z \frac{\partial \alpha^{sy}}{\partial y} \\ \alpha^{sy} + \frac{\partial w^{sy}}{\partial y} - x \frac{\partial \alpha^{sy}}{\partial y} \end{Bmatrix} \quad (2.52)$$

Rearranging the above the generalized strain components of the y-directional stiffener are given by

$$\{\boldsymbol{\varepsilon}^{sy}\} = \begin{Bmatrix} \varepsilon_y^{sy} \\ k_y^{sy} \\ k_{xy}^{sy} \\ \gamma_{yz}^{sy} \end{Bmatrix} = \begin{Bmatrix} \frac{\partial v^{sy}}{\partial y} + \frac{w^{sy}}{R_y} \\ \frac{\partial \beta^{sy}}{\partial y} \\ \frac{\partial \alpha^{sy}}{\partial y} \\ \beta^{sy} + \frac{\partial w^{sy}}{\partial y} \end{Bmatrix} = \sum_{i=1}^3 \begin{bmatrix} N_{i,y}^{sy} & \frac{N_i^{sy}}{R_y} & 0 & 0 \\ 0 & 0 & 0 & N_{i,y}^{sy} \\ 0 & 0 & N_{i,y}^{sy} & 0 \\ 0 & N_{i,y}^{sy} & 0 & N_i^{sy} \end{bmatrix} \begin{Bmatrix} u_i^{sy} \\ w_i^{sy} \\ \alpha_i^{sy} \\ \beta_i^{sy} \end{Bmatrix} \quad (2.53)$$

Derivatives with respect to y cannot be obtained directly. Hence these are obtained from the derivatives with respect to η as follows:

$$\frac{\partial N_i^{sy}}{\partial y} = \frac{\partial N_i^{sy}}{\partial \eta} \times \frac{\partial \eta}{\partial y} = \frac{1}{J^{sy}} \times \frac{\partial N_i^{sy}}{\partial \eta} \quad (2.54)$$

Where J^{sy} is the Jacobian of transformation for the y-stiffener and is given as

$$[J^{sy}] = \frac{\partial y}{\partial \eta} \quad (2.55)$$

The strain-displacement relationships of the y-directional stiffeners given in Eq. (2.53) can be written in a compact form as

$$\{\boldsymbol{\varepsilon}^{sy}\} = [B^{sy}] \{d_e^{sy}\} \quad (2.56)$$

2.3.4 Force-Strain Relationships

The stress resultants of the x-and y-directional stiffeners obtained from the stresses developed in the cross-section of the respective stiffeners as shown in Fig. 2.6 are given below.

For the x-directional stiffeners,

$$\begin{Bmatrix} N_x^{sx} \\ M_x^{sx} \\ T_x^{sx} \\ Q_{xz}^{sx} \end{Bmatrix} = \left(d_{st} + \frac{h}{2} \right) \int_{-\frac{b_{st}}{2}}^{+\frac{b_{st}}{2}} \begin{Bmatrix} \sigma_x^{sx} \\ \sigma_x^{sx} z \\ (\tau_{xy}^{sx} z - \tau_{xz}^{sx} z) \\ \tau_{xz}^{sx} \end{Bmatrix} dy dz \quad (2.57)$$

For the y-directional stiffeners,

$$\begin{Bmatrix} N_y^{sy} \\ M_y^{sy} \\ T_y^{sy} \\ Q_{yz}^{sy} \end{Bmatrix} = \left(d_{st} + \frac{h}{2} \right) \int_{-\frac{b_{st}}{2}}^{+\frac{b_{st}}{2}} \begin{Bmatrix} \sigma_y^{sy} \\ \sigma_y^{sy} z \\ (\tau_{yx}^{sy} z - \tau_{yz}^{sy} z) \\ \tau_{yz}^{sy} \end{Bmatrix} dx dz \quad (2.58)$$

where σ_x^{sx} is the normal stress along X axis and τ_{xy}^{sx} and τ_{xz}^{sx} are shear stresses in YZ plane along Y and Z axes, respectively, of the x-directional stiffeners. Similarly, σ_y^{sy} is the normal stress along Y axis and τ_{yx}^{sy} and τ_{yz}^{sy} are shear stresses in XZ plane along X and Z axes, respectively of the y-directional stiffeners.

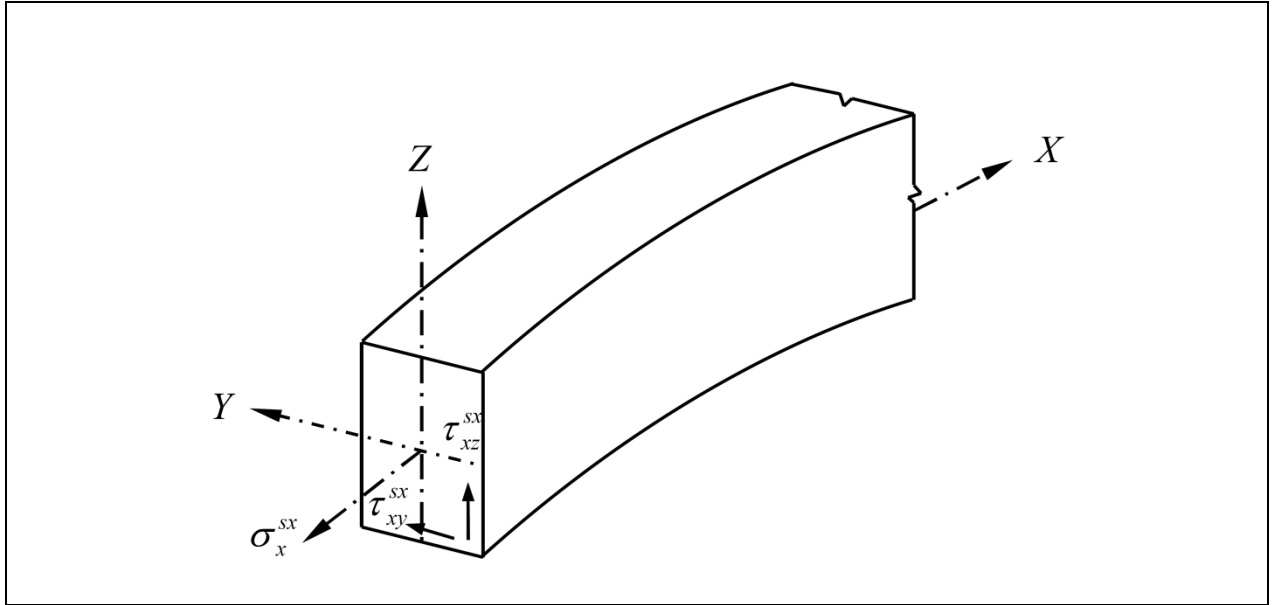


Figure 2.6 Stresses in x-directional stiffener cross-section.

The stress-strain relations of the stiffeners are obtained by a macro-mechanical analysis as in the case of the laminated shells. The depth of the stiffeners is made of composite laminate consisting of a number of laminae. The principal material axes are indicated by 1 and 2 and moduli of Elasticity of a lamina along these two directions are E_1 and E_2 respectively as in case of

laminated shells. θ is the angle that the major material principal axis of a lamina of the x- or y-stiffeners makes with their longitudinal axes.

In a similar way as in case of laminated shell the stress-strain relationships of a lamina of the x-stiffener are obtained by omitting the normal stress and strain along y-axis and are given by

$$\begin{Bmatrix} \sigma_x^{sx} \\ \tau_{xy}^{sx} \\ \tau_{xz}^{sx} \end{Bmatrix} = \begin{bmatrix} \bar{Q}_{11}^{sx} & \bar{Q}_{16}^{sx} & 0 \\ \bar{Q}_{16}^{sx} & \bar{Q}_{66}^{sx} & 0 \\ 0 & 0 & k_s^{sx} \bar{Q}_{44}^{sx} \end{bmatrix} \begin{Bmatrix} \epsilon_x^{sx} \\ \gamma_{xy}^{sx} \\ \gamma_{xz}^{sx} \end{Bmatrix} = \begin{bmatrix} \bar{Q}_{11}^{sx} & \bar{Q}_{16}^{sx} & 0 \\ \bar{Q}_{16}^{sx} & \bar{Q}_{66}^{sx} & 0 \\ 0 & 0 & k_s^{sx} \bar{Q}_{44}^{sx} \end{bmatrix} \begin{Bmatrix} \frac{\partial u^{sx}}{\partial x} + \frac{w^{sx}}{R_x} + z \frac{\partial \alpha^{sx}}{\partial x} \\ z \frac{\partial \beta^{sx}}{\partial x} \\ \alpha^{sx} + \frac{\partial w^{sx}}{\partial x} - y \frac{\partial \beta^{sx}}{\partial x} \end{Bmatrix} \quad (2.59)$$

where \bar{Q}_{11}^{sx} , \bar{Q}_{16}^{sx} , \bar{Q}_{66}^{sx} and \bar{Q}_{44}^{sx} are the off-axis elastic constants of a lamina of the x-directional stiffener and are obtained in a similar manner as in case of laminated shell. k_s^{sx} is the shear correction factor to account for parabolic variation of the transverse strains and is approximately taken as 5/6.

Since the laminate of the x-directional stiffener consists of a number of laminae, the total stress resultants for a nlx layered laminate are expressed as

$$\begin{aligned} N_x^{sx} &= \sum_{k=1}^{nlx} \int_{-\frac{b_{st}}{2}}^{\frac{b_{st}}{2}} \int_{z_{k-1}}^{z_k} \sigma_x^{sx} dy dz \\ &= \sum_{k=1}^{nlx} \int_{-\frac{b_{st}}{2}}^{\frac{b_{st}}{2}} \int_{z_{k-1}}^{z_k} \bar{Q}_{11}^{sx} \left(\frac{\partial u^{sx}}{\partial x} + \frac{w^{sx}}{R_x} + z \frac{\partial \alpha^{sx}}{\partial x} \right) dy dz + \sum_{k=1}^{nlx} \int_{-\frac{b_{st}}{2}}^{\frac{b_{st}}{2}} \int_{z_{k-1}}^{z_k} \bar{Q}_{16}^{sx} z \frac{\partial \beta^{sx}}{\partial x} dy dz \\ &= A_{11}^{sx} b_{st} \left(\frac{\partial u^{sx}}{\partial x} + \frac{w^{sx}}{R_x} \right) + B_{11}^{sx} b_{st} \left(\frac{\partial \alpha^{sx}}{\partial x} \right) + B_{16}^{sx} b_{st} \left(\frac{\partial \beta^{sx}}{\partial x} \right) \end{aligned} \quad (2.60)$$

$$\begin{aligned} M_x^{sx} &= \sum_{k=1}^{nlx} \int_{-\frac{b_{st}}{2}}^{\frac{b_{st}}{2}} \int_{z_{k-1}}^{z_k} \sigma_x^{sx} z dy dz \\ &= \sum_{k=1}^{nlx} \int_{-\frac{b_{st}}{2}}^{\frac{b_{st}}{2}} \int_{z_{k-1}}^{z_k} \bar{Q}_{11}^{sx} \left(\frac{\partial u^{sx}}{\partial x} + \frac{w^{sx}}{R_x} + z \frac{\partial \alpha^{sx}}{\partial x} \right) z dy dz + \sum_{k=1}^{nlx} \int_{-\frac{b_{st}}{2}}^{\frac{b_{st}}{2}} \int_{z_{k-1}}^{z_k} \bar{Q}_{16}^{sx} z^2 \frac{\partial \beta^{sx}}{\partial x} dy dz \end{aligned}$$

$$= B_{11}^{sx} b_{st} \left(\frac{\partial u^{sx}}{\partial x} + \frac{w^{sx}}{R_x} \right) + D_{11}^{sx} b_{st} \left(\frac{\partial \alpha^{sx}}{\partial x} \right) + D_{16}^{sx} b_{st} \left(\frac{\partial \beta^{sx}}{\partial x} \right) \quad (2.61)$$

$$\begin{aligned} T_x^{sx} &= \sum_{k=1}^{nlx} \int_{-\frac{b_{st}}{2}}^{\frac{b_{st}}{2}} \int_{z_{k-1}}^{z_k} (\tau_{xy}^{sx} z - \tau_{xz}^{sx} y) dy dz \\ &= \sum_{k=1}^{nlx} \int_{-\frac{b_{st}}{2}}^{\frac{b_{st}}{2}} \int_{z_{k-1}}^{z_k} \bar{Q}_{16}^{sx} \left(\frac{\partial u^{sx}}{\partial x} + \frac{w^{sx}}{R_x} + z \frac{\partial \alpha^{sx}}{\partial x} \right) z dy dz + \sum_{k=1}^{nlx} \int_{-\frac{b_{st}}{2}}^{\frac{b_{st}}{2}} \int_{z_{k-1}}^{z_k} \bar{Q}_{66}^{sx} z^2 \left(\frac{\partial \beta^{sx}}{\partial x} \right) dy dz \\ &\quad - \sum_{k=1}^{nlx} \int_{-\frac{b_{st}}{2}}^{\frac{b_{st}}{2}} \int_{z_{k-1}}^{z_k} k_s^{sx} \bar{Q}_{44}^{sx} y \left(\alpha^{sx} + \frac{\partial w^{sx}}{\partial x} - y \frac{\partial \beta^{sx}}{\partial x} \right) dy dz \\ &= \sum_{k=1}^{nlx} \int_{-\frac{b_{st}}{2}}^{\frac{b_{st}}{2}} \int_{z_{k-1}}^{z_k} \bar{Q}_{16}^{sx} \left(\frac{\partial u^{sx}}{\partial x} + \frac{w^{sx}}{R_x} \right) z dy dz + \sum_{k=1}^{nlx} \int_{-\frac{b_{st}}{2}}^{\frac{b_{st}}{2}} \int_{z_{k-1}}^{z_k} \bar{Q}_{16}^{sx} z^2 \left(\frac{\partial \alpha^{sx}}{\partial x} \right) dy dz \\ &\quad + \sum_{k=1}^{nlx} \int_{-\frac{b_{st}}{2}}^{\frac{b_{st}}{2}} \int_{z_{k-1}}^{z_k} (\bar{Q}_{66}^{sx} z^2 + k_s^{sx} \bar{Q}_{44}^{sx} y^2) \left(\frac{\partial \beta^{sx}}{\partial x} \right) dy dz - \sum_{k=1}^{nlx} \int_{-\frac{b_{st}}{2}}^{\frac{b_{st}}{2}} \int_{z_{k-1}}^{z_k} k_s^{sx} \bar{Q}_{44}^{sx} \left(\alpha^{sx} + \frac{\partial w^{sx}}{\partial x} \right) dy dz \end{aligned} \quad (2.62)$$

The last integration term in the above equation is zero for a symmetric cross-section. However, it is generally treated as zero for any cross section. The third term is interpreted as the torsional rigidity of the x- directional stiffener cross-section and expressed approximately as $\frac{1}{6}(\bar{Q}_{66}^{sx} + \bar{Q}_{44}^{sx})d_{st}b_{st}^3$, where d_{st} is the depth and b_{st} is the width of the stiffeners. Hence the equation becomes

$$T_x^{sx} = B_{16}^{sx} b_{st} \left(\frac{\partial u^{sx}}{\partial x} + \frac{w^{sx}}{R_x} \right) + D_{16}^{sx} b_{st} \left(\frac{\partial \alpha^{sx}}{\partial x} \right) + \frac{1}{6}(\bar{Q}_{66}^{sx} + \bar{Q}_{44}^{sx})d_{st}b_{st}^3 \left(\frac{\partial \beta^{sx}}{\partial x} \right) \quad (2.63)$$

$$\begin{aligned}
Q_{xz}^{sx} &= \sum_{k=1}^{nlx} \int_{-\frac{b_{st}}{2}}^{\frac{b_{st}}{2}} \int_{z_{k-1}}^{z_k} \tau_x^{sx} dy dz = \sum_{k=1}^{nlx} \int_{-\frac{b_{st}}{2}}^{\frac{b_{st}}{2}} \int_{z_{k-1}}^{z_k} k_s^{sx} \bar{Q}_{44}^{sx} \left(\alpha^{sx} + \frac{\partial w^{sx}}{\partial x} - y \frac{\partial \beta^{sx}}{\partial x} \right) dy dz \\
&= \sum_{k=1}^{nlx} \int_{-\frac{b_{st}}{2}}^{\frac{b_{st}}{2}} \int_{z_{k-1}}^{z_k} k_s^{sx} \bar{Q}_{44}^{sx} \left(\alpha^{sx} + \frac{\partial w^{sx}}{\partial x} \right) dy dz - \sum_{k=1}^{nlx} \int_{-\frac{b_{st}}{2}}^{\frac{b_{st}}{2}} \int_{z_{k-1}}^{z_k} k_s^{sx} \bar{Q}_{44}^{sx} y \left(\frac{\partial \beta^{sx}}{\partial x} \right) dy dz
\end{aligned} \tag{2.64}$$

The last term of the Eq. (2.64) is zero for the reason mentioned earlier and it takes the form

$$Q_{xz}^{sx} = k_s^{sx} A_{44}^{sx} b_{st} \left(\alpha^{sx} + \frac{\partial w^{sx}}{\partial x} \right) \tag{2.65}$$

Now the force vector is related to the generalized strain components as

$$\begin{Bmatrix} N_x^{sx} \\ M_x^{sx} \\ T_x^{sx} \\ Q_{xz}^{sx} \end{Bmatrix} = \begin{bmatrix} A_{11}^{sx} b_{st} & B_{11}^{sx} b_{st} & B_{16}^{sx} b_{st} & 0 \\ B_{11}^{sx} b_{st} & D_{11}^{sx} b_{st} & D_{16}^{sx} b_{st} & 0 \\ B_{16}^{sx} b_{st} & D_{16}^{sx} b_{st} & \frac{1}{6} (\bar{Q}_{66}^{sx} + \bar{Q}_{44}^{sx}) d_{st} b_{st}^3 & 0 \\ 0 & 0 & 0 & k_s^{sx} A_{44}^{sx} b_{st} \end{bmatrix} \begin{Bmatrix} \frac{\partial u^{sx}}{\partial x} + \frac{w^{sx}}{R_x} \\ \frac{\partial \alpha^{sx}}{\partial x} \\ \frac{\partial \beta^{sx}}{\partial x} \\ \alpha^{sx} + \frac{\partial w^{sx}}{\partial x} \end{Bmatrix} \tag{2.66}$$

where

$$\left. \begin{aligned} A_{ij}^{sx} &= \sum_{i=1}^{nlx} (\bar{Q}_{ij}^{sx})_k (z_k - z_{k-1}); \quad i, j = 1, 6 \\ B_{ij}^{sx} &= \frac{1}{2} \sum_{i=1}^{nlx} (\bar{Q}_{ij}^{sx})_k (z_k^2 - z_{k-1}^2); \quad i, j = 1, 6 \\ D_{ij}^{sx} &= \frac{1}{3} \sum_{i=1}^{nlx} (\bar{Q}_{ij}^{sx})_k (z_k^3 - z_{k-1}^3); \quad i, j = 1, 6 \\ A_{ij}^{sx} &= \sum_{i=1}^{nlx} (\bar{Q}_{ij}^{sx})_k (z_k - z_{k-1}); \quad i, j = 4 \end{aligned} \right\} \tag{2.67}$$

$$\text{Or, } \{F_e^{sx}\} = [D^{sx}] \{\epsilon^{sx}\} \tag{2.68}$$

In a similar manner, the force-strain relationships for the y-stiffener can be derived as

$$\begin{Bmatrix} N_y^{sy} \\ M_y^{sy} \\ T_y^{sy} \\ Q_{yz}^{sy} \end{Bmatrix} = \begin{bmatrix} A_{22}^{sy} b_{st} & B_{22}^{sy} b_{st} & B_{26}^{sy} b_{st} & 0 \\ B_{22}^{sy} b_{st} & D_{22}^{sy} b_{st} & D_{26}^{sy} b_{st} & 0 \\ B_{26}^{sy} b_{st} & D_{26}^{sy} b_{st} & \frac{1}{6}(\bar{Q}_{66}^{sy} + \bar{Q}_{55}^{sy}) d_{st} b_{st}^3 & 0 \\ 0 & 0 & 0 & k_s^{sy} A_{55}^{sy} b_{st} \end{bmatrix} \begin{Bmatrix} \frac{\partial v^{sy}}{\partial y} + \frac{w^{sy}}{R_y} \\ \frac{\partial \beta^{sy}}{\partial y} \\ \frac{\partial \alpha^{sy}}{\partial y} \\ \beta^{sy} + \frac{\partial w^{sy}}{\partial y} \end{Bmatrix} \quad (2.69)$$

where

$$\left. \begin{aligned} A_{ij}^{sy} &= \sum_{i=1}^{nly} (\bar{Q}_{ij}^{sy})_k (z_k - z_{k-1}), \quad i, j = 2, 6 \\ B_{ij}^{sy} &= \frac{1}{2} \sum_{i=1}^{nly} (\bar{Q}_{ij}^{sy})_k (z_k^2 - z_{k-1}^2), \quad i, j = 2, 6 \\ D_{ij}^{sy} &= \frac{1}{3} \sum_{i=1}^{nly} (\bar{Q}_{ij}^{sy})_k (z_k^3 - z_{k-1}^3), \quad i, j = 2, 6 \\ A_{ij}^{sy} &= \sum_{i=1}^{nly} (\bar{Q}_{ij}^{sy})_k (z_k - z_{k-1}), \quad i, j = 5 \end{aligned} \right\} \quad (2.70)$$

$$\text{or} \quad \{F_e^{sy}\} = [D^{sy}] \{\mathcal{E}^{sy}\} \quad (2.71)$$

2.3.5 Generalized Inertia Matrix

The generalized inertia matrix per unit length of the x- or y- directional stiffeners includes both the translatory and rotary inertia terms. Mass and moment of inertia are the measures of translatory and rotary inertial resistances respectively and are given by the following equations.

Mass per unit length of the x-stiffener is denoted by m and is given by

$$m_{sx} = \sum_{k=1}^{nlx} b_{st} (z_k - z_{k-1}) \rho_k \quad (2.72)$$

Mass moment of inertia per unit length is denoted by I_{msx} and is given by

$$I_{msx} = \frac{1}{3} \sum_{k=1}^{nlx} b_{st} (z_k^3 - z_{k-1}^3) \rho_k \quad (2.73)$$

Equivalent mass polar moment of inertia per unit length is denoted by J_{msxe} and given by

$$J_{msxe} = \frac{1}{3} \sum_{k=1}^{nlx} b_{st} (z_k - z_{k-1}) \rho_k b_{st}^3 \quad (2.74)$$

where ρ_k is the mass density of k th layer of x-directional stiffener b_{st} and d_{st} are width and depth of the stiffeners, respectively. z_k and z_{k-1} are the distances measured from the mid-surface of stiffener laminate to the bottom of the k th and $(k-1)$ th laminae.

Incorporating both the translatory and rotary inertia terms the generalized inertia matrix $[m^{sx}]$ of the x-directional stiffeners takes the following form,

$$[m^{sx}] = \begin{bmatrix} m_{sx} & 0 & 0 & 0 \\ 0 & m_{sx} & 0 & 0 \\ 0 & 0 & I_{msx} & 0 \\ 0 & 0 & 0 & J_{msxe} \end{bmatrix} \quad (2.75)$$

In a similar manner, the generalized inertia matrix of the y-directional stiffeners is obtained and is given by

$$[m^{sy}] = \begin{bmatrix} m_{sy} & 0 & 0 & 0 \\ 0 & m_{sy} & 0 & 0 \\ 0 & 0 & J_{msye} & 0 \\ 0 & 0 & 0 & I_{msy} \end{bmatrix} \quad (2.76)$$

where

$$m_{sy} = \sum_{k=1}^{nly} b_{st} (z_k - z_{k-1}) \rho_k \quad (2.77)$$

$$I_{msy} = \frac{1}{3} \sum_{k=1}^{nly} b_{st} (z_k^3 - z_{k-1}^3) \rho_k \quad (2.78)$$

$$J_{msye} = \frac{1}{3} \sum_{k=1}^{nly} b_{st} (z_k - z_{k-1}) \rho_k b_{st}^3 \quad (2.79)$$

ρ is the mass density of y-directional stiffeners b_{st} and d_{st} are width and depth of the stiffeners, respectively.

2.4 COMPATIBILITY BETWEEN SHELL AND STIFFENER

In order to maintain compatibility between the shell and stiffener elements, the stiffener nodal degrees of freedom have to be transformed to shell degrees of freedom considering the eccentricity and curvature of the stiffener.

Considering the effect of eccentricity and curvature the axial displacement of any point in the mid-surface of the x-stiffener u^{sx} can be expressed in terms of the axial displacement u of a point in the mid-surface of the shell as

$$u^{sx} = u \left(1 + \frac{e}{R_x} \right) + e\alpha \quad (2.80)$$

where $e = (h + d_{st})/2$

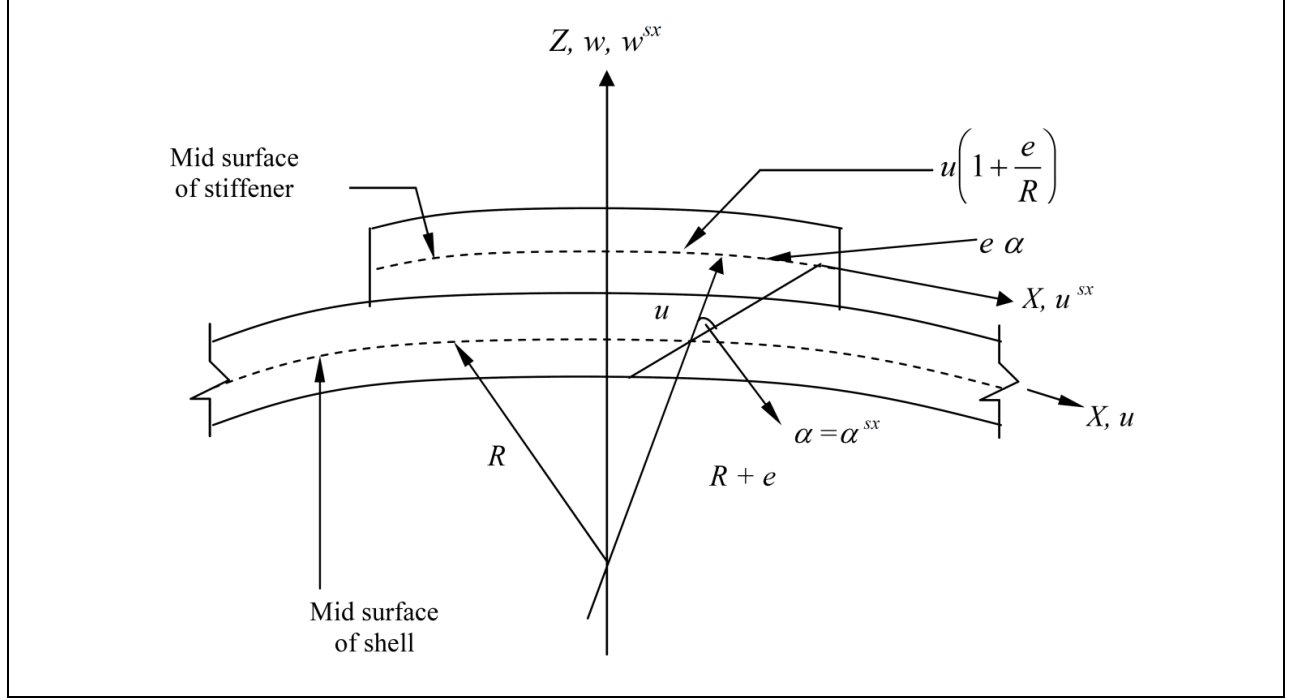


Figure 2.7 Effect of curvature and eccentricity on axial displacement of stiffener.

The points of the stiffener and the shell considered here are collinear in the Z -direction (Fig. 2.7). As the remaining degrees of freedom of the stiffener will be the same as those of the shell mid-surface, the displacement vector of the x -stiffener can be related to that of the shell mid-surface as

$$\begin{Bmatrix} u^{sx} \\ w^{sx} \\ \alpha^{sx} \\ \beta^{sx} \end{Bmatrix} = \begin{Bmatrix} \left(1 + \frac{e}{R_x}\right) & 0 & 0 & 0 & 0 \\ 0 & 0 & 1 & 0 & 0 \\ 0 & 0 & 0 & 1 & 0 \\ 0 & 0 & 0 & 0 & 1 \end{Bmatrix} \begin{Bmatrix} u \\ v \\ w \\ \alpha \\ \beta \end{Bmatrix} \quad (2.81)$$

or in compact form

$$\{\delta^{sx}\} = [T_{ce}^{sx}] \{\delta\} \quad (2.82)$$

Moreover, as the stiffener element is considered within the shell element the displacements at the nodes of the stiffeners (slave nodes) are constrained to follow the displacements at the nodes of the shell element (master nodes). Thus axial displacement at the i th node of the stiffener

$$u_i^{sx} = (N_{i1}u_1 + N_{i2}u_2 + \dots + N_{i8}u_8) \left(1 + \frac{e}{R_x}\right) + e(N_{i1}\alpha_1 + N_{i2}\alpha_2 + \dots + N_{i8}\alpha_8) \quad (2.83)$$

Here $N_{i1}, N_{i2}, \dots, N_{i8}$ represent the quadratic shape functions of shell evaluated at the i th nodal point of the stiffener.

Considering all the displacements at the i th node of x-stiffener the above equation takes the following form

$$\begin{Bmatrix} u_i^{sx} \\ w_i^{sx} \\ \alpha_i^{sx} \\ \beta_i^{sx} \end{Bmatrix} = [T_{ce}^{sx}] \{\delta\} = [T_{ce}^{sx}] \sum_{j=1}^8 \begin{bmatrix} N_{ij} & 0 & 0 & 0 & 0 \\ 0 & N_{ij} & 0 & 0 & 0 \\ 0 & 0 & N_{ij} & 0 & 0 \\ 0 & 0 & 0 & N_{ij} & 0 \\ 0 & 0 & 0 & 0 & N_{ij} \end{bmatrix} \begin{Bmatrix} u_j \\ v_j \\ w_j \\ \alpha_j \\ \beta_j \end{Bmatrix} \quad (2.84)$$

Thus the nodal degrees of freedom of the x-stiffener can be expressed in terms of the shell nodal degrees of freedom as

$$\sum_{i=1}^3 \begin{Bmatrix} u_i^{sx} \\ w_i^{sx} \\ \alpha_i^{sx} \\ \beta_i^{sx} \end{Bmatrix} = \sum_{i=1}^3 [T_{ce}^{sx}] \sum_{j=1}^8 \begin{bmatrix} N_{ij} & 0 & 0 & 0 & 0 \\ 0 & N_{ij} & 0 & 0 & 0 \\ 0 & 0 & N_{ij} & 0 & 0 \\ 0 & 0 & 0 & N_{ij} & 0 \\ 0 & 0 & 0 & 0 & N_{ij} \end{bmatrix} \begin{Bmatrix} u_j \\ v_j \\ w_j \\ \alpha_j \\ \beta_j \end{Bmatrix} \quad (2.85)$$

Here N_{ij} means j th quadratic shape function of shell evaluated at the i th nodal point of the stiffener.

The above equation can be written in a compact form as

$$\{d_e^{sx}\} = [T_{ce}^{sx}] [T_{sx}^{sh}] \{d_e\} = [T^{sx}] \{d_e\} \quad (2.86)$$

Using the above values of $\{d_e^{sx}\}$ the displacement vector of the x-stiffener can be expressed in terms of the shell nodal degrees of freedom as

$$\{\delta^{sx}\} = [N^{sx}] [T^{sx}] \{d_e\} \quad (2.87)$$

Similarly, the nodal degrees of freedom of the y-directional stiffeners are transformed to the shell nodal degrees of freedom as

$$\{d_e^{sy}\} = [T_{ce}^{sy}] [T_{sy}^{sh}] \{d_e\} = [T^{sy}] \{d_e\} \quad (2.88)$$

Displacement vector of the y-stiffener can be expressed as

$$\{\delta^{sy}\} = [N^{sy}] [T^{sy}] \{d_e\} \quad (2.89)$$

2.5 MULTIPOINT CONSTRAINTS ALGORITHM FOR DELAMINATION

A cross-sectional view of delamination crack front of a plate element is shown in Fig 2.8. The undelaminated region is modeled as element 1, where the delaminated region as element 2 and 3. The contact between the delaminated layers during deformation is not considered in the present formulation. The nodal displacement given by Gim (1994) of element 2 and 3 at the crack tip are expressed as:

$$\left. \begin{aligned} u_i &= u'_i - (z - z_i)\alpha_i \\ v_i &= v'_i - (z - z_i)\beta_i \\ w_i &= w'_i \end{aligned} \right\} \quad (2.90)$$

where u'_i, v'_i, w'_i are the mid-plane displacements and z_i is the z coordinates of the mid-plane of element i .

The transverse displacements and rotations of all the three elements at common node have the same values and are expressed as:

$$\left. \begin{aligned} w_1 &= w_2 = w_3 = w \\ \alpha_1 &= \alpha_2 = \alpha_3 = \alpha \\ \beta_1 &= \beta_2 = \beta_3 = \beta \end{aligned} \right\} \quad (2.91)$$

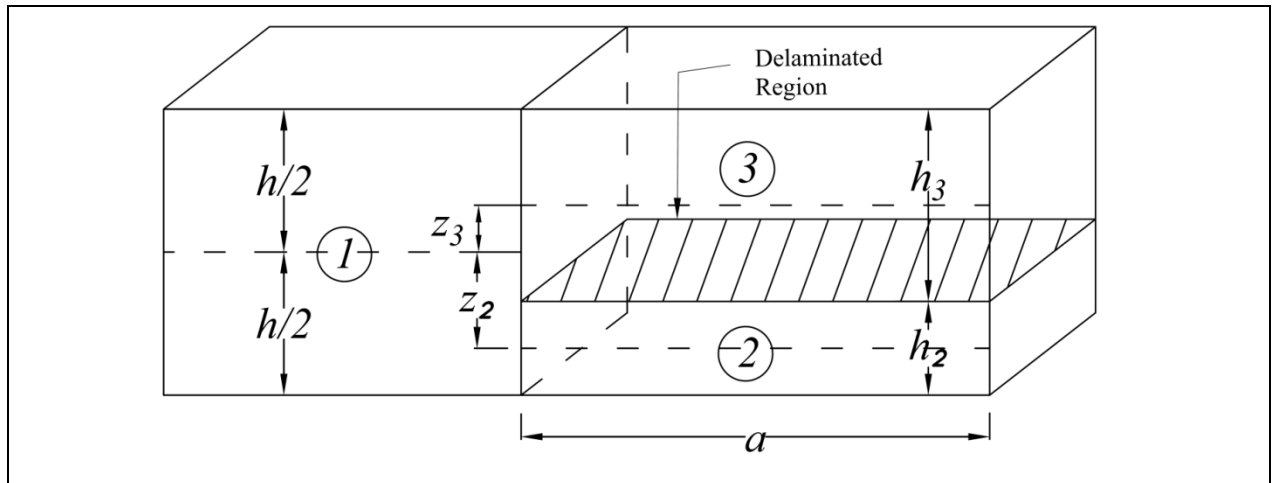


Figure 2.8 Shell elements at a delamination crack tip

The in-plane displacement of all the three elements at the crack node is equal and as a result, the mid-plane displacements of elements 1, 2 and 3 are related as:

$$\left. \begin{aligned} u'_2 &= u'_1 - z_2\alpha & \text{and} & & v'_2 &= v'_1 - z_2\beta \\ u'_3 &= u'_1 - z_3\alpha & \text{and} & & v'_3 &= v'_1 - z_3\beta \end{aligned} \right\} \quad (2.92)$$

where u'_1 is the mid- plane displacement of element 1. Equations (2.90),(2.91) and (2.92) relating the nodal displacements and rotations of elements 1, 2 and 3 at the delamination crack tip, are multipoint constraint equations used in the finite element formulation to satisfy the compatibility of displacements and rotations.

Mid-plane strains given by Gim (1994) between the element 2 and 3 are related as

$$\{\varepsilon'\}_i = \{\varepsilon'\}_1 + z_i \{\kappa\} \quad (i = 2, 3) \quad (2.93)$$

where $\{\kappa\}$ is the curvature vector being identical at the crack tip for element 2 and 3. This equation can be considered as a special case for element 1, when z_1 is equal to zero.

The in-plane stress resultants, $\{N\}$ and the moment resultants $\{M\}$ of element 2 and 3 can be expressed as

$$\{N\}_i = [A]_i \{\varepsilon'\}_1 + (z_i [A]_i + [B]_i) \{\kappa\} \quad (i = 2, 3) \quad (2.94)$$

$$\{M\}_i = [B]_i \{\varepsilon'\}_1 + (z_i [B]_i + [D]_i) \{\kappa\} \quad (i = 2, 3) \quad (2.95)$$

where $[A]$, $[B]$ and $[D]$ are extension, bending-extension coupling and bending stiffness coefficients of the composite laminate, respectively and as follows (Gim, 1994) :

$$[A]_i = \int_{-\frac{h}{2}+z_i}^{\frac{h}{2}+z_i} [\bar{Q}] dz, [B]_i = \int_{-\frac{h}{2}+z_i}^{\frac{h}{2}+z_i} [\bar{Q}](z - z_i) dz \text{ and } [D]_i = \int_{-\frac{h}{2}+z_i}^{\frac{h}{2}+z_i} [\bar{Q}](z - z_i)^2 dz \quad (2.96)$$

2.6 FORMULATING THE GENERAL DYNAMIC PROBLEM

Hamilton's principle applied to the dynamic analysis of elastic bodies' states that "among all admissible displacements which satisfy the specific boundary conditions, the actual solution makes the functional $\int (T+W) dt$ stationary, where T and W are the kinetic energy and work done by conservative and non-conservative forces, respectively. The stationary value is actually a minimum".

2.6.1 Strain Energy of rotating stiffened shell

In the case of a dynamic problem without damping, the conservative forces are the elastic forces developed within the deformed body and the non-conservative forces are the external forcing functions.

The work done U_I by conservative forces in rotating shell element having stiffeners in the X- and Y- directions is given by

$$U_1 = U_1^{sh} + U_1^{sx} + U_1^{sy} + U_1^{Rot} \quad (2.97)$$

where

$$U_1^{sh} = \frac{1}{2} \int_v \{\varepsilon\}^T \{\sigma\} dv = \frac{1}{2} \int_v \{\varepsilon\}^T \{\sigma\} h dA$$

or,

$$U_1^{sh} = \frac{1}{2} \iint_A \{\varepsilon\}^T [D] \{\varepsilon\} dA \quad (2.98)$$

$$U_1^{sx} = \frac{1}{2} \int \{\varepsilon^{sx}\}^T [D^{sx}] \{\varepsilon^{sx}\} dx \quad (2.99)$$

$$U_1^{sy} = \frac{1}{2} \int \{\varepsilon^{sy}\}^T [D^{sy}] \{\varepsilon^{sy}\} dy \quad (2.100)$$

The strain energy contribution resulting from the initial stresses generated due to rotation is expressed as

$$U_1^{Rot} = \int_{vol} \{\varepsilon'\}^T [\sigma_0] dv \quad (2.101)$$

ε' and σ_0 are the nonlinear strain components and initial stress vector resulting from rotation.

The non-linear strain components can be written as Cook (2007)

$$\{\varepsilon'\} = \frac{1}{2} \begin{bmatrix} \theta_x^T & 0 & 0 \\ 0 & \theta_y^T & 0 \\ \theta_y^T & \theta_x^T & 0 \\ \theta_z^T & 0 & \theta_x^T \\ 0 & \theta_z^T & \theta_y^T \end{bmatrix} \begin{Bmatrix} \theta_x \\ \theta_y \\ \theta_z \end{Bmatrix} = \frac{1}{2} [A] \{\theta\} \quad (2.102)$$

where

$$\left. \begin{aligned} \theta_x^T &= \left[\frac{\partial u}{\partial x} + \frac{w}{R_x}, \frac{\partial v}{\partial x}, \frac{\partial w}{\partial x} - \frac{u}{R_x} \right] \\ \theta_y^T &= \left[\frac{\partial u}{\partial y}, \frac{\partial v}{\partial y} + \frac{w}{R_y}, \frac{\partial w}{\partial y} - \frac{v}{R_y} \right] \\ \theta_z^T &= \left[\frac{\partial u}{\partial z}, \frac{\partial v}{\partial z}, \frac{\partial w}{\partial z} \right] \end{aligned} \right\} \quad (2.103)$$

or

$$\{\theta\} = [G] \{d_e\} \quad (2.104)$$

[G] represents the matrix of the derivatives of the shape functions.

Substituting the relevant strain-displacement relations for the shell in equation (2.98) one obtains

$$U_1^{sh} = \frac{1}{2} \iint_A \{d_e\}^T [B]^T [D][B] \{d_e\} dx dy \quad (2.105)$$

$$U_1^{sh} = \frac{1}{2} \{d_e\}^T [K_e^{sh}] \{d_e\} \quad (2.106)$$

where the element elastic stiffness matrix is

$$[K_e^{sh}] = \iint_A [B]^T [D][B] dx dy \quad (2.107)$$

Similarly, the Equation (2.99) can be written as

$$U_1^{sx} = \frac{1}{2} \int \{d_e^{sx}\}^T [B^{sx}]^T [D^{sx}] [B^{sx}] \{d_e^{sx}\} dx \quad (2.108)$$

Using the relation between the elemental degrees of freedom of the shell and the x-stiffener one obtains

$$\begin{aligned} U_1^{sx} &= \frac{1}{2} \int \{d_e\}^T [T^{sx}]^T [B^{sx}]^T [D^{sx}] [B^{sx}] [T^{sx}] \{d_e\} dx \\ &= \frac{1}{2} \{d_e\}^T [K_e^{sx}] \{d_e\} \end{aligned} \quad (2.109)$$

where $[K_e^{sx}] = \int [T^{sx}]^T [B^{sx}]^T [D^{sx}] [B^{sx}] [T^{sx}] dx$ is the stiffness matrix of the X-directional stiffener.

Similarly for y-directional stiffener

$$\begin{aligned} U_1^{sy} &= \frac{1}{2} \int \{d_e\}^T [T^{sy}]^T [B^{sy}]^T [D^{sy}] [B^{sy}] [T^{sy}] \{d_e\} dy \\ &= \frac{1}{2} \{d_e\}^T [K_e^{sy}] \{d_e\} \end{aligned} \quad (2.110)$$

where $[K_e^{sy}] = \int [T^{sy}]^T [B^{sy}]^T [D^{sy}] [B^{sy}] [T^{sy}] dy$ is the stiffness matrix of the Y-directional stiffener.

Using Eqs. (2.102) and (2.104), the Eq. (2.101) can be expressed as

$$\begin{aligned} U_1^{Rot} &= \frac{1}{2} \int_{vol} \{\theta\}^T [A] [\sigma_0] dv \\ &= \frac{1}{2} \int_{vol} \{d_e\}^T [G]^T [A]^T [\sigma_0] dv \end{aligned} \quad (2.111)$$

Again,

$$[A]^T [\sigma_0] = [M_\sigma] \{\theta\} = [M_\sigma] [G] \{d_e\} \quad (2.112)$$

where the matrix $[G]$ consists of derivatives of shape functions and $[M_\sigma]$ denotes the matrix of initial stresses.

The Equation (2.111) becomes

$$\begin{aligned} U_1^{Rot} &= \frac{1}{2} \int_A \{d_e\}^T [G]^T [M_\sigma] [G] \{d_e\} dx dy \\ &= \frac{1}{2} \{d_e\}^T [K_\sigma] \{d_e\} \end{aligned} \quad (2.113)$$

where the element geometric stiffness matrix is

$$[K_\sigma] = \int_A [G]^T [M_\sigma] [G] dx dy \quad (2.114)$$

Total potential energy of the rotating shell containing both X-and Y-directional stiffener is

$$\begin{aligned} U_1 &= \frac{1}{2} \{d_e\}^T [K_e^{sh}] \{d_e\} + \frac{1}{2} \{d_e\}^T [K_e^{sx}] \{d_e\} + \{d_e\}^T [K_e^{sy}] \{d_e\} + \frac{1}{2} \{d_e\}^T [K_\sigma] \{d_e\} \\ &= \frac{1}{2} \{d_e\}^T \left([K_e^{sh}] + [K_e^{sx}] + [K_e^{sy}] \right) \{d_e\} + \frac{1}{2} \{d_e\}^T [K_\sigma] \{d_e\} \end{aligned} \quad (2.115)$$

2.6.2 Kinetic Energy of rotating stiffened shell

Kinetic energy U_2 of vibration of an element is given by

$$U_2 = U_2^{sh} + U_2^{sx} + U_2^{sy} \quad (2.116)$$

Two coordinate system (X', Y', Z') and (x, y, z) are used for modeling a rotating shell as shown in Fig 2.9.

Total kinetic energy of a rotating shell can be expressed as

$$U_2^{sh} = \frac{1}{2} \int_v \rho \vec{V} \cdot \vec{V} dv \quad (2.117)$$

where, \vec{V} is the absolute velocity vector of an arbitrary point on the shell with respect to inertial reference frame (X', Y', Z') and ρ is the mass density of the composite shell. It is assumed that the panel rotates about the inertial coordinate system (X', Y', Z') with an angular velocity component $\Omega = \Omega' k'$ about the Z' axis, wherein k' is the unit vector along Z' axis.

The components of angular velocity with respect to the shell local coordinate system are given as

$$\{\Omega'_x, \Omega'_y, \Omega'_z\} = \{0, 0, \Omega'\} [T_{\theta_y}]^T [T_{\theta_x}]^T \quad (2.118)$$

where

$$[T_{\theta_x}]^T = \begin{bmatrix} 1 & 0 & 0 \\ 0 & \cos \varphi & -\sin \varphi \\ 0 & \sin \varphi & \cos \varphi \end{bmatrix} \text{ and } [T_{\theta_y}]^T = \begin{bmatrix} \cos \lambda & 0 & -\sin \lambda \\ 0 & 1 & 0 \\ \sin \lambda & 0 & \cos \lambda \end{bmatrix} \quad (2.119)$$

where Ω' is the speed of rotation of the stiffened shell about z-axis of the inertial coordinate system (x', y', z') , λ is the precone angle and φ is the skew angle. The order of rotation is φ and λ .

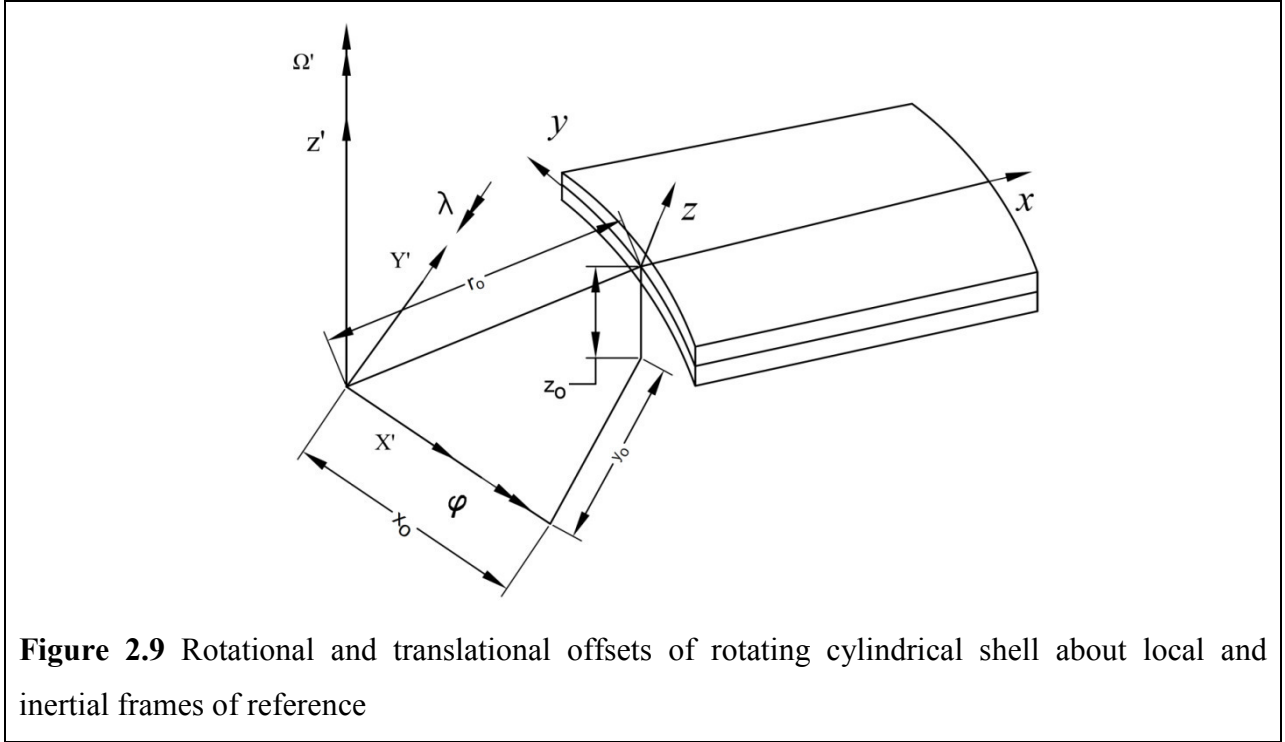


Figure 2.9 Rotational and translational offsets of rotating cylindrical shell about local and inertial frames of reference

The fixed translation offsets expressed with reference to cylindrical stiffened shell coordinate systems are given as

$$\{h_x, h_y, h_z\} = \{x_0, y_0, z_0\} [T_{\theta_y}]^T [T_{\theta_x}]^T \quad (2.120)$$

Unit vectors for the inertial reference system and local coordinate axes are (i', j', k') and (i, j, k) , respectively. According to Chasle's theorem,

$$\vec{V} = \frac{d\vec{r}}{dt} + (\Omega' k') X \vec{r} \quad (2.121)$$

where, \vec{r} is the position vector from the origin of the inertial reference frame to a point on the deformed cylindrical stiffened shell. Position vector and the angular velocity vector can be written as

$$\vec{r} = (h_x + x + u)\mathbf{i} + (h_y + y + v)\mathbf{j} + (h_z + z + w)\mathbf{k} \quad (2.122)$$

$$\vec{\Omega}' = \Omega'_x \mathbf{i} + \Omega'_y \mathbf{j} + \Omega'_z \mathbf{k} \quad (2.123)$$

where (x, y, z) are the coordinates of the point in the shell coordinate system (local coordinate axes), (h_x, h_y, h_z) are the fixed translational offsets of the shell coordinate axes from the inertial axes expressed with reference to the shell coordinate system, (u, v, w) are the elastic deflections of a point and $(\Omega'_x, \Omega'_y, \Omega'_z)$ are the component of angular velocity with respect to the shell coordinate system. The velocity vector is given by

$$\begin{aligned} \vec{V} = & \left[\dot{u} + \Omega'_y (h_z + z + w) - \Omega'_z (h_y + y + v) \right] \mathbf{i} + \left[\dot{v} + \Omega'_z (h_x + x + u) - \Omega'_x (h_z + z + w) \right] \mathbf{j} \\ & + \left[\dot{w} + \Omega'_x (h_y + y + v) - \Omega'_y (h_x + x + u) \right] \mathbf{k} \end{aligned} \quad (2.124)$$

where, dot (.) represents derivatives with respect to time and $\vec{V} \cdot \vec{V} = |\vec{V}|^2$

Computing $|\vec{V}|^2$ and cancelling the terms which gives no contribution when Lagrange's equation of motion is applied and substituting the result in kinetic energy expression, we have,

$$\begin{aligned} U_2^{sh} = & \frac{1}{2} \int_{vol} \rho \begin{Bmatrix} \dot{u} \\ \dot{v} \\ \dot{w} \end{Bmatrix}^T \begin{Bmatrix} \dot{u} \\ \dot{v} \\ \dot{w} \end{Bmatrix} dv + \frac{1}{2} \int_{vol} \rho \begin{Bmatrix} \dot{u} \\ \dot{v} \\ \dot{w} \end{Bmatrix}^T [A_1] \begin{Bmatrix} u \\ v \\ w \end{Bmatrix} dv + \frac{1}{2} \int_{vol} \rho \begin{Bmatrix} u \\ v \\ w \end{Bmatrix} [A_2] \begin{Bmatrix} u \\ v \\ w \end{Bmatrix} dv \\ & + \int_{vol} \rho \begin{Bmatrix} h_x + x \\ h_y + y \\ h_z + z \end{Bmatrix}^T [A_2] \begin{Bmatrix} u \\ v \\ w \end{Bmatrix} dv \end{aligned} \quad (2.125)$$

where, $[A_1]$ and $[A_2]$ are expressed as,

$$[A_1] = \begin{bmatrix} 0 & -2\Omega'_z & 2\Omega'_y \\ 2\Omega'_z & 0 & -2\Omega'_x \\ -2\Omega'_y & 2\Omega'_x & 0 \end{bmatrix} \quad (2.126)$$

$$[A_2] = \begin{bmatrix} \Omega_y'^2 + \Omega_z'^2 & -\Omega'_x \Omega'_y & -\Omega'_x \Omega'_z \\ -\Omega'_x \Omega'_y & \Omega_x'^2 + \Omega_z'^2 & -\Omega'_y \Omega'_z \\ -\Omega'_x \Omega'_z & -\Omega'_y \Omega'_z & \Omega_x'^2 + \Omega_y'^2 \end{bmatrix} \quad (2.127)$$

The displacement vector at any point in the element can be written as

$$\{d\} = \{u, v, w\}^T = [N]\{d_e\} \quad (2.128)$$

where $[N]$ stands for the shape function matrix and $\{d_e\}$ stands for the element nodal displacement vector. Substituting the above relation, the expression for kinetic energy of an element

$$\begin{aligned}
U_2^{sh} &= \frac{1}{2} \int_{vol} \rho \{ \dot{d}_e \}^T [N]^T [N] \{ \dot{d}_e \} dv + \frac{1}{2} \int_{vol} \rho \{ \dot{d}_e \}^T [N]^T [A_1] [N] \{ d_e \} dv \\
&\quad + \frac{1}{2} \int_{vol} \rho \{ d_e \}^T [N]^T [A_2] [N] \{ d_e \} dv \\
&\quad + \int_{vol} \rho \begin{Bmatrix} h_x + x \\ h_y + y \\ h_z + z \end{Bmatrix}^T [A_2] [N] \{ d_e \} dv \\
U_2^{sh} &= \frac{1}{2} \{ \dot{d}_e \}^T [M_e^{sh}] \{ \dot{d}_e \} + \frac{1}{2} \{ \dot{d}_e \}^T [C_e] \{ d_e \} + \frac{1}{2} \{ d_e \}^T [K_{rot}] \{ d_e \} + \{ d_e \}^T [F_{\Omega e}] \quad (2.129)
\end{aligned}$$

where, the element mass matrix of the shell is

$$[M_e^{sh}] = \rho \int_v [N]^T [N] dv$$

or,
$$[M_e^{sh}] = \int_A [N]^T [m] [N] dx dy \quad (2.130)$$

The element Coriolis matrix (skew symmetric) is

$$[C_e] = \rho \int_v [N]^T [A_1] [N] dv \quad (2.131)$$

The elemental rotational stiffness matrix (symmetric and positive definite) is

$$[K_{Rot}] = \rho \int_v [N]^T [A_2] [N] dv \quad (2.132)$$

The element centrifugal force vector is

$$[F_{\Omega e}] = \rho \int_v [N]^T [A_2] \begin{Bmatrix} h_x + x \\ h_y + y \\ h_z + z \end{Bmatrix} dv \quad (2.133)$$

The kinetic energy of the stiffeners can be expressed as

$$U_2^{sx} = \frac{1}{2} \int \{ \dot{\delta}^{sx} \}^T [m^{sx}] \{ \dot{\delta}^{sx} \} dx \quad (2.134)$$

$$U_2^{sy} = \frac{1}{2} \int \{ \dot{\delta}^{sy} \}^T [m^{sy}] \{ \dot{\delta}^{sy} \} dy \quad (2.135)$$

where the dot (.) represents derivative with respect to time.

Using the relation between $\{\delta^{sx}\}$ and $\{d_e\}$

$$U_2^{sx} = \frac{1}{2} \int \{\dot{d}_e\}^T [T^{sx}]^T [N^{sx}]^T [m^{sx}] [N^{sx}] [T^{sx}] \{\dot{d}_e\} dx \quad (2.136)$$

$$U_2^{sx} = \frac{1}{2} \{\dot{d}_e\}^T [M_e^{sx}] \{\dot{d}_e\} \quad (2.137)$$

Similarly

$$U_2^{sy} = \frac{1}{2} \int \{\dot{d}_e\}^T [T^{sy}]^T [N^{sy}]^T [m^{sy}] [N^{sy}] [T^{sy}] \{\dot{d}_e\} dy \quad (2.138)$$

$$U_2^{sy} = \frac{1}{2} \{\dot{d}_e\}^T [M_e^{sy}] \{\dot{d}_e\} \quad (2.139)$$

The total kinetic energy of the rotating shell element containing both x- and y-directional stiffener is

$$U_2 = \frac{1}{2} \{\dot{d}_e\}^T [M_e^{sh}] \{\dot{d}_e\} + \frac{1}{2} \{\dot{d}_e\}^T [C_e] \{\dot{d}_e\} + \frac{1}{2} \{d_e\}^T [K_{rot}] \{d_e\} + \{d_e\}^T [F_{\Omega e}] \\ + \frac{1}{2} \{\dot{d}_e\}^T [M_e^{sx}] \{\dot{d}_e\} + \frac{1}{2} \{\dot{d}_e\}^T [M_e^{sy}] \{\dot{d}_e\} \quad (2.140)$$

On arrangement of terms the Eq.(2.140) can be rewrite as

$$U_2 = \frac{1}{2} \{\dot{d}_e\}^T ([M_e^{sh}] + [M_e^{sx}] + [M_e^{sy}]) \{\dot{d}_e\} + \frac{1}{2} \{\dot{d}_e\}^T [C_e] \{\dot{d}_e\} + \frac{1}{2} \{d_e\}^T [K_{rot}] \{d_e\} \\ + \{d_e\}^T [F_{\Omega e}] \quad (2.141)$$

2.6.3 Work done due to external load

Work done U_3 by surface tractions in an element is given by

$$U_3 = - \int \int_A \{\delta\}^T [q] dA \quad (2.142)$$

where $\{q\} = [q_x \quad q_y \quad q_z \quad \mu_x \quad \mu_y]^T$ (2.143)

in which q_x , q_y , and q_z are the uniformly distributed loads per unit area along X, Y and Z axes, respectively, and μ_x and μ_y are the moments per unit area along X and Y axes, respectively. In case of shells subjected to transverse loads only q_x , q_y , μ_x and μ_y vanish and q_z remains, which is represented by the scalar notation p hereafter.

From Equations (2.6) and (2.142), it is obtained that

$$\begin{aligned}
U_3 &= -\iint_A \{d_e\}^T [N]^T [p] dx dy \\
&= -\{d_e\}^T \{F_e\}
\end{aligned} \tag{2.144}$$

where $\{F_e\} = \{F_e^{sh}\} = \iint_A [N]^T \{p\} dx dy$, the consistent element nodal load vector.

2.6.4 Governing equation

Hamilton's principle may be used to derive Lagrange's equation of motion given by

$$\frac{d}{dt} \left\{ \frac{\partial U_2}{\partial \dot{d}_e} \right\} - \left\{ \frac{\partial U_2}{\partial d_e} \right\} + \left\{ \frac{\partial}{\partial d_e} (U_1 + U_3) \right\} = 0 \tag{2.145}$$

The equation can be written as,

$$\frac{d}{dt} \left\{ \frac{\partial U_2}{\partial \dot{d}_e} \right\} - \left\{ \frac{\partial U_2}{\partial d_e} \right\} + \left\{ \frac{\partial U_1}{\partial d_e} \right\} = - \left\{ \frac{\partial U_3}{\partial d_e} \right\} \tag{2.146}$$

Substituting Equations (2.115), (2.141) and (2.144) in Equation (2.146) and solving one gets,

$$[M_e] \{\ddot{d}_e\} + [C_e] \{\dot{d}_e\} + ([K_e] + [K_{\sigma e}] - [K_{Rot}]) \{d_e\} = \{F_{\Omega e}\} + \{F_e\} \tag{2.147}$$

For moderate rotational speed, Coriolis matrix and rotational stiffness matrix are neglected and finally, the dynamic equilibrium equation reduces to

$$[M_e] \{\ddot{d}_e\} + ([K_e] + [K_{\sigma e}]) \{d_e\} = \{F_{\Omega e}\} + \{F_e\} \tag{2.148}$$

or

$$\begin{aligned}
[M_e] &= [M_e^{sh}] + [M_e^{sx}] + [M_e^{sy}] \\
&= \text{mass matrix of the shell element} \\
&\quad + \text{mass matrix of the x-stiffener element} \\
&\quad + \text{mass matrix of the y-stiffener element}
\end{aligned} \tag{2.149}$$

and

$$\begin{aligned}
[K_e] &= [K_e^{sh}] + [K_e^{sx}] + [K_e^{sy}] \\
&= \text{Stiffness matrix of shell element} \\
&\quad + \text{Stiffness matrix of the x-stiffener element} \\
&\quad + \text{Stiffness matrix of y-stiffener element}
\end{aligned} \tag{2.150}$$

Transforming the integrals to local natural coordinates of ξ, η of the element, the element matrices can be expressed as

$$[K_e^{sh}] = \int_{-1}^{+1} \int_{-1}^{+1} [B]^T [D] [B] |J| d\xi d\eta \tag{2.151}$$

$$[K_{\sigma e}] = \int_{-1}^{+1} \int_{-1}^{+1} [G]^T [M_{\sigma}] [G] |J| d\xi d\eta \quad (2.152)$$

$$[M_e^{sh}] = \int_{-1}^{+1} \int_{-1}^{+1} [N]^T [m] [N] |J| d\xi d\eta \quad (2.153)$$

$$\{F_e\} = \{F_e^{sh}\} = \int_{-1}^{+1} \int_{-1}^{+1} [N]^T \{p\} |J| d\xi d\eta \quad (2.154)$$

The numerical integrations of the above equations are performed by using Gaussian quadrature of order (2×2) to avoid shear locking (Cook , 2007).

Transforming the integrals of the x - stiffener element to local natural coordinate ξ , the element matrices can be expressed as

$$[K_e^{sx}] = \int_{-1}^{+1} [T^{sx}]^T [B^{sx}]^T [D^{sx}] [B^{sx}] [T^{sx}] [J^{sx}] d\xi \quad (2.155)$$

$$[M_e^{sx}] = \int_{-1}^{+1} [T^{sx}]^T [N^{sx}]^T [m^{sx}] [N^{sx}] [T^{sx}] [J^{sx}] d\xi \quad (2.156)$$

In a similar manner, the element matrices of the y -directional stiffener element are expressed as

$$[K_e^{sy}] = \int_{-1}^{+1} [T^{sy}]^T [B^{sy}]^T [D^{sy}] [B^{sy}] [T^{sy}] |J^{sy}| d\eta \quad (2.157)$$

$$[M_e^{sy}] = \int_{-1}^{+1} [T^{sy}]^T [N^{sy}]^T [m^{sy}] [N^{sy}] [T^{sy}] |J^{sy}| d\eta \quad (2.158)$$

Numerical integrations of the above equations are performed by using 2 point Gaussian quadrature.

The element mass and stiffness matrices of the stiffened shell are transformed to global axes system (X-Y-Z) without using the transformation matrices. This is so, because, the shell elements are rectangular and their local axes are parallel to the global axes X and Y respectively. The local axis Z' is also nearly parallel to the global axis Z because the shell is shallow and hence does not have a very sharp curvature. These matrices and element load vectors are assembled with proper correspondence to the degrees of freedom for all nodes. Thus, the global stiffness $[K]$ and mass $[M]$ matrices and global load vectors $\{F(\Omega)\}$ and $\{F\}$ of the stiffened shell are given by,

$$[K] = \sum_{i=1}^{NE} [K_e], [M] = \sum_{i=1}^{NE} [M_e], \{F(\Omega)\} = \sum_{i=1}^{NE} \{F_{\Omega e}\} \text{ and } \{F\} = \sum_{i=1}^{NE} \{F_e\} \quad (2.159)$$

The dynamic equation of motion in the global form reduces to

$$[M] \{\ddot{d}\} + ([K] + [K_\sigma]) \{d\} = \{F(\Omega)\} + \{F\} \quad (2.160)$$

where $\{d\}$ is a global displacement vector.

$[K_\sigma]$ depends on initial stress distribution due to the rotation and is obtained by iterative procedure (Sreenivasamurthy and Ramamurti, 1981) upon solving

$$([K] + [K_\sigma]) \{d\} = \{F(\Omega)\} \quad (2.161)$$

Initially, the stresses are taken equal to zero and

$$[K] \{d\} = \{F(\Omega)\} \quad (2.162)$$

gives a stress distribution σ^0 ; then solution of

$$([K] + [K_{\sigma^0}]) \{d\} = \{F(\Omega)\} \quad (2.163)$$

gives a new stress distribution σ^1 , and the stresses are found to converge within another two iterations.

2.7 IMPOSITION OF BOUNDARY CONDITIONS AND SOLUTION PROCEDURE

Imposing boundary conditions means the presence or absence of the generalized displacements u , v , w , α and β in the different nodes of the discretized structure. The zero displacement boundary conditions are incorporated by deleting the corresponding rows and columns from the global matrices and the load vector.

The boundary condition adopted for the entire analysis of the cantilevered stiffened shell is

$$\text{at } x=0 \quad u=v=w=\alpha=\beta=0 \quad (2.164)$$

Solution techniques of the static, free vibration and low velocity impact problems are elaborated in the following subsections.

2.7.1 Formulating Static Problem

If the inertia force term, the force resulting from initial stresses due to rotation and the force rotation of equation (2.160) are dropped and the displacement and external load vectors are assumed to be time independent, the following equation of static equilibrium is obtained,

$$[K] \{d\} = \{F\} \quad (2.165)$$

The above equation is solved by the Gauss elimination technique (Bathe, 2006) and from the global nodal displacement vector $\{d\}$ thus obtained, the element displacement vector $\{d_e\}$ is known.

Using $\{d_e\}$ in equation (2.19) the strains can be evaluated at the Gauss points, which when used in equation (2.32) the generalized force and moment resultants are obtained at the Gauss points. These values are extrapolated to the nodes by shape functions to obtain the nodal values. Since stresses are discontinuous at nodes due to C^0 continuity of the shape functions, these are calculated taking the average value of stresses at that node from various elements associated with that node.

2.7.2 Formulating Free Vibration Problem

Natural frequencies and eigenvectors are obtained about the deformed configuration. For the static analysis, the time-dependent terms in Eq. (2.160) are neglected and the following form is obtained

$$([K] + [K_\sigma])\{d_{static}\} = \{F(\Omega)\} \quad (2.166)$$

where, $\{d_{static}\}$ is the static equilibrium solution as a result of the centrifugal load.

In case of the dynamic analyses, both the static as well as the time-dependent components are considered where the displacement vector $\{d\}$ is expressed as the sum of a static and a dynamic term. Thus,

$$\{d\} = \{d_{static}\} + \{d_p\} \quad (2.167)$$

where $\{d_p\}$ is a small linear time-dependent perturbation about the static deflected position $\{d_{static}\}$.

The equation of motion for free vibration is given by

$$[M]\{\ddot{d}\} + ([K] + [K_\sigma])\{d\} = 0 \quad (2.168)$$

Assuming harmonic vibrations, $\{d\} = \{d\}e^{i\omega_n t}$, we have

$$([K] + [K_\sigma] - \omega_n^2 [M])\{d\} = 0 \quad (2.169)$$

This is a standard eigenvalue problem, and is solved for the eigenvalues and eigenvectors by the QR iteration algorithm (Bathe, 2006).

$$[A]\{d\} = \lambda\{d\} \quad (2.170)$$

where $[A] = ([K] + [K_\sigma])^{-1}[M]$ and $\lambda = 1/\omega_n^2$

2.7.3 Formulating low velocity Impact Problem

Neglecting the effect of damping, the dynamic equilibrium equation is given by

$$[M]\{\ddot{d}\} + ([K] + [K_\sigma])\{d\} = \{F(\Omega)\} + \{F_C\} \quad (2.171)$$

where, $\{d\}$ and $\{\ddot{d}\}$ are the global displacement and acceleration vectors respectively, $\{F(\Omega)\}$ is the nodal equivalent centrifugal forces and $\{F_C\}$ is the global contact force vector resulting from single or multi-site impact and is given by

$$\{F_C\} = \{0 \quad 0 \quad 0 \quad \dots \quad F_{C_i} \dots F_{C_j} \quad \dots \quad 0 \quad 0 \quad 0\}^T \quad (2.172)$$

Where, F_{C_i} and F_{C_j} are the contact forces at the nodes i and j where the impacts occur.

$[K_\sigma]$ depends on the initial stress distribution and is obtained by the iterative procedure upon solving

$$([K] + [K_\sigma])\{d\} = \{F(\Omega)\} \quad (2.173)$$

For impact, the equation of motion for each rigid impactor is given by

$$m_i \ddot{w}_i + F_C = 0 \quad (2.174)$$

where m_i and \ddot{w}_i are the mass and acceleration of the impactor respectively.

The local indentation at the indentation point is given by

$$\bar{\alpha}(t) = w_i - w_s \cos \Phi \quad (2.175)$$

where, Φ , w_s and w_i are the twist angle, displacements of the mid-plane of the cylindrical shell and the displacement of the spherical impactor at the impact point in the direction of impact, respectively.

The contact forces based on modified Hertzian contact law during loading, unloading and reloading cycle are determined as (Sun and Chen, 1985)

$$F_C = k\bar{\alpha}^{1.5} \quad 0 < \bar{\alpha} \leq \bar{\alpha}_m \quad \text{Loading} \quad (2.176)$$

$$F_C = F_m \left[\frac{\bar{\alpha} - \bar{\alpha}_0}{\bar{\alpha}_m - \bar{\alpha}_0} \right]^{2.5} \quad \text{Unloading} \quad (2.177)$$

$$F_C = F_m \left[\frac{\bar{\alpha} - \bar{\alpha}_0}{\bar{\alpha}_m - \bar{\alpha}_0} \right]^{1.5} \quad \text{Reloading} \quad (2.178)$$

where k is the contact stiffness, $\bar{\alpha}$ is the depth of indentation, F_m is the maximum contact force just before unloading, $\bar{\alpha}_m$ is the maximum indentation obtained at the end of loading cycle and $\bar{\alpha}_0$ is the permanent indentation in a loading/unloading cycle. The contact stiffness k of the cylindrical shell is determined using the following relation proposed by Yang and Sun (1982)

$$k = \frac{4}{3} \frac{\left[\frac{1}{r_i} + \frac{1}{2R_y} \right]^{-1/2}}{\left[\frac{(1-\nu_i^2)}{E_i} + \frac{1}{E_2} \right]} \quad (2.179)$$

where r_i , ν_i and E_i are the radius, Poisson's ratio and modulus of elasticity of the spherical impactor, respectively. E_2 is the modulus of elasticity of the cylindrical shell transverse to fibre direction. The permanent indentation $\bar{\alpha}_0$ is determined from the following equations (Sun and Chen, 1985)

$$\bar{\alpha}_0 = 0 \quad \text{when } \bar{\alpha}_m < \bar{\alpha}_{cr} \text{ and} \quad (2.180)$$

$$\bar{\alpha}_0 = \beta_c (\bar{\alpha}_m - \bar{\alpha}_{cr}) \quad \text{when } \bar{\alpha}_m \geq \bar{\alpha}_{cr} \quad (2.181)$$

where β_c is a constant and $\bar{\alpha}_{cr}$ is the critical indentation beyond which permanent indentation occurs. For graphite epoxy laminates, the values of $\bar{\alpha}_{cr}$ and β_c are 1.667×10^{-2} cm and 0.094, respectively (Sun and Chen, 1985).

As the load vector $\{F_C\}$ of equation (2.171) is transient in character then the above equation represents the basic equation of forced vibration. The Equation (2.171) is regarded as a system of ordinary differential equations with constant coefficients and is made to be satisfied at discrete points of time. Newmark's direct time integration scheme (Bathe, 2006) (the constant average-acceleration method) is used to approximate the time derivatives. Use of this unconditionally stable scheme in equation (2.171) with time step Δt yields for the $(n+1)$ th time step at time $t+\Delta t$ the following relation,

For cylindrical shell:

$$[\hat{K}] \{d\}_{n+1} = \{\hat{F}\}_{n+1} \quad (2.182)$$

where $[\hat{K}] = [K] + [K_\sigma] + a_0 [M]$ (2.183)

and
$$\{\hat{F}\}_{n+1} = \{F(\Omega)\} + \{F_C\}_{n+1} + [M] \left(a_0 \{d\}_n + a_1 \{\dot{d}\}_n + a_2 \{\ddot{d}\}_n \right) \quad (2.184)$$

For Impactors:

$$\hat{k}_i (w_i)_{n+1} = (\hat{F}_C)_{n+1} \quad (2.185)$$

where $\hat{k} = a_0 m_i$, the effective stiffness of the impactor and

$$(\hat{F}_C)_{n+1} = (F_C)_{n+1} + m_i (a_0 (w_i)_n + a_1 (\dot{w}_i)_n + a_2 (\ddot{w}_i)_n) \quad (2.186)$$

with
$$a_0 = 1/(\beta' \Delta t^2), \quad a_1 = a_0 \Delta t, \quad a_2 = 1/2\beta' - 1 \quad (2.187)$$

The acceleration vector $\{\ddot{d}\}$ and the velocity vector $\{\dot{d}\}$ of the shell can be computed from the displacement vector $\{d\}$ as,

$$\{\ddot{d}\}_{n+1} = a_0 (\{d\}_{n+1} - \{d\}_n) - a_1 \{\dot{d}\}_n - a_2 \{\ddot{d}\}_n \quad (2.188)$$

and
$$\{\dot{d}\}_{n+1} = \{\dot{d}\}_n + a_3 \{\ddot{d}\}_n + a_4 \{\ddot{d}\}_{n+1} \quad (2.189)$$

while that of the impactor is

$$(\ddot{w}_i)_{n+1} = a_0 ((w_i)_{n+1} - (w_i)_n) - a_1 (\dot{w}_i)_n - a_2 (\ddot{w}_i)_n \quad (2.190)$$

$$(\dot{w}_i)_{n+1} = (\dot{w}_i)_n + a_3 (\ddot{w}_i)_n + a_4 (\ddot{w}_i)_{n+1} \quad (2.191)$$

with
$$a_3 = (1 - \alpha') \Delta t \text{ and } a_4 = \alpha' \Delta t \quad (2.192)$$

Values of α' and β' are taken as 0.5 and 0.25, respectively as proposed by Newmark assuming constant average acceleration. Equation (2.182) is analogous to equation (2.165) and is solved in the same way as equation (2.165) and the dynamic stresses are obtained at each time step. Time step for each impact case is chosen to satisfy the convergence of the time-based response.

CHAPTER 3

FREE VIBRATION ANALYSIS OF PRETWISTED ROTATING DELAMINATED COMPOSITE STIFFENED CYLINDRICAL SHELLS

3.1 GENERAL

A cantilever pretwisted cylindrical shell has significant applications in turbomachinery, impeller and fan blades. Extensive use of cantilever composite shells are also found in mechanical, aerospace, automobile and marine industries owing to their light weight combined with high strength. In addition to this, the specific properties of composite materials can also be easily tailored by controlling the fiber orientation and stacking sequence of the constituent layers. Major cause of failure in turbomachinery blades is due to fatigue, which is a consequence of the resonant vibrations resulting in large operating stresses. Moreover, high rotational speeds in turbomachinery blades results in centrifugal forces of considerable magnitude, which manifest itself through geometric stiffness known as centrifugal stiffening and this, could be regarded as problem of initial stresses of the shell. In order to control the resonant vibrations and increase the overall stiffness, the composite shells are very often stiffened by adding stiffeners at suitable orientations. An in-depth understanding of the dynamic behavior of pretwisted cylindrical stiffened shells is extremely important from the design point of view in order to avoid harmful resonances and predict beforehand the probability of failure in these composite structures. A twisted stiffened shell structures pose geometrical complexities in most practical applications which sometimes make their behavior highly unpredictable in different service environments. In addition, certain dynamic parameters must always be taken into consideration when these structural elements are in rotation which results in initial stresses. However, the determination of the vibration response of stiffened shells is extremely difficult and hence requires the help of numerical techniques. Finite element method is an efficient tool available to the designers for the dynamic analysis of such type of applications provided accurate mathematical models are developed which can correctly predict the performance of such structures to a reasonable degree of accuracy.

Delamination or interlaminar debonding is one of the most commonly occurred damage mode in laminated composite structures and the failure of a delaminated composite

may become much more drastic because of initial stresses due to rotation. Generally, vibrations of the composite structures are closely related to their natural frequencies and hence the prior knowledge of the vibration characteristics of the stiffened shell with and without delamination is extremely helpful to prevent vibration induced failures.

This chapter is thereby aimed at a finite-element based analysis to determine the natural frequencies of graphite-epoxy composite pretwisted rotating cylindrical stiffened shells with and without delamination. This chapter is presented under two headings i.e. free vibration of a generalized stiffened cylindrical shell and free vibration of long, intermediate and short cylindrical stiffened shells based on Aas-Jakobsen's parameters. Numerical results are obtained corresponding to various twist angles, rotational speeds, number of fiber-orientation angles, position of stiffeners, eccentricity of stiffeners, location of delamination and percentage of delamination.

3.2 CONVERGENCE AND VALIDATION

Mesh convergence study of a cylindrical shell stiffened eccentrically at the bottom is furnished in the Table 3.1, considering mesh sizes of 4×4 , 6×6 , 8×8 and 10×10 . It is noticed that the results of 8×8 and 10×10 are close to each other and percentage of difference is less than unity. Hence, 8×8 mesh size consisting of 64 elements and 225 nodes is considered for the full stiffened shell discretization.

Table 3.1 Convergence study for non-dimensional fundamental frequencies ($\varpi = \omega_n L^2 \sqrt{\rho / E_{11} h^2}$) of eight layered symmetric cross ply and angle ply stiffened cylindrical shell. ($L/b = 1, b/h = 100, b/R_y = 0.5, b_{st} = 2h$ and $d_{st} = 4h, E_1 = 138.0$ GPa, $E_2 = 8.96$ GPa, $G_{12} = G_{13} = 7.1$ GPa, $G_{23} = 2.84$ GPa, $\nu_{12} = 0.3, n_x = n_y = 1$)

Stacking sequence	(4×4) Mesh	(6×6) Mesh	(8×8) Mesh	(10×10) Mesh
[45/-45/45/-45] _s	2.77369	2.74317	2.73081	2.73002
[0/90/0/90] _s	2.31306	2.29573	2.29275	2.29200

Accuracy of the developed computer code for free vibration analysis of the rotating delaminated stiffened panel with pretwist, the following problems are taken up from the existing literature for the purpose of comparing the present results with those obtained by earlier investigators.

1. Non-dimensional fundamental frequencies of an isotropic rotating cantilever plate, solved by Sreenivasamurthy and Ramamurthi (1981) and Karmakar and Kishimoto (2006).

2. Non-dimensional fundamental frequencies of three layer graphite-epoxy twisted plate, solved by Qatu and Leissa (1991).
3. Natural frequencies (Hz) of simply supported antisymmetric cross-ply crossed stiffened plate with "eccentric at bottom" stiffeners, solved by Nayak and Bandyopadhyay (2005) and Das and Chakravorty (2011).
4. Natural frequency (Hz) of cantilever cylindrical shell with eccentric orthogonal stiffeners, solved by Mustafa and Ali (1987) and Sinha and Mukhopadhyay (1994).
5. First natural frequency of composite cantilever beam with delamination at different locations, solved by Krawczuk et al.(1997).
6. Fundamental frequencies (Hz) of simply supported composite cylindrical shells with centrally located mid-surface delamination, solved by Parhi et al.(2001) and Acharyya et al. (2009).

Table 3.2 Non-dimensional fundamental frequencies ($\varpi = \omega_n L^2 \sqrt{\rho h / D}$) of an isotropic rotating cantilever plate. ($L/b=1$, $h/L=0.12$, $D = Eh^3 / 12(1-\nu^2)$, $\nu=0.3$, E is the Young's Modulus of Elasticity)

Non-dimensional speed $\Omega = \Omega' / \omega_0$	Sreenivasamurthy and Ramamurthi (1985)	Karmakar and Kishimoto (2006)	Present FEM
0.0	3.43685	3.41969	3.41748
0.2	3.51858	3.49992	3.49764
0.4	3.75280	3.72887	3.72640
0.6	4.12875	4.07813	4.07538
0.8	4.56786	4.51561	4.51250
1.0	5.09167	5.01415	5.01066

Table 3.3 Non-dimensional fundamental frequencies ($\varpi = \omega_n L^2 \sqrt{\rho / E_{11} h^2}$) of three layer [$\theta, -\theta, \theta$] graphite-epoxy twisted plates. ($L/b = 1, b/h = 20$, Twist angle(ϕ) = 30° , $E_{11} = 138.70$ GPa, $E_{22} = 8.96$ GPa, $G_{12} = 7.1$ Gpa, $\nu_{12} = 0.3$)

θ (Deg.)	Qatu and Leissa (1991)	Present FEM
0	0.9553	0.9431
15	0.8759	0.8629
30	0.6923	0.6812
45	0.4831	0.4752
60	0.3283	0.3245
75	0.2582	0.2572
90	0.2434	0.2431

Table 3.2 presents non-dimensional fundamental frequencies of an isotropic rotating cantilever plate, and Table 3.3 furnishes the non-dimensional fundamental frequencies of a three layer graphite epoxy twisted plates with different fibre orientation. Table 3.4 shows the conformity of the present result with Nayak and Bandyopadhyay(2005)and Das and Chakravorty (2011), which comprises natural frequencies of antisymmetric cross-ply and crossed stiffened plate with "eccentric at bottom" stiffeners. Further, Table 3.5 ensures the correctness of the present result with Mustafa and Ali(1987) and Sinha and Mukhopadhyay(1994)for an isotropic orthogonally stiffened cylindrical cantilever shell.

Table 3.4 Natural frequencies (Hz) of simply supported antisymmetric cross-ply($0^0/90^0$) crossed stiffened plate with "eccentric at bottom" stiffeners($0^0/90^0$) ($L = b = 254$ mm, $h = 12.7$ mm, $b_{st} = 6.35$ mm, $d_{st} = 25.4$ mm, $E_{11} = 144.8$ GPa, $E_{22} = 9.67$ GPa, $G_{12} = G_{13} = 4.14$ GPa, $G_{23} = 3.45$ GPa, $\nu = 0.3$, $\rho = 1389.23$ kg/m³ and $n_x = n_y = 1$, stiffeners are centrally placed)

Mode Number	Nayak and Bandyopadhyay(2005)	Das and Chakravorty (2011)	Present FEM
1	1141.00	1123.17	1142.03
2	2394.17	2367.77	2398.12
3	2415.82	2407.57	2417.10
4	2646.18	2656.00	2646.31

Table 3.5 Natural frequency (Hz) of cantilever cylindrical shell with eccentric orthogonal stiffeners.($L=b=0.3048$ m, $R=2L$, $h=3.175$ mm, $\rho=7800$ kg/m³, $E = 209 \times 10^9$ N/m², $\nu=0.30$, $n_x=3$, $n_y=2$, stiffeners divide the planform of the shell equally)

Mode number	Mustafa and Ali (1987)		Sinha and Mukhopadhyay (1994)	Present FEM
	Eight-node element	Nine-node element		
1	116	115	116	117.98
2	162	160	154	156.03
3	318	313	314	322.71
4	488	479	499	454.36

For delamination modeling, the results obtained for the fundamental frequency of a composite cantilever beam by varying the relative position of delamination along the span are well confirmed with that of Krawczuk et al. (1997) and is illustrated in Figure 3.1 while the fundamental frequency of simply supported composite cylindrical shell with different percentage of delamination reported by Parhi et al. (2001) and Acharyya et al. (2009) is

shown in Table 3.5. The ability of the present formulation in respect of rotation, twist angle, stiffeners and delamination is well established. Thus, it is evident that this model can successfully analyze free vibration problems of delaminated rotating stiffened shell with pretwist.

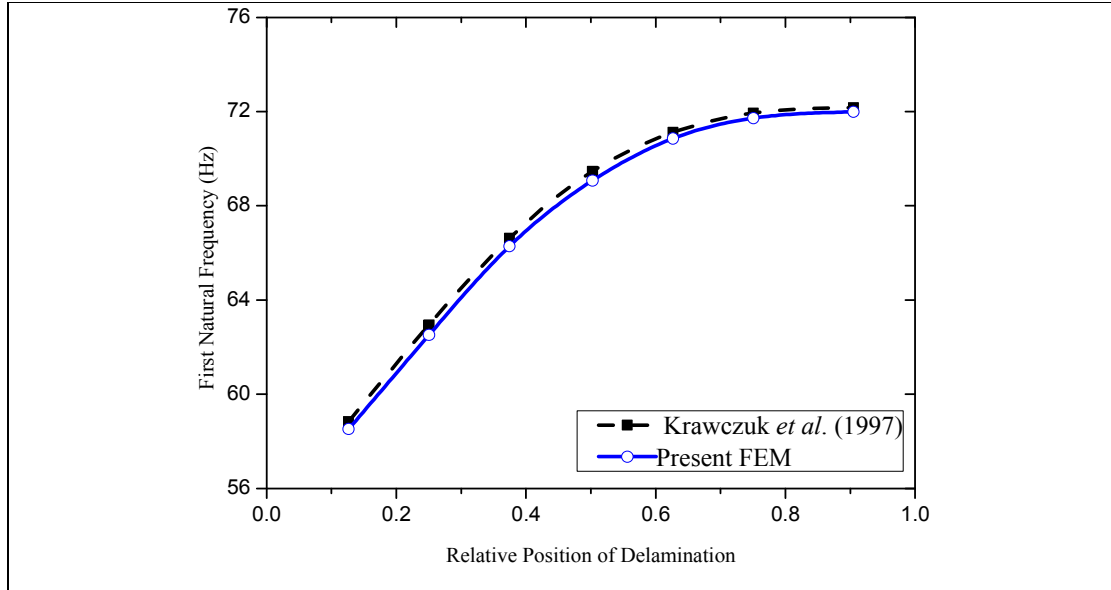


Figure 3.1 The influence of relative position of delamination on the first natural frequency of composite $[0^0/0^0/0^0/0^0/0^0/0^0]$ cantilever beam. ($E_1=57.864$ GPa, $E_2=4.2742$ GPa, $\nu_{12}=0.32$, $G_{12}=G_{13}=G_{23}=1.583$ GPa, $\rho=1380$ kg/m³, $L=600$ mm, $b=50$ mm, $h=25$ mm, $a=37.5$ mm, $h'/h=0.5$, Relative position of delamination= d/L)

Table 3.6 Fundamental frequencies (Hz) of composite $([0^0/90^0]_2)$ cylindrical shells for different extents of centrally located mid-surface delamination for simply supported boundary conditions. $E_{11}=172.5$ GPa, $E_{22}=6.9$ GPa, $G_{12}=G_{13}=3.45$ GPa, $G_{23}=1.38$ GPa, $\rho=1600$ kg/m³, $\nu_{12}=0.25$, $L=b=0.5$ m, $c=d$, $L/h=100$, lamination: $(0^0/90^0)_2$.

R/L	C/L	Parhi et al.(2001)	Acharyya et al. (2009)	Present FEM
5.0	0	129.04	128.99	129.03
	0.5 (25%)	104.56	104.51	104.55
	0.75 (56.25%)	98.24	98.19	98.24
10.0	0	103.03	103.04	103.02
	0.5 (25%)	69.60	69.61	69.60
	0.75 (56.25%)	59.88	59.92	59.92

3.3 FREE VIBRATION OF A GENERALIZED DELAMINATED STIFFENED CYLINDRICAL SHELL

Parametric studies are carried out in respect of number of stiffeners in x- and y-directions, location of delamination, fibre orientation, stiffener depth to shell thickness ratio, twist angle and rotational speed to investigate the effect on natural frequencies of stiffened shells. The stiffened shells with two different angle of twist namely 15^0 and 30^0 in addition to untwisted one are considered for the present study. The non-dimensional natural frequencies for the stiffened cylindrical shells ($R_x = 0$) having square plan form, thicknessratio ($b/h = 100$) and curvature ratio ($b/R_y = 0.5$) are obtained corresponding to different location of delamination along the thickness and span of the stiffened shell. The non-dimensional frequencies of the stiffened shell are also presented corresponding to different non-dimensional rotational speeds ($\Omega = \Omega' / \omega_n = 0.00, 0.50$ and 1.00). The graphite-epoxy composite is considered for the analysis, whose material properties are as follows (Qatu and Leissa, 1991): $E_1 = 138.0$ GPa, $E_2 = 8.96$ GPa, $G_{12} = G_{13} = 7.1$ GPa, $G_{23} = 2.84$ GPa, $\nu_{12} = 0.30$

As far as delamination is concerned, the width of delamination is always assumed same as that of the shell as earlier considered by Krawczuk et al. (1997) and Shen and Grady (1992). A number of problems have been considered by the authors to check the effect of the non-dimensional frequencies ($\varpi = \omega_n L^2 \sqrt{\rho / E_1 h^2}$) of cantilever stiffened cylindrical shells with the following variations:

1. Un-stiffened shell (A), shell with one x-directional stiffener (B), shell with one y-directional stiffener (C) and shell with one stiffener in each direction i.e. crossed stiffened (D) are taken into consideration.
2. Position of delamination is kept varying along the length and across the thickness for a typical shell with different stiffener arrangements such as B, C, D for different twist angles.
3. The stiffener depth to shell thickness ratio has been varied for three types of delaminated stiffened structures (B,C and D) for various twist angles.
4. A typical shell with a particular stiffener arrangement subjected to various non-dimensional rotational speeds is studied by varying stacking sequence and twist angles. The fibreorientations of the shell and of stiffeners are varied from 0^0 to 90^0 with an increment of 15^0 for the particular lamination.

3.3.1 Effect of delamination on un-stiffened shell, stiffened shell and twisted stiffened shell

Figure 3.2 presents the variation of non-dimensional fundamental frequency (NDFF) with fibre orientation angle of eight layered $[\theta/-\theta/\theta/-\theta]_s$ symmetric untwisted shell, crossed stiffened shell (without delamination) and crossed stiffened shell with a delamination of 33% at the mid-plane of the shell. It is evident that addition of stiffener increases both stiffness and mass of the shell, but as stiffness is more significant than mass, the fundamental frequency increases by considerable amount. Percentage increases in non-dimensional fundamental frequency due to addition of one crossed stiffener are 22.75, 27.59, 37.39, 31.26, 13.81, 25.62 and 48.11 for fibre orientation of 0° , 15° , 30° , 45° , 60° , 75° and 90° respectively. It reveals that percentage increase in NDFF of the shell increases with variation of fiber angle from 0° to 30° and 60° to 90° but reduces within the range 30° to 60° irrespective of delamination. It is further noted that appearance of delamination on the shell reduces the NDFF of the unstiffened shell and crossed stiffened structure to a significant amount because of the reduction of elastic stiffness of the structure. In unstiffened shell the decrease of frequency due to delamination is found for all the angles of fibre orientation but in cross stiffened shell the reduction is found insignificant at $\theta = 60^\circ$ and 75° . The frequency drop is maximum at the fiber orientation 45° and 30° for delaminated unstiffened and crossed stiffened shell, respectively. The NDFF is obtained maximum at $\theta = 30^\circ$ and minimum at $\theta = 90^\circ$ for crossed stiffened shell irrespective of presence of delamination.

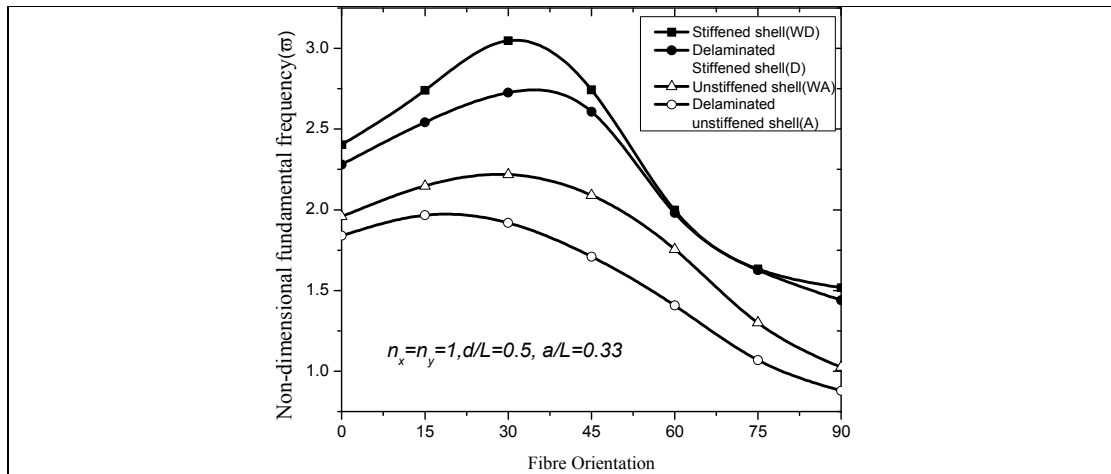


Figure 3.2 Effect of fiber orientation on non-dimensional fundamental frequency for crossed stiffened shell without delamination (WD), delaminated stiffened shell (D), undelaminated unstiffened shell (WA) and delaminated unstiffened shell (A). $L/b = 1$, $b/h = 100$, $b/R_y = 0.5$, $b_{st} = 2h$ and $d_{st} = 4h$, $\Phi = 0^\circ$

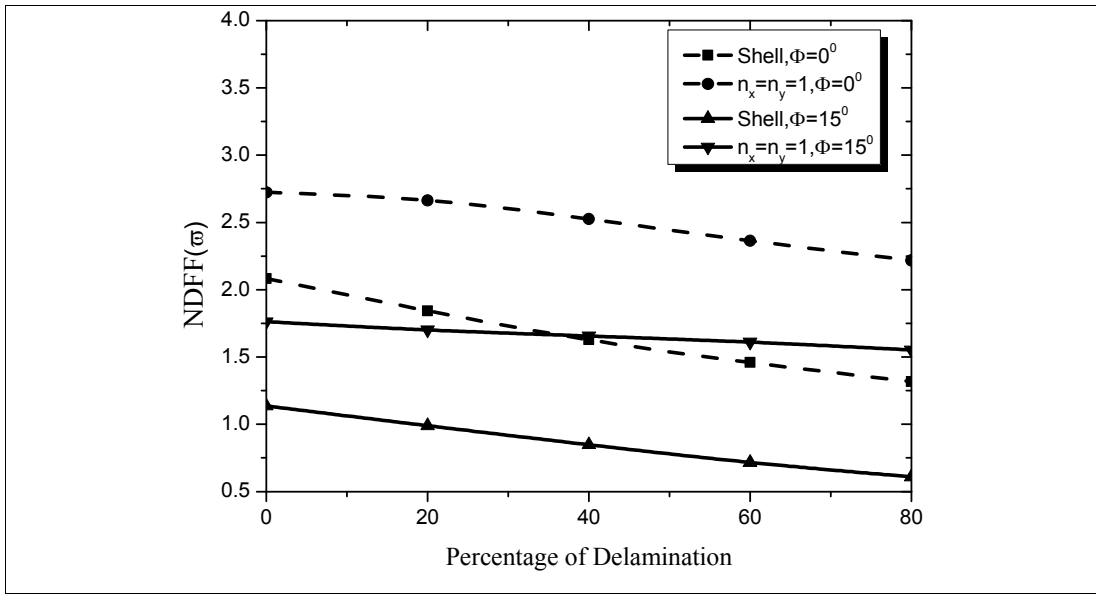


Figure 3.3 Effect of percentage of delamination at the mid plane on NDFF of [45/-45/45/-45]_s laminated stiffened shell along the length. $L/b = 1$, $b/h = 100$, $b/R_y = 0.5$, $b_{st} = 2h$ and $d_{st} = 4h$

Figure 3.3 shows the variation of non-dimensional fundamental frequency (NDFF) with percentage of delamination present in a symmetric angle ply bare and cross stiffened shell. Here four cases are considered such as untwisted unstiffened shell, twisted unstiffened shell, untwisted crossed stiffened shell, and twisted crossed stiffened shell to study the effect of percentage of delamination present in the shell on natural frequency. Obviously, appearance of delamination in the shell reduces the value of natural frequency due to reduction of elastic stiffness, which reflects in the Figure 3.3 for all the cases. Higher is the percentage of delamination, lower is the fundamental frequency. Increasing the twist angle leads to reduction in the value of fundamental frequency irrespective of the presence of delamination for both stiffened and unstiffened shells. The drop of non-dimensional fundamental frequency in case of twisted stiffened shell is marginal for the increase in percentage of delamination. The most interesting point observed from this analysis is that in stiffened shell, the value of NDFF corresponding to 80% delamination is still more than that of the value of bare shell without delamination.

3.3.2 Effect of delamination along the span of the laminated shell

The non-dimensional fundamental frequencies of the four models (A,B,C,D) with varying relative position of delamination along the span of the cantilever for untwisted and twisted symmetric cross-ply composite ($[0/90/0/90]_s$) is illustrated in Figure 3.4.

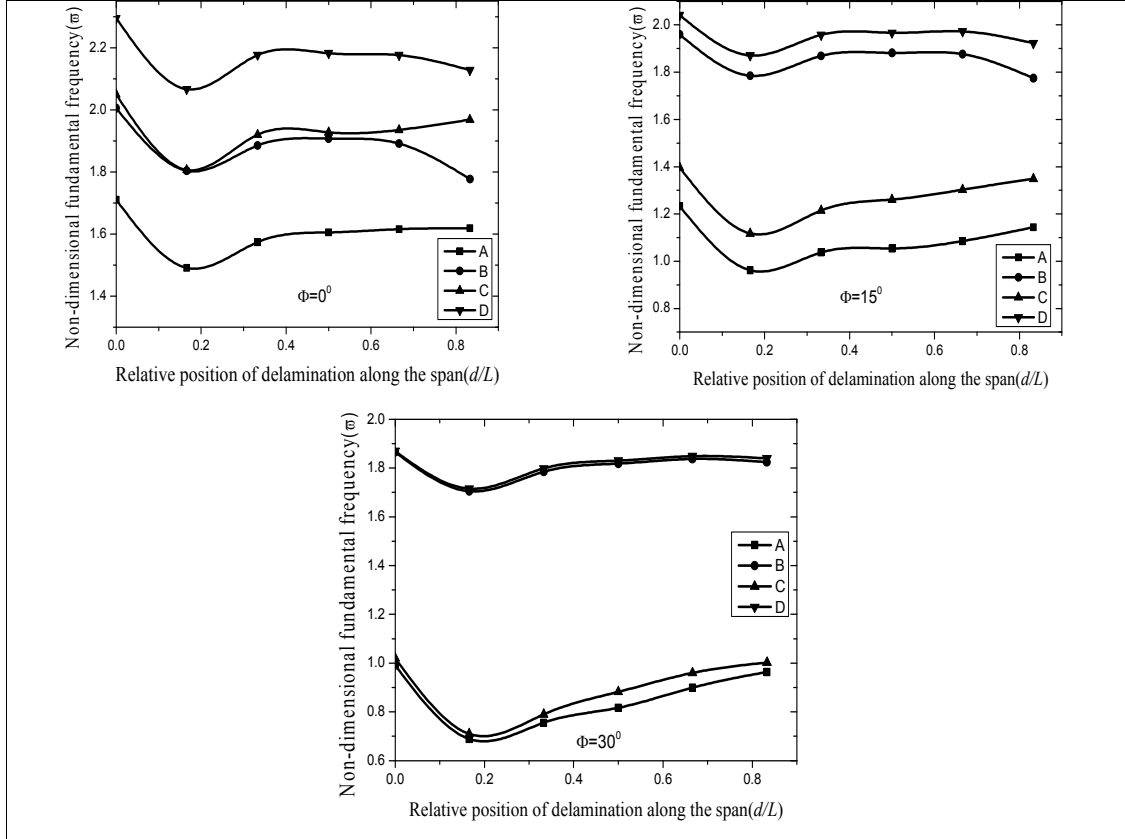


Figure 3.4 Variation of non-dimensional fundamental frequency of symmetric cross ply composite ($[0/90/0/90]_s$) stiffened shell with relative position of delamination along the span (d/L). $L/b = 1, b/h = 100, b/R_y = 0.5, b_{st} = 2h$ and $d_{st} = 4h$

Delamination of 33.3% ($a/L = 0.333$) is considered at the mid-plane of the shell. NDFF are observed to decrease with the increase of twist angle for both shell and stiffened shell. Delamination located near the fixed end of the cantilever have lower frequency than that located towards the free end for unstiffened shell and y-directional stiffened shell as corroborate by Krawczuk et al. (1997). But for x-directional and crossed stiffened shell, this trend is found up to the mid span and then decreases gradually for twist angle 0° and 15° . This can be due to the fact that the effect of mass for x-stiffener is more towards the free end compared to y-stiffener. However, for 30° of twist angle, x-directional and crossed stiffened shell NDFF increases as delamination shifts from fixed to free end but the increase is

marginal. At $\Phi = 0^\circ$, the performance of y-stiffener is better than x-stiffener but in twisted shell x-stiffener provides higher value of fundamental frequency compared to y-stiffener.

3.3.3 Effect of delamination along the thickness of the laminated stiffened shell

Figure 3.5 furnishes the non-dimensional fundamental frequency of a symmetric angle ply composite ($[45/-45/45/-45]_s$) for various relative position of delamination across the thickness of the shell. A delamination of 33.3% of the length of the shell is considered at mid span ($d/L=0.5$).

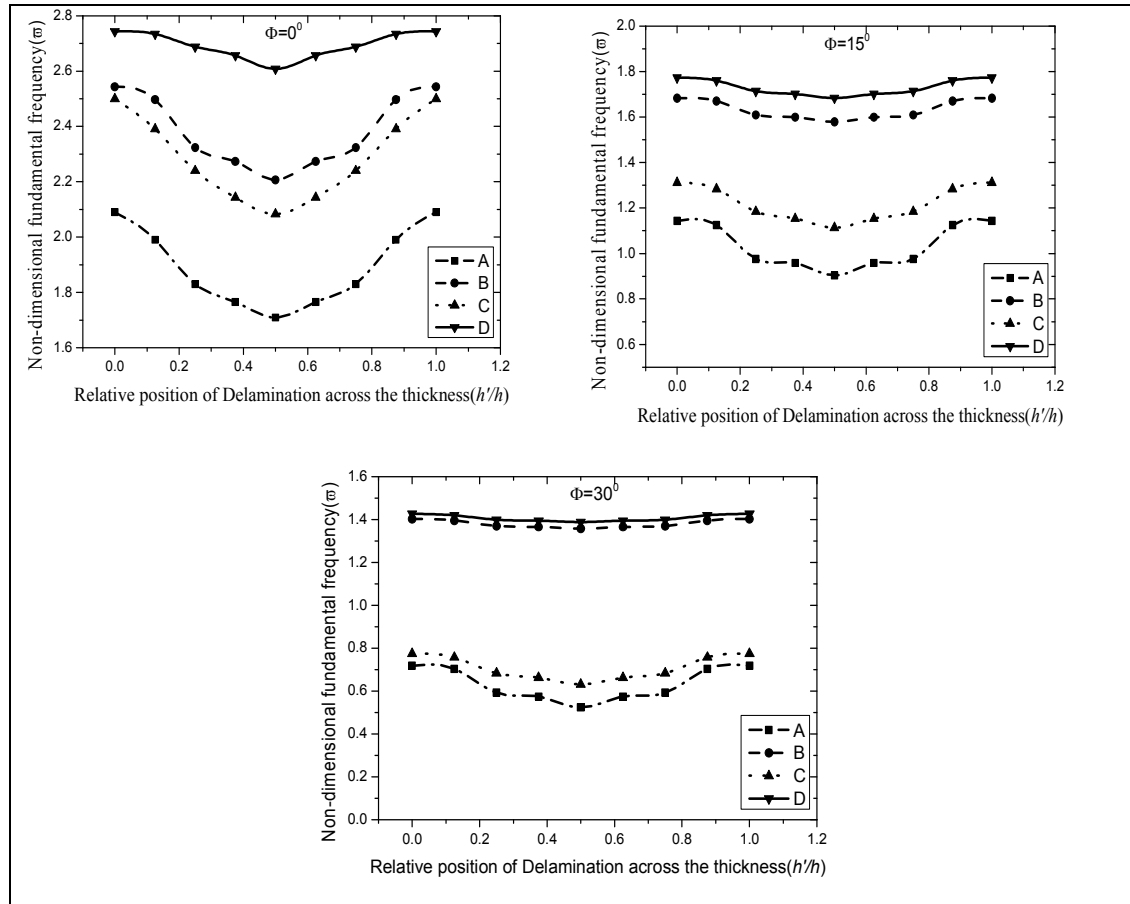


Figure 3.5 Variation of non-dimensional fundamental frequency by varying relative position of delamination across the thickness. $L/b = 1, b/h = 100, b/R_y = 0.5, b_{st} = 2h, d_{st} = 4h, a/L = 0.333, d/L = 0.5$

For all the models, the fundamental frequency attains a minimum value at the mid-plane ($h'/h = 0.5$) irrespective of angle of twist and maximum with no delamination ($h'/h = 0.0, 1.0$). As delamination moves from top ply to mid-plane, there is a reduction in the value of fundamental frequency and, thereafter, it increases till the bottom ply. Increase in twist angle reduces the percentage of decrease/increase in fundamental frequency as the case may be.

Response curves of model B and D at higher angle of twist shows marginal variation in fundamental frequency for different relative position of delamination. At $\Phi = 30^\circ$, the frequency response curves of x-directional and cross stiffened shell are very close to each other, the same trend is also noticed for y- directional stiffened and bare shell. Hence, for higher angle twisted shell x- directional stiffener is preferable than others. It is observed in both untwisted and twisted shell that higher value of fundamental frequency is obtained with x- stiffeners compared to y-stiffeners because it renders high elastic stiffness to the shell.

3.3.4 Effect of stiffener depth to shell thickness

Figure 3.6 shows the effect of the stiffener depth on non-dimensional fundamental frequency of delaminated eccentric stiffened cylindrical shell for model B,C and D. It is observed that NDFF value initially increases but then attains a saturation at $d_{st}/h=4$ and remains almost constant for all models (B, C and D) corresponding to untwisted stiffened shell. For twisted angle 15° and 30° , the fundamental frequency increases with increase in d_{st}/h ratio for model B and D but model C exhibits the same trend both for untwisted and twisted shell.

It is very interesting to note that the NDFF increases with stiffener depth for model B and D but for set up C it remains almost constant for twisted shells. In the range of d_{st}/h from 0 to 4, the NDFF is less for higher angle of twist but the reverse trend is observed when $d_{st}/h > 4.0$ for model B. The same observation is also obtained for the model D but the value of d_{st}/h about which the trend is reversed is 4.5. This may be due to increase in stiffness by the x- directional stiffener particularly at larger cross-sectional area to overcome the combined effect of delamination and twist. In general, it is observed that increase in twist angle reduces the effect of delamination but when $d_{st}/h < 4.0$, the area of the beam is not sufficient to overcome the effect of twist and delamination. For model C, higher is the angle of twist, lower is the NDFF. On comparing model B with D, it is noted that beyond the value of d_{st}/h is equal to 4.5, higher values of fundamental frequency are achieved by the latter for any value of twist angle, although increase of twist angle usually leads to decrease in the fundamental frequency. Further, it is noted that in untwisted case curved y- stiffener renders considerably greater elastic stiffness to the shell as compared to x- stiffener, whereas for twisted shell higher stiffness is provided by x- stiffener.

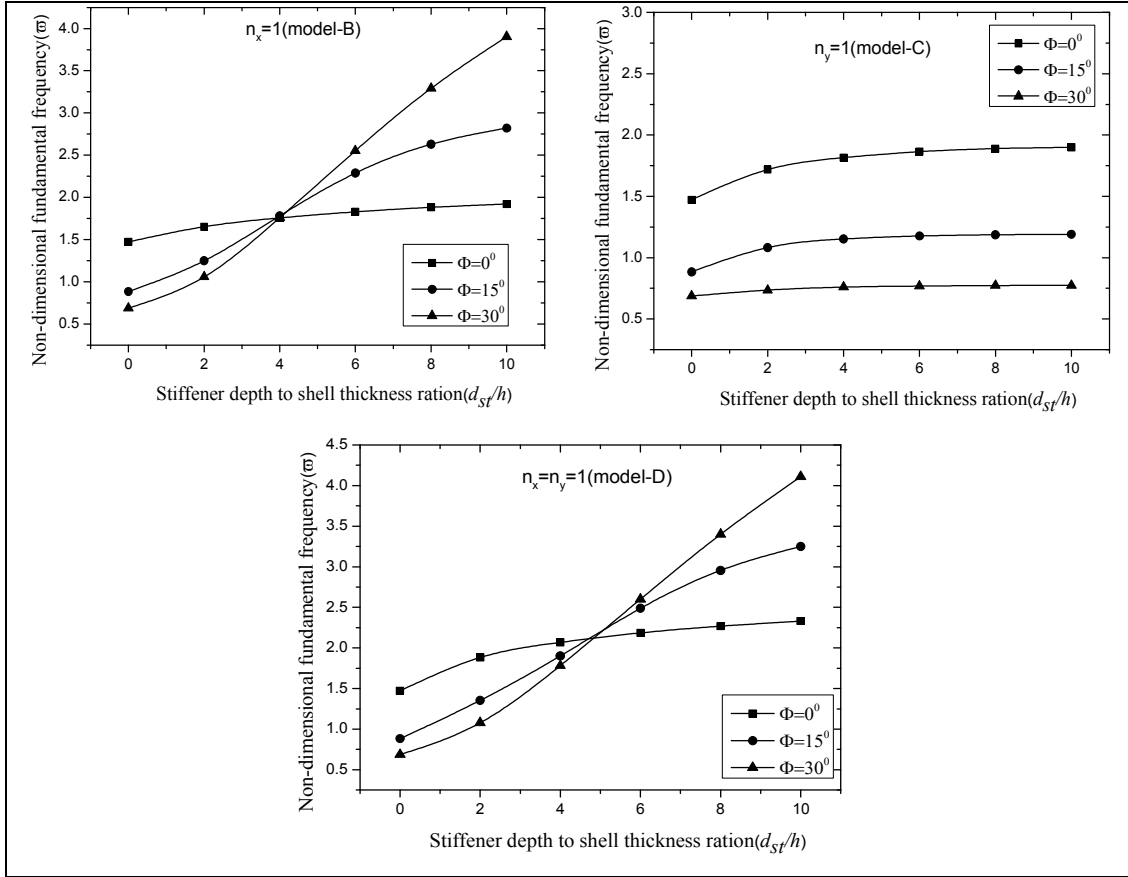


Figure 3.6 Variation of non-dimensional fundamental frequency with stiffener depth to shell thickness ratio of delaminated stiffened composite([0/90/0/90]_s) cylindrical shell, $L/b = 1$, $b/h = 100$, $b/R_y = 0.5$, $b_{st} = 2h$, $a/L = 0.666$, $d/L = 0.5$, $h'/h = 0.5$

3.3.5 Effect of stacking sequence, angle of twist, and rotation

The variation of non-dimensional fundamental frequency of composite cylindrical stiffened shell with one eccentric stiffener in each direction at bottom with a mid-plane delamination of 33.3% centered at a relative distance, $d/L=0.5$ from the fixed end of the cantilever is shown in the Table 3.7. The eight layered $[\theta/-\theta/\theta/-\theta]_s$ delaminated stiffened shell considered is allowed to rotate at 50% ($\Omega=0.5$) and 100% ($\Omega=1.0$) of its natural frequency.

Non-rotating un-twisted cantilever stiffened shell and its delaminated cases shows that maximum value of NDFF is obtained at fibre angle 30° and minimum value at $\theta=90^\circ$. The value of NDFF increases from 0° to 30° of fibre angle and then gradually decreases to minimum. For twist angle 15° and 30° , maximum value is obtained at fibre angle 15° and 0° respectively, whereas minimum is being attained when the fibres are parallel to the fixed

edge ($\theta=90^0$). Increasing twist angle for a particular fibre angle reduces the NDFF value

Table 3.7 Variation of non-dimensional fundamental frequency of delaminated angle ply symmetrical composite ($[\theta/-\theta/\theta/-\theta]_s$) cylindrical stiffened shells for various fibre orientations and twist angles at different rotational speeds. $L/b=1$, $b/h=100$, $b/R_y=0.5$, $a/L=0.333$, $d/L=0.5$, $h'/h=0.5$, $n_x=n_y=1$, $b_{st}=2h$, $d_{st}=4h$, eccentric stiffener at bottom.

Φ	θ	Stiffened	Delaminated Stiffened Shell		
		shell	$\Omega=0.0$	$\Omega=0.5$	$\Omega=1.0$
		NDFF	NDFF	NDFF	NDFF
0^0	0	2.4036	2.2806	2.6242	3.3062
	15	2.7405	2.5427	2.8804	3.4684
	30	3.0480	2.7256	3.0561	3.2777
	45	2.7432	2.6080	2.8641	3.1043
	60	1.9978	1.9796	2.1862	2.6482
	75	1.6329	1.6258	1.7925	2.1693
	90	1.5168	1.4394	1.6058	1.9260
	0	2.2306	2.0874	2.3346	2.9605
	15	2.2544	2.1149	2.3558	2.9750
15^0	30	2.1504	2.0331	2.2501	2.8220
	45	1.7731	1.6837	1.8532	2.3037
	60	1.3474	1.2887	1.4166	1.7551
	75	1.0508	1.0104	1.1104	1.3758
	90	0.9288	0.8959	0.9831	1.2173
	0	2.2430	2.1823	2.3067	2.8564
30^0	15	2.1600	2.1026	2.2214	2.7863
	30	1.8625	1.8124	1.9173	2.4512
	45	1.4266	1.3882	1.4737	1.9004
	60	1.0328	1.0074	1.0765	1.3903
	75	0.7951	0.7774	0.8304	1.0699
	90	0.7224	0.7079	0.7520	0.9661

except at $\theta=0^0$ wherein 30^0 angle of twist shows a higher value compared to 15^0 angle of twist. The percentage difference between maximum and minimum frequency values of

undelaminated stiffened shell are 50.23, 58.8 and 67.79 and for delaminated 47.18, 57.64 and 67.56 for $\Phi=0^0$, 15^0 and 30^0 , respectively. But these percentages are reduced in case of delaminated stiffened shell. Figure 3.7 shows that the variation of relative frequency(Delaminated frequency/undelaminated frequency) with fiber angles .It depicts that the fluctuation is more for untwisted stiffened shell wherein the relative frequency is almost constant at $\Phi=30^0$. Increase in twist angle reduces the fluctuation of relative frequency and makes it steady. For $\Phi=15^0$, the relative frequency rises gradually with fibre orientation.

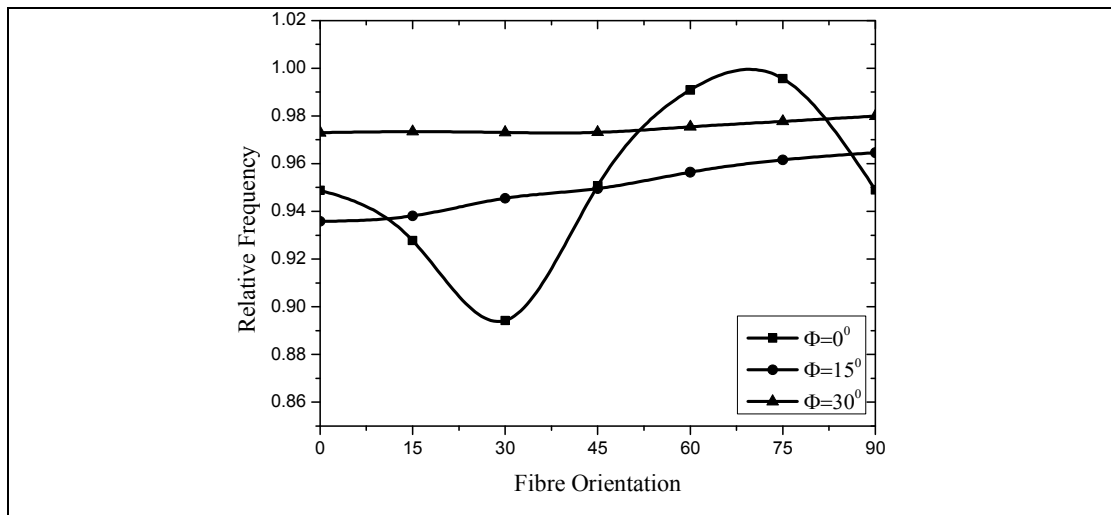


Figure 3.7 Variation of relative frequency with fiber angle orientation. Relative Frequency=Delaminated frequency/undelaminated frequency.

The non-dimensional fundamental frequency always increases with increase in rotational speed of the delaminated stiffened cantilever shell irrespective of twist angle and fiber orientation as observed earlier by Sreenivasamurthy and Ramamurti (1981). The centrifugal force due to rotation increases the stiffening effect which in turn increases the value of fundamental frequency, which can be clearly observed from the Figure 3.8, whereas the non-dimensional fundamental frequency curves show a specific pattern in opposition to the variation in fibre angles. The shell with two stiffeners in x-and y-direction have the maximum rotating frequency as compared to one stiffener in each direction in twisted shell, whereas for untwisted shell the reverse trend is observed at $\theta = 60^0$ and 75^0 . The stiffening effect of two stiffeners in each direction is found more than that of one stiffener except at $\theta = 60^0$ and 75^0 of the delaminated untwisted shell. Maximum value of rotating frequency is obtained at $\theta = 0^0$ and minimum at $\theta = 90^0$.

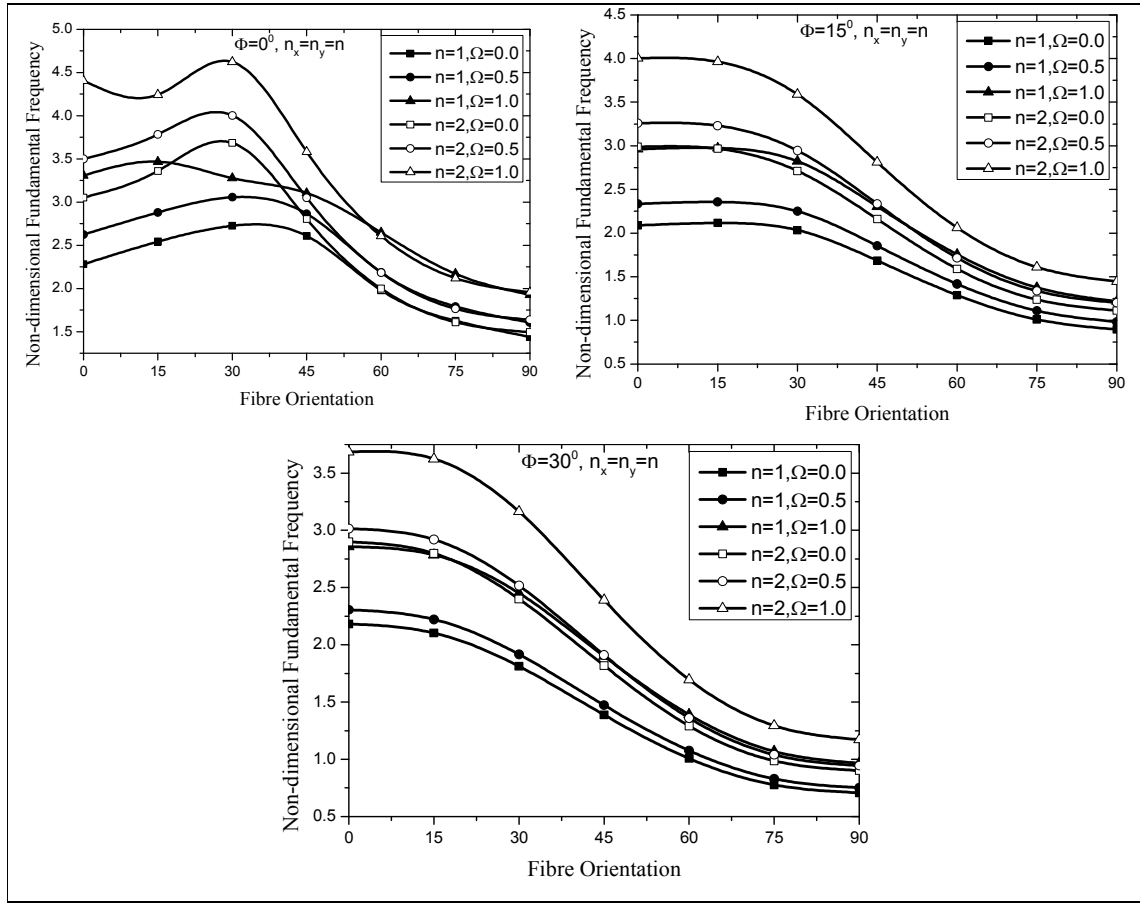


Figure 3.8 Variation of NDFF with fibre angle orientation at stationary ($\Omega=0.0$) and rotating ($\Omega=0.5$ and 1.0) conditions with one and two stiffener in each directions. $L/b=1$, $b/h=100$, $b/R_y=0.5$, $b_{st}=2h$, $d_{st}=4h$, $a/L=0.333$, $d/L=0.5$, $h'/h=0.5$

3.3.6. Mode shapes

In Table 3.8, surface and contour plot for the first four mode shapes of eight layered graphite epoxy square cylindrical shells and stiffened cylindrical shells without delamination are depicted for stacking sequence $[45/-45/45/-45]_s$. It is observed that the symmetrical mode shapes are found in all modes of vibration of the un-stiffened shell. The four mode shapes of the un-stiffened shell are first torsion mode (1T), first span-wise bending mode(1B), first cord wise bending mode(1C) and finally second torsional mode(2T). In case of the stiffened shell, the four mode shapes are 1B, 1T, 1C, and 2T. Due to the addition of stiffener, the first mode of the shell is converted to bending mode because of the decrease of torsional rigidity.

A set of mid surface contour plot for first four mode shapes of the delaminated stiffened shell for different twist angles and rotational speeds are illustrated in Table 3.9. For

untwisted($\Phi=0^0$) stationary stiffened shell, first mode is the first twisting mode(1T) and second mode confirms first span wise bending mode(1B) while third and fourth mode reveals first cord wise bending(1C) and second torsion(2T) respectively. Introduction of rotation in untwisted stiffened shell induces torsion along with bending in all mode shapes. For twisted stiffened stationary shells($\Phi=15^0,30^0$), first span wise bending(1B) is observed in the fundamental mode. The second mode is first twisting mode(1T) for the stationary stiffened shell of twist angle $\Phi=15^0$ while the second mode of 30^0 twisted stationary stiffened shell is the coupled bending and twisting mode. The third and fourth modes are combination of bending and torsion for twisted stiffened shells($\Omega = 0.0$).The first span wise bending modes(1B) of the twisted stiffened shell is not much influenced by rotation while the dominance of torsion mode is clearly observed with increase in the rotational speed in second, third, and fourth modes of the twisted shell.

Table 3.8 Effect of stiffener on First four mode shapes of eight layered symmetric angle ply $[45/-45/45/-45]_s$ cylindrical shell, $n_x = n_y = 1$, $b_{st} = 2h$, $d_{st} = 4h$

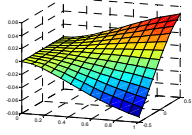
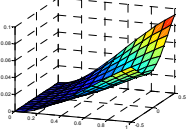
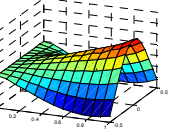
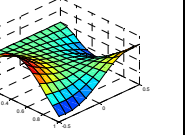
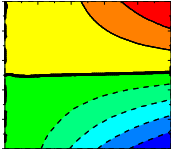
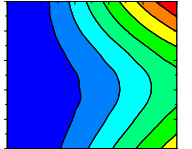
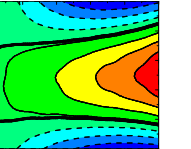
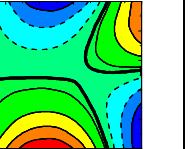
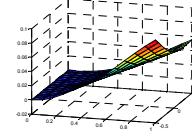
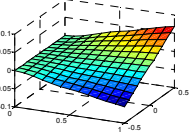
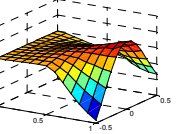
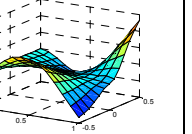
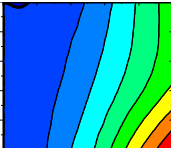
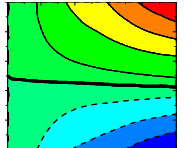
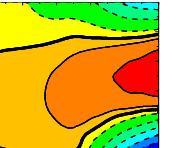
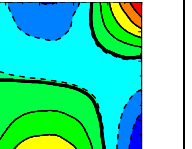
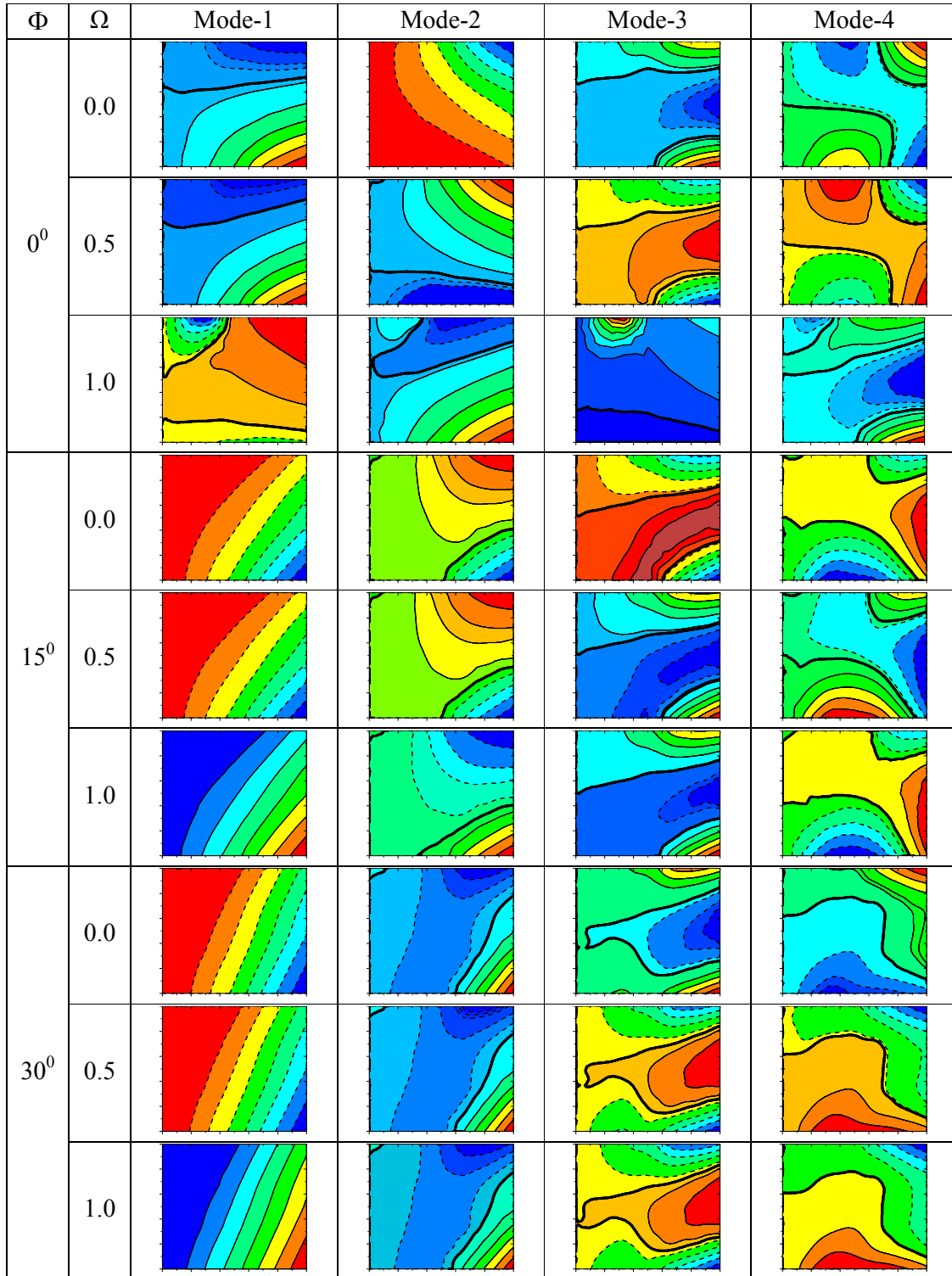
	Mode-1	Mode-2	Mode-3	Mode-4
Unstiffened Shell				
				
Stiffened Shell				
				

Table 3.9 Effect of twist angle and rotation on first four mode shapes of eight-layered symmetric mid-plane delaminated angle ply composite($[45/-45/45/-45]_s$) stiffened cylindrical shell, $a/L=0.333$, $d/L=0.5$, $n_x = n_y = 1$, $b_{st} = 2h$, $d_{st} = 4h$.



3.4 FREE VIBRATION OF LONG, INTERMEDIATE AND SHORT CYLINDRICAL STIFFENED SHELLS

The present analysis is based on long, intermediate and short cylindrical stiffened shells. The long, intermediate and short shells are categorized by Aas-Jakobsen's parameters (Γ, Λ) are defined as (Karmakar et al. , 2005 and Chakravorty and Bandyopathyay, 1994):

$$\Gamma = \left(\frac{12\pi^4 R^6}{L^4 h^2} \right) \text{ and } \Lambda = \left(\frac{\pi^2 R^2}{L^2 \Gamma^2} \right) \quad (3.1)$$

The dimensions of the shells considered for the present analysis are as follows:

1. Long shell ($\Gamma < 7, \Lambda < 0.12$): $L=1.0$ m, $b=0.5$ m, $h=0.005$ m, $R=0.5$ m, $\Gamma=5.40$, $\Lambda=0.084$.
2. Intermediate shell ($7 < \Gamma < 10, 0.12 < \Lambda < 0.15$): $L=0.8$ m, $b=0.5$ m, $h=0.005$ m, $R=0.8$ m, $\Gamma=8.60$, $\Lambda=0.1334$.
3. Short shell ($\Gamma > 10, \Lambda > 0.15$): $L=0.6$ m, $b=0.5$ m, $h=0.005$ m, $R=0.9$ m, $\Gamma=10.84$, $\Lambda=0.188$.

Following material properties of graphite-epoxy composite are considered for the parametric analysis (Qatu and Leissa, 1991).

$$E_1 = 138.0 \text{ GPa}, E_2 = 8.96 \text{ GPa}, G_{12} = G_{13} = 7.1 \text{ GPa}, G_{23} = 2.84 \text{ GPa}, \nu_{12} = 0.3$$

For all the examples considered, the stiffeners are of rectangular in cross-section and follow the nodal lines. Unless and otherwise specified, the stiffeners have same ply orientation and number of layers as that of the shell. The thickness of plies in the laminate is equal (thickness of laminate /number of plies). The stiffeners are placed in such a way that it divides the planform of shell equally. The stacking sequences of the laminates are always expressed from the top ply to bottom ply along the z -axis. The delamination in the shell is always considered through the complete width of the shell. The cantilever stiffened shells are always considered to rotate about z - axis. The boundary conditions adopted for the cantilever stiffened shells are expressed as

$$\text{At } x = 0, \quad u = v = w = \alpha = \beta = 0 \quad (3.2)$$

Following examples are considered by the authors to study the effect of delamination, twist angle, number of layers, eccentricity of stiffeners, stacking sequence and rotation on non-dimensional fundamental frequencies ($\varpi = \omega_n b^2 \sqrt{\rho / E_1 h^2}$) of the long, intermediate and short cylindrical stiffened shells.

1. The effect of delamination on the fundamental frequency of both un-stiffened and stiffened long, intermediate and short shells are presented by varying its position across the thickness at different twist angles.
2. Three models considered for analysis: Model-A: long shells with three stiffeners in each direction, Model-B: Intermediate shells with three stiffeners in each direction and Model-C: Short shells with three stiffeners in each direction. Effect of eccentricity of stiffeners on fundamental frequencies of delaminated Model- A, B, and C composed of both angle ply and cross-ply at various twist angles are presented.
3. Effect of twist angle and rotation on non-dimensional fundamental frequencies of Model- A, B, and C have been furnished.
4. Effect of the number of layers of ply in long, intermediate, and short stiffened shells composed of both cross ply and angle ply on fundamental frequency have been investigated.
5. Mode shapes of both un-stiffened and stiffened long cylindrical shell of a symmetric cross-ply laminate are presented to show the effect of rotation and twist angle.

3.4.1 Effect of delamination

Figure 3.9 shows the variation of fundamental frequencies of eight layered 50% delaminated ($d/L = 0.5$) cross-ply un-stiffened/stiffened cylindrical shells at twist angles of 0^0 and 15^0 by varying the relative position of delamination (h'/h) across the thickness. It reveals that delamination reduces the fundamental frequency of the shell because of the decrease in elastic stiffness. But the addition of stiffeners increases the elastic stiffness thereby minimizes the effect of delamination to some extent as observed from the Figure 4(b) and (d). It reveals that minimum fundamental frequencies are obtained at $h'/h = 0.5$ (delamination in between fourth and fifth layer) in all cases considered irrespective of twist angle. It may be noted that increase in twist angle increases the effect of delamination in un-stiffened shell whereas the same is reduced in the case of stiffened shell. It is to be noted that lower value of frequency is always obtained at all the positions of delamination (h'/h) in long shells with stiffener while the higher value of the same is always observed in the short shells with or without stiffeners. At $\Phi = 15^0$, lower value of frequency is obtained in the un-stiffened intermediate shell. Thus an increase in twist angle improves the performance of un-stiffened long shell over the intermediate shell. The reduction of the fundamental frequency is more remarkable in the short shell as compared to long and intermediate shells with and without stiffeners at all twist angles.

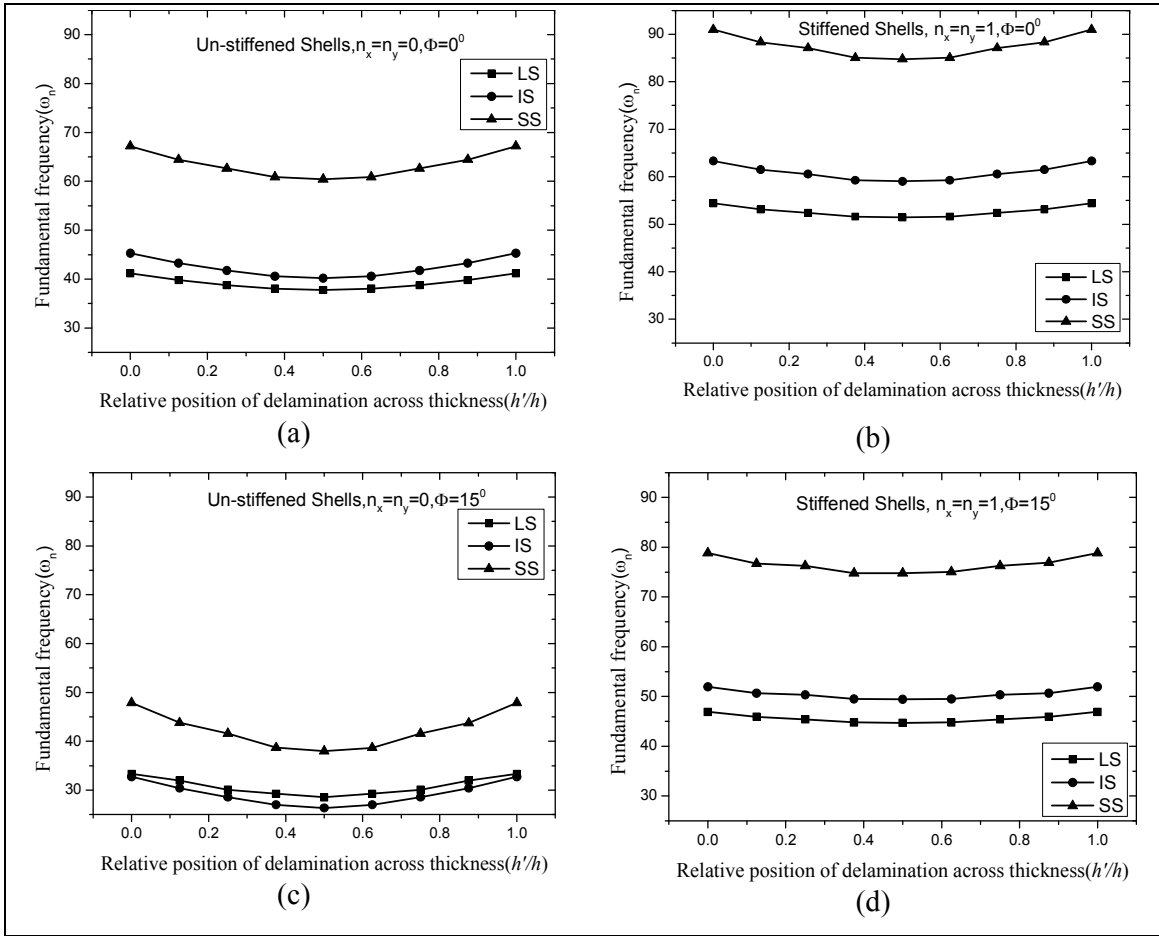


Figure 3.9 Variation of fundamental frequency with relative position of delamination across the thickness of un-stiffened and stiffened composite $([0/90/0/90]_s)$ cylindrical shells at $\Phi=0^\circ$ and 15° , $b_{st} = 2h$, $d_{st} = 4h$, $a/L = 0.50$, $d/L=0.5$, $n_x = n_y=1$, $\rho=22080 \text{ kg/m}^3$, LS: Long Shell, IS: Intermediate Shell, SS: Short Shell

3.4.2 Effect of eccentricity of stiffeners

General studies of the three different types of stiffeners (eccentric at the top, eccentric at the bottom and concentric) with three stiffeners in each direction are furnished in the Table 3.10. This analysis is carried out both for untwisted and twisted long, intermediate and short shells with cross ply and angle ply laminates. As expected the maximum fundamental frequency is obtained in the short stiffened shells while minimum in the long stiffened shells. It reveals that eccentric type (both top and bottom) stiffeners have higher frequency values than the concentric one except at $\Phi=0^\circ$ of the long shell (angle ply), wherein concentric stiffeners

have a higher value of frequency than eccentric at the bottom. Eccentric stiffener gives higher fundamental frequencies due to the fact that first and second moment of area of the stiffeners

Table 3.10 Fundamental frequencies (ω_n) of graphite-epoxy composite (angle-ply [45/-45/-45/45] and cross-ply [0/90/90/0]) delaminated cylindrical shells with three different types of stiffeners. $b_{st} = 2h$, $d_{st} = 4h$, $a/L = 0.50$, $d/L = 0.5$, $n_x = n_y = 3$, $\rho = 22,080 \text{ kg/m}^3$.

Shell type	Twist angle (Φ)	Eccentric at top		Eccentric at bottom		Concentric	
		Cross-ply	Angle-ply	Cross-ply	Angle-ply	Cross-ply	Angle-ply
Long (A)	0	67.2041	73.84112	58.5489	63.888	57.3976	64.16858
	15	59.7850	58.03164	53.3261	49.59684	46.7079	45.99072
	30	49.3829	43.9063	45.6075	37.29379	35.2949	30.35583
Inter (B)	0	82.0161	81.18147	73.2946	67.19441	69.6070	65.90301
	15	72.4418	63.25742	66.4006	52.88882	51.6418	43.8244
	30	62.8471	49.42301	59.4087	42.92528	40.7651	28.12739
Short (C)	0	126.0694	129.3994	111.8239	108.5053	101.8717	102.8382
	15	113.6170	97.19132	107.1126	83.32453	78.3388	62.17428
	30	102.1756	79.04906	99.0094	70.88367	65.8384	41.71002

increases with eccentricity, thereby increases the stiffness without increasing the mass. Comparing between the two eccentric kinds, eccentric at the top provides higher values of the fundamental frequency. The increase in twist angle reduces the fundamental frequency as normally expected. From the Table 3.9, it is observed that compared to the untwisted case, percentage of decrease of fundamental frequency for a given twist angle of 15° in the long, intermediate and short shell of cross-ply laminate with eccentric at top stiffeners are 12.40, 13.12, and 10.95, with eccentric bottom stiffeners are 9.79, 10.38, and 4.39, and with concentric stiffeners are 22.88, 34.78, and 30.03, respectively. The percentage of the decrease due to 15° twist angle in the case of angle-ply laminates with eccentric top stiffeners are 27.24, 28.33, and 33.13, while with eccentric bottom stiffeners, these values are 28.81, 27.04, and 30.22, but with concentric stiffeners these are 39.52, 50.37, and 65.40 for long, intermediate, and short shells, respectively. Hence, the observation made here is that cross-ply laminates are preferably suitable for twisted stiffened shells than angle ply because of the less percentage of decrease in fundamental frequencies. In the case of untwisted stiffened shells, angle-ply laminates show better performances than cross-ply for long and short shells, while the use of cross-ply is beneficial in intermediate shells. It is also observed that for the

high value of the angle of twist ($\Phi=30^0$), short shells are preferred because of the decrease of fundamental frequencies due to twist are less than that of long and intermediate shells.

3.4.3 Effect of twist angle and rotation

Effect of rotational speed on the non-dimensional fundamental frequencies (NDFF) of the mid-plane delaminated long, intermediate and short stiffened shells at different twist angles are shown in Table 3.11. It reveals that for untwisted rotating delaminated stiffened shells, the NDFF are observed to attain maximum value in short stiffened shells, while minimum values are attained in long shells. The increase in twist angle is found to reduce the fundamental frequency in all the shells as corroborated by Qatu and Leissa(1991). The percentage decrease of stationary non-dimensional fundamental frequencies for twist angle of 15^0 , compared to untwist cases of delaminated long, intermediate and short stiffened shells having eccentric top stiffeners are 21.41, 22.08 and 24.89 but with eccentric bottom stiffeners, the values are 22.37, 21.29 and 23.21 while with concentric stiffeners these are 28.33, 33.50 and 39.54, respectively. A similar observation for twist angle of 30^0 is also observed, and thus, the study reveals that the percentage reduction in fundamental frequency due to twist angle is observed maximum always in short stiffened shells and minimum in most of the cases for long shells except with eccentric bottom stiffener. Considering the fact that the percentage decrease in fundamental frequency is found to be maximum in concentric stiffeners and minimum in eccentric stiffeners, it can be said that eccentric top stiffeners will be favorable by the designers.

Effect of centrifugal stiffening is found in all types of shell irrespective of the type of stiffeners and twist angles. Percentage of increase in non-dimensional fundamental frequencies at low speed ($\Omega=0.5$) and high speed ($\Omega=1.0$) at different twist angles of this results are also presented in Figure 3.10. The percentage of increase in rotating NDFF at low speed of untwisted ($\Phi=0^0$) stiffened shells is found to be maximum at 7.32 (Intermediate shell with eccentric bottom stiffeners) whereas for twist angle 15^0 and 30^0 the values are 8.96(short shell with eccentric top stiffeners) and 12.67(short shell with eccentric top stiffeners), respectively. However, for high speed the maximum rise in rotating frequency at twist angles $0^0, 15^0$ and 30^0 are 25.82 (long shell with concentric stiffeners), 29.03 (long shell with concentric stiffeners) and 35.79 (short shell with eccentric top stiffeners), respectively. It may be noted that at low/high speeds the percentage of increase in frequency rises rapidly with twist angle in shells with eccentric top stiffeners but the same value decreases with increase in twist angle, and it is observed in shells with eccentric bottom stiffeners except in

intermediate and short shell at high speed. In concentric stiffened shells, the gain in rotating fundamental frequency increases with twist angle at low/high speed but for the long shells rise of the curve is poor towards higher twist angles.

Table 3.11 Non-dimensional fundamental frequency(NDFF) of delaminated four layered angle ply [45/-45/-45/45] stiffened long, intermediate and short shells at rotating state for different twist angles. $b_{st} = 2h$, $d_{st} = 4h$, $a/L = 0.50$, $d/L=0.5$, $n_x = n_y=3$.

Shell Type	Twist Angle (Φ)	Eccentric top			Eccentric bottom			Concentric		
		$\Omega=0$	$\Omega=0.5$	$\Omega=1.0$	$\Omega=0$	$\Omega=0.5$	$\Omega=1.0$	$\Omega=0$	$\Omega=0.5$	$\Omega=1.0$
LONG (A)	0	1.4768	1.5687	1.8220	1.2778	1.3668	1.5640	1.2834	1.3730	1.6147
	15	1.1606	1.2572	1.4805	0.9919	1.0517	1.2105	0.9198	0.9958	1.1868
	30	0.8781	0.9818	1.1803	0.7459	0.7789	0.9067	0.6071	0.6583	0.7873
INTER (B)	0	1.6236	1.7331	2.0255	1.3439	1.4423	1.6617	1.3181	1.4035	1.6294
	15	1.2651	1.3753	1.6197	1.0578	1.1263	1.3146	0.8765	0.9404	1.1031
	30	0.9885	1.1110	1.3360	0.8585	0.8964	1.0892	0.5625	0.6078	0.7206
SHORT (C)	0	2.5880	2.7590	3.2176	2.1701	2.3205	2.6496	2.0568	2.1858	2.5192
	15	1.9438	2.1181	2.4997	1.6665	1.7767	2.0849	1.2435	1.3319	1.5581
	30	1.5810	1.7813	2.1468	1.4177	1.4747	1.8069	0.8342	0.9005	1.0690

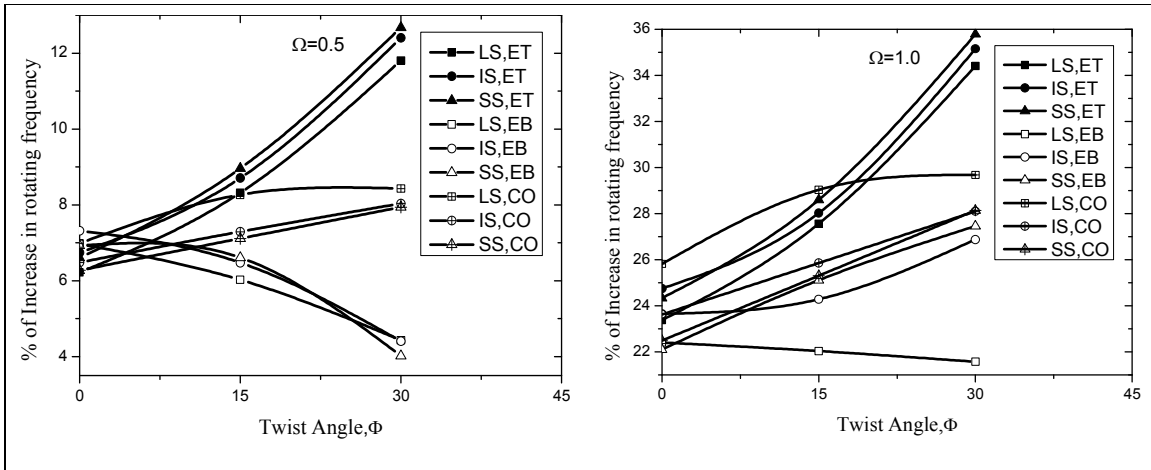


Figure 3.10 Percentage increase in rotating frequencies with respect to twist angles of composite ([45/-45/-45/45]) stiffened shells at $\Omega=0.5$ and $\Omega=1.0$. $b_{st} = 2h$, $d_{st} = 4h$, $a/L = 0.50$, $d/L=0.5$, $n_x = n_y=3$. Note: LS: Long shell, IS: Intermediate shell, SS: Short shell, ET: Eccentric at top, EB: Eccentric at Bottom, CO: Concentric

3.4.4 Effect of number of layers in the laminate

A comparative study is presented considering 4-, 6-, 8-, 10- and 12-layered composite stiffened shells for different twist angles composed of cross-ply (0/90) and angle-ply(-45/45) laminates. Crossed stiffened shells ($n_x = n_y = 1$, eccentric top) are considered with a delamination of 50% ($a/L = 0.50$) at the mid-plane of the shell. The values of non-dimensional fundamental frequency (NDFF) of both un-delaminated and delaminated cases are furnished in graphical form in Figure 3.11 (a) and (b).

The short stiffened shell with angle-ply laminates for the higher number of layers has high-frequency values than others. Considering untwisted and un-delaminated stiffened shells, the value of fundamental frequency increases with increase in the number of layers in long, intermediate and short stiffened shells with cross-ply or angle-ply but the value of fundamental frequency is very close to each other in cross ply laminates at $n=6$ and 8. The increase in fundamental frequency is very rapid in long stiffened shell with angle ply laminates. In the case of the intermediate shell with angle-ply, it is observed that NDFF value increases up to $n=6$ and, thereafter, it almost remains constant. The presence of delamination in the three shells reduces the fundamental frequency to a great extent in both cross-ply and angle-ply laminates. It evident that the effect of delamination on the non-dimensional fundamental frequency decreases with an increase in the number of layers in angle-ply laminates though it is found to be almost uniform in cross-ply laminates irrespective of the number of layers.

It is found that increase in twist angle in all the three types of stiffened shells decreases the fundamental frequency. It is also observed that increase in twist angle improves the performance of cross-ply over angle ply laminates in terms of increase in NDFF in general for lower number of layers. At $\Phi=30^0$, the value of the fundamental frequency of cross-ply laminates are much more than angle-ply laminates in intermediate and short stiffened shells for any number of layers. The dominance of cross-ply over angle-ply laminates is also observed at $\Phi=15^0$ in all types of the shell with the lower number of layers. In addition to this, the value of non-dimensional frequencies of the twisted stiffened shells with angle-ply rises with the increase in the number of layers but the value fluctuates incase of cross-ply laminates.

Figure 3.12 shows the percentage drop in fundamental frequency due to 50% mid-plane delamination at various twist angles in long, intermediate and short stiffened cylindrical shell. Maximum drop in fundamental frequency is observed always in angle ply laminates at

$\Phi=0^0$, $n=4$ for all the three types of shells. The minimum drop is also found in angle ply at $\Phi=0^0$, $n=12$ except short shell, wherein cross-ply laminates attains minimum frequency drop at $\Phi=30^0$, $n=12$. The percentage reduction in frequency is maximum in untwisted shell as compared to twisted shells in case of the cross-ply laminates for any number of layers. The maximum percentage decrease in non-dimensional fundamental frequency for cross-ply laminated is found 7.10% in intermediate stiffened shell at $\Phi=0^0$, $n=4$ while for angle ply it is noticed 26.77 % in short stiffened shell at $\Phi=0^0$, $n=4$. Further, it may be noted that percentage decrease in fundamental frequency due to delamination reduces as twist angle increases in all the cases except at $n=10,12$ for long, $n=8,10,12$ for intermediate and $n=12$ for short shell in the case of angle-ply laminates. From the previous study, it is evident that short stiffened shells are highly efficient in increasing fundamental frequency but the decrease in fundamental frequency due to delamination in this shell is found to be maximum as compared to long and intermediate shells.

3.4.5 Mode shapes

Effect of twist angle and rotational speed on the mode shapes of long un-stiffened and stiffened cylindrical shell with delamination are furnished in Table 3.12. Dark lines in the figures are nodal line with zero displacements while the solid and dashed lines represent positive and negative displacements, respectively. The first four mode shapes of the stationary untwisted long cylindrical shell are, in order, the first torsional mode(1T), the first spanwise bending mode(1B), the first chordwise bending(1C) and finally second torsional mode(2T). It is noticed that at stationary condition the mode shapes of the untwisted delaminated shell are symmetric about the x-axis. As the rotational speed increases, the symmetry of the mode shapes completely vanishes and abrupt changes in contour lines is noticed especially when $\Omega=1.0$. The first four mode shapes of the stationary stiffened untwisted long cylindrical shell are 1T, 1B, 1C and 2T. Due to stiffening effect of the stiffeners, the symmetry of the mode shapes is maintained at low speeds ($\Omega=0.5$) but at high speed ($\Omega=1.0$) the symmetry of mode shapes are disturbed. It may be observed that due to the rotation, the third mode of the stationary stiffened shell becomes the fourth mode at high speed ($\Omega=1.0$) in the case of the untwisted stiffened shell. When the un-stiffened and stiffened shell have a twist of 30^0 , the first mode does not remain the torsional mode as in untwisted cases but it changes to first bending mode. However, an increase in twist angle in cylindrical stiffened shells also demolishes the symmetry of mode shapes by reducing the elastic stiffness of the structures.

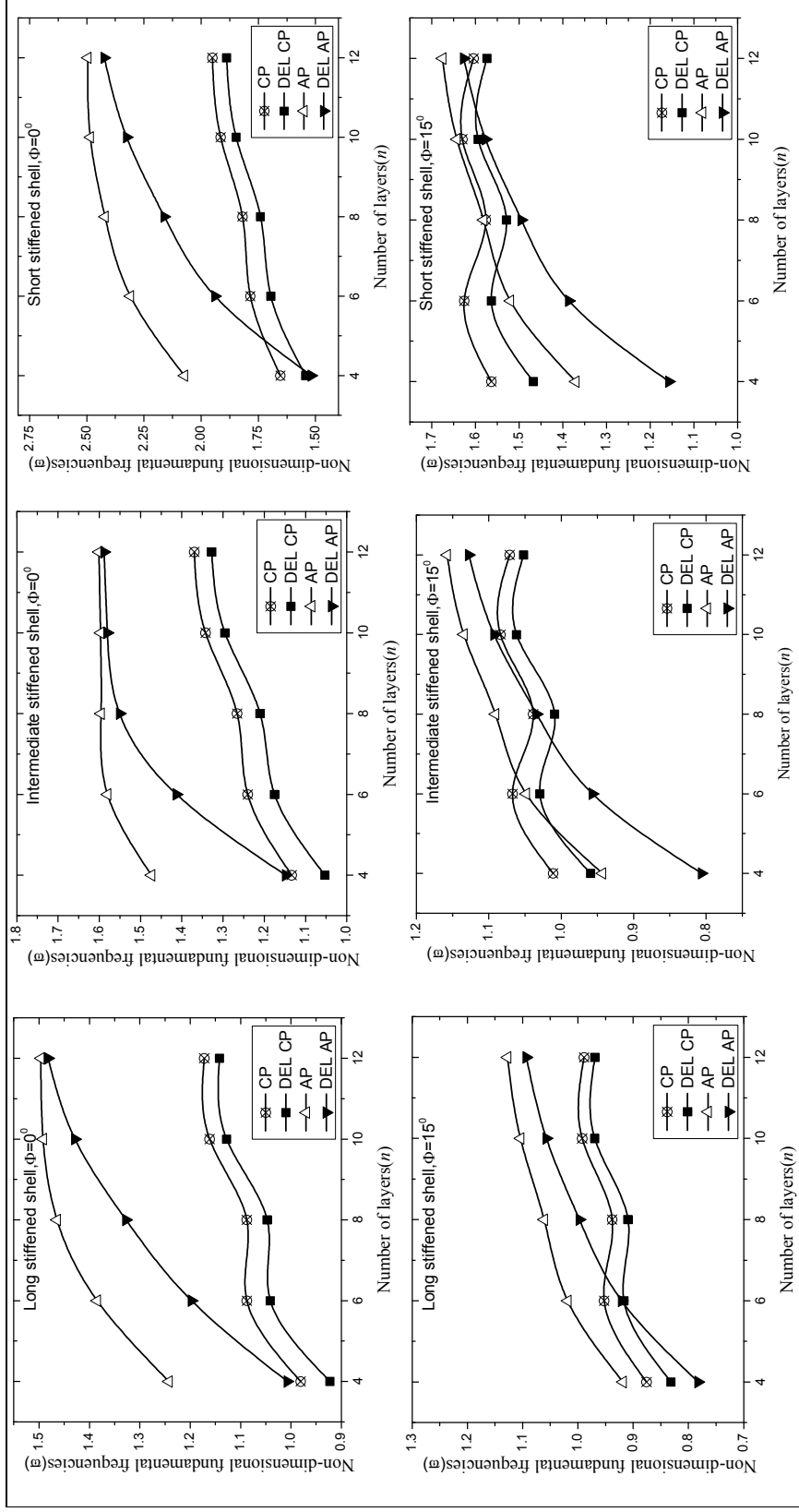


Figure 3.11 (a) Variation of non-dimensional fundamental frequencies with number of layers in undelaminated and delaminated untwisted/twisted stiffened shells Note: CP: Cross-ply without delamination, AP: Angle-ply without delamination, DEL CP: Cross-ply with delamination, DEL AP: Angle-ply with delamination, $n_x = n_y = 1$, $b_{st} = 2h$, $d_{st} = 4h$, $a/L = 0.50$, $d/L = 0.5$.

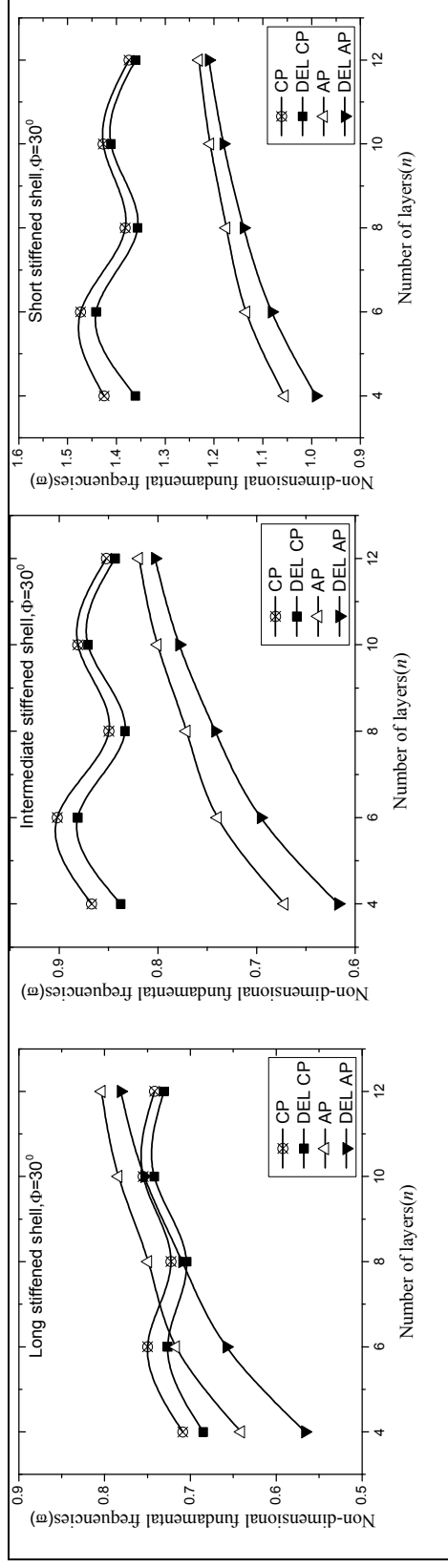


Figure 3.11 (b) Variation of NDFP with number of layers in undelaminated and delaminated untwisted/twisted stiffened shells Note: CP: Cross-ply without delamination, AP: Angle-ply without delamination, DEL CP: Cross-ply with delamination, DEL AP: Angle-ply with delamination, $n_x = n_y = 1, b_{st} = 2h, d_{st} = 4h, a/L = 0.50, d/L = 0.5$.

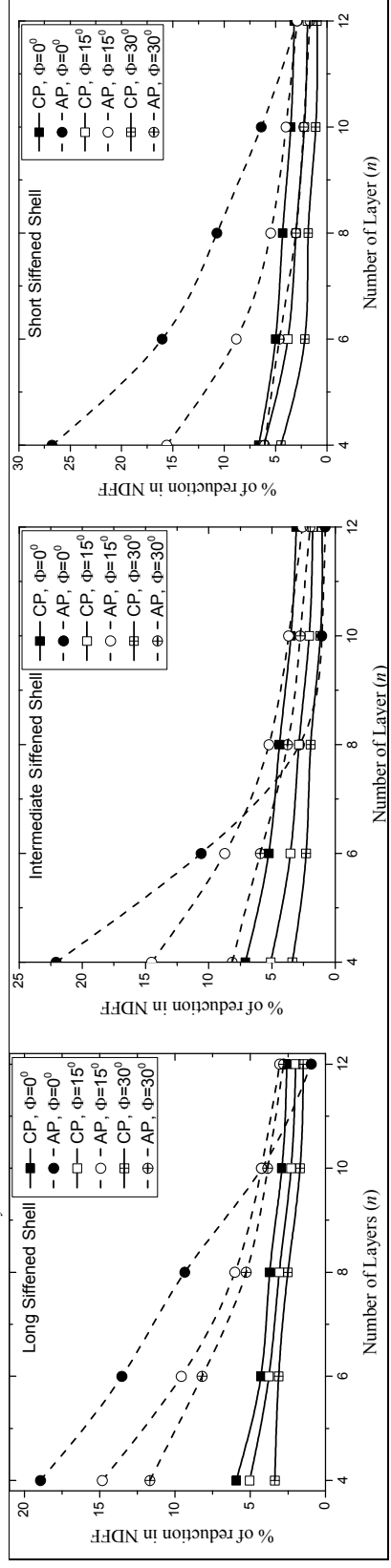


Figure 3.12 Percentage reduction in fundamental frequency of Long, intermediate and short crossed stiffened and short crossed stiffened (eccentric at top) shell with number of layer due to 50% delamination at different twist angles. Note: CP: Cross ply, AP: Angle ply, $n_x = n_y = 1, b_{st} = 2h, d_{st} = 4h, a/L = 0.50, d/L = 0.5$.

Table 3.12 Effect of rotation and twist angle on first four mode shapes of symmetric delaminated cross-ply[0/90/90/0] un-stiffened and stiffened cylindrical long shell $a/L = 0.333$, $d/L = 0.5$, $n_x = n_y = 1$, $b_{st} = 2h$, $d_{st} = 4h$.

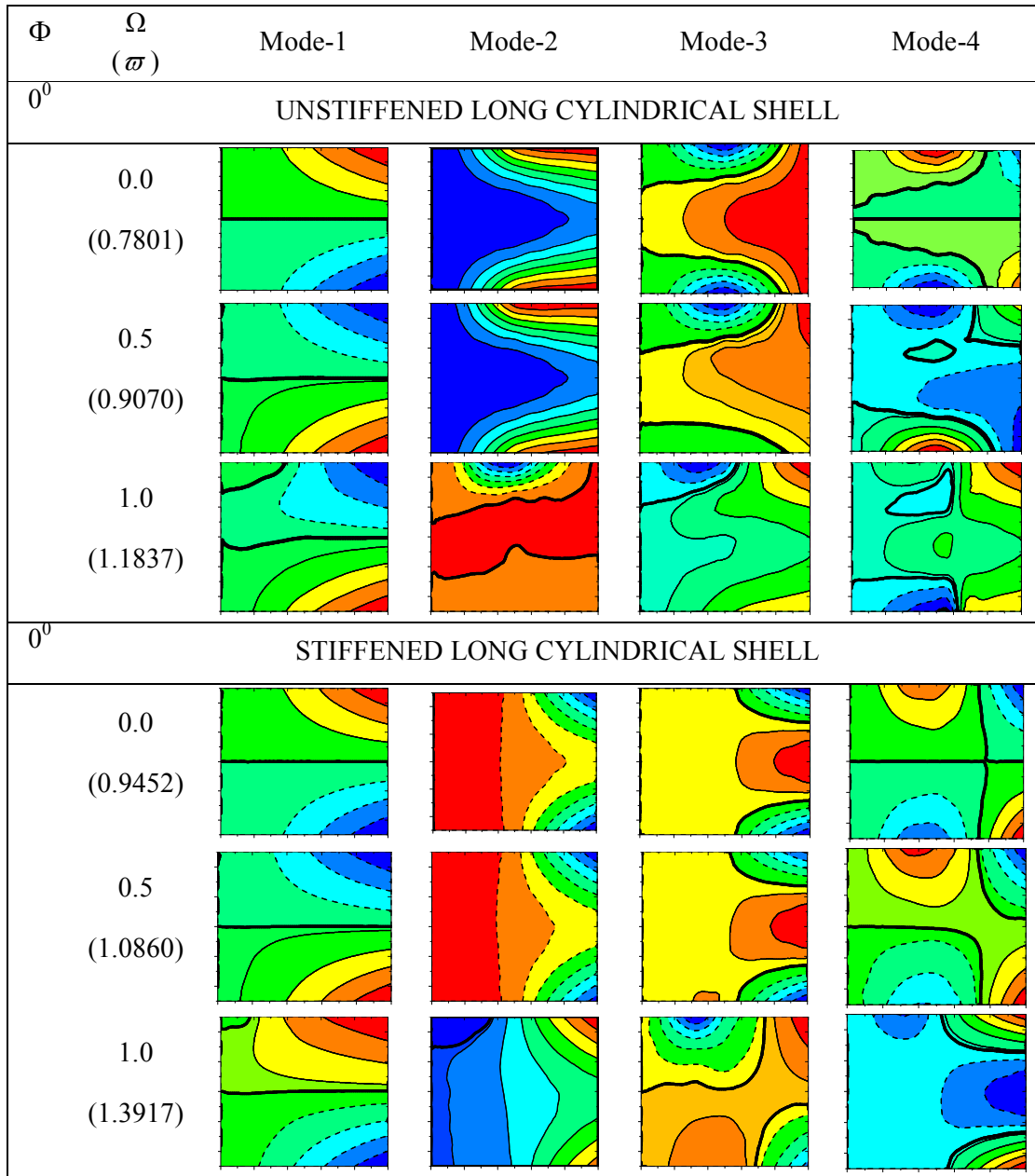
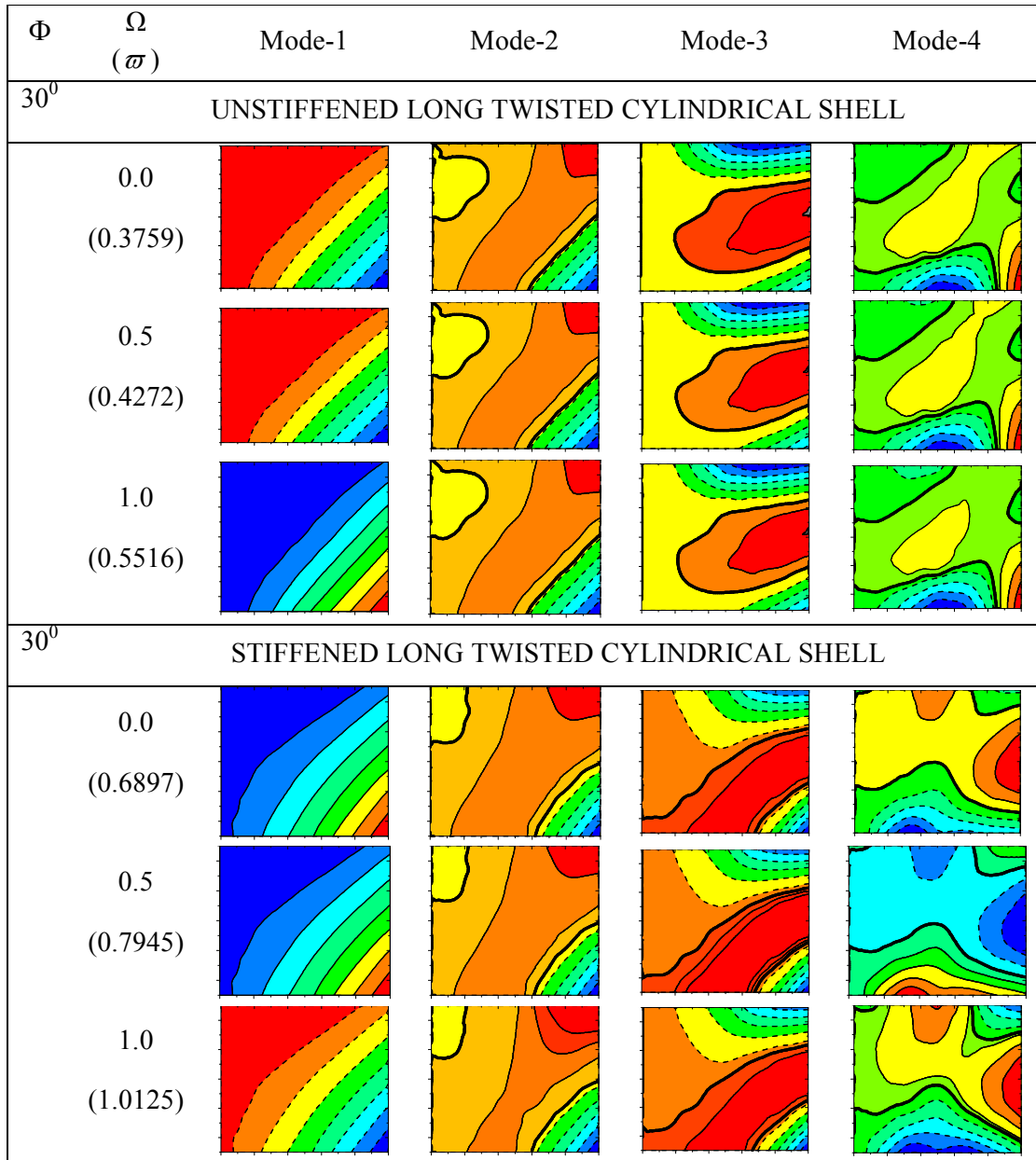


Table 3.12Continued



CHAPTER 4

TRANSIENT RESPONSE OF DELAMINATED COMPOSITE PRETWISTED STIFFENED SHELLS UNDER LOW VELOCITY IMPACT

4.1 GENERAL

Composite materials have little or no plastic deformation when receiving load exceeding the elastic deformation energy and hence, they are immediately damaged and their mechanical property is rapidly degraded. Such a composite structure has so weak characteristic to compressive strength that decreases strength of material when impact occurs, and it would lead to lifetime decrease and cause unexpected problems. The most severe type of loading on a composite structure is impact by a foreign object during manufacture, maintenance, transportation and service operation of different components and is generally found in aircraft wings, fan blades in jet engine and protruded section in automobiles. Impact of masses moving at relatively low velocities (less than 10 m/s) with underwater vehicles, windmill blades, automobile or aircraft bodies, steam turbine blades or spaceships is quite common in actual practice. Turbomachinery blades are under a preload resulting from the centrifugal forces and as a consequence, the initial stresses may aggravate the damage due to impact especially in the presence of delaminations. An impact of a specific energy may cause these cracks to grow beyond a critical limit thereby leading to premature failure of the stiffened shells. In most practical applications as in hailstorm or ballistic attacks, impact on composite laminates is never a localized phenomenon and the loading and unloading cycles of multiple impactors can greatly influence the contact force and displacement. Therefore, an organized analytic method to predict the dynamic response of delaminated composite stiffened cylindrical shells under single/multiple impacts is needed to establish a design method to make the composite structures more reliable and safer.

In this chapter, transient response of delaminated composite stiffened cylindrical shells subjected to low velocity single impact or multiple impact is presented. Dynamic response of specific problems of delaminated composite stiffened cylindrical shells is investigated with the following objectives:

1. Convergence study of the present finite element code developed is carried out for low velocity impact analysis of stiffened shells with cantilevered boundary condition.

2. The impact response of some benchmark problems in the literature is compared with those obtained by the author to establish the validity of the present code.
3. An extensive parametric study of transient response characteristics of several additional examples of delaminated stiffened cylindrical shells with pretwist is carried out with a view to arriving at some meaningful conclusions.

The detailed response characteristics of stiffened panels are reported under two different sections. Impact response of the stiffened cylindrical shell with delamination is presented in section 4.3 while the multiple impact response of the delaminated panel is furnished in section 4.4.

4.2 CONVERGENCE AND VALIDATION

The convergence of the present finite element formulation is studied with respect to time step for cantilevered cylindrical stiffened shell with one central eccentric bottom stiffener along each orthogonal (x-/y-) direction. The contact force and shell displacement at the centre of the delaminated twisted panel is presented in Fig 4.1. Previous study for free vibration analysis revealed that the results are found to be converged at the mesh sizes of 8×8 . Hence, mesh size of 8×8 is used to check the time convergence study of the stiffened panel subjected to low velocity impact. Contact force history and central vertical displacement of the shell are illustrated in Fig 4.1 corresponding to time step $0.5 \mu\text{s}$, $1.0 \mu\text{s}$, $1.5 \mu\text{s}$ and $2.0 \mu\text{s}$, respectively. It is evident that the response of both contact force and shell displacement corresponding to time step $1 \mu\text{s}$ is acceptable because there is no significant variation of the parameters with respect to time steps. Hence, the time step of $1 \mu\text{s}$ is considered for further study with mesh size 8×8 for full stiffened shells with cantilevered boundary condition.

The validity of the present formulation is established by comparing the present results of transient dynamic response of specific problems with those available in literature. The accuracy of the formulation with respect to stiffener, pretwist, delamination and rotation have already furnished in Chapter-3. The size of delamination is assumed to remain same during the transient state (very small duration) of the impact loading. Hence the growth of the delamination area is not considered in the present study. The width of delamination is also equal to the width of the shell. In order to establish the accuracy of the code in respect of low velocity impact formulation, the following examples are taken from the existing literature for comparison:

1. Fully clamped square laminated composite ($0^0/90^0/0^0$) plate impacted by a striker with initial velocity of 22.6 m/s solved by Chun and Lam (1998).

2. Simply supported square laminated composite ($[0^0/90^0/0^0/90^0/0^0]_s$) plate impacted by a striker with initial velocity of 3 m/s solved by Sun and Chen (1985).
3. A composite($[0^0/90^0/90^0/0^0]$) beam impacted simultaneously at two different locations by two strikers with initial velocity of 2 m/s each solved by Lam and Sathiyamoorthy (1999).

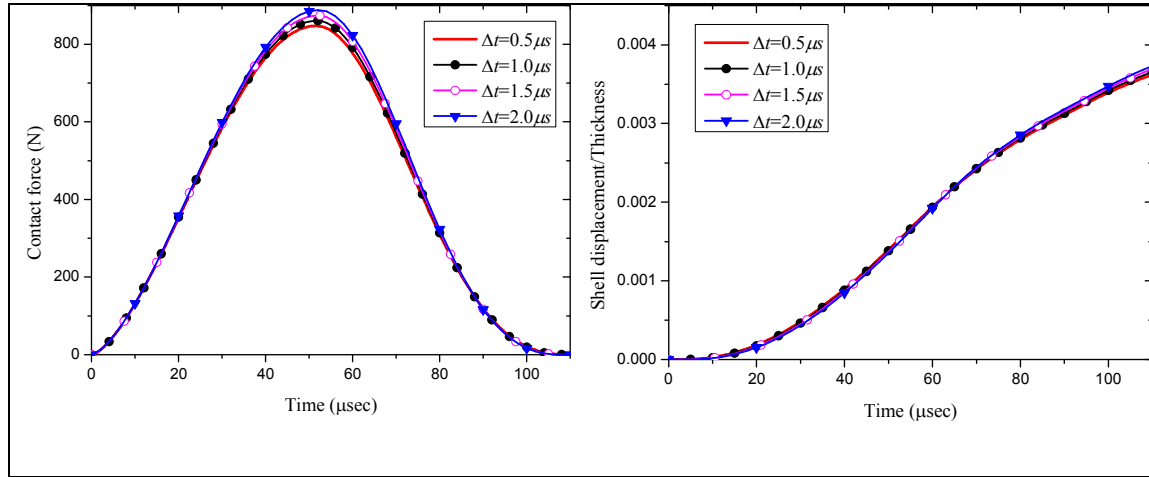


Figure 4.1 Convergence of transient response with respect to different time steps for cantilevered delaminated composite ($[0/90/0/90/0]_s$) cylindrical cross stiffened shell under low velocity impact. $L= 0.5\text{m}$, $b= 0.3\text{ m}$, $h=0.005\text{m}$, $b_{st}=2h$, $d_{st}=4h$, $n_x= n_y=1, a/L=0.5, d/L=0.5$, $\Phi=30^0$, $v_i=3\text{ m/s}$, $E_i=210\text{ GPa}$, $r_i=6.35\text{ mm}$, $\rho_i=7960\text{ kg/m}^3$, $\nu_i=0.3$.

Fig. 4.2 shows contact force and in-plane stress histories of a fully clamped square laminated composite ($0^0/90^0/0^0$) square plate obtained by Chun and Lam(1998) are compared with the results obtained by employing the present formulation. The time step chosen for time integration is $2\mu\text{sec}$. The present results are in good agreement with the literature. Contact force and central deflection histories of a symmetrical laminated cross ply square plate under simply supported boundary condition obtained employing the present formulation are compared with those obtained by Sun and Chen (1985) and is shown in Fig 4.3. Minor variation of the result with those of Sun and Chen is due to the fact that the present analysis is carried out using the full plate while they have considered a quarter plates with symmetric boundary conditions. In addition, the number of nodes, the order of numerical integration and the convergence time steps considered are different in each case. Since, the results of dynamic response of shell structures with multiple low velocity impacts are not available in the literature; the results of the present formulation shown in Fig 4.4 are compared with the results of Lam and Sathiyamoorthy (1999), wherein a symmetric composite $[0^0/90^0/90^0/0^0]$ beam is impacted at two different locations. Contact force and shell displacement results show slight variation with those obtained by Lam and Sathiyamoorthy (1999), which is due

to the fact that they have used energy approach to obtain the results. Hence, the formulation of the present code can accurately predict the transient response of the delaminated stiffened shell with pretwist subjected to low velocity impact.

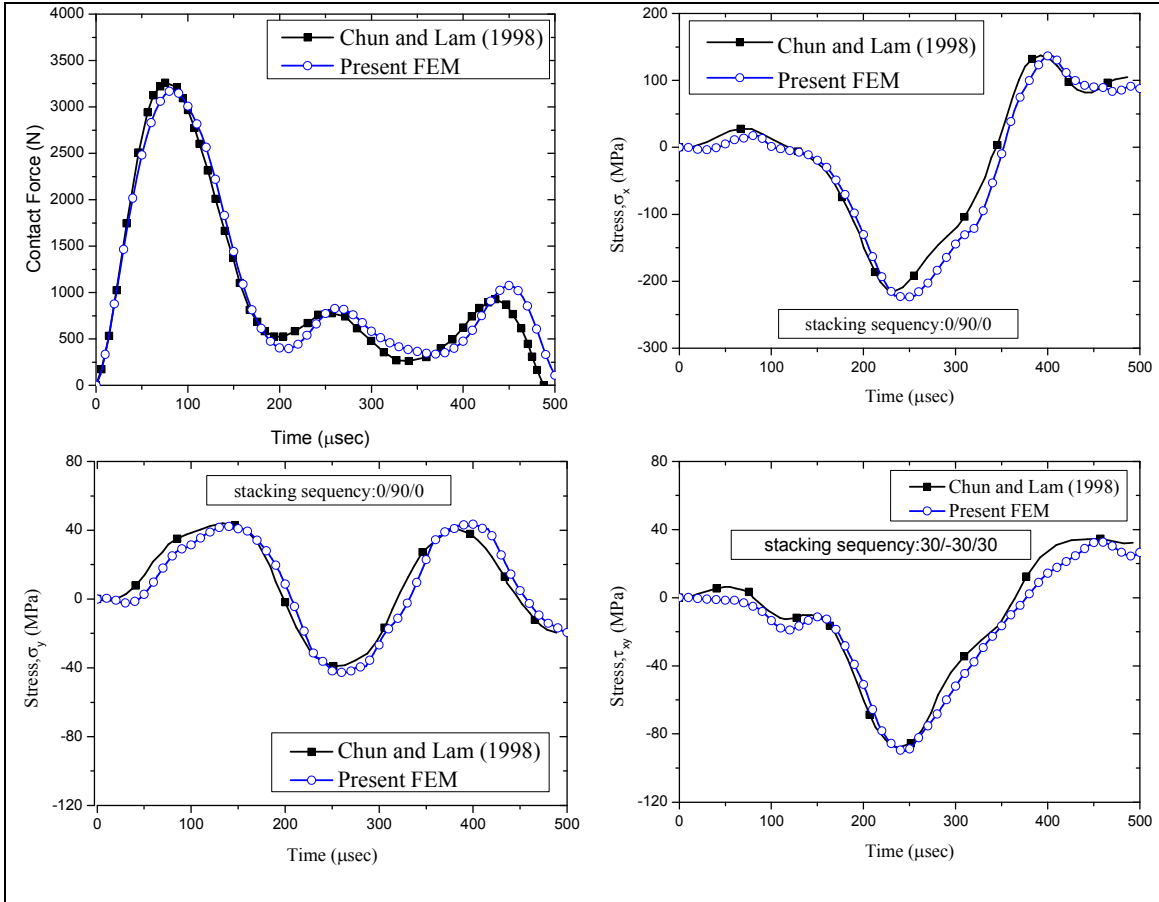


Figure 4.2 Contact force and in-plane stress history of a clamped square composite plate, impacted at the center of the plate. $E_1 = 142.73$ GPa, $E_2 = 13.79$ GPa, $G_{12} = 4.64$ GPa, $\nu_{12} = 0.30$, $\rho = 1.61 \times 10^3$ kg/m³, $L = b = 0.14$ m, $h = 3.81 \times 10^{-3}$ m, mass of striker = 0.014175 kg, velocity of striker = 22.6 m/s, contact stiffness ($k_c = 1 \times 10^8$ N/m^{1.5})

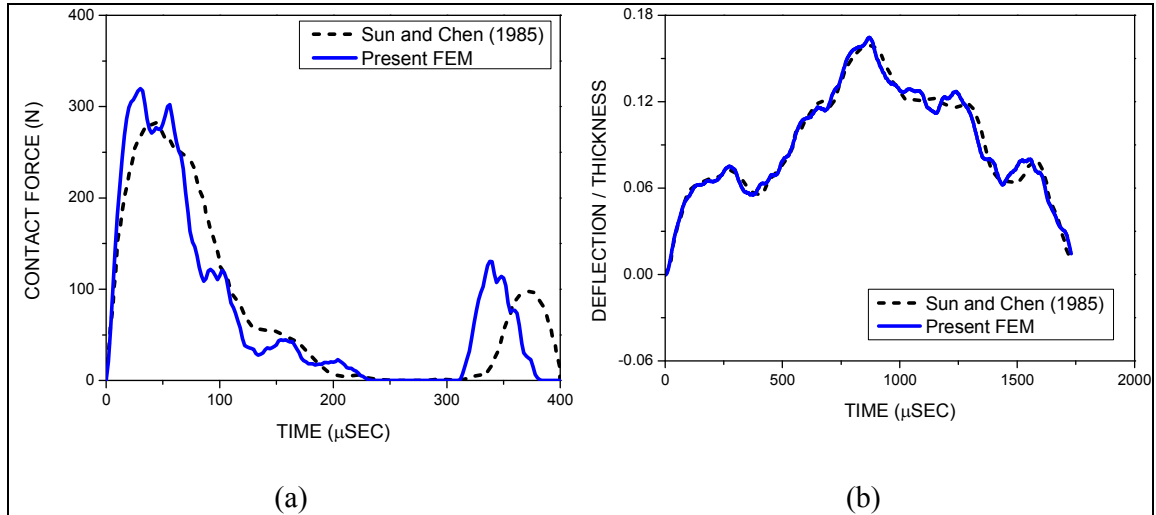


Figure 4.3 Impact responses of a cross ply $([0/90/0/90/0]_s)$ composite plate impacted centrally by spherical steel ball under simply supported boundary conditions. $L = 20$ cm, $b = 20$ cm, $h = 0.269$ cm, $E_1 = 120$ GPa, $E_2 = 7.9$ GPa, $G_{12} = G_{23} = G_{13} = 5.5$ GPa, $\nu_{12} = 0.30$, $\rho = 1.58 \times 10^{-5}$ N-sec²/cm⁴, $V_i = 300$ cm/sec, $\rho_i = 7.96 \times 10^{-5}$ N-sec²/cm⁴. (a) Contact force history (b) Central deflections.

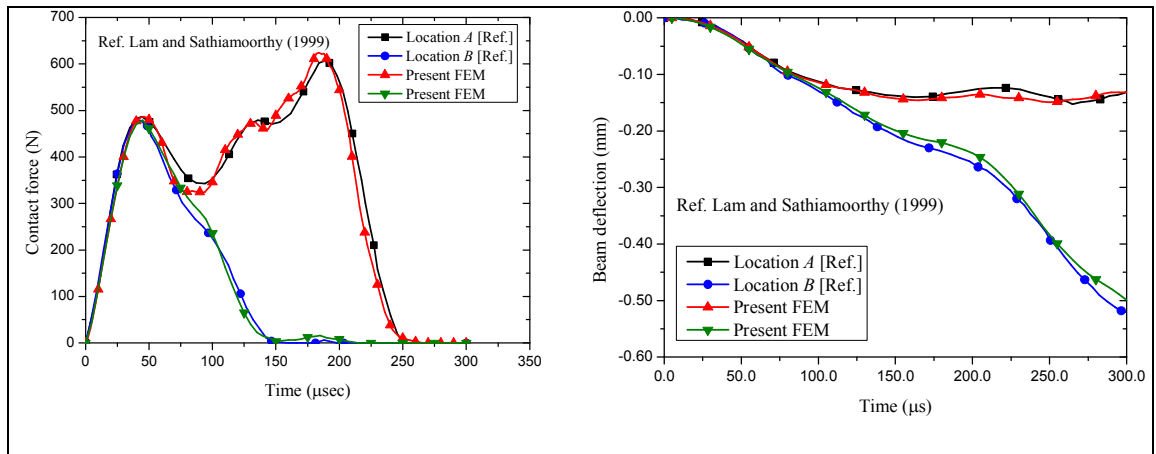


Figure 4.4 Contact force and beam displacement histories of a cantilever composite $([0^0/90^0/90^0/0^0])$ beam at locations A and B . $L = 0.3$ m, $b = 0.01$ m, $h = 0.01$ m, $r_{iA} = r_{iB} = 0.01$ m, $v_{iA} = v_{iB} = 2.0$ m/s, $E_1 = 144.80$ GPa, $E_2 = 9.65$ GPa, $G_{12} = G_{13} = 4.14$ GPa, $G_{23} = 3.45$ GPa, $\nu_{12} = 0.30$, $\rho = 1389.23$ kg/m³. $A (L/6, b/2)$, $B (5L/6, b/2)$

4.3 RESPONSE OF PRETWISTED DELAMINATED STIFFENED SHELL

Stiffeners of rectangular cross-section are considered for the analysis wherein they have the same stacking sequence as that of the shell. Delamination crack front always stretches across the full width of the shell. Delaminated stiffened shell is always assumed to be impacted at the center by a spherical impactor. The contact between the delaminated layers during impact is not considered in the present study. The value of mass density and Young's modulus of the spherical impactor are 7960 kg/m^3 and 210 GPa , respectively. Parametric studies are carried out to investigate dynamic impact responses of the stiffened cylindrical shell due to variation of stiffener orientation and eccentricity, delamination location, twist angles, stiffener width to shell thickness ratio and diameter of the impactor. Transient response, which includes the histories of contact force, shell displacement, moments, and shell velocities are always evaluated at the center of the shell. In some cases the in-plane stresses are evaluated at a particular location of the graphite epoxy composite stiffened cylindrical shell fixed at one end having the following material (Sun and Chen, 1985) and geometric properties.

$$E_1=120 \text{ GPa}, E_2= 7.9 \text{ GPa}, \nu_{12}=0.30, G_{12}=G_{23}=G_{13}=5.5\text{GPa}, \rho=1580\text{kg/m}^3$$
$$L=0.5 \text{ m}, b=0.3 \text{ m}, h=0.005 \text{ m}, R_y=2.0 \text{ m}.$$

In general, the occurrence of high value of stress may be expected in the zone, which is away from the stiffener. Hence, a point $(L/2, b/4, h/2)$ at the top surface, which was earlier considered by Chun and Lam (1998) is chosen to compute the values of the impact induced in-plane stresses. The boundary condition of the stiffened shell for the entire analysis is given by

$$\text{At } x=0, \quad u = v = w = \alpha = \beta = 0 \quad (4.1)$$

4.3.1 Effect of stiffener orientation

Transient impact response of 50% mid-plane delaminated composite $([0/90/0/90/0]_s)$ un-stiffened and stiffened cylindrical shell are shown in Fig 4.5. A comparative study between un-stiffened shell, shell with one x-directional stiffener and shell with one y-directional stiffener are carried out wherein the striker is impacted at the centre of the shell with an initial velocity of 5 m/s . In general, adding stiffener increases the elastic stiffness which in turn increases the contact force response as compared to the un-stiffened shell. Contact force of the stiffened shells are much higher than the un-stiffened shell but the results of both x- and y-directional stiffened shells are found close to each other. However, the maximum value of contact force is observed in y-directional stiffened cylindrical shell.

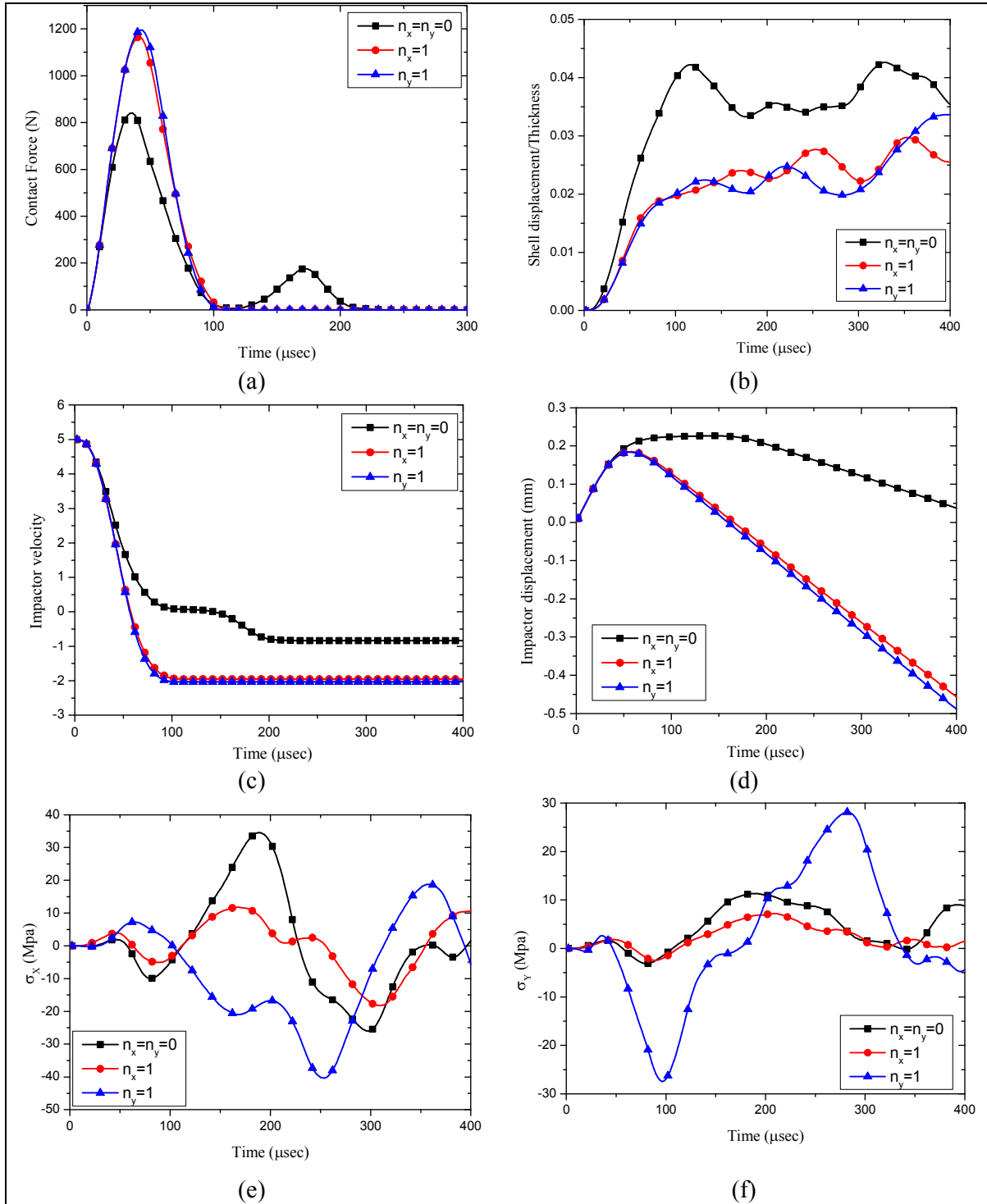


Figure 4.5 Effect of adding stiffener along x- and y-direction on the transient impact responses of the delaminated composite cylindrical shell, $a/L=0.50$, $d/L=0.5$, $b_{st}=h$, $d_{st}=2h$, $d_i=1.27$ cm, $v_i=5$ m/s. (a) Time history of contact force; (b) Time history of shell displacement/thickness; (c) Time history of impactor velocity; (d) Time history of impactor displacement; (e) Time history of σ_x ; (f) Time history of σ_y .

Normalized shell displacement is found maximum in the un-stiffened shell while minimum in stiffened shells. Impactor velocity is found to reduce rapidly in stiffened shell as compared to the un-stiffened shell. After the completion of the unloading cycle, the impactor is observed to have a constant velocity in all cases. Velocity of the impactor in the case of the un-stiffened shell is noticed to decrease in two stages because of the reloading taking place between 120 μ sec to 230 μ sec. Impactor displacement increases continuously until the completion of loading cycle and then decreases but the rate of decrease in displacement of the impactor in stiffened shell is found faster than that of the un-stiffened shell. The in-plane dynamic stresses σ_x , and σ_y are determined at $(L/2, b/4, h/2)$, which is the mid-point of the normal line from the impact point to the x-axis and on the upper surface of the shell. The values of normal stress σ_x are found greater than σ_y in all the cases considered. Addition of x- and y-directional stiffener induces greater magnitude of σ_x and σ_y during loading cycle while reduces the magnitude of σ_y during unloading cycle. The maximum value of σ_x reduces to 65.98% and 45.58% of the maximum value of σ_x when compared with the un-stiffened shell for x-directional and y-directional stiffeners, respectively. The maximum value of σ_y is found to increase with y-directional stiffener while it diminishes with x-directional stiffener compared to the maximum value of σ_y of the un-stiffened shell. Hence, the use of x-directional stiffener is found advantageous than y- stiffener. The magnified deformation of the mid-plane of the un-stiffend ($n_x=n_y=0$)/stiffened shell ($n_x=1, n_y=1$ and $n_x=n_y=1$) are illustrated in Figure 4.16 corresponding to the instant of attaining the peak value of contact force.

4.3.2 Effect of delamination across the thickness

Dynamic impact response of composite ([0/90/0/90/0]_s) stiffened shell containing 75% mid-span delamination located at three different positions ($h'/h=0.1, 0.5, 0.8$) across the thickness have been shown in Fig 4.6. Cylindrical shell is appended by one x- directional stiffener ($n_x=1$) along the centreline. Contact force history reveals that the peak value of contact force obtained is 1261.71 N corresponding to $h'/h=0.1$ while minimum value is obtained for $h'/h=0.5$. Contact force decreases when delamination moves from top surface to mid-plan and thereafter again increases till the bottom ply. However, the variation of delamination across the thickness has the sharp distinction in the normalized displacement, impactor velocity and impactor displacement of the cantilever stiffened shell. During loading cycle, the normalized displacement for $h'/h=0.1, 0.5$ and 0.8 have no variation thereafter significant variation is observed. Normalized displacement is found maximum in the mid-plane ($h'/h=0.5$) delaminated stiffened shell while minimum for $h'/h=0.1$.

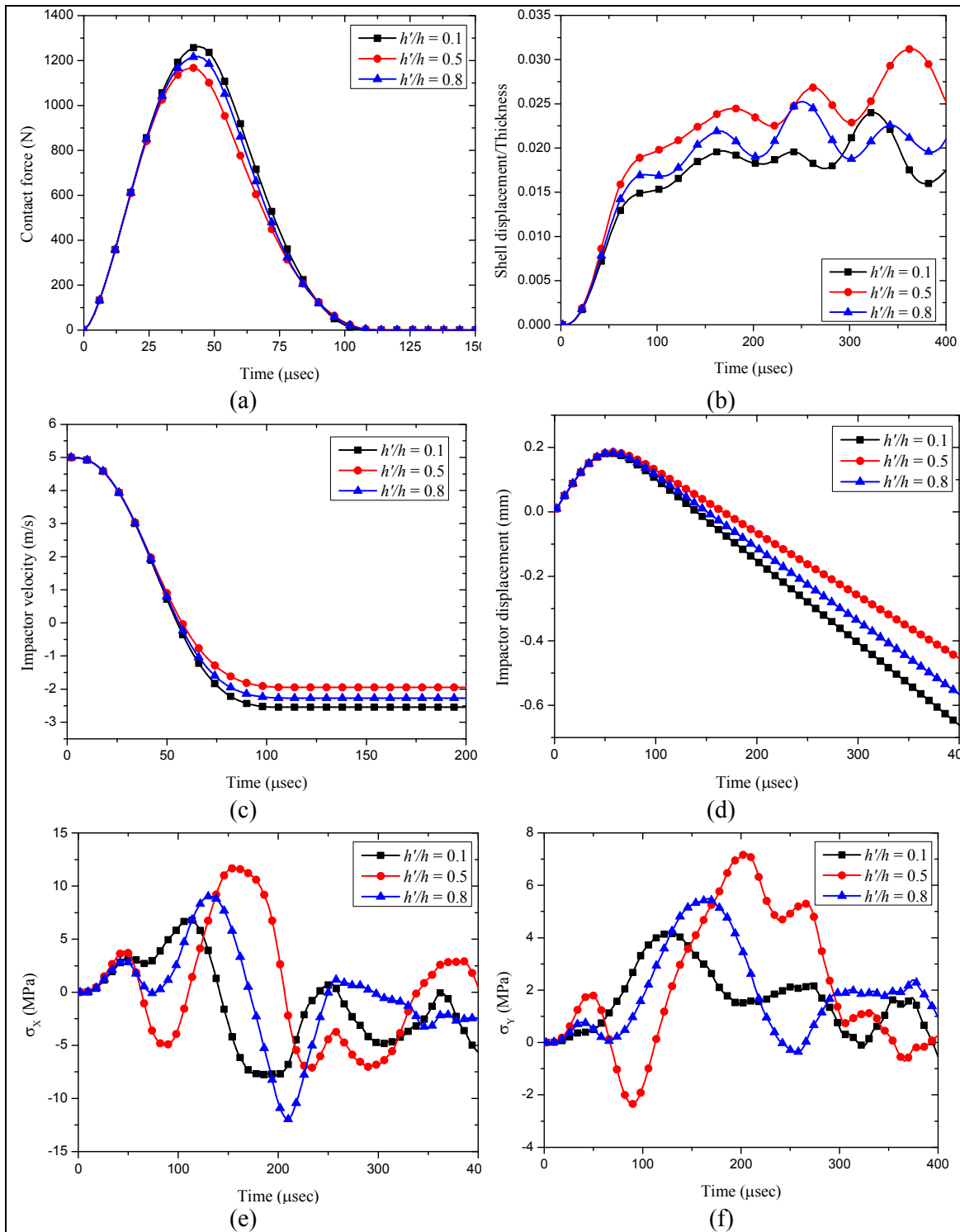


Figure 4.6 Dynamic impact response of delaminated composite([0/90/0/90/0]_s) stiffened cylindrical shell for various position of delamination across the thickness, $n_x=1$, $a/L=0.75$, $d/L = 0.5$, $b_{st} = h$, $d_{st} = 2h$, $v_i = 5$ m/s, $d_i = 1.27$ cm. (a) Time history of contact force; (b) Time history of shell displacement/thickness; (c) Time history of impactor velocity; (d) Time history of impactor velocity; (e) Time history of σ_x ; (f) Time history of σ_y .

It reveals that the displacement response of the stiffened shell increases as delamination moves from top ply to middle ply and thereafter again decreases towards the bottom ply. It is evident that the impactor displacement and velocity of all the three case are identical during loading while in un-loading cycle, both the velocity and displacement of the impactor are found to be maximum for $h'/h= 0.5$. Dynamic stresses (σ_x and σ_y) are obtained on the top surface of the stiffened shell corresponding to point $(L/2, b/4, h/2)$ wherein it is observed that both the stresses increases during loading cycle and σ_y is found greater than σ_x irrespective of the position of delamination. It may be noted that maximum value of σ_x and σ_y are obtained corresponding to $h'/h =0.5$ and gradually decreases as delamination moves away from mid plane and found minimum at $h'/h =0.1$. Mid-plane delamination induces high value of in-plane dynamic stresses, which is undesirable. Hence, mid-plane delamination is found to be risky for the stiffened shell panel.

4.3.3 Effect of Eccentricity of stiffeners

Fig 4.7 illustrates the effect of eccentricity of the stiffeners on the dynamic response of delaminated composite ($[0/90/0/90/0]_s$) stiffened cylindrical shell wherein eccentric bottom, concentric and eccentric top stiffeners are considered for the analysis. It is already observed by Nayak and Bandyopadhyay (2005) that the effect of eccentricity can be judged when the shell is appended with more than three numbers of stiffeners. Hence the analysis has been carried out with three numbers of stiffeners in each direction. Contact force histories have the marginal variation with the eccentricity of stiffeners, however, the maximum contact force is found in eccentric top and bottom stiffeners. Normalized displacement and velocity of the concentric stiffened shell are identified maximum followed by the eccentric bottom and eccentric top stiffeners. But the normalized displacement and velocity response curves of the eccentric bottom and top stiffened shell are very close to each other. Moreover, it is evident that during loading cycle the displacement of shells are identical in all the cases while the deviation of the response curves starts immediately during the commencement of the unloading cycle. Eccentric stiffener renders more elastic stiffness than that of concentric one because of the high value of the first and second moment of area. The normal stresses σ_x and σ_y are computed at the top surface of the shell $(L/2, b/4, h/2)$ and are presented in Fig 4.7 (e) and (f) wherein the opposite nature of the stresses corresponding to eccentrically top and eccentrically bottom is observed. From failure point of view, the concentric stiffeners are found more suitable than eccentric stiffeners because of the lowest value of in-plane stress but the fabrication of concentric stiffener is tough compared to eccentric stiffeners.

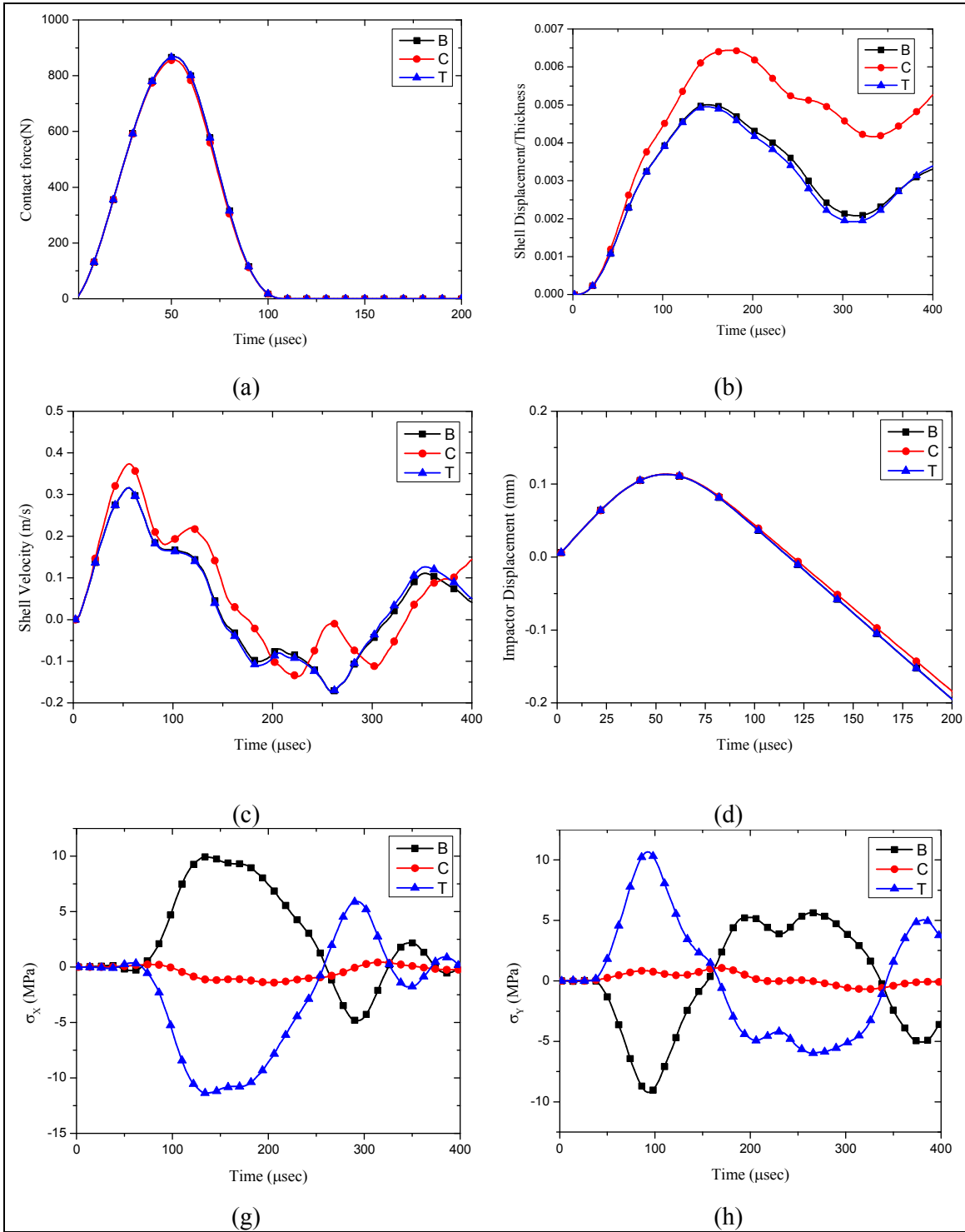


Figure 4.7 Effects of eccentricity of stiffeners on the transient response of the composite $([0/90/0/90/0]_s)$ stiffened cylindrical shell, $n_x=n_y=3$, $d/L=0.5$, $a/L=0.5$, $b_{st}=2h$, $d_{st}=4h$, $d_i=1.27$ cm, $v_i=3$ m/s. (a) Time history of contact force; (b) Time history of shell displacement/thickness; (c) Time history of shell velocity; (d) Time history of impactor displacement; (e) Time history of σ_x ; (f) Time history of σ_y . Note: B: Eccentric bottom, C: Concentric, T: Eccentric top.

4.3.4 Effect of stiffener depth to shell thickness ratio

Fig 4.8 shows the transient response of delaminated composite ($[0/90/0/90/0]_s$) stiffened cylindrical shell with the variation of stiffener depth to shell thickness ratio wherein 50% mid-plane delamination is considered at the mid-span. Four cases are considered such as $d_{st}/h = 1.0, 2.0, 3.0$ and 4.0 and the impactor is striking at the center of the shell with an initial velocity of 3 m/s. As expected, the maximum value of contact force is observed for $d_{st}/h = 4.0$ followed by $d_{st}/h = 3.0$ and 2.0 while the minimum value of contact force is found for $d_{st}/h = 1.0$. This is due to the fact that with the increase of stiffener depth overall structural stiffness increases. Further, it may be noted that the period of loading and unloading cycle for $d_{st}/h = 4.0, 3.0$ and 2.0 are completed earlier compared to $d_{st}/h = 1.0$. It is observed that increase in d_{st}/h reduces the target displacement wherein maximum and minimum normalized displacement are obtained for $d_{st}/h = 1.0$ and 4.0 , respectively. Impactor displacement and velocity for all the four cases show a similar trend wherein both impactor displacement and velocity decreases at a rapid rate for higher d_{st}/h . Impactor displacement and velocity are maximum for $d_{st}/h = 1.0$ followed by $d_{st}/h = 2.0, 3.0$ and 4.0 wherein the impactor velocity is decreasing continuously till the end of loading and unloading cycle and then remains constant. Impactor displacement is observed to increase gradually until the end of loading cycle and thereafter it decreases. The in-plane normal stresses σ_x and σ_y are computed at the top surface of the shell ($L/2, b/4, h/2$) and are presented in Fig 4.8 (e) and (f). It is evident that increase in d_{st}/h ratio leads to reduce the value of in-plane normal stresses. Finally, the study reveals that increase in d_{st}/h ratio results in higher value of contact force, which in turn reduces the target point displacement, velocity, stress resultants, impactor velocity, impactor displacement and stresses.

4.3.5 Effect of initial twist

Dynamic response of composite ($[0/90/0]_s$) stiffened cylindrical shell containing 75% delamination ($a/L=0.75$) located at $0.5L$ from the fixed end have been presented in Fig 4.9 corresponding to twist angle $0^\circ, 30^\circ$ and 45° , respectively wherein the delaminated stiffened shell is impacted at the center of the shell by the striker with an initial velocity of 7 m/s. The low-velocity impact responses of the twisted stiffened shells are compared with that of the untwisted stiffened shell. It is evident that the contact force increases with increase in twist angles wherein maximum contact force is obtained at $\Phi=45^\circ$ and minimum at $\Phi = 0^\circ$. The normalized shell displacement, impactor velocity and impactor displacement decreases with increase in twist angle, which may be due to the coupling in twisted laminate

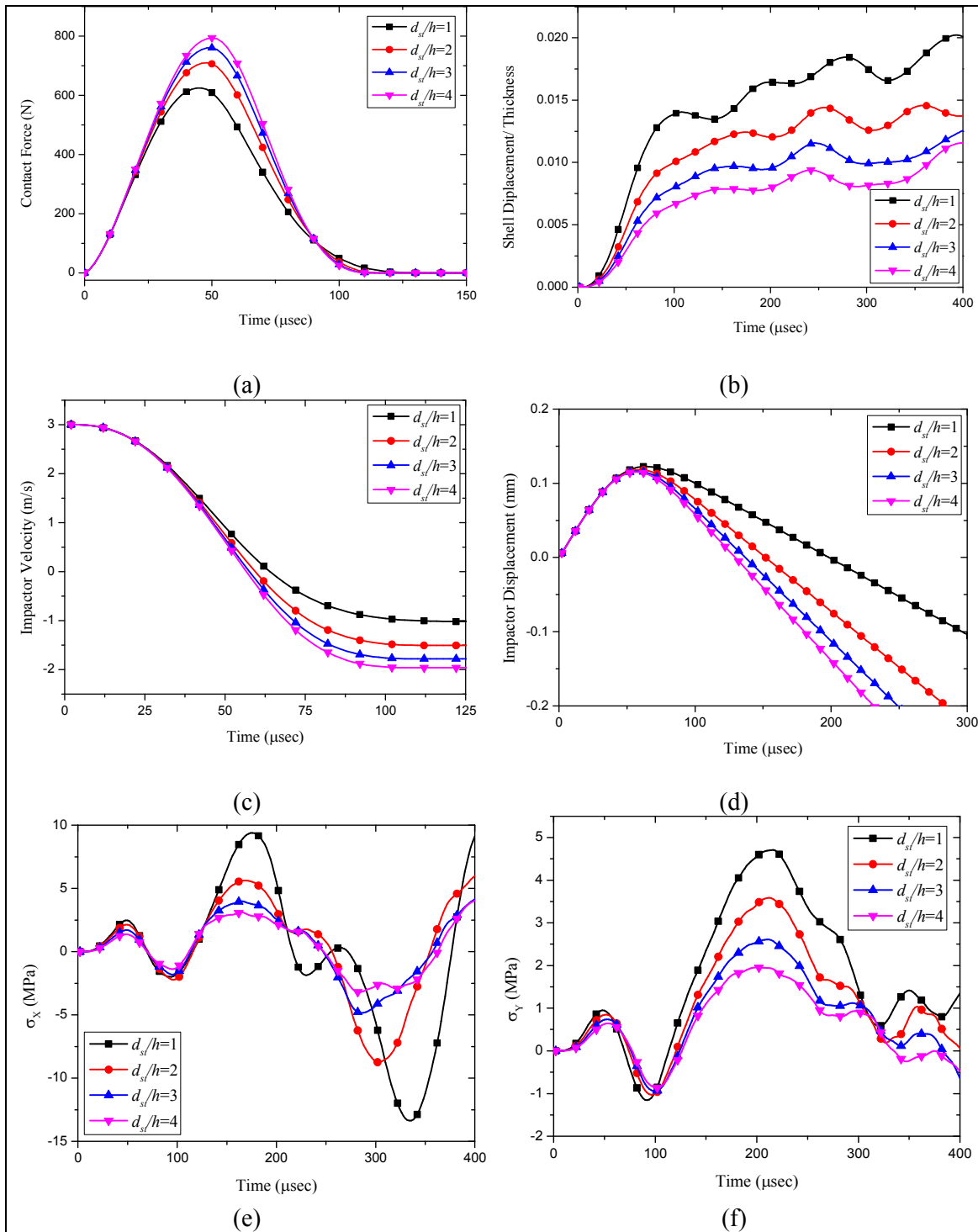


Figure 4.8 Effect of stiffener depth to shell thickness ratio on the transient response of the composite([0/90/0/90/0]_s) stiffened cylindrical shell, $n_x=1$, $d/L=0.5$, $a/L=0.5$, $b_{st}=2h$, $d_i=1.27$ cm, $v_i=3$ m/s.(a) Time history of contact force; (b) Time history of shell displacement/thickness; (c) Time history of impactor velocity; (d) Time history of impactor displacement; (e) Time history of σ_x ; (f) Time history of σ_y .

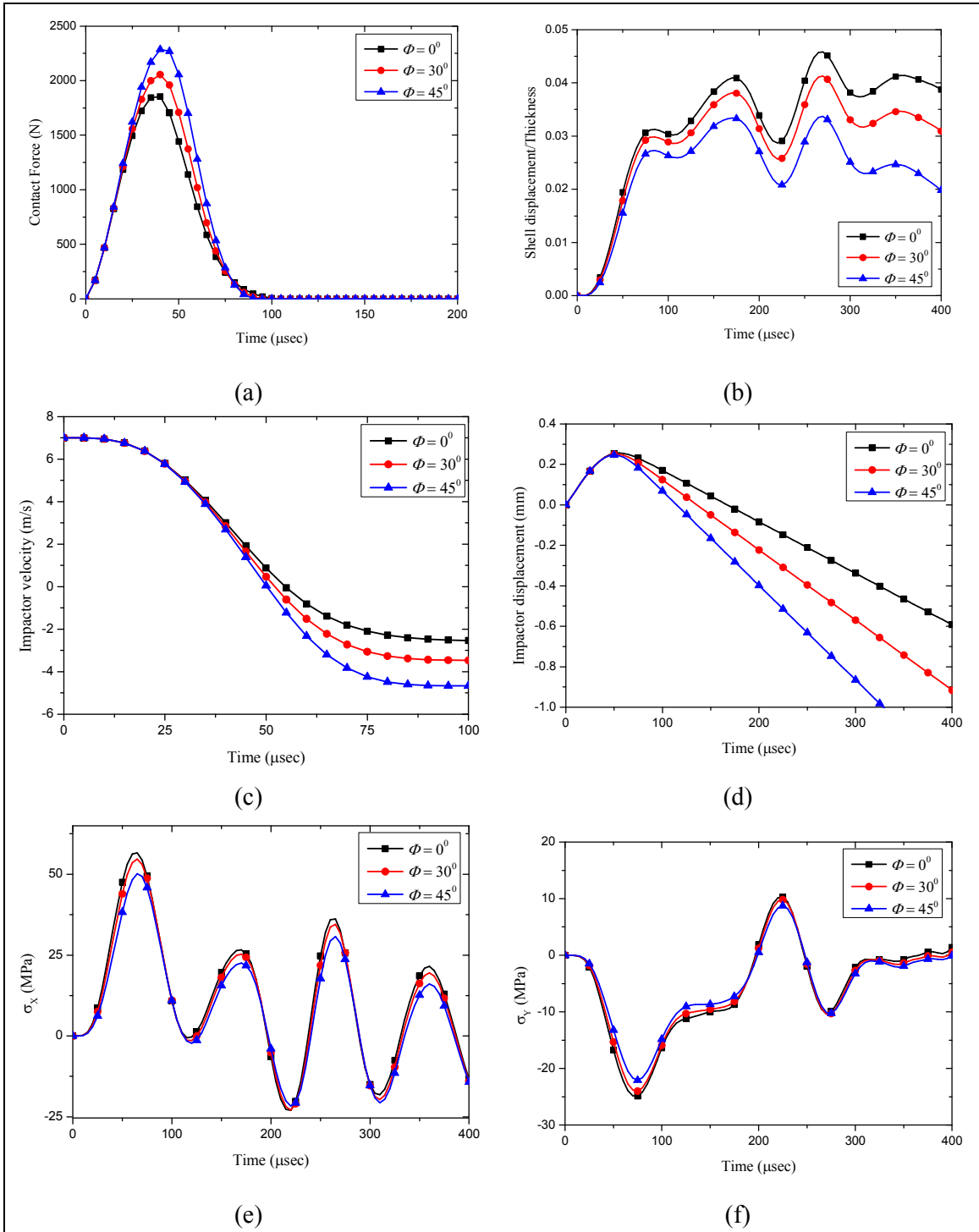


Figure 4.9 Effect of twist angle on the dynamic impact response of the delaminated composite([0/90/0]_s) stiffened cylindrical shell, $n_x=1$, $a/L=0.75$, $d/L=0.5$, $b_{st}=h$, $d_{st}=2h$, $d_t=1.27$ cm, $v_i=7$ m/s.(a) Time history of contact force; (b) Time history of shell displacement/thickness; (c) Time history of impactor velocity; (d) Time history of impactor displacement; (e) Time history of σ_x ; (f) Time history of σ_y .

leads to greater structural stiffness thus increases the contact force and reduces the other parameters. Time histories of the normalized displacement of the three cases during loading cycle shows insignificant variation but thereafter large difference between them is identified with the increase in time wherein the trend of variation is similar. Impactor velocity in all the cases is decreasing with time and at the end of unloading cycles attains constant values wherein the rate of decrease in striker velocity is found maximum at higher twist angle. No significant deviation in the time histories of impactor displacement is observed during the loading cycle, on the other hand at the beginning of unloading cycle the magnitude starts decreasing and deviation of the curves show higher rate for larger twist angle. Time histories of the in-plane stresses (σ_x and σ_y) of the twisted and untwisted stiffened shell at $(L/2, b/2, h/2)$ are also presented, wherein it is evident that the increase in twist angle reduces the value of stresses in conformity with the displacement.

4.3.6 Effect of diameter of impactor

Dynamic response of the twisted composite ($[0/90/0]_s$) cylindrical stiffened shell having 75% mid-plane delamination ($a/L=0.75$) with changes in diameter of the impactor is shown in the Fig 4.10. Three cases have been considered wherein the impactors strike the stiffened shell at the centre with a fixed initial velocity of 7 m/s. Diameters of the impactors assumed in the three cases are 1cm, 2cm and 3 cm, respectively. The maximum value of contact force is found with the impactor having diameter 3cm while the minimum is observed corresponding to diameter 1cm. Further, it may be noted that in all the cases considered in the present study, increase in contact force reduces the contact period but in this particular case both contact force and contact period increases simultaneously with increase in diameter of the impactor. Reloading is observed at 200 μ sec corresponding to $d_i=2$ cm for a small period of time. Time period of unloading cycle is extended with the increase in diameter of the impactor while maximum contact duration of unloading cycle is identified for $d_i=3$ followed by $d_i=2$ and $d_i=1$. Similarly, there is the corresponding increase in shell displacement are found with increase in the diameter of the impactor due to increase in inertia of the impactor. Time histories of shell displacement/thickness are found to be maximum for $d_i=3$ cm followed by $d_i=2$ cm and the minimum is observed for $d_i=1$ cm. Gradually decrease in impactor velocity is observed with large diameter whereas rapid drop of the impactor velocity is observed with small diameter. Displacement of the impactor is found to increase continuously for $d_i=3$ cm within the time frame of analysis while in the other cases the drop in impactor displacement is observed. The in-plane dynamic stresses σ_x and σ_y , at $(L/2, b/4, h/2)$ are also furnished in

Fig4.13 (e) and (f).Both the stresses are found to increase with increase in diameter of the impactor.

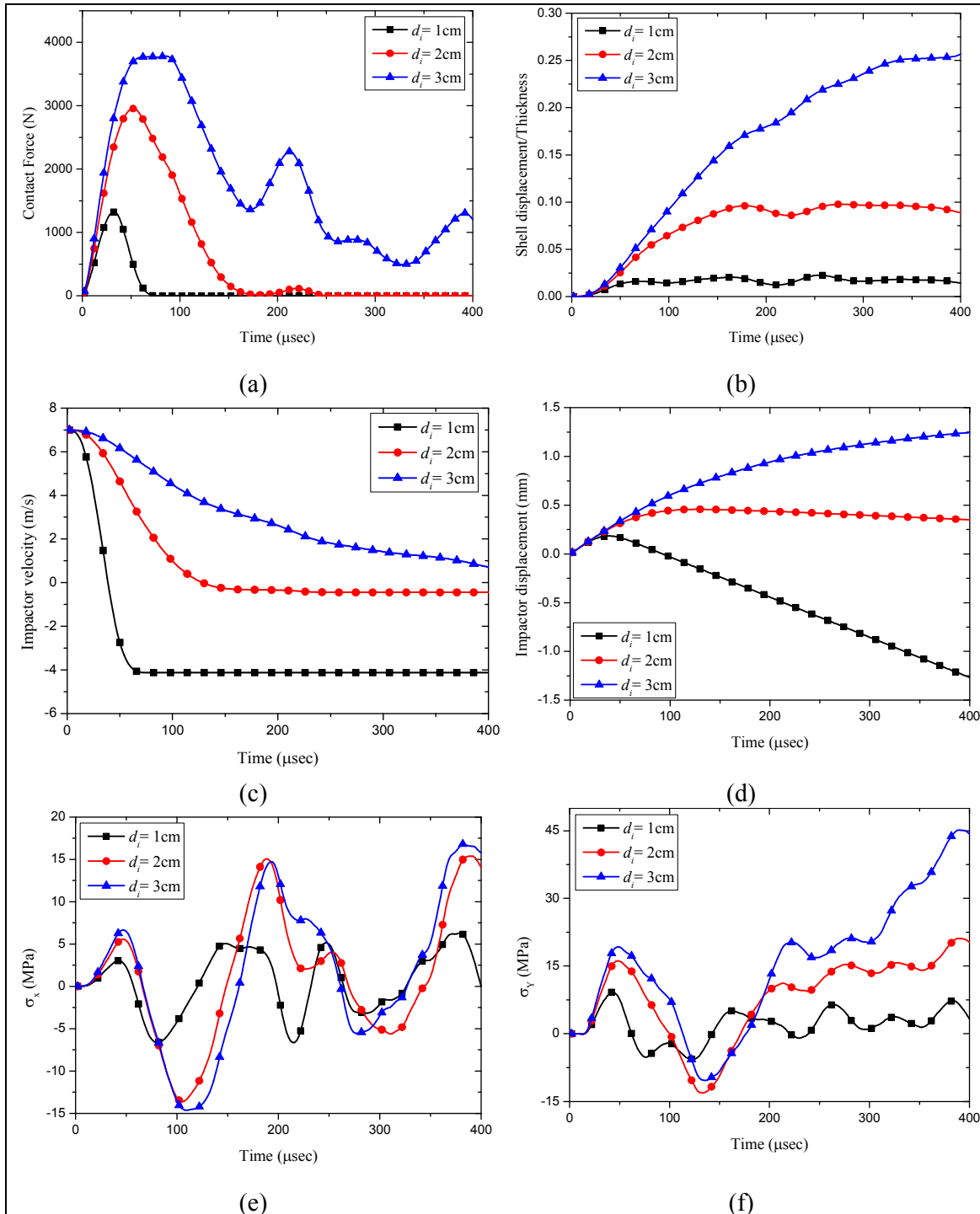


Figure 4.10 Transient impact response of the delaminated twisted composite($[0/90/0]_S$) stiffened cylindrical shell for various impactor diameters, $n_x=1$, $d/L=0.75$, $a/L=0.5$, $b_{st}=h$, $d_{st}=2h$, $\Phi = 30^\circ$, $v_i = 7\text{ m/s}$.(a) Time history of contact force; (b) Time history of shell displacement/thickness; (c) Time history of impactor velocity; (d) Time history of impactor displacement; (e) Time history of σ_x ;(f) Time history of σ_y .

4.4 RESPONSE OF DELAMINATED STIFFENED SHELL UNDER MULTIPLE IMPACT

Graphite epoxy composite laminated stiffened cylindrical shell is impacted by two spherical rigid impactors at two different locations simultaneously or with a time lag between the two impacts is presented. The material properties of the stiffened shell and the impactor are remaining same as in the previous cases. The delamination is always considered to be stretched across the full width of the shell. Stiffeners of rectangular section are always placed along the mesh lines and have the same ply orientation as that of the composite shell. The geometry of stiffened shell and impactor is also same as the previous case unless until it is specified. Two spherical impactor are always assumed to strike at center $[C (L/2, b/2)]$ and at the free end $[F(L, b/2)]$, respectively. The in-plane stresses (σ_x and σ_y) are computed at the top surface. The parameters such as stiffener orientation, twist angle, percentage of delamination, stiffener depth to shell thickness ratio and delayed impact are varied to examine the effects on the transient response of the structure.

4.4.1 Effect of stiffener

Fig 4.11 shows the variation contact force, shell displacement, and in-plane stresses (σ_x and σ_y) at the impacted points (C and F) of the stiffened shells with stiffeners orientated in x - and y -directions. Here two configuration of the undelaminated stiffened panel are considered wherein one panel is stiffened with an x -directional stiffener while the other with a y -directional stiffener. It is evident that contact force at the center (C) is found maximum while minimum at the free end (F) in both the stiffened panels. At C and F maximum contact force is observed with the panel having x -directional stiffener while the variation of contact force at the center is found insignificant with respect to orientation of the stiffeners. The distinct variation of the contact force at the free end is depicted with respect to x - and y -directional stiffeners. It is evident that maximum contact force is obtained with x -directional stiffener irrespective of the impacted points. It may be observed that the time period of loading and unloading are found maximum at the free end of the stiffened shell. The shell displacement curve shows maximum deflection at the free end in the two types of stiffened structures. The displacement at the free end of the y -directional stiffened shell is found more than that of the x -directional stiffened shell. However, the nature of σ_x is found tensile at the center of both x - and y -directional stiffened shells and compressive at the free end. The value of σ_x is found maximum at C in the x -directional stiffened shell. In x -directional stiffened shell, the value of σ_y is found minimum at both the locations compared to y -directional

stiffened shell. From the above discussion it reveals that an x-directional stiffener renders maximum stiffness to the shell than a y-stiffener and the value of impact induced stress, σ_x is obtained maximum.

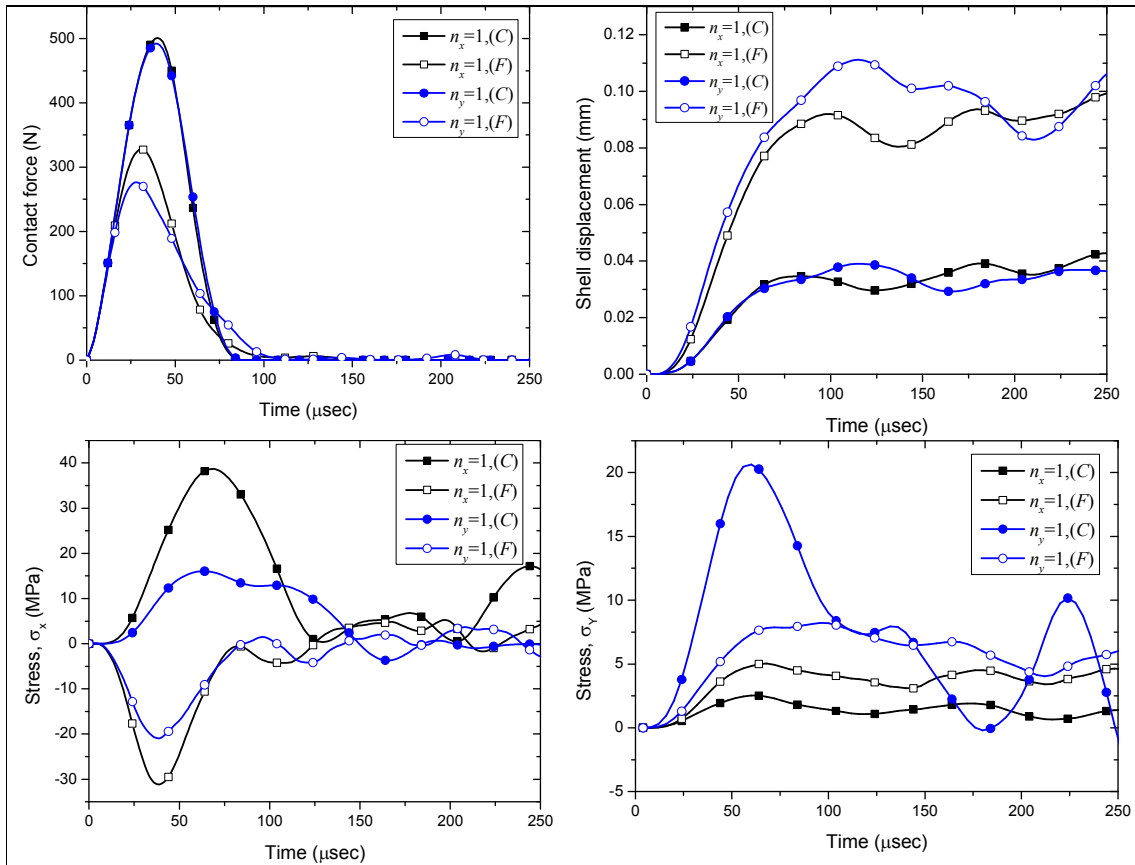


Figure 4.11 Effect of orientation of stiffener on the transient response of the undelaminated untwisted composite stiffened cylindrical shell $v_c=v_f=3$ m/s, $b_{st}=d_{st}=h$.

4.4.2 Effect of twist angle

Effect of pretwist angle of the composite stiffened panel on its transient response due to simultaneous impact of two spherical balls at the center (C) and free end (F) is depicted in Fig 4.12 wherein three values of twist angles are considered such as 0° , 15° and 30° , respectively. In each case, a delamination of 50% ($a/L=0.50$) located at the mid span is considered. It is evident that increase in twist angle, increases the contact force at the two locations while the duration of loading and unloading remains unchanged. Contact force is observed maximum at location C as compared to free end though the impact velocity of impactor at the two locations is same. However, the shell displacements at the impacted points are found to be reduced with increase in twist angle but the degree of reduction in shell displacement is marginal with change in twist angle. As expected, the shell displacement is

obtained maximum at the free end (F) irrespective of delamination and twist angle. The decrease in shell displacement at the two locations due to rise in twist angle is due to decrease in structural stiffness. It is earlier reported by Qatu and Leissa (1991) that the natural frequency of the twisted plate decreases with increase in twist angle. Hence, the present results exhibit the same tendency of reducing structural stiffness at higher twist angle. Higher twist angle reduces the magnitude of both σ_x and σ_y while the maximum value of in-plane stresses are obtained at the center corresponding to untwisted stiffened shell. The nature of stress σ_x is found compressive at F while tensile at the center C within the period of loading and unloading. The value of σ_y is found significantly smaller than σ_x at both the locations irrespective of twist angle.

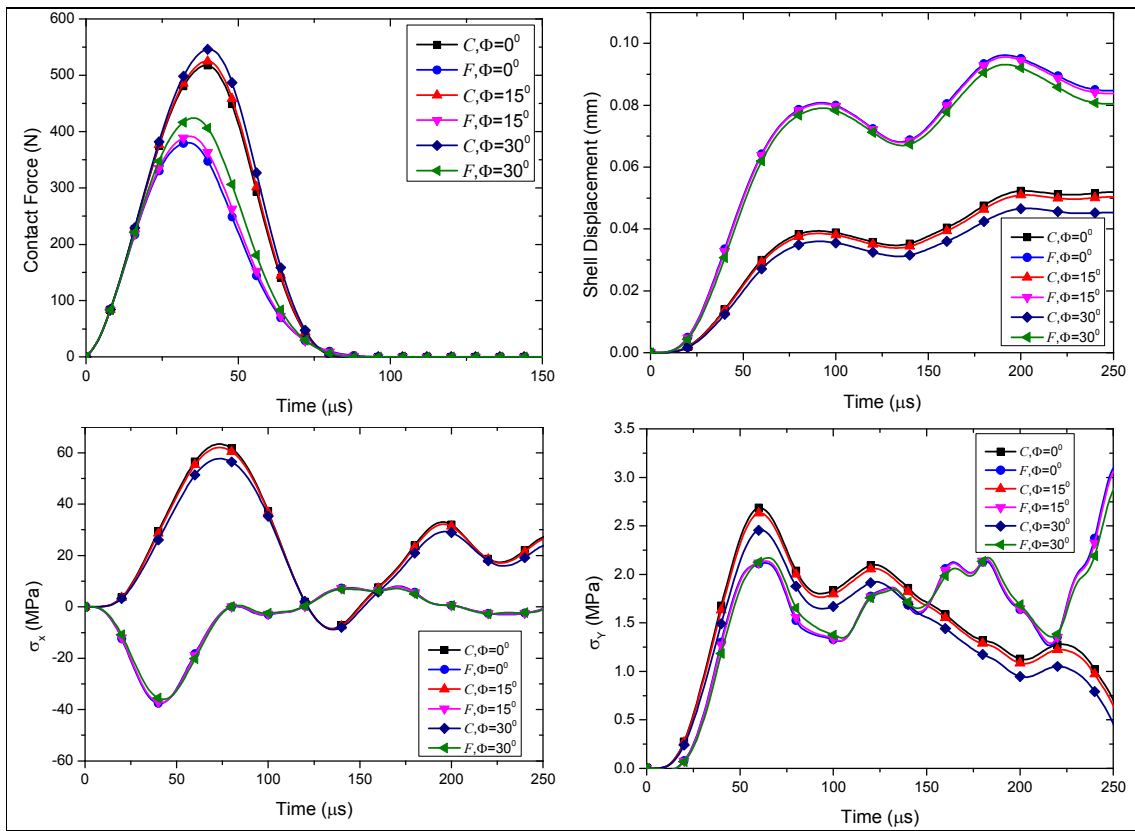


Figure 4.12 Effect of twist angle on the transient response of the delaminated composite stiffened cylindrical shell $v_c=v_f=3$ m/s, $n_x=1$, $a/L=0.50$, $d/L=0.5$, $h'/h=0.5$, $b_{st}=d_{st}=h$.

4.4.3 Effect of delamination

Presence of delamination reduces the strength of the shell while the size of delamination has adverse effect on the dynamic characteristics of the shell. Effect of percentage of delamination (PD) on the dynamic response of a twisted cylindrical shell with one x-directional stiffener subjected to transverse impact at two different locations

simultaneously is illustrated in Fig 4.13. Comparison studies between two cases are presented here with delamination of 0 % and 75% located at the mid span of the shell. It reveals that the peak value of contact force is obtained highest in undelaminated case (PD= 0%) while lowest value of the same is identified for delaminated case at the center due to degradation in elastic stiffness. The increase in percentage of delamination reduces the contact force thereby increases the shell displacement, which in turn increases the value of impact induced in-plane stress particularly at *C*. Contact force is found identical at the free end in both the cases while the shell displacement curves shows similar trend up to 100 μ s and thereafter deviation in the nature of the curves are observed. At the free end, all the parameters have shown almost identical response, which is due to the fact that the point *F* is located out of delamination zone. Delamination effect is found prominent at the center(*C*) of the shell because it is within the delamination zone. Delamination in the stiffened shell is found to intensify the magnitude of σ_x and σ_y at the center while its effect at the free end is found insignificant.

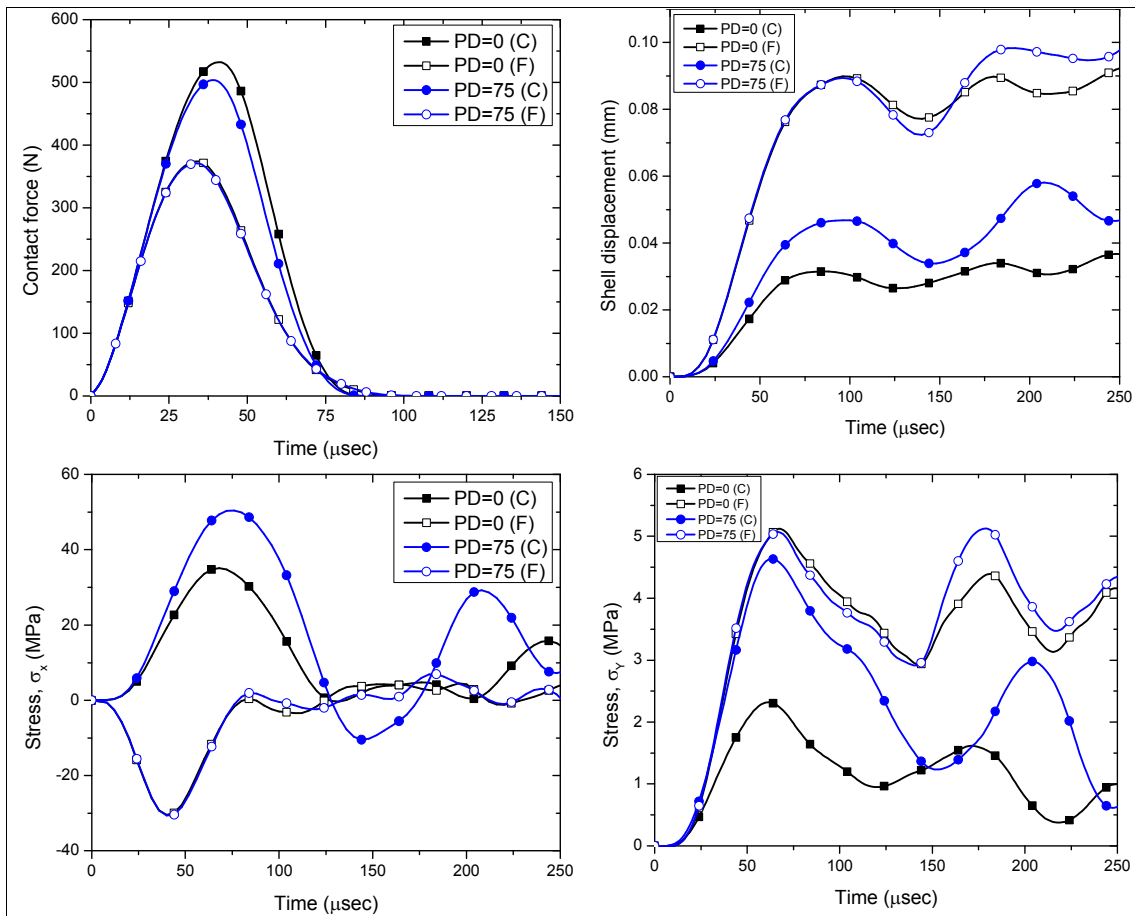


Figure 4.13 Effect of percentage of delamination on the transient response of the composite stiffened cylindrical shell. $n_x=1$, $v_c=v_f=3\text{m/s}$, $\Phi=30^\circ$, $d/L=0.5$, $b_{st}=d_{st}=h$.

4.4.4 Effect of stiffener depth to shell thickness ratio

The effect of stiffener depth to shell thickness ratio (d_{st}/h) on transient response of the delaminated twisted stiffened shell subjected to simultaneous impact at two locations is presented in the Fig 4.14. The twisted stiffened shell contains a 50 % mid-plane delamination.

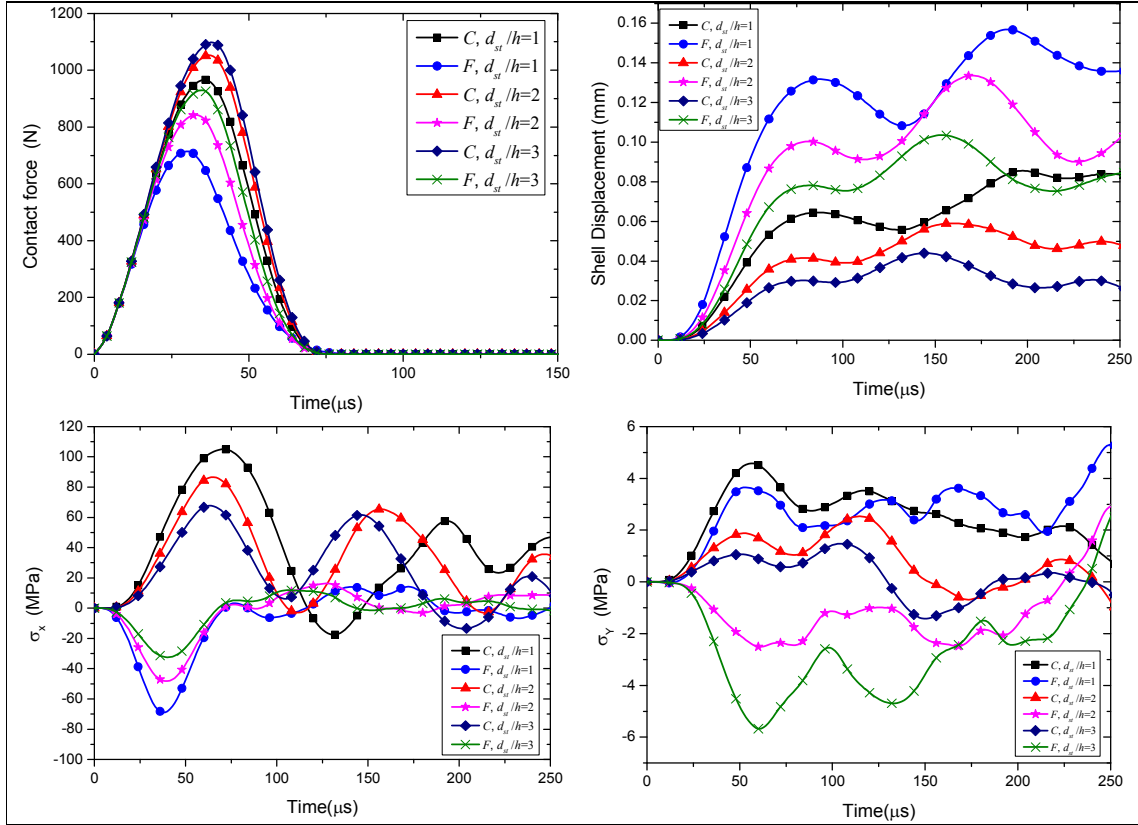


Figure 4.14 Effect of stiffener depth to shell thickness ratio on the transient response of the delaminated composite stiffened cylindrical shell $v_c=v_f= 5$ m/s, $n_x=1$, $a/L=0.50$, $d/L=0.5$, $h'/h=0.5$, $\Phi=15^\circ$.

Simultaneous impact at the two locations take place on three different models wherein the depth of the stiffener have three different values such as $d_{st}/h=1.0$, 2.0 and 3.0 , respectively. Increase in the values of d_{st}/h , intensifies the contact force at both the location of the twisted stiffened shell while reduces the value of shell displacement at C and F . The maximum value of contact force is identified at the center C corresponding to $d_{st}/h=3.0$ while the minimum value at the free end F corresponding to $d_{st}/h=1.0$. The shell displacement is found greater at the free end (F) corresponding to $d_{st}/h=1.0$ than that of the other values of d_{st}/h while shell displacement at center (C) corresponding to $d_{st}/h=3.0$ is found the smallest one. The magnitude of stress σ_x is found to reduce at the location C and F with increase in the value of d_{st}/h within time step of $100\mu s$ thereafter anomalous behavior is observed. The magnitude of

the stress σ_y is found much less than that of σ_x wherein the nature is found tensile at the center(C) for all the values of d_{st}/h within the time step of $100\mu s$ but the nature changes from tensile to compressive at (F) with increase in the value of d_{st}/h from 1.0 to 3.0. At F, the nature of stress σ_y is tensile corresponding to $d_{st}/h = 1.0$ while further increase in d_{st}/h the stress at F becomes compressive.

4.4.5 Effect of delayed impact

Transient response of the delaminated twisted composite stiffened shell impacted by two masses at different time and location is illustrated in Fig4.15. Twisted delaminated cylindrical stiffened shell is first impacted at location C and then the second impactor strikes at location F after a definite time (t_d) of the first impact.

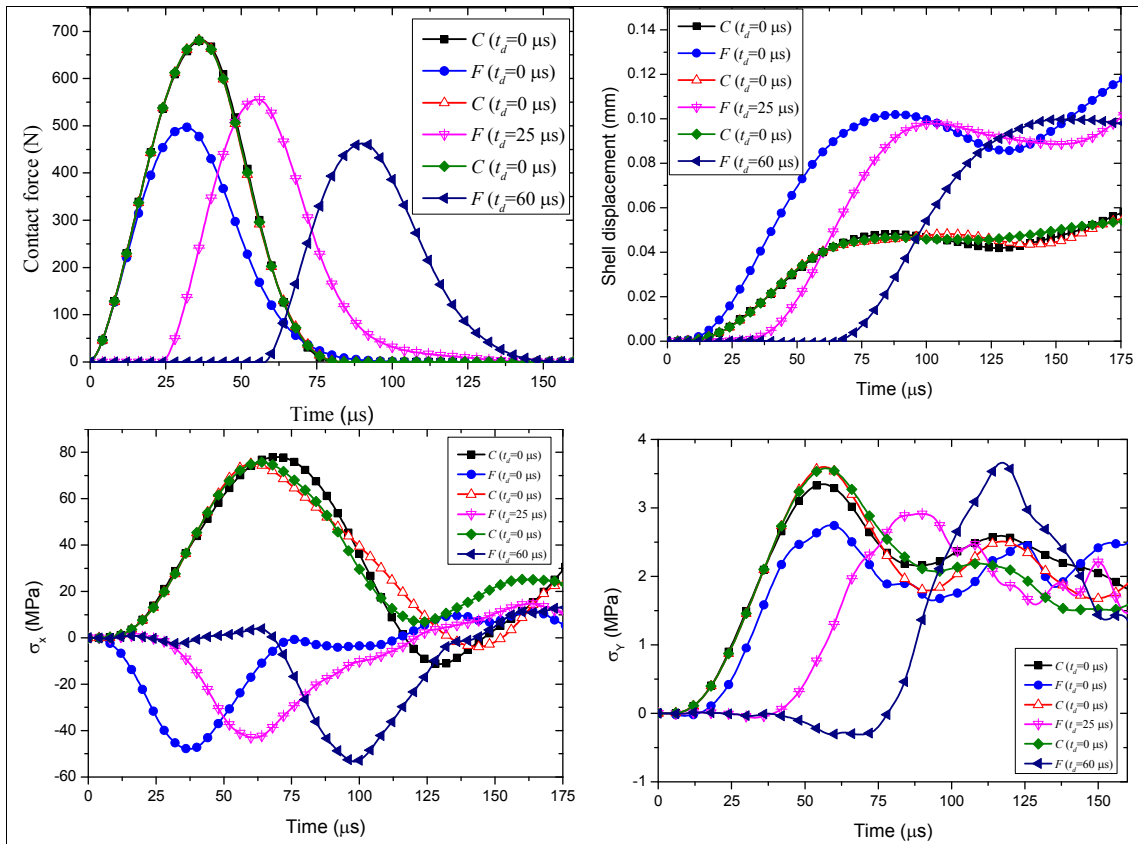


Figure 4.15 Effect of delay impact on the transient response of the delaminated composite stiffened cylindrical shell. $v_c=v_f= 4$ m/s, $n_x=1$, $a/L=0.50,d/L=0.5$, $h'/h=0.5$, $\Phi=15^0$, $b_{st}=d_{st}=h$.

Initial velocity of the two impactors is 4 m/s. Three cases have been considered in the present study wherein the first case, both the impactor strikes simultaneously, in second case the second impactor strikes after $25\mu s$ of the first impact and in the third case, the second impactors strike after $60\mu s$ of the first impact. A time delay of $25\mu s$ and $60\mu s$ is considered

in the second and third case i.e. the instant when the first impactor is approaching maximum indentation and the first impact is about to complete the unloading cycle, respectively. In all the three cases, the contact force, shell displacement and in-plane stresses (σ_x and σ_y) response at location C i.e. the first impact is almost obtained identical but it is noted that the response at location F is different and depends upon the time of delay. It is evident that the contact force at location (F) is found greater in the second case than the first case while the contact force at F in the third case is the smallest one. Hence, it may be noted that the contact force at F increases with increase in time delay till the completion of loading cycle of the first impact, thereafter it decreases with increase in time of delay. Shell displacement response depicts that the displacement at F decreases in the second case and increases in the third case. Response of stress σ_x have similar trend as that of the shell displacement while σ_y is found increasing with time delay and attained maximum in the third case corresponding to $t_d=60 \mu\text{s}$. Hence, it can be understood that the transient response of the stiffened shell in delayed impact at any location completely depends on the response of the first impact.

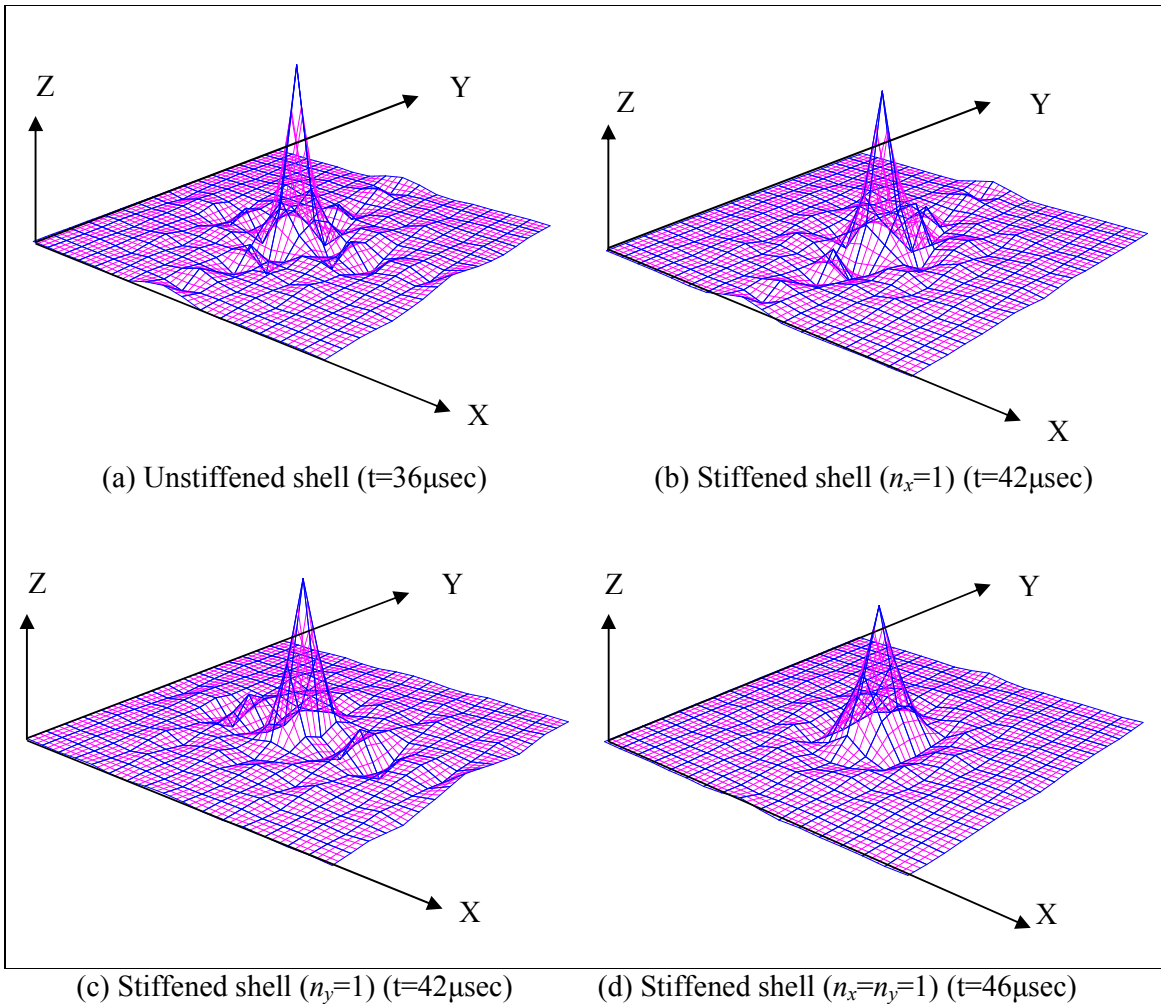


Figure 4.16 The magnified deformation configuration of the mid-plane of the delaminated composite shells with and without stiffener at the times corresponding to their peak value of contact forces. Stiffeners are placed eccentrically at bottom. $a/L=0.50$, $d/L=0.5$, $b_{st}=h$, $d_{st}=2h$, $v_i=5$ m/s

CHAPTER 5

CONCLUSIONS

5.1 GENERAL

The results of the dynamic behavior of delaminated pretwisted composite cylindrical stiffened shells within the scope of the present investigation are summarized in this chapter. The computer codes are developed based on the present finite element formulation to generate numerical results for free vibration and transient response under low velocity impact of the delaminated composite pretwisted stiffened cylindrical shells. The convergence of the finite element solution is obtained by varying mesh sizes and time steps as in the case of transient response. The present study is carried out to investigate the effect of various triggering parameters on vibratory characteristics and transient response of the delaminated pretwisted composite shallow stiffened cylindrical shells subjected to low velocity impact. The results of the problem, presented and discussed in the previous Chapter 3 and Chapter 4 for free vibration and transient dynamic response analyses subjected to low velocity normal impact, respectively, are computed with two specific objectives in mind, viz. first to establish the validity of the formulation proposed herein and secondly, to arrive at some pertinent characteristics of delaminated stiffened shells. Important conclusions drawn from the present investigation and discussion in Chapters 3 and 4 are summarized in Section 5.2. These results could be served as reference solutions for future investigators. Important information documented in the present report is not claimed to be complete in all respects and accordingly further extension of the same and the scope for future research has been suggested in the section 5.4.

5.2 CONCLUSIONS

Major conclusions drawn from free vibration and transient responses of the delaminated stiffened shells are furnished below.

5.2.1 FREE VIBRATION ANALYSIS

1. In untwisted angle ply composite stiffened shell, the x-directional stiffener is found to render maximum stiffness than the curved y-directional stiffener whereas in cross-ply laminate, y-directional stiffener is proved to be providing maximum stiffness. But in

the twisted shell, x -directional stiffeners are found advantageous than y -directional stiffener incase of both cross-ply and angle-ply laminates.

2. Numerical examples illustrate that not only the size but also the location of delamination has momentous effect on the natural frequency of the stiffened shell. The effect of delamination in the shell cannot be eliminated but the results show that its effect can be reduced to a great extent with adding up stiffeners. Moreover, it is evident that at $\theta = 60^0$ and 75^0 the effect of delamination in stiffened shell is insignificant.

Delamination located near the fixed end of the cantilever has lower frequency than that located towards the free end for unstiffened shell and y -directional stiffened shell. But for x -directional and cross stiffened shell, this trend is found up to the mid span and then decreases gradually. Considering position of delamination along thickness direction, the fundamental frequency attains minimum value at the mid-plane ($h'/h=0.5$) irrespective of the angle of twist.

3. Thickness of the x - directional stiffeners has a strong influence in increasing the fundamental frequency of the twisted stiffened shell. In untwisted stiffened shells and twisted shells with y -directional stiffener, the rate of increase of fundamental frequency gradually decreases with the increase in the value of thickness of stiffener.
4. Eccentric stiffeners are proved to be more efficient in increasing the fundamental frequency than concentric one. Eccentric top stiffeners provide higher value of fundamental frequency than eccentric bottom irrespective of twist angles and rotational speeds. The decrease in fundamental frequency as a result of twist angle is also found to be minimum in all types of shells when integrated with eccentric top stiffener.
5. Among the three types of shells (long, intermediate and short), short cantilever stiffened shell is always found to provide higher value of fundamental frequencies irrespective of twist angle and delamination. In contrast, the effect of delamination in reducing fundamental frequency are found to be more pronounced in case of short shells.
6. Increase in the number of layers in angle ply and cross-ply laminates increases the non-dimensional fundamental frequency in untwisted shells whereas fluctuation in the values of fundamental frequency is observed in twisted cross-ply laminates. Comparing between cross ply and angle ply laminates in the three types of shells;

angle-ply is found highly efficient for untwisted cases while cross-ply laminates are more suitable for twisted shells.

7. Effect of delamination on fundamental frequency is found to be maximum with less number of layers while it is minimum for higher number of layers in angle-ply laminates, but it remains almost identical for any number of layers in cross-ply laminates.
8. Influence of delamination in stiffened shell in terms of reduction in fundamental frequencies reduces with increase of twist angle.
9. Increase in the rotational speed of the stiffened shells leads to an increase in fundamental frequencies as observed for all the cases of stiffener arrangement due to centrifugal stiffening irrespective of delamination and twist angle. However, the rotating effect on the fundamental frequencies is found to be more pronounced in twisted shells with eccentric top stiffeners in all types of shells considered.
10. The Fundamental mode shape illustrates that the symmetry mode disappears with increase of initial twist and rotational speed. On the other hand, fundamental mode of the twisted stiffened shell is found insensitive to rotational speed.

5.2.2 TRANSIENT RESPONSE DUE TO LOW VELOCITY IMPACT

5.2.2.1 IMPACT BY SINGLE MASS

1. With the addition of stiffener the contact force increases, while there is a decrease in shell displacement resulting from the increase in elastic stiffness of the cylindrical shell. Contact duration between the impactor and shell are reduced due to addition of stiffener. Maximum contact force is found in case of y-directional stiffened shell as compared to x-directional stiffened shell. The x-directional stiffener is found advantageous than y-directional stiffener because of reduced the value of in-plane stresses.
2. The effect of delamination on contact force response of stiffened twisted cylindrical shell is found to be insignificant but the presence of delamination is manifested only in the displacement histories. Delamination at the mid-plane ($h'/h=0.5$) minimizes the contact force while maximizes the values of impact induced stresses (σ_x and σ_y). Thus, from design point of view, delamination at the mid-plane ($h'/h=0.5$) is observed to be unsafe.
3. Eccentricity of stiffener has marginal effect on the history of contact force, impactor displacement and velocity. However, the lower contact force is observed in concentric

stiffened shell. Eccentric top and bottom stiffeners produce stresses of opposite nature, which is an important finding for the design engineers to select the stiffener as per the limiting value of stresses corresponding to particular loading condition and depending on the material of the structure. From failure point of view, concentric stiffeners are more suitable than eccentric because the values of induced stresses are marginally low.

4. Increase in twist angle intensifies the contact force while minimizes the shell displacement, in-plane stress, impactor displacement, and impactor velocity. However, a rapid drop in impactor velocity and displacement is observed with increase in twist angle.
5. A larger value of d_{st}/h intensifies the contact force and reduces the shell displacement and in-plane normal stresses. The rate of decrease in in-plane stresses are reduced with increase in thickness of the stiffener. The rapid drop in velocity and displacement of the impactor is also observed at the higher value of d_{st}/h .
6. Impactor velocity has a significant effect on the contact force, moment resultants and displacement, which have rising trend with the increase of impactor's initial velocity. Contact duration between the impactor and stiffened shell are reduced with increase in initial velocity of impactor.
7. Increase in diameter of impactor not only increases the contact force but also enlarges the contact period and also increases the induced stresses. Reloading also takes place depending upon the mass of the impactor depending on its diameter and mass density.

5.2.2.1 IMPACT BY MULTIPLE MASSES

1. It is observed that x-directional stiffener induces greater value of σ_x while y-directional stiffener induces greater value of σ_y at both the impact locations compared to single impact.
2. Increase in percentage of delamination reduces the contact force sharply for multiple impacts while increasing the value of shell displacements which in turn increases the value of impact induced in-plane stresses particularly within the area of delamination.
3. Increase in stiffener depth to shell thickness ratio reduces the value of simultaneous impact induced stresses σ_x at center consistently as in the case of single impact but for multiple impact the variation of σ_y is unpredictable at the free end wherein the nature of stress changes.
4. On the time delayed case, the impact response depends upon the loading and unloading cycle of the previous impacts. It is observed that if time delay is much less

than the loading unloading time period of the first impact then the contact force at the second impactor position increases appreciably in comparison with zero time delay.

5.3 CONTRIBUTIONS OF THE PRESENT WORK

1. The advantage of use of this formulation over the available commercial packages is that there is no further increase in the total number of degrees of freedom for stiffener thereby increase computational efficiency and reduce computational time.
2. It is recommended that x-directional eccentric top stiffeners have better performance.
3. Based on the analysis of the delaminated stiffened shell, it is recommended that the fiber orientation of both the shell and stiffener should be kept within the range of 60 to 70 degree to minimize effect of delamination.
4. Delamination at the mid-plane of the stiffened shell minimizes the contact force while maximizes the values of impact induced stresses (σ_x and σ_y). Thus, from design point of view, delamination at the mid-plane is observed to be unsafe.
5. The stresses produced by eccentric stiffeners is an important finding for the design engineers to select the stiffener as per the limiting value of stresses corresponding to particular loading condition and depending on the material of the structure.

5.4 SCOPE OF FUTURE WORK

In view of the technical importance and need for in-depth investigations of the composite pretwisted cylindrical stiffened shells in relation to analysis, design, modeling and construction, it can be said that only a few aspects have been attempted in the context of the present work. Some of the possible areas for further research including those found necessary during the course of the present investigation are summarized below:

1. In this present investigation, the linear analyses have been carried out. The investigation may be extended to carry out the analysis of laminated twisted stiffened shells with geometric and material non-linearity.
2. Experimental investigation of the present work may be carried out to validate the findings using the proposed finite element formulation.
3. First ply failure and progressive failure analysis of the rotating pretwisted laminated stiffened shell may be carried out to understand the philosophy of the failure process in the entire structure.
4. Environmental effect on the composite materials is severe. A sudden change in temperature and moisture causes additional stresses and deformations on the structures. So, the present work can be extended to include such hygrothermal effect.

5. Effort may be made to carry out the present investigation considering reinforcement of carbon nanotubes (CNTs) and graphene sheets because of their remarkable mechanical, electrical and thermal properties.

The above extension plans are merely the suggestive but not exhaustive topics to be taken up for extensive investigation so that the designers acquire a thorough and comprehensive knowledge of the behavior of rotating pretwisted stiffened shell with which a full exploitation of these advanced materials can be made successfully.

REFERENCES

1. Abrate S. Impact on laminated composite materials. *Appl Mech Rev.* 1991 ;44(4):155-190.
2. Abrate S. Modeling of impacts on composite structures. *Composite structures.* 2001 ;51(2):129-38.
3. Acharyya AK, Chakravorty D, Karmakar A. Bending characteristics of delaminated composite cylindrical shells—a finite element approach. *Journal of Reinforced Plastics and Composites.* 2009 ;28(8):965-78.
4. Achenbach JD, Sun CT, Herrmann G. On the vibrations of a laminated body. *Journal of Applied Mechanics.* 1968 ;35(4):689-96.
5. Aggour H, Sun CT. Finite element analysis of a laminated composite plate subjected to circularly distributed central impact loading. *Computers & structures.* 1988;28(6):729-36.
6. Ahmed SR, Modak P. Stress analysis of symmetric and anti-symmetric discretely stiffened laminated cantilever beams using displacement-potential field. *Applied Mathematics and Computation.* 2015;258:465-82.
7. Aktaş M, Atas C, İçten BM, Karakuzu R. An experimental investigation of the impact response of composite laminates. *Composite Structures.* 2009 ;87(4):307-13.
8. Akterskaia M, Jansen E, Hühne S, Rolfes R. Efficient progressive failure analysis of multi-stringer stiffened composite panels through a two-way loose coupling global-local approach. *Composite Structures.* 2018 ;183:137-45..
9. Alfano G, Crisfield M. Finite element interface models for the delamination analysis of laminated composites: mechanical and computational issues. *International journal for numerical methods in engineering.* 2001;50(7):1701-36.
10. Allix O, Corigliano A. Geometrical and interfacial non-linearities in the analysis of delamination in composites. *International Journal of Solids and Structures.* 1999 ;36(15):2189-216.
11. Allix O, Leveque D, Perret L. Identification and forecast of delamination in composite laminates by an interlaminar interface model. *Composites Science and Technology.* 1998;58(5):671-8.

12. Alnefaie K. Finite element modeling of composite plates with internal delamination. *Composite Structures*. 2009;90(1):21-7.
13. Ambur DR, Jaunky N, Hilburger MW. Progressive failure studies of stiffened panels subjected to shear loading. *Composite Structures*. 2004;65(2):129-42.
14. Anyfantis KN, Tsouvalis NG. Post buckling progressive failure analysis of composite laminated stiffened panels. *Applied Composite Materials*. 2012 ;19(3-4):219-36.
15. Armentani E, Caputo F, Esposito R, Godono G. Evaluation of energy release rate for delamination defects at the skin/stringer interface of a stiffened composite panel. *Engineering fracture mechanics*. 2004 ;71(4):885-95.
16. Asha AV, Sahu SK. Parametric instability of twisted cross-ply laminated panels. *Aerospace Science and Technology*. 2011 ;15(6):465-75.
17. Ashton JE, Whitney JM. *Theory of laminated plates*. CRC Press; 1970.
18. Aslan Z, Karakuzu R, Okutan B. The response of laminated composite plates under low-velocity impact loading. *Composite Structures*. 2003;59(1):119-27.
19. Aymerich F, Dore F, Priolo P. Prediction of impact-induced delamination in cross-ply composite laminates using cohesive interface elements. *Composites science and technology*. 2008;68(12):2383-90.
20. Babu AA, Vasudevan R. Vibration analysis of rotating delaminated non-uniform composite plates. *Aerospace Science and Technology*. 2017 ;60:172-82.
21. Bathe KJ. *Finite element procedures*. Klaus-Jurgen Bathe; 2006.
22. Bert CW, Malik M. Differential quadrature method in computational mechanics: a review. *Applied Mechanics Reviews*. 1996;49:1-28.
23. Bert CW, Malik M. On the relative effects of transverse shear deformation and rotary inertia on the free vibration of symmetric cross-ply laminated plates. *Journal of sound and vibration*. 1996;193(4):927-33.
24. Bhar A, Phoenix SS, Satsangi SK. Finite element analysis of laminated composite stiffened plates using FSDT and HSDT: A comparative perspective. *Composite Structures*. 2010 ;92(2):312-21.
25. Bhaskar K, Pydah A. An elasticity approach for simply-supported isotropic and orthotropic stiffened plates. *International Journal of Mechanical Sciences*. 2014;89:21-30.
26. Bhimaraddi A, Carr AJ, Moss PJ. Finite element analysis of laminated shells of revolution with laminated stiffeners. *Computers & structures*. 1989 ;33(1):295-305.

27. Bisagni C. Progressive delamination analysis of stiffened composite panels in post-buckling. In Proceedings of the AIAA/ASME/ASCE/AHS/ASC 47th Structures, Structural Dynamics & Materials Conference, *AIAA paper* 2006; (No. 2006-2178).
28. Borrelli R, Riccio A, Sellitto A, Caputo F, Ludwig T. On the use of global–local kinematic coupling approaches for delamination growth simulation in stiffened composite panels. *Composites Science and Technology*. 2015;115:43-51.
29. Cairns DS, Lagace PA. Transient response of graphite/epoxy and kevlar/epoxy laminates subjected to impact. *AIAA journal*. 1989 ;27(11):1590-6.
30. Cao D, Liu B, Yao M, Zhang W. Free vibration analysis of a pre-twisted sandwich blade with thermal barrier coatings layers. *Science China Technological Sciences*. 2017 ;60(11):1747-61.
31. Cappello F, Tumino D. Numerical analysis of composite plates with multiple delaminations subjected to uniaxial buckling load. *Composites Science and Technology*. 2006 ;66(2):264-72.
32. Caputo F, De Luca A, Lamanna G, Borrelli R, Mercurio U. Numerical study for the structural analysis of composite laminates subjected to low velocity impact. *Composites Part B: Engineering*. 2014 ;67:296-302.
33. Carnegie W. Vibrations of pre-twisted cantilever blading allowing for rotary inertia and shear deflection. *Journal of Mechanical Engineering Science*. 1964 ;6(2):105-9.
34. Carnegie W. Vibrations of pre-twisted cantilever blading. *Proceedings of the Institution of Mechanical Engineers*. 1959a;173(1):343-74.
35. Carnegie W. Vibrations of rotating cantilever blading: theoretical approaches to the frequency problem based on energy methods. *Journal of Mechanical Engineering Science*. 1959b;1(3):235-40.
36. Carrera E, Filippi M, Zappino E. Free vibration analysis of rotating composite blades via Carrera Unified Formulation. *Composite Structures*. 2013 ;106:317-25.
37. Castro SG, Donadon MV. Assembly of semi-analytical models to address linear buckling and vibration of stiffened composite panels with debonding defect. *Composite Structures*. 2017 ;160:232-47.
38. Chai H, Babcock CD. Two-dimensional modelling of compressive failure in delaminated laminates. *Journal of Composite Materials*. 1985;19(1):67-98.
39. Chakravorty D, Bandyopadhyay JN. Effects of release of boundary constraints on the natural frequencies of clamped, thin, cylindrical shells. *Computers & Structures*. 1994 ;52(3):489-93.

40. Chandiramani NK, Shete CD, Librescu LI. Vibration of higher-order-shearable pretwisted rotating composite blades. *International Journal of Mechanical Sciences*. 2003 ;45(12):2017-41.
41. Chandrashekhara K, Kolli M. Free vibration of eccentrically stiffened laminated plates. *Journal of reinforced plastics and composites*. 1997;16(10):884-902.
42. Chao CC, Lee JC. Vibration of eccentrically stiffened laminates. *Journal of Composite Materials*. 1980;14(3):233-44.
43. Chattopadhyay B, Sinha PK, Mukhopadhyay M. Finite element analysis of blade-stiffened composite plates under transverse loads. *Journal of reinforced plastics and composites*. 1993;12(1):76-100.
44. Chattopadhyay B, Sinha PK, Mukhopadhyay M. Finite element free vibration analysis of eccentrically stiffened composite plates. *Journal of reinforced plastics and composites*. 1992 ;11(9):1003-34.
45. Chen H, Wang M, Bai R. The effect of nonlinear contact upon natural frequency of delaminated stiffened composite plate. *Composite Structures*. 2006 ;76(1):28-33.
46. Chen JK, Sun CT. Dynamic large deflection response of composite laminates subjected to impact. *Composite Structures*. 1985 ;4(1):59-73.
47. Chen JK, Sun CT. Nonlinear transient responses of initially stressed composite plates. *Computers & structures*. 1985;21(3):513-20.
48. Chen P, Xiong J, Shen Z. Thickness effect on the contact behavior of a composite laminate indented by a rigid sphere. *Mechanics of Materials*. 2008 ;40(4):183-94.
49. Cho M, Kim JS. Higher-order zig-zag theory for laminated composites with multiple delaminations. *Journal of Applied Mechanics*. 2001;68(6):869-77.
50. Choi IH. Geometrically nonlinear transient analysis of composite laminated plate and shells subjected to low-velocity impact. *Composite Structures*. 2016;142:7-14.
51. Christoforou AP, Swanson SR. Analysis of impact response in composite plates. *International Journal of Solids and Structures*. 1991;27(2):161-70.
52. Christoforou AP, Yigit AS. Characterization of impact in composite plates. *Composite structures*. 1998 ;43(1):15-24.
53. Christoforou AP, Yigit AS. Impact of composite structures—the momentum balance method. *Journal of composite materials*. 1996 ;30(10):1068-87.
54. Chun LU, Lam KY. Dynamic response of fully-clamped laminated composite plates subjected to low-velocity impact of a mass. *International journal of solids and structures*. 1998 ;35(11):963-79.

55. Cook RD. *Concepts and applications of finite element analysis*. John Wiley & Sons; 2007.
56. Craig TJ, Dawe DJ. Flexural vibration of symmetrically laminated composite rectangular plates including transverse shear effects. *International journal of solids and structures*. 1986 ;22(2):155-69.
57. Crawley EF, Dugundji J. Frequency determination and non-dimensionalization for composite cantilever plates. *Journal of Sound and Vibration*. 1980 ;72(1):1-10.
58. Crawley EF. The natural modes of graphite/epoxy cantilever plates and shells. *Journal of composite Materials*. 1979 ;13(3):195-205.
59. Dai HL, Liu HB, Zheng ZQ. Investigation on thermomechanical behavior of a HSLA-stiffened rectangular plate under low-velocity impact. *Journal of Thermal Stresses*. 2016 ;39(7):795-819.
60. Damjanović E, Marjanović M, Nefovska-Danilović M. Free vibration analysis of stiffened and cracked laminated composite plate assemblies using shear-deformable dynamic stiffness elements. *Composite Structures*. 2017 ;180:723-40.
61. Das HS, Chakravorty D. Bending analysis of stiffened composite conoidal shell roofs through finite element application. *Journal of Composite Materials*. 2011;45(5):525-42.
62. Davies GA, Hitchings D, Ankersen J. Predicting delamination and debonding in modern aerospace composite structures. *Composites Science and Technology*. 2006 ;66(6):846-54.
63. Dávila CG, Bisagni C. Fatigue life and damage tolerance of postbuckled composite stiffened structures with initial delamination. *Composite Structures*. 2017 ;161:73-84.
64. Deb A, Booton M. Finite element models for stiffened plates under transverse loading. *Computers & Structures*. 1988 ; 28(3):361-72.
65. Deb Nath SK, Afsar AM, Reaz Ahmed S. Displacement potential solution of a deep stiffened cantilever beam of orthotropic composite material. *The Journal of Strain Analysis for Engineering Design*. 2007;42(7):529-40.
66. Dey S, Karmakar A. Free vibration analyses of multiple delaminated angle-ply composite conical shells—A finite element approach. *Composite structures*. 2012a Jun;94(7):2188-96.
67. Dey S, Karmakar A. Natural frequencies of delaminated composite rotating conical shells—a finite element approach. *Finite Elements in Analysis and Design*. 2012b ;56:41-51.

68. Di Sciuva M. Bending, vibration and buckling of simply supported thick multilayered orthotropic plates: an evaluation of a new displacement model. *Journal of Sound and Vibration*. 1986 ;105(3):425-42.
69. Dokainish MA, Rawtani S. Bending of pretwisted cantilever plates (Finite element bending stiffness matrices for deflections analysis of pretwisted cantilever plate subjected to static loads). *CASI TRANSACTIONS*. 1969a; 2: 89-94.
70. Dokainish MA, Rawtani S. Vibration analysis of pretwisted cantilever plates(Finite element method for calculating natural frequencies and mode shapes of pretwisted cantilever plates assembly of flat triangular elements). *CASI TRANSACTIONS*. 1969b;2: 95-100.
71. Dokainish MA, Rawtani S. Vibration analysis of rotating cantilever plates. *International Journal for Numerical Methods in Engineering*. 1971;3(2):233-48.
72. Duffield RC, Willems N. Parametric resonance of stiffened rectangular plates. *Journal of Applied Mechanics*. 1972;39(1):217-26.
73. Egle DM, Sewall JL. An analysis of free vibration of orthogonally stiffened cylindrical shells with stiffeners treated as discrete elements. *AIAA Journal*. 1968;6(3):518-26.
74. English SA, Briggs TM, Nelson SM. Quantitative validation of carbon-fiber laminate low velocity impact simulations. *Composite Structures*. 2016 ;135:250-61.
75. Faggiani A, Falzon BG. Predicting low-velocity impact damage on a stiffened composite panel. *Composites Part A: Applied Science and Manufacturing*. 2010 ;41(6):737-49.
76. Fang M, Zhu X, Li T, Zhang G. Free Vibration Characteristics of a Finite Ring-Stiffened Elliptic Cylindrical Shell. *Journal of Vibration and Acoustics*. 2017;139(6):061012.
77. Fleming DC. Delamination modeling of composites for improved crash analysis. *Journal of Composite Materials*. 2001;35(19):1777-92.
78. Geubelle PH, Baylor JS. Impact-induced delamination of composites: a 2D simulation. *Composites Part B: Engineering*. 1998 ;29(5):589-602.
79. Ghosh AK, Biswal KC. Free-vibration analysis of stiffened laminated plates using higher-order shear deformation theory. *Finite elements in analysis and design*. 1996;22(2):143-61.
80. Gim CK. Plate finite element modeling of laminated plates. *Computers & Structures*. 1994 ; 52(1):157-68.

81. Gioncu V. *Thin reinforced concrete shells: special analysis problems*. John Wiley & Sons, New York; 1979.
82. Goldsmith W. *Impact: The theory and physical behavior of colliding solids*. 1960. Edward Arnold, London.
83. Gong SW, Lam KY. Transient response of stiffened composite plates subjected to low velocity impact. *Composites Part B: Engineering*. 1999;30(5):473-84.
84. Goswami S, Mukhopadhyay M. Finite element analysis of laminated composite stiffened shell. *Journal of Reinforced Plastics and Composites*. 1994;13(7):574-616.
85. Grassi M, Zhang X. Finite element analyses of mode I interlaminar delamination in z-fibre reinforced composite laminates. *Composites science and technology*. 2003 ;63(12):1815-32.
86. Gruben G, Sølvernes S, Berstad T, Morin D, Hopperstad OS, Langseth M. Low-velocity impact behaviour and failure of stiffened steel plates. *Marine Structures*. 2017 ;54:73-91.
87. Guo J, Guan Z, Qiu C. Buckling response of reinforced composite stiffened panel with cover in shear load. In *Material Engineering and Mechanical Engineering: Proceedings of Material Engineering and Mechanical Engineering (MEES2015) 2016* (pp. 682-696).
88. Guo M, Harik IE, Ren WX. Free vibration analysis of stiffened laminated plates using layered finite element method. *Structural engineering and mechanics*. 2002;14(3):245-62.
89. Hammami M, El Mahi A, Karra C, Haddar M. Experimental analysis of the linear and nonlinear behaviour of composites with delaminations. *Applied Acoustics*. 2016 ;108:31-9.
90. Hao P, Wang B, Tian K, Li G, Sun Y, Zhou C. Fast procedure for Non-uniform optimum design of stiffened shells under buckling constraint. *Structural and Multidisciplinary Optimization*. 2017b;55(4):1503-16.
91. Hao P, Wang B, Tian K, Liu H, Wang Y, Niu F, Zeng D. Simultaneous buckling design of stiffened shells with multiple cutouts. *Engineering Optimization*. 2017a ;49(7):1116-32.
92. Haoran C, Ruixiang B, Man W. Study on failure process of delaminated stiffened composite plates under compression. *Acta Mechanica Sinica*. 2003;19(4):289-99.

93. Heimbs S, Heller S, Middendorf P, Hähnel F, Weiße J. Low velocity impact on CFRP plates with compressive preload: Test and modelling. *International Journal of Impact Engineering*. 2009;36(10):1182-93.
94. Hertz H. Über die Berührung fester elastischer Körper. *Journal für die reine und angewandte Mathematik*. 1882;92:156-171.
95. Hirwani CK, Panda SK, Mahapatra TR. Thermomechanical deflection and stress responses of delaminated shallow shell structure using higher-order theories. *Composite Structures*. 2018 ;184:135-45.
96. Hirwani CK, Patil RK, Panda SK, Mahapatra SS, Mandal SK, Srivastava L, Buragohain MK. Experimental and numerical analysis of free vibration of delaminated curved panel. *Aerospace Science and Technology*. 2016;54:353-70.
97. Ho-Cheng H, Dharan CK. Delamination during drilling in composite laminates. *Journal of Engineering for Industry (Transactions of the ASME)*. 1990 ;112(3):236-9.
98. Hoppmann WH. Some characteristics of the flexural vibrations of orthogonally stiffened cylindrical shells. *The Journal of the Acoustical Society of America*. 1958 ;30(1):77-82.
99. Hu N, Fukunaga H, Kameyama M, Aramaki Y, Chang FK. Vibration analysis of delaminated composite beams and plates using a higher-order finite element. *International Journal of Mechanical Sciences*. 2002 ;44(7):1479-503.
100. Hu N, Sekine H, Fukunaga H, Yao ZH. Impact analysis of composite laminates with multiple delaminations. *International Journal of Impact Engineering*. 1999 ;22(6):633-48.
101. Johnson AF, Holzapfel M. Influence of delamination on impact damage in composite structures. *Composites science and technology*. 2006;66(6):807-15.
102. Johnson AF, Pickett AK, Rozycki P. Computational methods for predicting impact damage in composite structures. *Composites Science and Technology*. 2001 ;61(15):2183-92.
103. Jones RM. *Mechanics of composite materials*. McGraw Hill Kogakusha Limited, 1975.
104. Joshi SP, Sun CT. Impact induced fracture in a laminated composite. *Journal of Composite Materials*. 1985;19(1):51-66.
105. Ju F, Lee HP, Lee KH. Finite element analysis of free vibration of delaminated composite plates. *Composites Engineering*. 1995 Jan 1;5(2):195-209.

106. Karmakar A, Kishimoto K. Free Vibration Analysis of Delaminated Composite Pretwisted Rotating Shells— A Finite Element Approach. *JSME International Journal Series A Solid Mechanics and Material Engineering*. 2006;49(4):492-502.
107. Karmakar A, Roy H, Kishimoto K. Free vibration analysis of delaminated composite pretwisted shells. *Aircraft Engineering and Aerospace Technology*. 2005 Dec 1;77(6):486-90.
108. Karmakar A, Sinha PK. Failure analysis of laminated composite pretwisted rotating plates. *Journal of reinforced plastics and composites*. 2001;20(14-15):1326-57.
109. Kee YJ, Kim JH. Vibration characteristics of initially twisted rotating shell type composite blades. *Composite structures*. 2004 ;64(2):151-9.
110. Kielb RE, Leissa AW, Macbain JC. Vibrations of twisted cantilever plates—a comparison of theoretical results. *International Journal for Numerical Methods in Engineering*. 1985 Aug 1;21(8):1365-80.
111. Kim JH, Kim YY, Park Y, Kim CG. Low-velocity impact localization in a stiffened composite panel using a normalized cross-correlation method. *Smart Materials and Structures*. 2015 Mar 10;24(4):045036.
112. Kim SJ, Goo NS, Kim TW. The effect of curvature on the dynamic response and impact-induced damage in composite laminates. *Composites Science and Technology*. 1997 Jan 1;57(7):763-73.
113. Kirkhope J, Wilson GJ. A finite element analysis for the vibration modes of a bladed disc. *Journal of Sound and Vibration*. 1976 Dec 22;49(4):469-82.
114. Kolli M, Chandrashekhara K. Finite element analysis of stiffened laminated plates under transverse loading. *Composites science and technology*. 1996 Jan 1;56(12):1355-61.
115. Kong CW, Lee IC, Kim CG, Hong CS. Postbuckling and failure of stiffened composite panels under axial compression. *Composite Structures*. 1998 May 1;42(1):13-21.
116. Krawczuk M, Ostachowicz W, Zak A. Dynamics of cracked composite material structures. *Computational Mechanics*. 1997 Jul 4;20(1):79-83.
117. Krishnamurthy KS, Mahajan P, Mittal RK. Impact response and damage in laminated composite cylindrical shells. *Composite structures*. 2003 Jan 31;59(1):15-36.
118. Kubo JT, Nelson RB. Analysis of impact stresses in composite plates. In Foreign Object Impact Damage to Composites 1975 Jan. *ASTM International*.

119. Kumar NJ, Babu PR. Impact analysis of embedded delamination growth in stiffener of hybrid laminated composite stiffened panel. *International Journal of Computational Materials Science and Engineering*. 2017 Mar;6(01):1750001
120. Kumar SK, Cinefra M, Carrera E, Ganguli R, Harursampath D. Finite element analysis of free vibration of the delaminated composite plate with variable kinematic multilayered plate elements. *Composites Part B: Engineering*. 2014 Nov 30;66:453-65.
121. Kumar YS, Mukhopadhyay M. A new triangular stiffened plate element for laminate analysis. *Composites Science and Technology*. 2000 May 31;60(6):935-43.
122. Lal KM. Low velocity transverse impact behavior of 8-ply, graphite-epoxy laminates. *Journal of reinforced plastics and composites*. 1983 Oct;2(4):216-25.
123. Lam KY, Sathiyamoorthy TS. Response of composite beam under low-velocity impact of multiple masses. *Composite Structures*. 1999 Feb 1;44(2-3):205-20.
124. Lee CY, Chen JM. Interlaminar shear stress analysis of composite laminate with layer reduction technique. *International journal for numerical methods in engineering*. 1996 Mar 15;39(5):847-65.
125. Lee DM, Lee I. Vibration analysis of anisotropic plates with eccentric stiffeners. *Computers & structures*. 1995 Oct 3;57(1):99-105.
126. Lee JD, Du S, Liebowitz H. Three-dimensional finite element and dynamic analysis of composite laminate subjected to impact. *Computers & structures*. 1984 Jan 1;19(5-6):807-13.
127. Leissa A. Vibrational aspects of rotating turbomachinery blades. *Applied Mechanics Reviews*. 1981 May;34(5):629-35.
128. Leissa AW. Vibrations of turbine engine blades by shell analysis. *Shock Vib. Dig*. 1980;12(11):3-10.
129. Li C, Wu Z. Buckling of 120° stiffened composite cylindrical shell under axial compression—Experiment and simulation. *Composite Structures*. 2015 Sep 15;128:199-206.
130. Li D, Qing G, Liu Y. A layerwise/solid-element method for the composite stiffened laminated cylindrical shell structures. *Composite Structures*. 2013 Apr 30;98:215-27.
131. Li DH, Liu Y, Zhang X. Low-velocity impact responses of the stiffened composite laminated plates based on the progressive failure model and the layerwise/solid-elements method. *Composite Structures*. 2014 Apr 30;110:249-75.

132. Li G, Chakka VS. Isogrid stiffened syntactic foam cored sandwich structure under low velocity impact. *Composites Part A: Applied Science and Manufacturing*. 2010 Jan 31;41(1):177-84.
133. Li L, Xiaohui R. Stiffened plate bending analysis in terms of refined triangular laminated plate element. *Composite Structures*. 2010 Nov 30;92(12):2936-45.
134. Li N, Chen PH. Experimental investigation on edge impact damage and Compression-After-Impact (CAI) behavior of stiffened composite panels. *Composite Structures*. 2016 Mar 15;138:134-50.
135. Liao CL, Cheng CR. Dynamic stability of stiffened laminated composite plates and shells subjected to in-plane pulsating forces. *Journal of Sound and Vibration*. 1994 Jul 14;174(3):335-51.
136. Liao CL, Reddy JN. Analysis of anisotropic, stiffened composite laminates using a continuum-based shell element. *Computers & structures*. 1990 Jan 1;34(6):805-15.
137. Lim CW, Liew KM, Kitipornchai S. Free vibration of pretwisted, cantilevered composite shallow conical shells. *AIAA journal*. 1997 ;35(2):327-33.
138. Liu D. Impact-induced delamination—a view of bending stiffness mismatching. *Journal of Composite Materials*. 1988 Jul;22(7):674-92.
139. Lu X, Liu D. An interlaminar shear stress continuity theory for both thin and thick composite laminates. ASME, Transactions, *Journal of Applied Mechanics*. 1992 Sep 1;59(3):502-9.
140. Lu X, Yang JY, Wu YG, Zhang F, Li DH. An extended layerwise/solid-element method of stiffened composite plates with delaminations and transverse crack. *International Journal of Mechanics and Materials in Design*. 2017:1-4.DOI:<https://doi.org/10.1007/s10999-017-9378-1>
141. MacBain JC. Vibratory behavior of twisted cantilevered plates. *Journal of Aircraft*. 1975 Apr;12(4):343-9.
142. Maiti DK, Sinha PK. Bending, free vibration and impact response of thick laminated composite plates. *Computers & structures*. 1996 ;59(1):115-29.
143. Malik M, Bert CW. Differential quadrature analysis of free vibration of symmetric cross-ply laminates with shear deformation and rotatory inertia. *Shock and Vibration*. 1995;2(4):321-38.
144. McCallum S. The influence of preload and boundary conditions on pre-damaged composite plates subject to soft-body impact. *Materials & Design*. 2015 Oct 15;83:848-57.

145. McDonald D. A problem in the free vibration of stiffened cylindrical shells. *AIAA Journal*. 1970 Feb;8(2):252-8.
146. Merritt RG, Willems N. Parametric resonance of skew stiffened plates. *Journal of Applied Mechanics*. 1973 Jun 1;40(2):439-44.
147. Mikkor KM, Thomson RS, Herszberg I, Weller T, Mouritz AP. Finite element modelling of impact on preloaded composite panels. *Composite Structures*. 2006 Sep 30;75(1):501-13.
148. Milazzo A, Oliveri V. Buckling and postbuckling of stiffened composite panels with cracks and delaminations by Ritz approach. *AIAA Journal*. 2017; 55(3): 965-980.
149. Mili F, Necib B. Impact behavior of cross-ply laminated composite plates under low velocities. *Composite structures*. 2001 Mar 31;51(3):237-44.
150. Miller PR. Free vibrations of a stiffened cylindrical shell. Ministry of Aviation, *Aeronautical Research Council*; 1957.1-38
151. Mindlin RD. Influence of rotatory inertia and shear on flexural motions of isotropic, elastic plates. *J. appl. Mech.*. 1951;18-31.
152. Mohanty J, Sahu SK, Parhi PK. Numerical and experimental study on free vibration of delaminated woven fiber glass/epoxy composite plates. *International Journal of Structural Stability and Dynamics*. 2012 Mar;12(02):377-94.
153. Moon FC. Stress wave calculations in composite plates using the fast Fourier transform. *Computers & Structures*. 1973 Sep 1;3(5):1195-204.
154. Moon FC. Wave surfaces due to impact on anisotropic plates. *Journal of composite materials*. 1972 Jan;6(1):62-79.
155. Morin D, Kaarstad BL, Skajaa B, Hopperstad OS, Langseth M. Testing and modelling of stiffened aluminium panels subjected to quasi-static and low-velocity impact loading. *International Journal of Impact Engineering*. 2017 Mar 6.
156. Muc A, Stawiarski A. Location of delaminations in curved laminated panels. *Composite Structures*. 2015 Dec 1;133:652-658.
157. Mukherjee A, Menghani LC. Displacement and stress response of laminated beams and stiffened plates using a high-order element. *Composite structures*. 1994 Jan 1;28(1):93-111.
158. Murthy MV. An improved transverse shear deformation theory for laminated anisotropic plates. *NASA Technical Paper* 1903, 1981.

159. Mustafa BA, Ali R. Prediction of natural frequency of vibration of stiffened cylindrical shells and orthogonally stiffened curved panels. *Journal of Sound and Vibration*. 1987 Mar 8;113(2):317-27.
160. Nabi SM, Ganesan N. Comparison of beam and plate theories for free vibrations of metal matrix composite pre-twisted blades. *Journal of Sound and Vibration*. 1996;189(2):149-60.
161. Naganarayana BP, Huang BZ, Atluri SN. Multidomain modeling and analysis of delaminated stiffened composite shells. *AIAA journal*. 1996 Sep 1;34(9).
162. Nagashima T, Suemasu H. X-FEM analyses of a thin-walled composite shell structure with a delamination. *Computers & structures*. 2010 May 31;88(9):549-57.
163. Naini JK, Ramesh B P. Impact analysis of embedded delamination location in hybrid curved laminated composite stiffened panel. *Applied Composite Materials*. 2016 Aug 1;23(4):639-58.
164. Nanda N, Sahu SK. Free vibration analysis of delaminated composite shells using different shell theories. *International Journal of Pressure Vessels and Piping*. 2012 Oct 31;98:111-8.
165. Nath SD, Ahmed SR. Displacement potential solution of stiffened composite struts subjected to eccentric loading. *Applied Mathematical Modelling*. 2009 Mar 31;33(3):1761-75.
166. Nayak AN, Bandyopadhyay JN. Free vibration analysis of laminated stiffened shells. *Journal of Engineering Mechanics*. 2005 Jan;131(1):100-5.
167. Nguyen-Thoi T, Bui-Xuan T, Liu GR, Vo-Duy T. Static and Free Vibration Analysis of Stiffened Flat Shells by a Cell-Based Smoothed Discrete Shear Gap Method (CS-FEM-DSG3) Using Three-Node Triangular Elements. *International Journal of Computational Methods*. 2017 Dec 8:1850056.
168. Noor AK, Burton WS. Assessment of shear deformation theories for multilayered composite plates. *Appl. Mech. Rev.* 1989 Jan 1;42(1):1-3.
169. Oh J, Cho M, Kim JS. Dynamic analysis of composite plate with multiple delaminations based on higher-order zigzag theory. *International Journal of Solids and Structures*. 2005 Nov 30;42(23):6122-40.
170. Ojeda R, Prusty BG, Lawrence N, Thomas G. A new approach for the large deflection finite element analysis of isotropic and composite plates with arbitrary orientated stiffeners. *Finite Elements in Analysis and Design*. 2007 Sep 30;43(13):989-1002.

171. Olsson R. Analytical model for delamination growth during small mass impact on plates. *International Journal of Solids and Structures*. 2010 Oct 15;47(21):2884-92.
172. Olsson R. Analytical prediction of damage due to large mass impact on thin ply composites. *Composites Part A: Applied Science and Manufacturing*. 2015 May 31;72:184-91.
173. Pagano NJ, Hatfield HJ. Elastic behavior of multilayered bidirectional composites. *AIAA journal*. 1972 Jul;10(7):931-3.
174. Pagano NJ. Exact solutions for composite laminates in cylindrical bending. *Journal of composite materials*. 1969 Mar;3(3):398-411.
175. Pagano NJ. Exact solutions for rectangular bidirectional composites and sandwich plates. *Journal of composite materials*. 1970 Jan;4(1):20-34.
176. Pagano NJ. Influence of shear coupling in cylindrical bending of anisotropic laminates. *Journal of composite materials*. 1970 Mar;4(3):330-43.
177. Pardoen GC. Effect of delamination on the natural frequencies of composite laminates. *Journal of composite materials*. 1989 Dec;23(12):1200-15.
178. Parhi PK, Bhattacharyya SK, Sinha PK. Hygrothermal effects on the dynamic behavior of multiple delaminated composite plates and shells. *Journal of Sound and Vibration*. 2001 Nov 22;248(2):195-214.
179. Park H. Investigation on low velocity impact behavior between graphite/epoxy composite and steel plate. *Composite Structures*. 2017 Jul 1;171:126-30.
180. Patel SN, Datta PK, Sheikh AH. Buckling and dynamic instability analysis of stiffened shell panels. *Thin-Walled Structures*. 2006 Mar 31;44(3):321-33.
181. Peck SO, Springer GS. The behavior of delaminations in composite plates—analytical and experimental results. *Journal of Composite Materials*. 1991 Jul;25(7):907-29.
182. Phan ND, Reddy JN. Analysis of laminated composite plates using a higher-order shear deformation theory. *International Journal for Numerical Methods in Engineering*. 1985 Dec 1;21(12):2201-19.
183. Prusty BG, Ray C. Free vibration analysis of composite hat-stiffened panels by method of finite elements. *Journal of reinforced plastics and composites*. 2004 Mar;23(5):533-47.
184. Prusty BG. Free vibration and buckling response of hat-stiffened composite panels under general loading. *International Journal of Mechanical Sciences*. 2008 Aug 31;50(8):1326-33.

185. Prusty BG. Linear static analysis of composite hat-stiffened laminated shells using finite elements. *Finite elements in analysis and design*. 2003 Sep 30;39(12):1125-38.
186. Prusty BG. Progressive failure analysis of laminated unstiffened and stiffened composite panels. *Journal of reinforced plastics and composites*. 2005 Apr;24(6):633-42.
187. Pydah A, Bhaskar K. Accurate discrete modelling of stiffened isotropic and orthotropic rectangular plates. *Thin-Walled Structures*. 2015 Dec 31;97:266-78.
188. Qatu MS, Leissa AW. Free vibrations of completely free doubly curved laminated composite shallow shells. *Journal of Sound and Vibration*. 1991b Nov 22;151(1):9-29.
189. Qatu MS, Leissa AW. Natural frequencies for cantilevered doubly-curved laminated composite shallow shells. *Composite Structures*. 1991a Jan 1;17(3):227-55.
190. Qatu MS, Leissa AW. Vibration studies for laminated composite twisted cantilever plates. *International Journal of Mechanical Sciences*. 1991 Jan 1;33(11):927-40.
191. Qian Y, Swanson SR. A comparison of solution techniques for impact response of composite plates. *Composite Structures*. 1990 Jan 1;14(3):177-92.
192. Qing G, Qiu J, Liu Y. Free vibration analysis of stiffened laminated plates. *International Journal of Solids and Structures*. 2006 Mar 31;43(6):1357-71.
193. Ramamurti V, Kielb R. Natural frequencies of twisted rotating plates. *Journal of Sound and Vibration*. 1984 Dec 8;97(3):429-49.
194. Ramkumar RL, Chen PC. Low-velocity impact response of laminated plates. *AIAA J*. 1983 Oct;21(10):1448-52.
195. Rao JS, Banerjee S. Coupled bending-torsional vibrations of rotating cantilever blades—method of polynomial frequency equation. *Mechanism and Machine Theory*. 1977 Jan 1;12(4):271-80.
196. Rao JS, Gupta K. Free vibrations of rotating small aspect ratio pretwisted blades. *Mechanism and Machine Theory*. 1987 Jan 1;22(2):159-67.
197. Rao JS. Natural frequencies of turbine blading—a survey. *Shock and Vibration Digest*. 1973; 5(10):3-16.
198. Rao JS. Turbine blading excitation and vibration. *Shock and Vibration Digest*. 1977; 9(3):15-22.
199. Rao JS. Turbomachine Blade Vibration. *Shock and Vibration Digest*. 1980; 12(2): 19-26.

200. Rao JS. Turbomachine Blade Vibration. *Shock and Vibration Digest*. 1983; 15(5): 3-9.
201. Ravn-Jensen K. A shell analysis of turbine blade vibrations. *International Journal of Mechanical Sciences*. 1982 Jan 1;24(10):581-7.
202. Reddy JN. A general non-linear third-order theory of plates with moderate thickness. *International Journal of Non-Linear Mechanics*. 1990 ;25(6):677-686.
203. Reddy JN. A simple higher-order theory for laminated composite plates. *Journal of applied mechanics*. 1984 Dec 1;51(4):745-52.
204. Riccio A, Damiano M, Raimondo A, Di Felice G, Sellitto A. A fast numerical procedure for the simulation of inter-laminar damage growth in stiffened composite panels. *Composite Structures*. 2016 Jun 10;145:203-16.
205. Riccio A, Raimondo A, Caprio FD, Scaramuzzino F. Delaminations buckling and growth phenomena in stiffened composite panels under compression. Part II: a numerical study. *Journal of Composite Materials*. 2014b Sep;48(23):2857-70.
206. Riccio A, Raimondo A, Di Felice G, Scaramuzzino F. A numerical procedure for the simulation of skin–stringer debonding growth in stiffened composite panels. *Aerospace Science and Technology*. 2014 Dec 31;39:307-14.
207. Riccio A, Raimondo A, Fragale S, Camerlingo F, Gambino B, Toscano C, Tescione D. Delamination buckling and growth phenomena in stiffened composite panels under compression. Part I: An experimental study. *Journal of Composite Materials*. 2014a Sep;48(23):2843-55.
208. Riccio A, Raimondo A, Scaramuzzino F. A robust numerical approach for the simulation of skin–stringer debonding growth in stiffened composite panels under compression. *Composites Part B: Engineering*. 2015;71:131-42.
209. Riccio A, Raimondo A, Scaramuzzino F. A study on skin delaminations growth in stiffened composite panels by a novel numerical approach. *Applied composite materials*. 2013;20(4):465-88.
210. Riccio A, Ricchiuto R, Saputo S, Raimondo A, Caputo F, Antonucci V, Lopresto V. Impact behaviour of omega stiffened composite panels. *Progress in Aerospace Sciences*. 2016 ;81:41-8.
211. Rui-xiang B, Hao-ran C. Numerical analysis of delamination growth for stiffened composite laminated plates. *Applied mathematics and mechanics*. 2004;25(4):405-17.
212. Sadek EA, Tawfik SA. A finite element model for the analysis of stiffened laminated plates. *Computers & Structures*. 2000 ;75(4):369-83.

213. Sahoo S, Chakravorty D. Stiffened composite hyper shell roofs under free vibration: Behaviour and optimization aids. *Journal of sound and vibration*. 2006 ;295(1):362-77.
214. Sahoo S. Free vibration behavior of laminated composite stiffened elliptic parabolic shell panel with cutout. *Curved and Layered Structures*. 2015 ;2(1).
215. Sahoo SS, Panda SK, Sen D. Effect of delamination on static and dynamic behavior of laminated composite plate. *AIAA Journal*. 2016 .DOI: 10.2514/1.J054908
216. Sanders JL. An improved first approximation theory for thin shells (NASA TR-R24). *US Government Printing Office, Washington, DC*. 1959.
217. Sanga RP, Garnier C, Pantalé O. Finite Element Simulation of Low Velocity Impact Damage on an Aeronautical Carbon Composite Structure. *Applied Composite Materials*. 2016 ;23(6):1195-208.
218. Sankar BV, Sun CT. An efficient numerical algorithm for transverse impact problems. *Computers & structures*. 1985 ;20(6):1009-12.
219. Schonberg WP, Keer LM, Woo TK. Low velocity impact of transversely isotropic beams and plates. *International journal of solids and structures*. 1987 ;23(7):871-96.
220. Sekine H, Atobe S. Identification of locations and force histories of multiple point impacts on composite isogrid-stiffened panels. *Composite Structures*. 2009 ;89(1):1-7.
221. Sekine H, Hu T, Natsume T, Fukunaga H. Impact response analysis of partially delaminated composite laminates. *Transactions of the Japan Society of Mechanical Engineers, Series A*. 1997;63(608):787-93.
222. Seydel R, Chang FK. Impact identification of stiffened composite panels: I. System development. *Smart Materials and Structures*. 2001a ;10(2):354.
223. Seydel R, Chang FK. Impact identification of stiffened composite panels: II. Implementation studies. *Smart materials and structures*. 2001 ;10(2):370.
224. Shah S, Panda SK. Thermoelastic fracture behavior of bimodular functionally graded skin-stiffener composite panel with embedded inter-laminar delamination. *Journal of Reinforced Plastics and Composites*. 2017; 36(19): 1439-1452.
225. Shankar G, Kumar SK, Mahato PK. Vibration analysis and control of smart composite plates with delamination and under hygrothermal environment. *Thin-Walled Structures*. 2017 ;116:53-68.
226. Sharif-Khodaei Z, Ghajari M, Aliabadi MH. Determination of impact location on composite stiffened panels. *Smart Materials and Structures*. 2012 ;21(10):105026.

227. Shen MH, Grady JE. Free vibrations of delaminated beams. *AIAA journal*. 1992 May;30(5):1361-70.
228. Sheng GG, Wang X. The dynamic stability and nonlinear vibration analysis of stiffened functionally graded cylindrical shells. *Applied Mathematical Modelling*. 2017 ; 56: 389-403.
229. Shivakumar KN, Elber W, Illg W. Prediction of impact force and duration due to low-velocity impact on circular composite laminates. *Journal of applied mechanics*. 1985a Sep 1;52(3):674-680.
230. Shivakumar KN, Elber W, Illg W. Prediction of low-velocity impact damage in thin circular laminates. *AIAA journal*. 1985b ;23(3):442-449.
231. Simitises GJ, Sallam S, Yin WL. Effect of delamination of axially loaded homogeneous laminated plates. *AIAA journal*. 1985 ;23(9):1437-44.
232. Sinha G, Mukhopadhyay M. Finite element free vibration analysis of stiffened shells. *Journal of Sound and Vibration*. 1994 ;171(4):529-48.
233. Sinha SK, Turner KE. Natural frequencies of a pre-twisted blade in a centrifugal force field. *Journal of Sound and Vibration*. 2011 ;330(11):2655-81.
234. Sreenivasamurthy S, Ramamurti V. A parametric study of vibration of rotating pre-twisted and tapered low aspect ratio cantilever plates. *Journal of Sound and vibration*. 1981 ;76(3):311-28.
235. Sreenivasamurthy S, Ramamurti V. Coriolis effect on the vibration of flat rotating low aspect ratio cantilever plates. *The Journal of Strain Analysis for Engineering Design*. 1981 ; 16(2):97-106.
236. Sreenivasamurthy S, Ramamurti V. Effect of a tip mass on the natural frequencies of a rotating pre-twisted cantilever plate. *Journal of Sound and Vibration*. 1980 ;70(4):598-601.
237. Srivastava AK, Datta PK, Sheikh AH. Vibration and dynamic instability of stiffened plates subjected to in-plane harmonic edge loading. *International Journal of Structural Stability and Dynamics*. 2002 ;2(02):185-206.
238. Srivastava AK. Vibration and Dynamic Stability of Stiffened Plates with Cutout. *In Advances in Structural Engineering 2015* (pp. 95-102). Springer, New Delhi.
239. Suemasu H, Kurihara K, Arai K, Majima O, Ishikawa T. Compressive property degradation of composite stiffened panel due to debonding and delaminations. *Advanced Composite Materials*. 2006 ;15(2):139-51.

240. Sun CT, Chattopadhyay S. Dynamic response of anisotropic laminated plates under initial stress to impact of a mass. *Journal of applied mechanics*. 1975 ;42(3):693-8.
241. Sun CT, Chen JK. On the impact of initially stressed composite laminates. *Journal of Composite Materials*. 1985 ;19(6):490-504.
242. Sun CT, Lai RY. Exact and approximate analyses of transient wave propagation in an anisotropic plate. *AIAA Journal*. 1974;12(10):1415-7.
243. Sun CT, Liou WJ. Investigation of laminated composite plates under impact dynamic loading using a three-dimensional hybrid stress finite element method. *Computers & structures*. 1989 ;33(3):879-84.
244. Sun CT, Whitney JM, Rocchio JJ, Decker LJ. Dynamic response of laminated composite plates under initial stress. *AIAA JOURNAL*. 1976 ;14(2).
245. Sun CT, Whitney JM. Theories for the dynamic response of laminated plates. *AIAA J*. 1973 ;11(2):178-83.
246. Sun CT, Yang SH. Contact Law and Impact Responses of Laminated Composites. *Purdue univ lafayette in school of aeronautics and astronautics*; 1980.
247. Sun CT. Propagation of shock waves in anisotropic composite plates. *Journal of Composite Materials*. 1973 ;7(3):366-82.
248. Sun W, Guan Z, Ouyang T, Tan R, Zhong X. Effect of stiffener damage caused by low velocity impact on compressive buckling and failure modes of T-stiffened composite panels. *Composite Structures*. 2018;184:198-210.
249. Sun X, Tong M. Finite Element Analysis of Low-Velocity Impact Damage on Stiffened Composite Panels. *International Journal of Aerospace and Mechanical Engineering*. 2014;8(7):1259-63.
250. Swanson SR. Contact deformation and stress in orthotropic plates. *Composites Part A: Applied Science and Manufacturing*. 2005;36(10):1421-9.
251. Swanson SR. Hertzian contact of orthotropic materials. *International journal of solids and structures*. 2004;41(7):1945-59.
252. Tan TM, Sun CT. Use of statical indentation laws in the impact analysis of laminated composite plates. *Journal of applied mechanics*. 1985;52(1):6-12.
253. Think TI, Quoc TH. Finite element modeling and experimental study on bending and vibration of laminated stiffened glass fiber/polyester composite plates. *Computational Materials Science*. 2010;49(4):S383-9.

254. Tian K, Wang B, Hao P, Waas AM. A high-fidelity approximate model for determining lower-bound buckling loads for stiffened shells. *International Journal of Solids and Structures*. 2017. <https://doi.org/10.1016/j.ijsolstr.2017.10.034>.
255. Torabi K, Shariati-Nia M, Heidari-Rarani M. Experimental and theoretical investigation on transverse vibration of delaminated cross-ply composite beams. *International Journal of Mechanical Sciences*. 2016;115:1-1.
256. Torkamani S, Navazi HM, Jafari AA, Bagheri M. Structural similitude in free vibration of orthogonally stiffened cylindrical shells. *Thin-Walled Structures*. 2009;47(11):1316-30.
257. Tsai SW. *Composites design*. Think Composites, P. O. Box 581, Dayton, Ohio 45419, USA, 1988. 583. 1988.
258. Tuan TA, Quoc TH, Tu TM. Free Vibration Analysis of Laminated Stiffened Cylindrical Panels using Finite Element Method. *Journal of Science and Technology*. 2016;54(6):771.
259. Vaziri R, Quan X, Olson MD. Impact analysis of laminated composite plates and shells by super finite elements. *International journal of impact engineering*. 1996;18(7-8):765-82.
260. Venkatesh A, Rao KP. Analysis of laminated shells of revolution with laminated stiffeners using a doubly curved quadrilateral finite element. *Computers & structures*. 1985;20(4):669-82.
261. Venkatesh A, Rao KP. Analysis of laminated shells with laminated stiffeners using rectangular shell finite elements. *Computer Methods in Applied Mechanics and Engineering*. 1983;38(3):255-72.
262. Vlasov VZ. *Allgemeine Schalentheorie und ihre Anwendung in der Technik*. Akad.-Verlag; 1958.
263. Wagner W, Balzani C. Simulation of delamination in stringer stiffened fiber-reinforced composite shells. *Computers & Structures*. 2008;86(9):930-9.
264. Wah T. Flexural vibrations of ring-stiffened cylindrical shells. *Journal of Sound and Vibration*. 1966;3(3):242-51.
265. Wang JT, Raju IS, Sleight DW. Composite skin-stiffener debond analyses using fracture mechanics approach with shell elements. *Composites Engineering*. 1995;5(3):277-96.
266. Wang JT, Rinehart SA. Free vibrations of longitudinally stiffened cylindrical shells. *Journal of Applied Mechanics*. 1974 ;41(4):1087-93.

267. Wang SS. An analysis of delamination in angle-ply fiber-reinforced composites. ASME, Transactions, *Journal of Applied Mechanics*. 1980;47:64-70.
268. Weingarten VI. Free vibrations of ring-stiffened conical shells. *AIAA Journal*. 1965 ;3(8):1475-81.
269. Whitney JM, Analysis of anisotropic rectangular plates. *AIAA journal*, 1972; 10(10): 1344-1345.
270. Whitney JM, Leissa AW. Analysis of heterogeneous anisotropic plates. *Journal of Applied Mechanics*. 1969 ;36(2):261-6.
271. Whitney JM, Pagano NJ. Shear deformation in heterogeneous anisotropic plates. *Journal of applied mechanics*. 1970;37(4):1031-6.
272. Whitney JM. The effect of transverse shear deformation on the bending of laminated plates. *Journal of Composite Materials*. 1969;3(3):534-47.
273. Whittingham B, Marshall IH, Mitrevski T, Jones R. The response of composite structures with pre-stress subject to low velocity impact damage. *Composite Structures*. 2004;66(1):685-98.
274. Wu HY, Fu-Kuo C. Transient dynamic analysis of laminated composite plates subjected to transverse impact. *Computers & structures*. 1989 ;31(3):453-66.
275. Wu HY, Springer GS. Impact induced stresses, strains, and delaminations in composite plates. *Journal of Composite Materials*. 1988 ;22(6):533-60.
276. Yam LH, Wei Z, Cheng L, Wong WO. Numerical analysis of multi-layer composite plates with internal delamination. *Computers & structures*. 2004 ;82(7):627-37.
277. Yang FJ, Cantwell WJ. Impact damage initiation in composite materials. *Composites science and technology*. 2010;70(2):336-42.
278. Yang IH, Shieh JA. Vibrations of initially stressed thick, rectangular, orthotropic plates. *Journal of sound and vibration*. 1987 ;119(3):545-58.
279. Yang J, Fu Y. Analysis of dynamic stability for composite laminated cylindrical shells with delaminations. *Composite structures*. 2007;78(3):309-15.
280. Yang PC, Norris CH, Stavsky Y. Elastic wave propagation in heterogeneous plates. *International Journal of solids and structures*. 1966;2(4):665-84.
281. Yang SH, Sun CT. Indentation law for composite laminates. *In Composite Materials: Testing and Design (6th Conference)* 1982; ASTM International.
282. Yazdani S, Rust WJ, Wriggers P. An XFEM approach for modelling delamination in composite laminates. *Composite Structures*. 2016 ;135:353-64.

283. Yazdani S, Rust WJ, Wriggers P. Delamination onset and growth in composite shells. *Computers & Structures*. 2018; 195:1-15.
284. Yetman JE, Sobey AJ, Blake JI, Sheno RA. Investigation into skin stiffener debonding of top-hat stiffened composite structures. *Composite Structures*. 2015 ;132:1168-81.
285. Yigit AS, Christoforou AP. On the impact between a rigid sphere and a thin composite laminate supported by a rigid substrate. *Composite Structures*. 1995;30(2):169-77.
286. Yuan WX, Dawe DJ. Free vibration and stability analysis of stiffened sandwich plates. *Composite structures*. 2004 ;63(1):123-37.
287. Zhang Z, Chen H, Ye L. Progressive failure analysis for advanced grid stiffened composite plates/shells. *Composite Structures*. 2008 Nov;86(1):45-54.
288. Zhao W, Kapania RK. Vibrational Analysis of Unitized Curvilinearly Stiffened Composite Panels Subjected to In-plane Loads. *In 57th AIAA/ASCE/AHS/ASC Structures, Structural Dynamics, and Materials Conference 2016* (p. 1500).

Appendix-I: Flowchart for the computational procedure

